DEVELOPMENT OF NEW NMR TECHNIQUES FOR CONFORMATIONAL ANALYSIS OF ^{13}C-ENRICHED OLIGOSACCHARIDES

Richard Harris

A Thesis Submitted for the Degree of PhD
at the
University of St Andrews

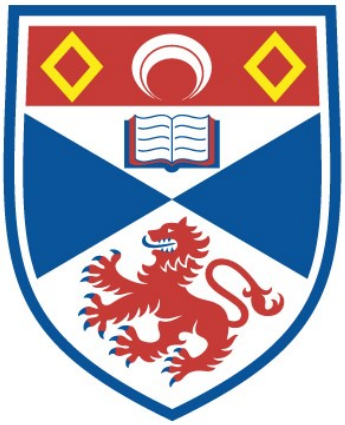

1998

Development of NMR methods for conformational analysis of ^{13}C-enriched oligosaccharides.

Richard Harris

A thesis submitted for the degree of Doctor of Philosophy.

School of Biomedical Sciences
University of St. Andrews
November 1997.

Table of Contents

Acknowledgements

I would like to thank my supervisor, Steve Homans, for all of his help and support throughout my Ph.D. project.

I would also like to thank Julia Richardson, Trevor Rutherford, and Charles Weller for all of their help with the NMR experiments and theory. I would like to thank Mark Milton, and Mark Probert, without whom the fully ^{13}C labelled sialyl Lewis^x would never have been made, to Martek Biosciences for the gift of labelled starting materials, and to Monica Palcic for the gift of fucosyltransferase. I would also like to acknowledge the kind gift of E-selectin by Beat Ernst, and the advice from Thomas Weimar on the transferred NOE study. In addition I would like to thank Mark Milton, again, for all of his help and advice with the computer modelling, especially the time-averaged restrained dynamics.

Finally I have to thank Graham Kiddle and Grant Fuller for keeping me entertained throughout the three years, and to my family for all their continued support during my life as a student.

Thank you all.

This work was funded by the BBSRC.

Declarations

I, Richard Harris, hereby certify that this thesis, which is approximately 50 000 words in length, has been written by me, that it is a record of work carried out by me and that it has not been submitted in any previous application for a higher degree.

14th November 1997 Richard Harris

I was admitted as a research student in October 1994 and as a candidate for the degree of Doctor of Philosophy in October 1994; the higher study for which this is a record was carried out in the University of St. Andrews between 1994 and 1997.

14th November 1997 Richard Harris

I hereby certify that the candidate has fulfilled the conditions of the Resolution and Regulations appropriate for the degree of Doctor of Philosophy in the University of St. Andrews and that the candidate is qualified to submit this thesis in application for that degree.

14th November 1997 Steve William Homans

In submitting this thesis to the University of St. Andrews I understand that I am giving permission for it to be made available for use in accordance with the regulations of the University Library for the time being in force, subject to copyright vested in the work not being affected thereby. I also understand that the title and abstract will be published, and that a copy of the work may be made and supplied to any *bona fide* library or research worker.

14th November 1997 Richard Harris

Abstract

The conformation and dynamics of sialyl Lewis^x and related oligosaccharides were investigated using high resolution nuclear magnetic resonance measurements, and molecular dynamics calculations.

In order to increase the number of structural parameters for inclusion in the molecular modelling simulations, the oligosaccharide sialyl Lewis^x was chemo-enzymatically synthesised to a high degree of carbon-13 enrichment (<99%). The incorporation of ^{13}C labelling allows editing of standard homonuclear NMR experiments by the ^{13}C chemical shift, thus overcoming the spectral overlap which plagues carbohydrate NMR.

Three dimensional heteronuclear NOESY/ROESY-HSQC experiments have allowed the unambiguous assignment and quantitation of NOEs/ROEs in a number of oligosaccharides including evidence that the anti-conformer is populated in aqueous solution for the Galβ1-4GlcNAc linkage in sialylα2,3-*N*-acetyllactosamine trisaccharide. Additional structural information was gained from the measurement of trans-glycosidic three bond carbon-carbon coupling constants. A Karplus relationship was derived for the C-O-C-C fragment allowing the back-calculation of $^3J_{COCC}$ values from molecular dynamics simulation for comparison to experimental data.

Additional distance restraints were derived from NOEs to exchangeable protons in low temperature studies using a mixed solvent system of H_2O/acetone-d_6. The increase in the number of distance restraints, have allowed the use time-averaged molecular dynamics simulations, and from these it is shown that NOEs to certain hydroxyls in sialyl Lewis^x can only be explained if these hydroxyls are constrained within hydrogen bonds.

Table of Figures

Chapter 1

Chapter 2

Chapter 6

List of Tables

Chapter 6

List of Abbreviations

COSY	Correlated Spectroscopy
ES	Excitation Sculpting
HMQC	Heteronuclear Multiple Quantum Coherence Spectroscopy
HOHAHA	Homonuclear Hartmann Hahn
HSQC	Heteronuclear Single Quantum Coherence Spectroscopy
LRCC	Long Range Carbon-Carbon Coupling Spectroscopy
LRCH	Long Range Carbon-Proton Coupling Spectroscopy
NMR	Nuclear Magnetic Resonance
NOE	Nuclear Overhauser Effect
NOESY	Nuclear Overhauser Effect Spectroscopy
ns	nanosecond
ROE	Rotating Frame Nuclear Overhauser Effect
ROESY	Rotating Frame Nuclear Overhauser Effect Spectroscopy
ps	picosecond
p-NP	*para*-nitrophenol
TOCSY	Total Correlated Spectroscopy
TRNOE	Transferred Nuclear Overhauser Effect
TRNOESY	Transferred Nuclear Overhauser Effect Spectroscopy
TSP	3-(trimethylsilyl) proprionic-2,2,3,3,-d_4-acid, sodium salt.
[U-^{13}C]	Uniformly carbon-13 enriched (excluding *N*-acetyl groups of acetylated sugars)

Symbols

^{1}H	Hydrogen atom (proton)
^{13}C	Carbon-13 atom
$^{n}J_{CH}$	n-bond carbon-proton coupling constant
$^{n}J_{CC}$	n-bond carbon-carbon coupling constant
$^{n}J_{HH}$	n-bond proton-proton coupling constant
δ	Chemical Shift
ϕ	Dihedral angle H_1-C_1-O_1-C_x in a glycosidic linkage
ϕ_1	Dihedral angle H_6-C_6-C_7-H_7 in the glycerol side chain
ϕ_2	Dihedral angle H_7-C_7-C_8-H_8 in the glycerol side chain
ϕ_3	Dihedral angle H_8-C_8-C_9-O_9 in the glycerol side chain
γ	Gyromagnetic ratio
$J(\omega)$	Spectral Density
k_{off}	Exchange off-rate
k_{on}	Exchange on-rate
K_D	Equilibrium dissociation constant
τ_c	Correlation time for molecular reorientation
τ_m	NOESY/ROESY mixing time
t_1	Acquisition time (1D NMR experiment); first evolution period (nD NMR experiment)
t_2	Acquisition time (2D NMR experiment); second evolution period (nD NMR experiment)
t_3	Acquisition time (3D NMR experiment)
T_1	Time constant of spin-lattice (longitudinal) relaxation
T_2	Time constant of spin-spin (transverse) relaxation)
ψ	Dihedral angle C_1-O_1-C_x-H_x in a glycosidic linkage

Chapter 1

Introduction

1.1 Biological Function of Carbohydrates

Until the late 1960's the biological role of carbohydrates was generally believed to be limited to energy storage and production, and as a structural material. That carbohydrates may play a role in cellular recognition and differentiation was first suggested by the discovery of the ABH blood group antigens, and the first evidence that carbohydrates can function as cellular receptors was the discovery that *N*-acetyl neuraminic acid (*see figure 1.1*) on the surface of erythrocytes is essential for the binding and entry of the influenza virus. Research over the last 30 years has expanded the range of biological processes in which carbohydrates play a pivotal role, for example, cell-cell recognition, toxin adhesion and invasion, immune evasion and activation, leukocyte extravasation, and the clearance of glycoproteins from the circulation by hepatic or reticuloendothelial cells (reviewed by Varki, 1993).

1.1.1 Carbohydrate Structure

In mammalian systems the oligosaccharides involved in cellular recognition are normally found as glycolipids, linked to either a ceramide tail, or as glycoproteins, covalently attached to the side chains of specific amino acids such as asparagine (Asn) via a nitrogen (*N*-linked), or serine (Ser) and threonine (Thr) via an oxygen (*O*-linked). The carbohydrate moieties of these glycoconjugates may range in size from 2 to 20 residues, and normally consist of neutral monosaccharides such as D-mannose (Man), D-glucose (Glc), and D-galactose (Gal); amino sugars such as *N*-acetyl-D-glucosamine, and *N*-acetyl-D-galactosamine; C-6 deoxy sugars for example L-fucose (Fuc); and the nine carbon atom sugars of the sialic acid family, of which *N*-acetyl neuraminic acid (Neu5Ac) is the most commonly found representative (Schauer, 1982) (for structures *see figure 1.1*).

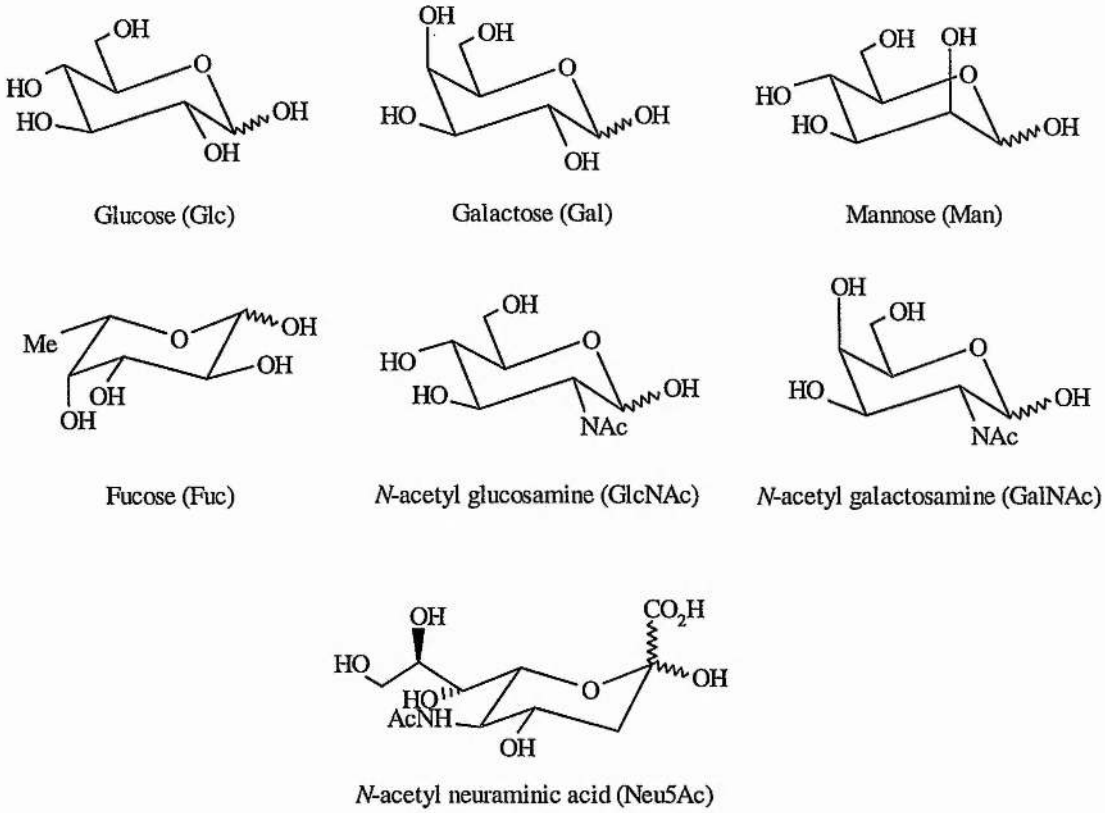

Figure 1.1 - Schematic representation of the most commonly found constituent monosaccharide units of glycoproteins and glycosphingolipids.

In contrast to nucleotides and amino acids in nucleic acids and proteins, respectively, which are only found in nature to link together in one way, the monosaccharide units in oligosaccharides are found to bond together in multiple ways to form a variety of differing structures from the same constituent sugars. Despite the potential complexity of oligosaccharide chains, glycosphingolipids and glycoprotein glycans commonly found in mammalian systems can be classified into a few distinct groups. Glycolipids may be arranged into the following sets (*figure 1.2*): "ganglio", "globo", "isoglobo", "lacto", and "neo-lacto" series.

Ganglio	
Galβ1-3GalNAcβ1-4Galβ1-4Glc-Cer	asialo-G_{M1}
Globo	
GalNAcβ1-3Galα1-4Galβ1-4Glc-Cer	globoside, Gb_4
Isoglobo	
GalNAcβ1-3Galα1-3Galβ1-4Glc-Cer	isogloboside
Lacto	
Galβ1-3GlcNAcβ1-3Galβ1-4Glc-Cer	lacto-*N*-tetraose
Neo-lacto	
Galβ1-4GlcNAcβ1-3Galβ1-4Glc-Cer	lacto-*N*-neotetraose

Figure 1.2 - Examples of the core structures of animal glycosphingolipids.

O-linked glycans are classified as belonging to one of six groups according to different core structures (*figure 1.3*). These cores can be elongated to form the backbone region by addition of galactose in β1-3 and β1-4 linkages, and *N*-acetylglucosamine in β1-3 and β1-6 linkages. Although the glycans are often linked to a serine or threonine residue via GalNAc, they may link through other residues such as fucose.

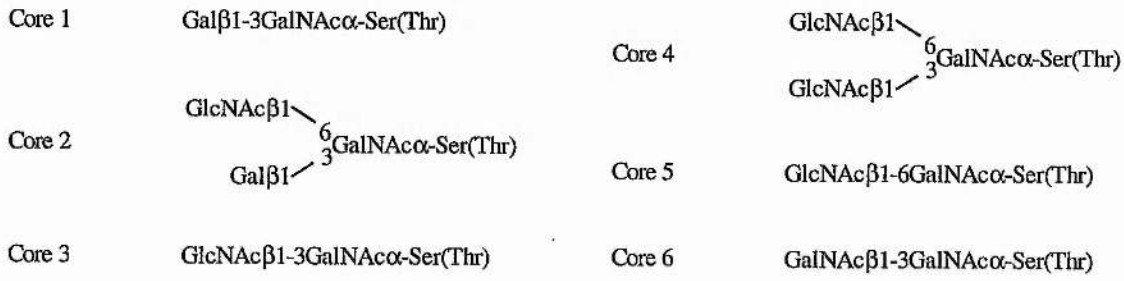

Figure 1.3 - Core structures found in *O*-linked glycans.

N-linked glycoprotein glycans fall into three broad families (*figure 1.4*): high mannose, complex, and hybrid type oligosaccharides. All *N*-linked oligosaccharides contain the pentasaccharide Manα1-6(Manα1-3)Manβ1-4GlcNAcβ1-4GlcNAc as a common core (the "trimannosyl core"). High mannose type sugars contain only α-mannosyl residues in addition to the trimannosyl core, complex type oligosaccharides contain no mannose residues other than those in the core, and the chains normally terminate with variations of the Neu5Acα2-3/6Galβ1-4GlcNAcβ1-R (where R = trimannosyl core), and hybrid type oligosaccharides have a combination of the complex and high mannose type characteristics.

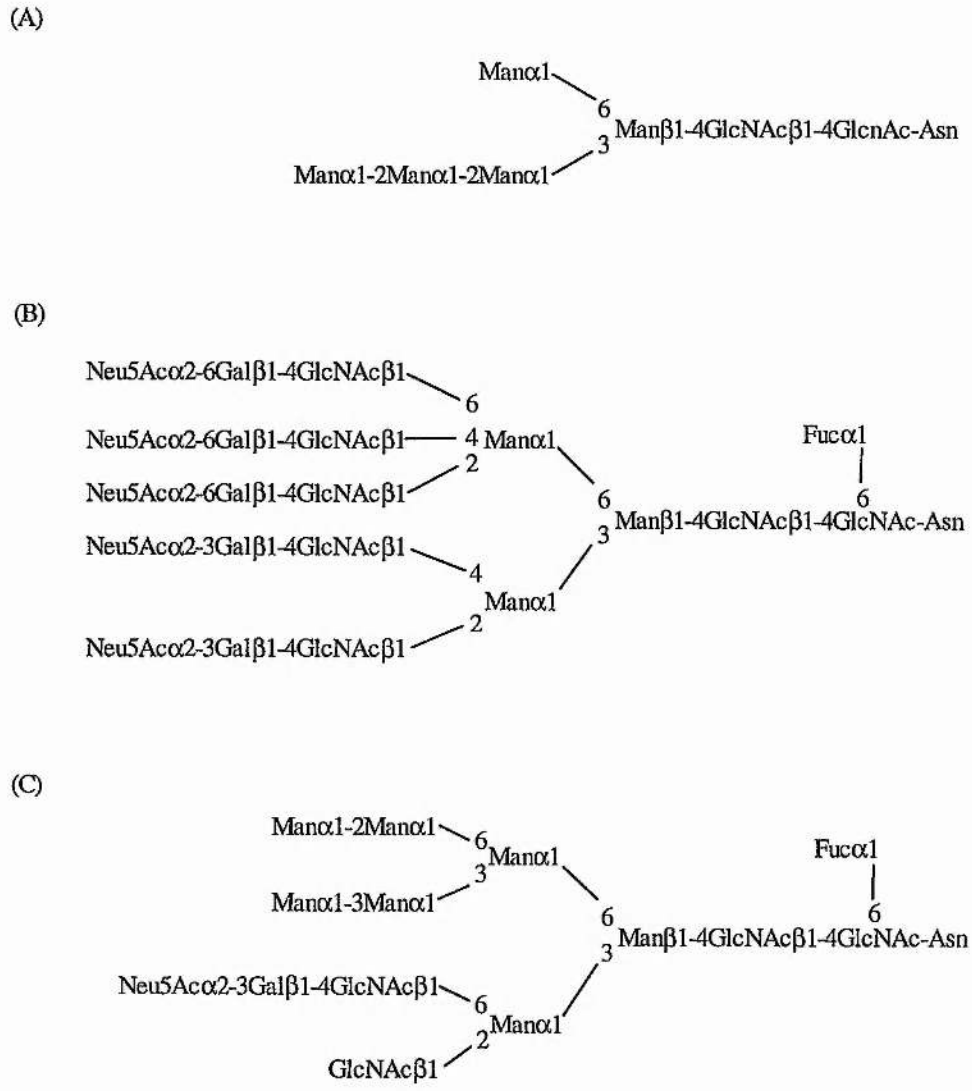

Figure 1.4 - Examples of the three major subgroups of *N*-linked sugar chains: (A) High Mannose type; (B) complex type; and (C) hybrid type.

1.1.2 Blood Group Antigens

Human blood group antigens are expressed on red blood cells, and at present over 200 antigens have been identified and assigned to 22 blood group systems (Daniels *et al.*, 1993). Of these the most well studied and characterised are the carbohydrate based blood group antigens, namely ABH, Lewis (Le), Ii, P-related, P_1, T and T_n (for recent reviews: Oriol *et al.*, 1986; Clausen and Hakomori, 1989; King, 1994; Greenwell, 1997), which may occur as either glycolipids or glycoproteins. For the purposes of this introduction only the structural characteristics of the ABH and Lewis blood group antigens will be discussed.

1.1.3.1 ABH and Lewis antigens

The ABO blood system, first to be identified, was discovered by Landsteiner in 1900 and remains the most important class of antigens for blood transfusion. By mixing the blood of different people, Landsteiner made the discovery that some combinations resulted in agglutination of the blood, whilst others did not. This subsequently lead to the suggestion that there were three blood group antigens, A, B, and O. The simplest way to demonstrate the presence of an antigen on erythrocytes is by testing whether they will be agglutinated by specific antibodies. Individuals who lack an antigen have, in their sera, natural antibodies that agglutinate cells carrying that antigen. So in the case of the ABO blood system, individuals of blood group A have anti-B antibodies, and those of blood group B have anti-A antibodies. Hence on mixing blood from two individuals from different blood groups will result in agglutination. In the 1940's it was first demonstrated that these antigens were not confined to the erythrocytes but were present in other cell type and in secretions (Hartmann, 1941), and so they are more appropriately termed 'histo-blood group antigens'.

Apart from antibodies, lectins may also be used to identify the antigens present as some are also blood group specific (Sharon and Lis, 1972). For example, the lectins of *Phaseolus limensis* (lime bean) and *Dolichos biflorus* are blood group A specific, whilst *Lotus tetragonolobus* and *Ulex europeus* are blood group O specific. Some of these lectins are still used in blood transfusion centres today.

The expression of these antigens on erythrocytes is controlled by allelic genes, with the A and B phenotypes controlled by the two allelic genes *A* and *B*, respectively. Contrary to earlier beliefs, there is evidence that there is no O gene product, and that the blood group

antigen on O cells, is a product of a different gene system, *Hh* (Watkins and Morgan, 1959). This conclusion is based upon the fact that individuals from blood groups A, B, and O often secrete a glycoprotein that inhibits the agglutination of O erythrocytes by anti-O reagents. Hence this glycoprotein is now called an H substance.

The nature of the relationship between the A, B, and H antigens became apparent when the structures were determined (*figure 1.5*), and found to be of carbohydrate structure (reviewed by Sharon and Lis, 1972). The H antigen is the precursor to both A and B antigens. The only difference between these is the terminal sugar residue, where GalNAc and Gal are the immunodominant sugars for A and B antigens, respectively. The H disaccharide may be synthesised on four main acceptor sequences, depending upon the source of the blood group substances (Clausen and Hakomori, 1989). Type 2 based ABH oligosaccharides are the major species in erythrocytes, glycoproteins, and glycolipids (reviewed by Hakomori, 1982), whilst type 1 and 3 glycolipids have been isolated as minor components (Breimer *et al.*, 1988; Clausen *et al.*, 1985). Type 1 is found mostly in milk oligosaccharides, and secreted glycoproteins. Type 3 is found in glycoconjugates of epithelial cells in the gut and lungs. Type 4 is associated with glycolipids particularly those found in the human kidney.

Type	Structure
1	Galβ1-3GlcNAcβ-R
2	Galβ1-4GlcNAcβ-R
3	Galβ1-3GalNAcβ-R
4	Galβ1-4GalNAcβ-R

H determinant: Galβ-(type 1 to 4 chain)
2
|
Fucα1

A determinant: GalNAcα1-3Galβ-(type 1 to 4 chain)
2
|
Fucα1

B determinant: Galα1-3Galβ-(type 1 to 4 chain)
2
|
Fucα1

Figure 1.5 - Acceptors for the synthesis of, and structures of the ABH determinants.

The Lewis blood group antigens are named after the first patient in which they were identified, (Mourant, 1946). There are six currently identified Lewis blood group antigens, namely Lewis^a, Lewis^b, Lewis^c, Lewis^d, Lewis^x, and Lewis^y (for structures *see figure 1.6*).

The Lewis[a] antigen is formed from the precursor of the H antigen. The Lewis[b] antigen is a hybrid structure of both H and Lewis[a] antigens and requires the glycosyltransferases involved in the production of both H and Lewis[a] antigens to be present.

The structures of the Lewis[a] and Lewis[b] antigens are based upon the type 1 chain, whilst Lewis[x] and Lewis[y] antigens are based upon the type 2 chain and are therefore regarded as their structural isomers.

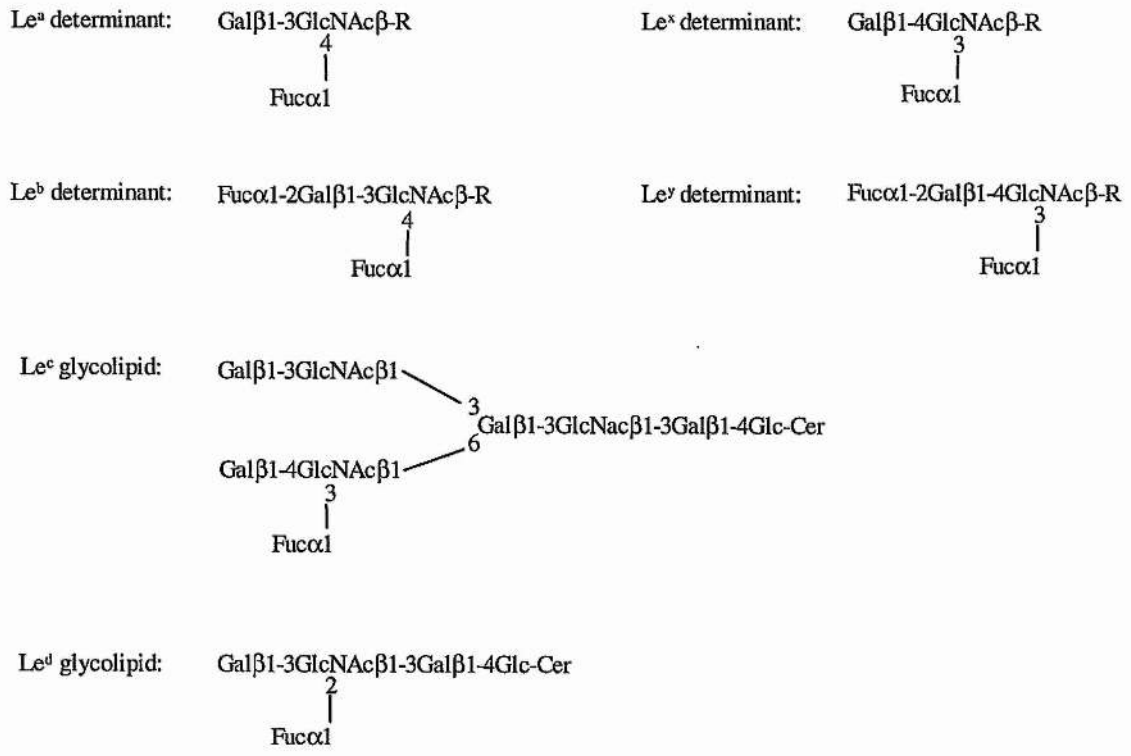

Figure 1.6 - Determinants of the Lewis[a], Lewis[b], Lewis[c], Lewis[d], Lewis[x], and Lewis[y] antigens.

1.1.3 Carbohydrates in disease

1.1.3.1 Oncology

Increased cellular glycosylation is a common change in malignancy, with altered glycosylation a unifying feature of cancer cells (Kim and Varki, 1997). De-differentiation of normal cells leads to cancerous growth and certain malignant cells exhibit glycolipid surface antigens resembling those occurring during early embryonysis, and are often termed oncodevelopmental (or oncofoetal) associated antigens (Hakomori, 1985). For example in foetal colon, blood group ABH and Lewis^b antigens are expressed during carcinomas of the colon, but are not usually expressed in the adult colon (Lloyd, 1987). Therefore, antibodies to these antigens can be used as markers in tumour diagnosis (reviewed by King, 1994).

The sialylated form of Lewis^x (sialyl Lewis^x) has been identified on carcinoma cells and a correlation between the metastatic potential of colon carcinoma cell lines in mice and the expression of this antigen has been demonstrated. The recognition of sialyl Lewis^x by a group of proteins, which allows leukocytes to migrate to areas of inflamed tissue (for discussion see section 1.1.4), is used by the carcinoma cells to facilitate evasion of the host's immune system.

1.1.3.2 Bacterial Infection

Some bacteria bind to epithelial cells by means of carbohydrate-protein interactions. Examples include the preferential binding of *Helicobacter pylori* to the surface of gastric epithelial cells in the stomach using Lewis^b antigen as its receptor; Cholera toxin an A-B toxin produced by *Vibrio cholerae*, uses the B-subunit to bind the glycosphingolipid GM_1, enabling the A subunit to enter the cell and activate cAMP production; and the influenza virus recognises and binds to glycoconjugates on cell surfaces through one of its surface proteins, haemagglutinin (reviewed in Edge, 1994).

1.1.4 Inflammation

It has been long recognised that the earliest cellular response to inflammatory stimuli or tissue damage is the rolling of leukocytes along the vessel wall near the sites of injury (Atherton and Born, 1972). This rolling behaviour, which is essential for the subsequent arrest and transmigration of the leukocytes through the endothelial cell wall (*figure 1.7*), is mediated principally by a group of three lectins, called the selectins (for recent reviews see Tedder, 1995b; Kansas, 1996; McEver, 1997). All three selectins have been shown to directly and independently mediate rolling *in vitro* and *in vivo* (Abbassi *et al.*, 1991; Lawrence and Springer, 1991; Ley *et al.*, 1991; Dore *et al.*, 1992; Abbassi *et al.*, 1993; Lawrence and Springer, 1993; Alon *et al.*, 1994; Jones *et al.*, 1994; Kubes and Kanwar, 1994; Ley *et al.*, 1995a; Luscinskas *et al.*, 1995). However, owing to the different mechanisms of expression (see later), selectins act at different times during the course of inflammatory response.

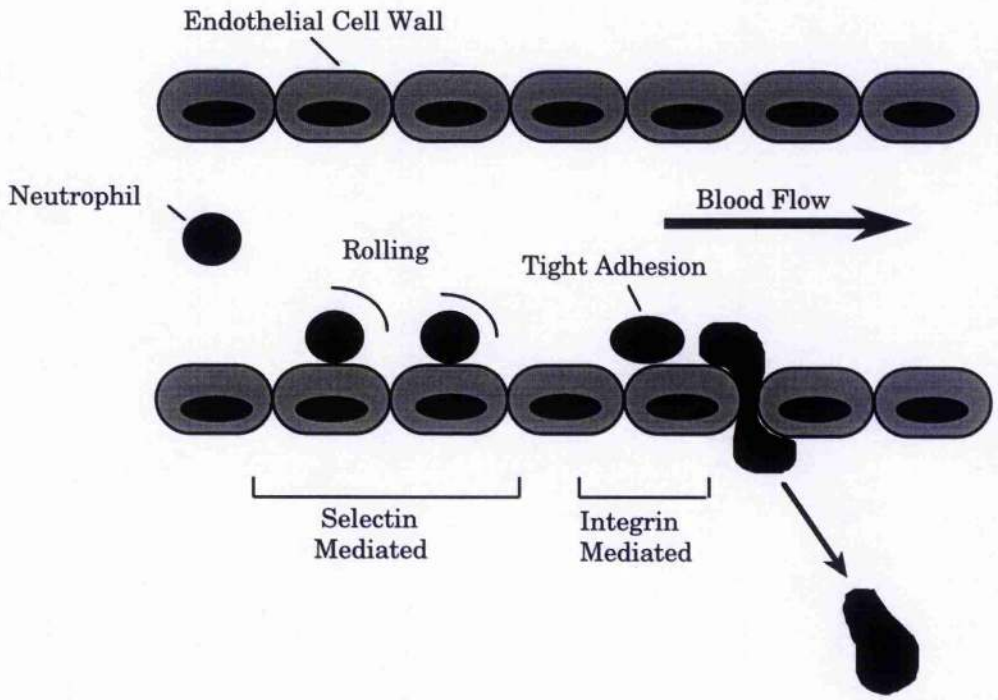

Figure 1.7 - A cartoon representation of diapedesis. Neutrophil entry into tissues is preceded by the initial tethering or capture of the neutrophils and subsequent rolling along the endothelial cell wall, both processes are mediated by the selectins. During rolling the leukocytes can interact with locally produced inflammatory mediators and chemokines which allow tight binding to occur (mediated by the integrins and immunoglobulin superfamily), followed by transmigration through the cell wall to the area of tissue injury.

The earliest response to inflammatory stimuli, within 20 minutes after induction, is predominately mediated by P-selectin (Ley *et al.*, 1993; Ley *et al.*, 1995a; Ley *et al.*, 1995b; Dore *et al.*, 1992; Nolte *et al.*, 1994; Mayadas *et al.*, 1993). Subsequently, the levels of P-selectin activity decrease, whilst rolling after 20 minutes is principally mediated by L-selectin. It is only after two hours that E-selectin plays a part in the rolling phenomena, although both L-selectin and P-selectin also appear to have a role in the later periods in inflammatory response.

One important aspect of the selectin function is the ability of cooperativity, especially on populations of leukocytes that can potentially use more than one selectin simultaneously (Ley and Tedder, 1995). For example, comparison of spontaneous rolling flux in normal (wild type) mice against mice deficient in L- or P-selectin show that there is a higher flux of rolling at nearly all times for the wild type as compared to the combination of both deficient mice (Ley *et al.*, 1995a). Therefore, interaction of neutrophils with endothelium is more efficient when more than one selectin is present. This can be explained in terms of the differences in the characteristic rolling velocities that each selectin can sustain. L-selectin supports the greatest rolling velocities, between 50 to 150 μms^{-1}, whilst P-selectin mediates slower rolling, between 20 to 50 μms^{-1}, and E-selectin the slowest of all, between 3 to 10 μms^{-1} (Ley *et al.*, 1993; Kunkel *et al.*, 1995; Jung *et al.*, 1996; Kunkel *et al.*, 1996). This therefore suggests that L-selectin is involved in the initial capture or tethering of the leukocytes which is likely to then facilitate and enhance slower rolling mediated by E- or P-selectin. Consistent with this proposal is evidence where spontaneous rolling occurs at the lower rolling velocity of P-selectin in normal mice even though both L- and P-selectin are present (Ley *et al.*, 1995a).

Another factor important in the rolling phenomenon, is that of "tensile strength" (Alon *et al.*, 1995), which is the resistance of the selectin interaction to break down on increasing the applied force. Without tensile strength the rolling phenomenon would not occur because the selectin-ligand interaction would have vanishingly short lifetimes, lower than the minimum required to maintain rolling. This factor may be important in distinguishing the selectins from other molecules which have similar rates of interaction but cannot mediate rolling (Alon *et al.*, 1995).

The generation of mice lacking one or more of the selectins (Mayadas *et al.*, 1993; Arbones *et al.*, 1994; Labow *et al.*, 1994) has provided further insight into the recruitment of leukocytes and the roles of the selectins. In mice deficient of both E- and P-selectin (Bullard *et al.*, 1996), the recruitment of neutrophils is completely absent during early time points, which suggests that whilst L-selectin can capture the neutrophils it is incapable of efficiently arresting the neutrophils and allowing transmigration. However, recruitment of neutrophils to the peritoneum after 24 hours is at normal levels, and leukocytes can be also be found in the dermis, suggesting that additional L-selectin dependent pathways are active. To summarise the findings on knockout mice, L-selectin deficient mice show defects in leukocyte recruitment up to 48 hours after initiation (Tedder *et al.*, 1995a), whilst P-selectin knockout mice show partial defects at early stages in the inflammatory response but not during late stage (Mayadas *et al.*, 1993), and no significant defects can be found in E-selectin knockout mice (Labow *et al.*, 1994). In the E- and P-selectin knockout mice there are near total defects in the early stages but recruitment appears to be normal after 24 hours. Hence cooperativity is important for effective leukocyte recruitment during inflammation, but functions of individual selectins are distinguishable and not completely essential, in all settings of chronic inflammation.

This same mechanism which recruits leukocytes to areas of inflamed tissue can ultimately lead to the over recruitment, resulting in swelling and tissue damage. Diseases, such as rheumatoid arthritis, are the product of such up-regulated accumulation of leukocytes to healthy tissue, and in cases where the blood supply to tissues is removed, such as in heart attacks or during surgery, subsequent resumption of the blood flow often results in leukocytes destroying tissues damaged by lack of oxygen leading to necrosis. Therefore, the selectin - ligand interaction is a possible target for therapeutic intervention, but an understanding of the three dimensional structure of, and the ligands for the selectins is needed.

1.2 Selectins

1.2.1 Structure

The selectins are a group of three proteins which enable adhesion between the endothelial cell wall and leukocytes, and although they have had a wide selection of names, are now referred to as E(endothelial)-, P(platelet)-, and L(leukocyte)-selectin. They are multi-domain proteins, with a unique overall structure (*figure 1.8A*). The primary sequence shows highly conserved regions in the lectin and EGF domains (~65%), and very high conservation between different mammalian species. The lectin domain is essential for binding carbohydrates, and is homologous to others found in mammalian proteins which require Ca^{2+} to bind carbohydrates. The EGF domain influences the lectin's ability to mediate cell binding, possibly through stabilising the protein. Although, the crystal structure of the lectin and EGF domains of E-selectin (Graves *et al.*, 1994) showed that these were distinct domains with little apparent association (*figure 1.8B*).

The complement regulatory domains (CRDs) although not essential for binding, have been reported to facilitate lectin activity, possibly by contributing to the conformational stabilisation or to the orientation of the protein within the membrane. The number of CRDs is dependent upon the selectin and mammalian system; for humans E-selectin has six CRDs, P-selectin has nine; and L-selectin has two. The CRDs also may also have a function in mediating receptor oligomerisation. The number of CRDs is thought to extend the lectin and EGF domains the appropriate distance away from the membrane for optimal ligand binding.

The cytoplasmic tail is believed to have a different function for each of the selectins, for example, in L-selectin the tail is believed to regulate the affinity of the protein, and modulate cell-cell binding, whilst in P-selectin, it directs the protein to storage in platelet granules by an, as yet, undefined sorting signal.

(A)

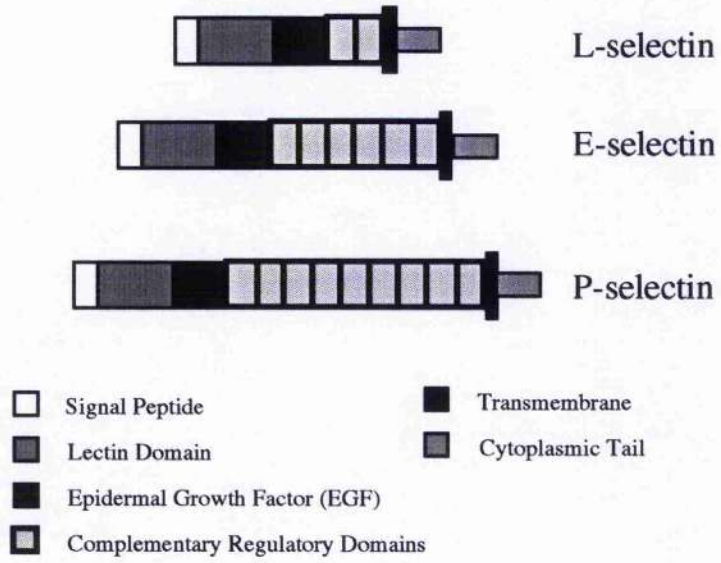

(B)

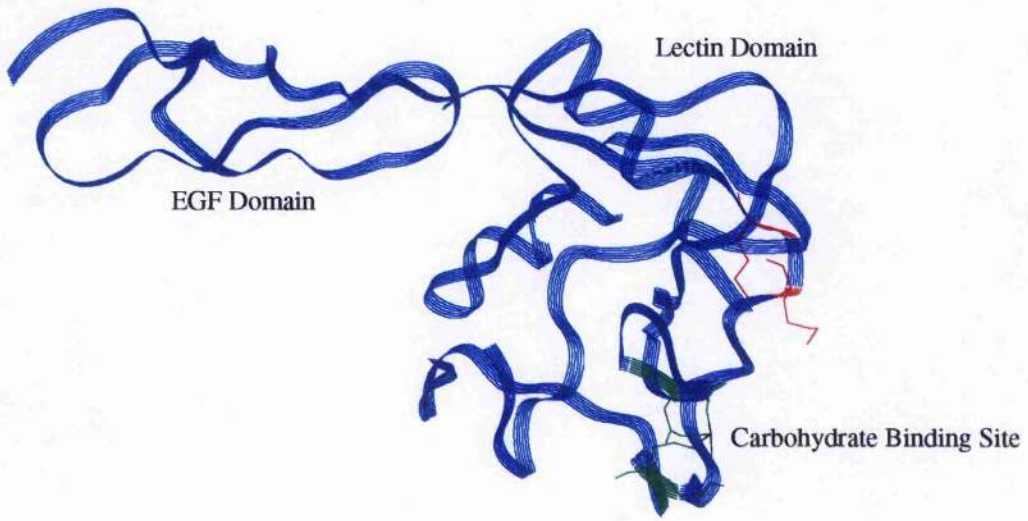

Figure 1.8 - (A) A schematic representation of the overall structure of the selectins, and (B) a ribbon representation of the lectin and EGF domains derived from the x-ray crystal structure (Graves *et al.*, 1994) with the amino acids involved in the calcium binding site and those involved in recognition of sialyl Lewis^x highlighted.

Although the selectins have similarities with C-type lectins (such as the requirement for a calcium ion for binding, the high conservation of amino acids in the CRDs between selectins and lectins, and the possibility of mutating a small number of amino acids in the mannose binding protein (MBP) lectin domain to confer E-selectin binding activity) they also exhibit significant differences. The selectins only require a single Ca^{2+} ion for binding whereas MBP is known to require two ions for binding. Selectins have only a single carbohydrate binding domain per whole protein, whilst other known C-type lectins, except proteoglycan C-type lectin, have multiple carbohydrate binding domains per protein. The transmembrane orientation of the selectins is type I which is similar to the macrophage mannose receptor, but other C-type lectins exhibit type II. Finally, the selectins are unique in that they have all three lectin, EGF, and CRD domains together, unlike all other lectins, and hence the spatial arrangement of these domains may be important in the receptor function.

1.2.2 Expression

1.2.2.1 E-Selectin

Previously known as Endothelial Leukocyte Adhesion Molecule 1 (ELAM-1), E-selectin or CD62E is a 95-115 kDa glycoprotein which is expressed on the surface of endothelial cells. Its expression occurs via *de novo* protein synthesis, and is induced by the activation of the endothelium by certain cytokines, including interleukin 1 (IL-1), and tumour necrosis factor (TNF) (Bevilacqua *et al.*, 1987). Maximum levels of E-selectin are found at the cell surface 3 - 6 hours after activation with cytokines, but this declines back to basal levels after 24 hours by shedding from the cell surface even in the constant presence of cytokines. The loss of E-selectin from activated endothelial cells is due to the down-regulation of transcription within 6 to 9 hours of induction (Bevilacqua *et al.*, 1989) and the rapid degradation in lysosomes (von Asmuth *et al.*, 1992; Smeets *et al.*, 1993; Subramanian *et al.*, 1993). Increased amounts of E-selectin in the serum of patients is indicative of various inflammatory syndromes (Gearing and Newman, 1994), for example patients with septic shock.

1.2.2.3 P-Selectin

P-Selectin or CD62P (previously known as PADGEM, or GMP-140), is a 140 kDa glycoprotein and unlike E-selectin is preformed and stored in secretory granules of platelets and endothelial cells (Hsu-Lin *et al.*, 1984; McEver *et al.*, 1989). Its rapid expression at the cell surface by the process of degranulation, occurs within minutes after stimulation of the endothelial cells by either histamine or thrombin, and is also expressed later on in the course of inflammatory response by gene induction by TNF-α, lipopolysaccharides (LPS), or IL-1, leading to expression between 2 and 4 hours after induction.. The cytoplasmic tail has multiple motifs (though these are not completely defined) and this dynamic pattern may be important in the regulation of the expression of P-selectin at the surface (Kansas, 1996). The exact role of acylation and phosphorylation of certain amino acids in the tail is still unclear (Fujimoto and McEver, 1993), however, the cytoplasmic tail is implicated in a number of important regulatory functions. First, the sorting of P-selectin into granules is controlled by sequences in the cytoplasmic tail which interacts with the sorting machinery in cells that have the regulated sorting pathway (Disdier *et al.*, 1992). Second, the transient expression on the surface of endothelial cells is due to the rapid internalisation (McEver *et al.*, 1989) and followed by lysosome degradation which is regulated by amino acids within the cytoplasmic tail (Green *et al.*, 1994).

1.2.2.3 L-Selectin

L-Selectin, CD62L, or 'the homing receptor', is a 90-100 kDa glycoprotein which is expressed on all types of leukocytes (Gallatin *et al.*, 1993; Tedder *et al.*, 1990). This broad expression is required for L-selectin to be involved in the recirculation of lymphocytes, and the adhesion of leukocytes to the endothelium. L-selectin is shed from the surface of leukocytes after stimulation with cytokines or phorbol esters, by the induction of a conformational change exposing nascent epitopes near the membrane which are vulnerable to proteolytic cleavage (Chen *et al.*, 1995). High levels of L-selectin are found in the serum of patients with AIDS or leukaemia, but decreased levels in people suffering from adult respiratory distress syndrome. Although currently not understood, a possible reason for this shedding may be that soluble L-selectin acts as a buffer to prevent leukocyte rolling at sites of subacute inflammation (Tedder *et al.*, 1995b).

1.2.3 Additional Selectin Functions

Apart from the function of leukocyte rolling, the selectins have also been implicated in a number of other biologically important functions. For a normal immune response the circulation of mature T and B lymphocytes throughout the secondary lymphoid organs is required as it ensures that a full complement of antigen receptors are exposed to the full range of antigens present in the system. Entry to these secondary lymphoid organs by lymphocytes occurs across specialised endothelial cells, known as high endothelial venules (HEV) (Picker and Butcher, 1992), and L-selectin is the principal if not sole HEV receptor for lymphocyte traffic to the lymph nodes (Kansas, 1996). Additionally L-selectin may play a role in interactions between leukocytes, and in particular neutrophils, which may be important in the amplification of the inflammatory response. It has been noted that neutrophils can roll on other neutrophils and that this is blocked by monoclonal antibodies to L-selectin (Bargatze *et al.*, 1994). Neutrophil aggregation can also be blocked by a monoclonal antibody to L-selectin or carbohydrates that inhibit L-selectin activity (reviewed by Kansas, 1996).

The fact that P-selectin is found on platelets suggests a role in platelet-leukocyte interactions during wound healing and hemostasis, which could amplify the recruitment to sites of vascular injury (Larsen *et al.*, 1989). P-selectin is known to mediate platelet binding to monocytes which in turn induces tissue factor, thereby activating the blood coaggulation cascade (Celi *et al.*, 1994). E-selectin has been implicated as a tissue specific homing receptor for leukocyte recruitment specifically to the skin, particularly in the case of memory T cells (Picker *et al.*, 1991).

In summary, although the selectins are involved in the recruitment of leukocytes to areas of inflamed tissue, it is apparent that their role is not limited to this alone and each selectin may have a more specialised function within the immune response.

1.2.4 Carbohydrate Ligands

The identification of the physiological ligands for the selectins is complicated because, like most lectins, they bind to a wide variety of carbohydrate epitopes *in vivo*. The dependence of the selectins upon a carbohydrate ligand was illustrated in two patients with leukocyte adhesion deficiency type II disease, which is an inherited inability to recruit neutrophils to the sites of inflammation (Harlan, 1993). This inability to generate the ligands required for selectin mediated rolling is attributed to a defect in the fucose metabolism, and they are, therefore, unable to synthesise fucosylated carbohydrates. The observation that cell adhesion is sensitive to neuraminidase, indicates that fucose and sialic acid residues are essential for selectin binding, and a prototype carbohydrate ligand, sialyl Lewis^x, Neu5Acα2-3Galβ1-4[Fucα1-3]GlcNAc, was proposed as the minimal required structure (*figure 1.9*).

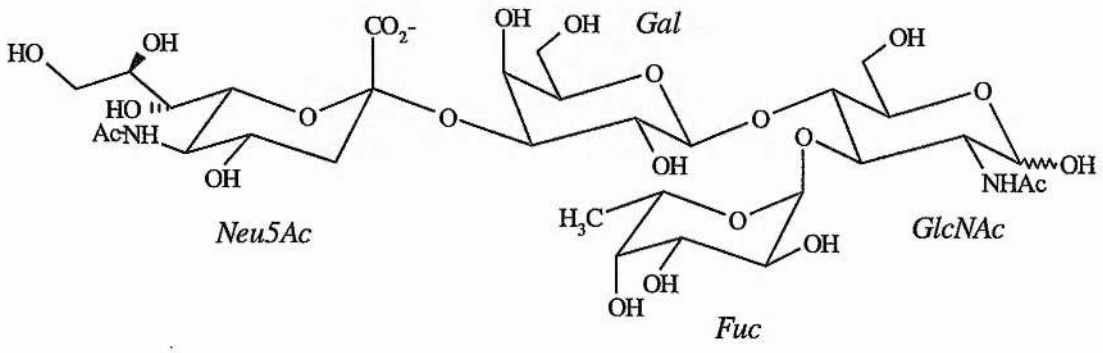

Figure 1.9 - Schematic representation of the sialyl Lewis^x antigen, the minimal ligand proposed for selectin binding.

All three selectins can bind to sialyl Lewis^x, although with varying affinities, but they also bind with higher affinity to carbohydrate determinant on a limited number of glycoproteins or proteoglycans (reviewed by Rosen and Bertozzi, 1994). Therefore, a distinction must be made between structures which can interact with the selectins under certain conditions *in vitro*, and those structures which do interact under physiological conditions *in vivo*. Hence, the simple tetrasaccharides originally proposed as ligands and which may contribute to the biologically active ligand, may be thought as markers for construction of the biological relevant ligands.

1.2.5 Glycoprotein Ligands

Purified forms of the selectins or IgG fusion proteins exhibit a higher level of specificity in comparison to monoclonal antibodies against their putative ligands. This suggests that the selectins recognise not just a simple oligosaccharide, but a three dimensional surface composed of several carbohydrate moieties contributed by several molecular species attached to a specific glycoprotein.

Mouse L-selectin binds to at least three heavily glycosylated mucin-like proteins in vivo, namely GLYCAM-1, CD34, and MAdCAM-1. Each glycoprotein bears sulfated, sialylated, and fucosylated *O*-linked oligosaccharide chains that appear essential for L-selectin binding (reviewed by Kansas, 1996). Although first reported to be the ligand for L-selectin, and thought to be constitutively expressed on peripheral lymph node HEV, GLYCAM-1 contains no apparent transmembrane region, and it appears that it is predominately released into circulation where it competitively inhibits, rather than promotes, L-selectin mediated attachment (Tedder *et al.*, 1995b).

The second glycoprotein, a glycoform of CD34, is constitutively expressed on most endothelial and hematopoietic stem cells, and therefore has been proposed to regulate tissue specific selectin binding because of the tissue-specific glycosylation of CD34. In mice it is universally expressed on the endothelium both during mouse development and in the mature animal, so it is perfectly placed as a ligand for L-selectin. In CD34 knockout mice normal levels of rolling and lymphocyte homing is observed, and in purified human tonsil, CD34 accounts for approximately half of the L-selectin activity. Therefore, the third ligand, MAdCAM-1, may constitute the principal adhesive ligand(s) for L-selectin, although it has yet to be identified at the molecular level. Interestingly, in knockout mice of both CD34 and GLYCAM-1, an up-regulation of this third ligand is seen, indicating the evolution of dynamic mechanisms to maintain adequate levels of lymphocyte traffic and recirculation.

The *O*-linked carbohydrates of GLYCAM-1 have been characterised (Hemmerich *et al.*, 1995), and two of the more prominent structures obtained from β-elimination are novel sulfated derivatives of the sialyl Lewis^x motif; 6'-sulfo-sialyl Lewis^x, where the sulfate group is at the 6 position of the galactose residue; and 6-sulfo-sialyl Lewis^x, where the 6 position of the GlcNAc residue is sulfated, and both of these moieties are contained within the core-2 *O*-

linked glycans, *i.e.*, Galβ1-3[GlcNAcβ1-6]GalNAc. These ligands provide all the requirements for L-selectins ligands, but whether these are the actual recognition motifs, or whether CD34 or MAdCAM-1 contain these or different oligosaccharides structures is as yet unknown.

The P Selectin Glycoprotein Ligand -1 (PSGL-1) is a disulfide linked homo-dimer of two identical ~120kDa type I mucin-like proteins which have a unique structure (Moore *et al.*, 1992). This glycoprotein is expressed by all blood neutrophils, monocytes, and lymphocytes but requires specific glycosylation for its function. Studies on the P-selectin - PSGL-1 binding have provided the first direct evidence that leukocyte rolling under physiological shear forces requires the specific interaction of a selectin with a single cell-surface glycoprotein. A specific anti-PSGL-1 monoclonal antibody completely inhibits P-selectin mediated rolling of leukocytes (Moore *et al.*, 1995). PSGL-1 is mainly *O*-linked glycosylated, although it has two or three *N*-linked sugars which do not appear to be necessary for binding, with extensive branched chain polylactosamine glycans, which contain fucose and sialic acid and many terminate in the sialyl Lewis^x motif (Moore *et al.*, 1994). The structure of these glycans has been characterised (Wilkins *et al.*, 1996) and contain *N*-acetyllactosamine, sialylα2,3-*N*-acetylactosmine, Lewis^x, and sialyl Lewis^x motifs in differing quantities (*figure 1.10*).

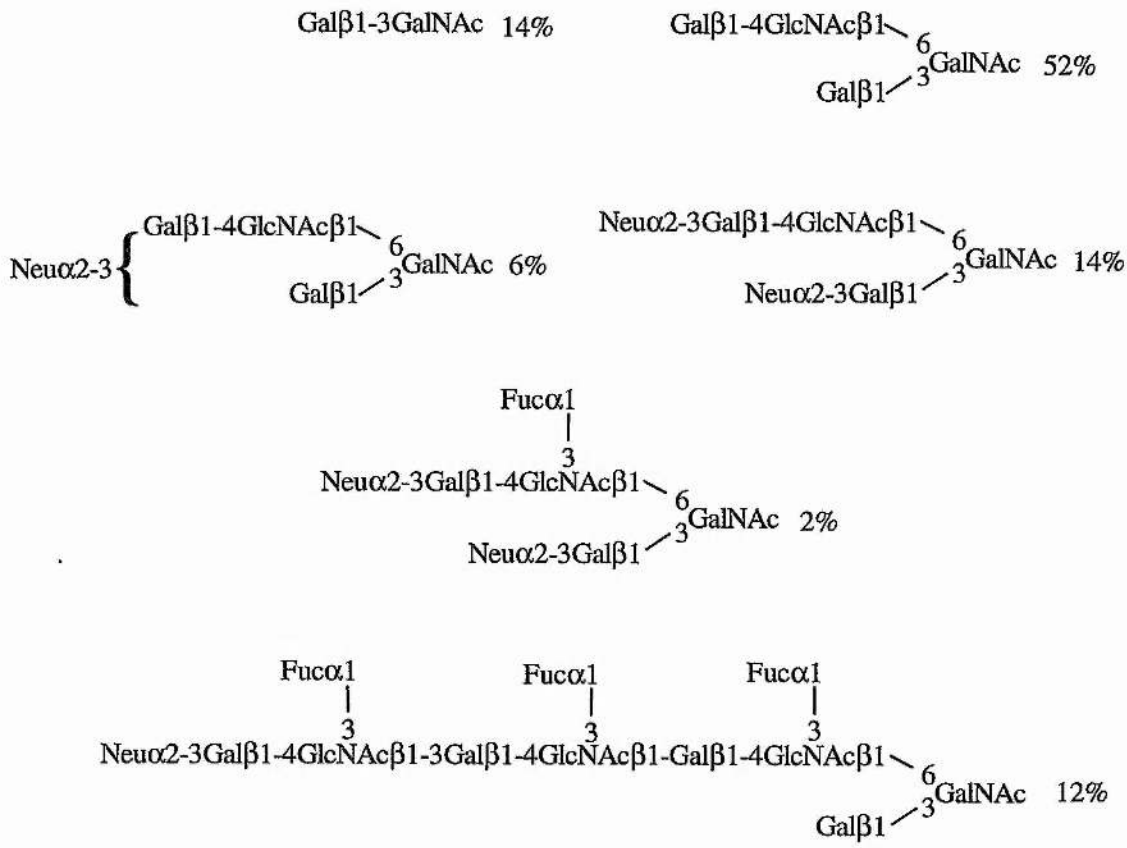

Figure 1.10 - Structures and percentages of the *O*-glycans in PSGL-1 (from Wilkins *et al.*, 1996)

1.3 Carbohydrate Therapeutics

With the diverse role that oligosaccharides play in biological functions it is apparent that the prevention of carbohydrate recognition may have potentially important therapeutic benefits. The selectin - carbohydrate ligand interaction has been targeted for possible therapeutic intervention because of the over recruitment of leukocytes, resulting in tissue damage and swelling. In fact, at present several companies are testing sialyl Lewis^x antigen in clinical trials for reperfusion injury, and there are currently some fifteen carbohydrate drugs undergoing clinical trials for ailments including cancer, diarrhoea, thrombosis, diabetes, ulcers, epilepsy, and Parkinson's disease (reviewed by McAuliffe and Hindsgaul, 1997). Carbohydrate based drugs may also have added benefits such as low toxicity and immunogenicity. In the treatment of microbial infections, carbohydrate-based drugs only prevent the adhesion of microbes, thus there is less evolutionary pressure for mutation,

reducing the likelihood of resistance. The mode of action of these carbohydrate drugs is varied:

1. Inhibition of protein attachment

The most common approach is to design a drug based upon the natural carbohydrate receptor which would bind irreversibly and competitively with the natural substrate, thus preventing cellular adhesion. This method is the current approach for mimics to the sialyl Lewis^x - selectin interaction for the treatment of reperfusion injury, where the accumulation of leukocytes in tissues after heart attack and surgery can lead to tissue damage. The clearance of bacteria and their toxins from the gastrointestinal tract with oligosaccharides is used in nature. The high levels of oligosaccharides present in mammalian milk, often found on the surface of the gut, is believed to protect infants from infection. Mimics of this process include the development of a Gb_3 conjugate linked to an insoluble powder to prevent verotoxin adhesion.

2. Alteration of carbohydrate biosynthesis

Many diseases are associated with defects in oligosaccharide metabolism, such as diabetes. Azasugars (nitrogen analogous of carbohydrates) are believed to be a possible treatment by inhibiting sucrase and amylase, responsible for the breakdown of polysaccharides in the gut, and therefore prevent the adsorption of glucose into the bloodstream. Inhibition of the catabolism of Neu5Ac terminating oligosaccharides has been successfully used in the treatment of influenza (von Itzstein *et al.*, 1993).

3. Eliciting an immune response

Cells undergoing oncogenesis often express a different range of glycoproteins due to defects in the sugar metabolic pathways with higher densities of smaller gangliosides present at the expense of more complex gangliosides (reviewed by Oettgen, 1989). The treatment of cancer patients by stimulating anti-ganglioside antibodies has had some limited success (Livingston *et al.*, 1987). The present treatment consists of injecting patients with a glycopeptide hapten found on the surface of these cancer cell lines which elicits an immune response against these cells. This treatment is being applied successfully to the treatment of lung, breast, colon, and ovarian cancers.

1.3.1 Rational Drug Design

A prerequisite for the rational design of drugs is a detailed understanding of the interaction of a carbohydrate with its receptor. A high resolution three dimensional structure of the complex is required, and several crystallographic studies have been described recently which illustrate in detail the precise nature of certain carbohydrate-protein interactions. The most celebrated example of model based drug design was the work performed in von Itzstein's laboratory on the development of an influenza sialidase inhibitor (von Itzstein *et al.*, 1993). Sialidase is critical in the release of newly synthesised influenza virions from infected cells by the cleavage of terminal Neu5Ac residues from host cell-surface glycans. Inhibition of this enzyme limits the establishment and progression of infection. Computer-aided molecular modelling was used to analyse the active site and predict the functional group changes which would increase the binding affinity of the sialic acid residue. Modelling studies predicted that the substitution of the 4-OH group with an amino or guanidynl group would produce an increase in overall binding. Results show that the 4-guanidino derivative has an inhibition constant, for various strains of influenza, in the 10^{-10} range. Additionally the affinity of this compound against human sialidases is a million times lower, therefore offering excellent selectivity for virus sialidases.

Detailed x-ray crystal structures of biologically important oligosaccharide complexes are rare, as the relatively flexible oligosaccharide often results in poor electron densities for the carbohydrate residues, and when observed they are often stabilised by crystal packing forces which may orient the sugar in an unnatural conformation. Many lectins only weakly bind isolated oligosaccharide analogues of their receptor glycans, and so may not be co-crystallised (Stein *et al.*, 1992). An additional problem is that carbohydrate binding sites in the well ordered solid state may not be active in the less well ordered solution state (*c.f.* Wright, 1992, with Wright and Kellog, 1996, and reviewed by Rossi, 1992).

In contrast, high resolution structural studies of glycan protein interactions by nuclear magnetic resonance spectroscopy can offer complimentary information on the structure of the carbohydrate in sugar-protein interactions. Solution studies also have an important potential advantages since a comparison of the solution structure of the free and bound conformations of the ligand is more meaningful, and moreover, the dynamics of the system are accessible.

1.4 NMR Spectroscopy

The nuclear magnetic resonance phenomenon, first observed in 1946, has become a widespread tool for the non-destructive analysis of both organic and inorganic compounds. NMR techniques can provide information on structure, conformation, and internal mobility. Comprehensive introductions include Sanders and Hunter (1987), and Derome (1987).

The fundamental basis of the NMR experiment is perturbation by a radio-frequency pulse of the equilibrium bulk magnetisation from an axis parallel to the external static magnetic field, B_0, into a vector perpendicular to this axis. The individual spins precess around this plane at a characteristic (Larmor) frequency (ω), which is dependent upon the shielding of the nucleus from the external field by nearby electron-inductive groups:

$$\omega=\gamma B_0 \qquad [1.1]$$

Once perturbed from its equilibrium position the magnetisation can be detected as an oscillating current in a coil orthogonal to the B_0 field. The detected signal, known as the Free Induction Decay (FID), is a function of time, which upon Fourier transformation is converted into a domain of the frequencies at which the nuclei are precessing.

1.4.1 Conformational Analysis

NMR can be used to study the conformation of oligosaccharides in free solution by the measurement of three parameters:

(a) Relaxation Properties (NOE, T_1, T_2)

(b) Spin-spin coupling constants (J)

(c) Conformation and structure dependent chemical shifts

and the conformation of oligosaccharides in complex proteins may be determined from:

(d) Line-shape analysis

(e) Transferred NOE

Detailed explanations of NMR relaxation phenomena are given by Noggle and Schirmer (1971), and Neuhaus and Williamson (1989), and analysis of the transferred NOE are given by Ni, (Ni, 1994, Ni and Scheraga 1994) and Clore and Gronenborn (1982; 1983).

After the application of a pulse or other perturbation, nuclei relax back to equilibrium by one of two mechanisms. Longitudinal relaxation (T_1) causes the population difference between two spin states of a given nucleus to return exponentially to equilibrium, due to transfer of energy to the surroundings or 'lattice'. In terms of the classical formalism, bulk magnetisation in the x-y plane returns to the +z axis. The second mechanism, spin-spin relaxation (T_2) causes a loss of phase coherence in the x-y plane due to mutual exchange of spin energy and resultant decay in the bulk intensity of transverse vectors (Bloch model).

Both mechanisms of relaxation are due to time-dependent magnetic or electric fields derived from random thermal motions within the sample. For both ^1H and ^{13}C nuclei, the major sources of such fields are the magnetic moments of neighbouring protons, and the intensity is termed the spectral density function, $J(\omega)$. Relaxation is most efficient for both T_1 and T_2 when the time-scale of such interactions is at or near the Larmor frequency, and T_2 is additionally sensitive to low frequency modulations of spin energy levels. Thus the relaxation mechanisms are dominated by the effects of dipole-dipole interactions with adjacent ^1H nuclei, with the strength of these dipolar interactions primarily dependent, among other factors, upon the internuclear distance, and the mobility of the vector within the static B_0 field, and hence are able to give information about both geometric and dynamic behaviour.

1.4.2 Nuclear Overhauser Effect

Consider a two spin system, I and S, that are not dipolar coupled, but are close in space. Transition probabilities between states can be defined as shown (*figure 1.11*), with the populations of each energy level given by the Boltzmann distribution.

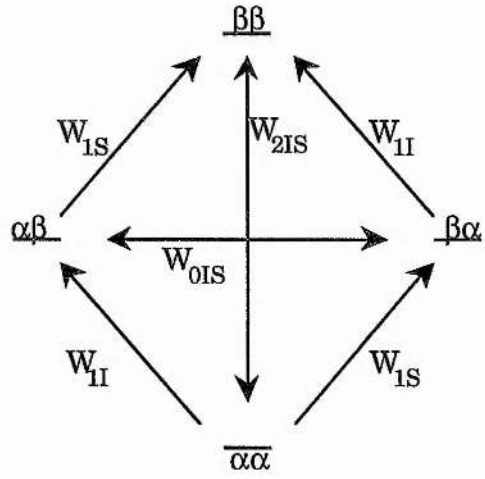

Figure 1.11 - Energy level diagram for two non-coupled spins, I and S, in close spatial proximity. W_1, W_2, and W_0 represent the transition probabilities for single, double, and zero quantum processes, respectively. Spin states are labelled α or β.

The application of a radio-frequency pulse at the frequency of spin S saturates this spin causing the equalisation of the populations across the S spin transitions, and relaxation will proceed by various pathways including double and zero quantum spin transitions, W_2 and W_0 respectively. W_2 transitions are promoted by magnetic fields fluctuating at ~2ω, and W_0 by low frequency fluctuations. In slowly tumbling molecules relaxation by the W_0 pathway will predominate causing a reduction in the intensity of the I spin, resulting in a -100% NOE at the limit, whilst in rapidly tumbling molecules, W_2 relaxation processes dominate causing a positive enhancement on the intensity of the I spin. When these energy level populations are disturbed from equilibrium, the I spin will also relax by transferring energy to other nearby spins, and these indirect enhancements are negative. After prolonged saturation of the S spin, the transfer of indirect NOE enhancements ('spin-diffusion') causes saturations of all the spins in the molecule, and the distance proportionality of the NOE magnitude is lost. Therefore, rate of cross-relaxation, σ, also proportional to r^{-6} is a more convenient parameter to use than the enhancement itself.

In a multi-spin system, the rate of intensity change for spin I is:

$$\frac{dI_z}{dt} = -R_I\left(I_z - I_z^0\right) - \sigma_{IS}\left(S_z - S_z^0\right) - \sum \sigma_{IM}\left(M_z - M_z^0\right) \qquad [1.2]$$

where I_z and I_z^0 are I spin intensities along the Z-axis at time zero and time t respectively. R_I is the relaxation rate of I, and M represents all other spins in the system. The initial rate, when $I_z=I_z^0$, $M_z=M_z^0$, and $S_z=0$, is given by:

$$\frac{dI_z}{dt} = \sigma_{IS} S_z^0 \qquad [1.3]$$

For homonuclear ^{1}H-^{1}H interactions, σ is given by:

$$\sigma_{IS} = \left(\frac{\mu_0}{4\pi}\right)^2 \frac{\gamma_I^2 \gamma_S^2 \hbar^2}{10 r_{IS}^{-6}} \left[6J(\omega_I + \omega_S) - J(\omega_I - \omega_S)\right] \qquad [1.4]$$

where $\hbar$ is Planck's constant divided by 2π, μ_0 is the permeability of free space, r_{IS} is the internuclear distance, and γ is the gyromagnetic ratio of proton spins, I and S. $J(\omega)$, the spectral density function is defined as:

$$J(\omega) = \frac{\tau_c}{1+\omega^2\tau_c^2} \qquad [1.5]$$

where τ_c, the correlation time for isotropic molecular reorientation, is inversely proportional to rates of molecular motions, and is identical for each ^{1}H-^{1}H vector in a rigid isotropically tumbling molecule.

Using the initial rate approximation, immediately after saturation of spin S, the NOE at spin I is affected by only one distance-dependent term, σ_{IS}, and therefore, in such situations, all enhancements behave as though they were in a two-spin system, and NOEs measured during truncated driven experiments, when the saturation period is within the linear build-up region, are in proportion to the internuclear separation from spin S. With longer presaturation times, indirect enhancements develop, and the distance specificity is lost.

If all constant terms in equation 1.4 are gathered together as a single term, k, the equation simplifies to:

$$\sigma_{IS}=kr_{IS}^{-6} \qquad [1.6]$$

Then, when an NOE enhancement is observed between two other spins (I and M) and the distance between I and S is known, the I-M distance can be estimated from a simple ratio calculation:

$$r_{IM} = r_{IS}\left(\frac{\sigma_{IS}}{\sigma_{IM}}\right)^{\frac{1}{6}} \qquad [1.7]$$

Due to the r^{-6} dependence small inaccuracies in measured NOE enhancements have negligible effects in calculated internuclear distances, and this reference distance method, also referred to as the isolated spin pair approximation (ISPA), may be used to model theoretical NOE intensities from static or dynamic structures provided that the following caveats are adhered to:

1. The accuracy of the calculated I-M distance relies upon that of the reference distance.
2. Inaccuracies are introduced by non-instantaneous saturation.
3. The method is only valid for the initial rate approximation.
4. Integration of spectra, particularly with overlapping signals may be inaccurate.
5. Internuclear vectors connecting IS and SM must have the same effective correlation time (τ_e). This will not be the case if the molecule exhibits anistropic tumbling or has flexibility in the S-M distance.
6. In the event of internal motions, enhancements are heavily weighted by conformations with the closest contact, due to the r^{-6} dependence, with the internuclear distance rather than the enhancement itself which is averaged.
7. Nuclei I, S, and M must have the same gyromagnetic ration, and must not be relaxed by a directly attached NMR 'active' nucleus.
8. Nuclei I, S, and M must not be undergoing chemical exchange.

Providing these conditions are satisfied, the I-M distance can be calculated to within ~10%. However, in flexible oligosaccharides inequalities of τ_c become relevant, and internal mobility adds uncertainties to the proportionality of σ and r^{-6} (Genest, 1989). For a flexible molecule in multi-site conformational exchange that is slow on the τ_c time-scale, the effective internuclear distance is simply a time-average of the separation at each individual conformation $\langle r^{-6} \rangle^{-1/6}$.

1.4.3 Full Relaxation Matrix Calculations

In contrast to the ISPA method, full relaxation matrix calculations offer a more theoretically rigorous method for the interpretation of (R)NOESY data. In full relaxation matrix calculations the longitudinal relaxation of a complete spin-system is determined, thus the effects of spin-diffusion, the presence of heteronuclei, and chemical exchange may be incorporated in calculations for a fixed or dynamic model of the system using a suitable parametrised algorithm. The full relaxation rate matrix, R, is calculated (assuming cross-correlation can be ignored) by solving a set of generalised Bloch equations, which govern the time dependence of the magnetisation M_{zI} of each spin I within the molecule, and is best calculated in the form of a matrix:

$$\frac{d}{dt}\begin{bmatrix} M_I \\ M_S \\ \vdots \\ M_n \end{bmatrix} = -\begin{bmatrix} R_{II} & R_{IS} & \cdots & R_{In} \\ R_{SI} & R_{SS} & \cdots & R_{Sn} \\ \vdots & \vdots & & \vdots \\ R_{n1} & R_{n2} & \cdots & R_{nn} \end{bmatrix}\begin{bmatrix} M_I \\ M_S \\ \vdots \\ M_n \end{bmatrix} \qquad [1.8]$$

with $M_I = M_{zI} - M_{zI}^0$. Here M_{zI}^0 is the z magnetisation of spin I at equilibrium. R_{II} is given by:

$$R_{II} = \sum_S \rho_{IS} + \rho_I^* \qquad [1.9]$$

the dipolar contributions to the spin-lattice relaxation rate ρ_{IS} are given by:

$$\rho_{IS} = \frac{\gamma_I^2 \gamma_S^2 \hbar^2}{10 r_{IS}^6} \sum_{S \neq I} \left[J_0(\omega) + 3J_1(\omega) + 6J_2(2\omega) \right] \qquad [1.10]$$

and ρ_I^* represents other (non-dipolar) relaxation sinks ('leakage') in macromolecule systems, and the cross-relaxation rate R_{IS} is equal to σ_{IS}.

If all inter-proton vectors are assumed to be rigid and to move isotropically, the spectral density function takes the form given in equation 1.5, and we can rewrite equation 1.8 as:

$$\frac{d}{dt}M = -RM \qquad [1.11]$$

where R is the relaxation rate matrix, and the solution is given by:

$$M(\tau_M) = e^{(-R\tau_M)}M(0) \qquad [1.12]$$

These equations can be generalised for the analysis of 2D NOESY spectra in which case $\mathbf{M}(\tau_M)$ is a matrix proportional to the normalised NOE intensities recorded with a mixing time τ_M and M(0) is the diagonal matrix containing the z magnetisations.

1.4.4 Spin-Spin Couplings Constants

The magnitude of spin-spin coupling constants is affected by the degree of atomic overlap, and is therefore related to the dihedral angle (θ) between vicinal coupled spins (Karplus, 1959; Karplus, 1963). The generalised Karplus relationship, applicable to both homonuclear and heteronuclear spin-coupling constants, takes the form:

$$J = A\cos^2\theta + B\cos\theta + C$$

where A, B, and C are constants for which different values have been proposed depending on the torsional angles under investigation, whilst Haasnoot has included additional terms for substituent electronegativities (Haasnoot *et al.*, 1980). The ^{1}H-^{1}H spin-coupling constants and chemical shifts of pro-R and pro-S hydroxymethyl resonances have been assigned unequivocally for several hexapyranosides, where $H6_{proR}$ invariably has a greater chemical shift and larger H5-H6 coupling constant compared to $H6_{proS}$. The rotomer distribution about the C5-C6 bond can, therefore, be found from the analysis of the ^{1}H-^{1}H spin-coupling constants (Wu *et al.*, 1983; Ohrui *et al.*, 1985).

1.4.4 Two and Three Dimensional NMR Spectroscopy

Resonance assignments of even simple oligosaccharides is often complicated by the tendency for the majority of resonances in both ^{1}H and ^{13}C spectra to lie within an unresolved envelope spanning only a few hundred Hertz. Anomeric proton and carbon resonances usually lie outside this envelope, being well resolved down-field due to the electron withdrawing effect exerted by the ring oxygen. Problems of coincident resonances are partially resolved by separation into a second or third dimension, increasing the spectral dispersion. The precise nature of the information contained in the spectrum depends upon the details of the pulse sequence and phase cycling used, however, a number of key points are shared by all multidimensional experiments. All nD experiments consist of 'building blocks' (Edison *et al.*, 1994) consisting of a sequence of pulses and delays to generate the required coherences which then are allowed to evolve under a free precession Hamiltonian during an incremented delay (t_1). In 3D experiments further building blocks are used to transfer magnetisation to other spins encoding additional information and may be recorded during a further incremental delay. The signal generated is then detected directly during acquisition, with two dimensional spectra processed by application of two orthogonal Fourier transformations, and where three dimensional spectra require a third orthogonal transformation.

1.4.5 Transferred NOE experiments

The transferred NOE or TRNOE occurs when a ligand is in exchange between free solution and a bound state in which it is complexed with a protein (Clore and Gronenborn, 1982, 1983; and reviewed by Clore and Gronenborn, 1981; Campbell and Sykes, 1993; Ni, 1994; Ni and Scheraga, 1994). Measurement of negative NOEs on the easily detectable free or averaged ligand resonances following the irradiation of other ligand resonances whilst bound to the protein, allows information about the bound conformation to be obtained. As oligosaccharides are often in fast exchange with their receptor proteins, K_D values are between ~10^{-3} to 10^{-6}M, a variety of glycan-protein interactions have been probed by TRNOE experiments (Bevilacqua *et al.*, 1990; Bevilacqua *et al.*, 1992; Bundle *et al.*, 1994; Cooke *et al.*, 1994; Andrews *et al.*, 1995; Asensio *et al.*, 1995; Scheffler *et al.*, 1995, 1997; Weimar *et al.*, 1995).

For a ligand in fast exchange between free and bound on the relaxation time-scale, <σ>, the overall cross-relaxation rate, is given by:

$$\langle \sigma_{IS} \rangle = N^F \sigma_{IS}^F + N^B \sigma_{IS}^B \qquad [1.13]$$

where N^F and N^B are the number of molecules in the free and bound states, respectively, and σ^F_{IS} and σ^B_{IS} are the cross-relaxation rates between spins I and S in the free and bound states. For the measurement of TRNOEs <σ> should be dominated by σ^B, and simply corresponds to the inequality:

$$\left| N^B \sigma_{IS}^B \right| >> \left| N^F \sigma_{IS}^F \right| \qquad [1.14]$$

The extent to which this inequality is fulfilled depends upon the relative correlation times (τ_c) of the free and bound states, the distances, r_{IS}, in both states, and the equilibrium dissociation constant K_D. If the complex is only weakly bound, then N^B will be small, and the TRNOE will disappear simply because there is insufficient ligand present in the bound state to contribute to the overall relaxation. Clearly, the minimum value of K_D required for a viable TRNOE will depend on values of σ^B_{IS} and σ^F_{IS}, where, the more slowly the complex tumbles the larger $|\sigma^B_{IS}|$ becomes, consequently the simpler it is to satisfy equation 1.14. One advantage of this condition is that ligands in complex with very large proteins, such as photon rhodopsin (>1000kDa) (Ni, 1994), which would normally be too large to study by conventional NMR spectroscopy, may be probed by TRNOEs.

At the opposite extreme, the TRNOE depends upon the rate of exchange between free and bound states being sufficient for an appreciable magnetisation flux to occur between them. If S^B is irradiated, the condition for appreciable enhancement transfer to occur from the bound signal I^B to the free signal I^F is:

$$k_{on}[P] >> R_I^F \qquad [1.15]$$

where R^F_I is the relaxation rate of spin I in the free state. Similarly, if the signal S^F is selectively irradiated, the saturation transfer from S^F to S^B is also a requirement for a viable TRNOE, and the relevant equality is:

$$k_{off} >> R_S^B \qquad [1.16]$$

where R^B_S is the relaxation rate of spin S in the bound state. Inequalities in equations 1.14 and 1.15 are likely to be broken for tightly bound complexes, and so for TRNOEs to be observed, inequalities equations 1.14, and 1.15, and for certain experiments equation 1.16must be observed.

The build-up and decay of TRNOEs over a series of NOESY mixing times can also be used to study the relative mobilities of ligand residues when bound to a protein. For a typical example, TRNOEs which show an increase in intensity followed by a decay over a small range of mixing times ($\tau_m \leq 100$ms) indicates the presence of spin diffusion as a result of restricted mobility of this residue and the close proximity of the protein. In comparison, TRNOEs which show significant increase in intensity even up to relatively long mixing times ($\tau_m > 500$ms) are characteristic of a group which has significant conformational mobility in the bound state. Thus it is possible to map oligosaccharide residues which makes significant contact with their receptor lectin (Casset *et al.*, 1997).

Due to the restricted mobility of a ligand in the bound state and the close proximity of often large proteins, spin-diffusion effects play an important role in the TRNOE phenomena, and failure to take this into account has resulted in misinterpretation of TRNOESY data. A notable example of this was the work by Glaudemans and co-workers, who examined the conformation of a disaccharide in complex with an antibody Fab fragment. The original study TRNOESY data suggested that there was a large conformational change between free and bound states (Glaudemans *et al.*, 1990), but in a following paper (Arepalli *et al.*, 1995) the authors concluded that the intra-residue TRNOE which was indicative of this new bound state conformation was in fact spin-diffusion as a result of magnetisation transfer via the protein. Such indirect (TR)NOEs may be identified by measuring transferred NOE enhancements in the rotating frame (TRROE) where, σ_{ROE} is positive regardless of the rate of rotational reorientation, giving rise to cross peaks with negative phase, and where ROE-ROE relays (equivalent to spin-diffusion in NOESY spectra) will always lead to cross-peaks having sign $(-1)^m$, where m is the number of ROE transfers (Farmer II *et al.*, 1987). Hence an ROE transfer from proton A to C via B will give rise to a cross-peak of opposite phase to a direct A to C ROE.

1.5 Carbohydrate Conformation

Carbohydrate conformations (reviewed by Stoddart, 1971) are defined by the conformations of individual residues and their linkage geometries. Hexapyranose rings occur predominately in the chair configuration and for the purpose of description the atoms are numbered with the ring oxygen as zero and the carbons follow sequentially from the anomeric carbon (atom one). A reference plane is defined as passing through four of six of the heavy atoms in the ring, with the lowest numbered atom lying above or below the plane (IUPAC-IUB, 1980). Alternative configurations are then described by a letter describing the conformation ('C' for chair). Superscript and subscripts denote the atoms lying above and below the plane of the ring, respectively. The $^4C_1$ configuration predominates in D-pyranose due to the relief of steric crowding, except D-arabinopyranoses which adopts $^1C_4$ configuration due to the distribution of hydroxyl groups and the absence of a 6-carboxy moiety (*figure 1.12*). *N*-acetyl neuraminic acid adopts a similar configuration to the arabinopyranoses except due to the different numbering system is defined as $^2C_5$. Measurement of homonuclear spin-coupling constants does not indicate large deviations from theoretical predictions, suggesting that in solution the pyranose rings are essentially rigid structures.

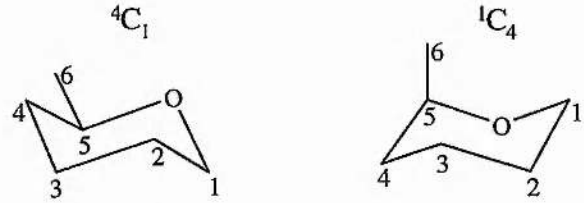

Figure 1.12 - Chair conformations of pyranose rings, showing atom numbers.

Linkage geometry is defined by the orientation of the glycosidic linkage. IUPAC-IUB (1970) describes these in terms of heavy atoms, however in discussing NMR-derived conformations it is more convenient to define them with respect to protons as follows, ϕ_H = H1-C1-O1-Cx, ψ_H = C1-O1-Cx-Hx. The subscript 'H' distinguishes these from the IUPAC definitions, and the 'Cx' and 'Hx' refer to the aglyconic atoms.

1.5.1 Theoretical Determination of Conformation

The incorporation of experimentally derived distance restraints (NOE measurements) in the determination of the structures of proteins and nucleic acids is now well established. In contrast, due to the small number of inter-residue contacts, experimental NOE data alone is not sufficient to define the geometry of oligosaccharides in solution. Therefore, theoretical support is required from computerised energy calculation routines, which modify/optimise the atomic co-ordinates of an input structure to determine the optimum (minimum energy) conformation. Methods for conformational searching and energy calculation procedures are reviewed by French and Brady (1989).

Full *ab initio* quantum mechanical computations of oligosaccharide conformations are unattainable for even a small disaccharide due to computationally intensive calculations required, so computations of oligosaccharide conformations have relied almost entirely on molecular mechanical methods (Brady, 1986; Brady, 1987; Homans *et al.*, 1987; Yan and Bush, 1990). In this approach the atoms are treated as point masses and charges, and the bonds are treated as springs, each bond type has an optimum value derived empirically from x-ray crystallography or *ab initio* studies on small molecules, and distortion from ideality increases the potential of the model in an analogous manner to the compression of a spring (*i.e.* $E=\frac{1}{2}Kx^2$). Using analogous classical descriptions an energy function can be defined for the model, whilst additional terms to account for empirical observations that are particular to carbohydrates, particularly the anomeric and exo-anomeric effects (reviewed by Tvaroska and Bleha, 1989) which drive the aglyconic carbon to take orientations of $\phi_H \sim +60°$ in β-D-glycosides, and $\phi_H \sim -60°$ in α-D-glycosides.

This approach was adopted for the commonly used HSEA (hard sphere exo-anomeric) approach (Thogerson *et al.*, 1982), where results obtained were in good agreement with experimental and theoretical data for the blood-group oligosaccharides (Lemieux *et al.*, 1980; Thogerson *et al.*, 1982), sucrose (Bock and Lemieux, 1982), and structures relating to the complex type *N*-linked glycans (Bock *et al.*, 1982). These studies proposed that oligosaccharides have essentially fixed orientations about the glycosidic linkages, with the exception of 1-6 linkages for which a number of orientations were predicted. However, in extending this approach to structures larger than 4-5 residues, agreement is poorer, and it becomes apparent that a degree of conformational flexibility may be present.

HSEA calculations give good results for static minimum energy structures with restricted values for ϕ and ψ torsion angles, but to investigate dynamic models where the potential energy surface encompasses a wide range of ϕ and ψ angles, it now appears that a full molecular mechanical force-field is more appropriate. The AMBER parametrisation is a full force-field (Weiner *et al.*, 1984; Weiner *et al.*, 1986), originally designed use with for nucleic acids and proteins, and has been extended to include carbohydrates (Homans, 1990a), based upon the work by Ha *et al.* (1988a).

HSEA calculations suggest deep potential wells supporting the concept of rigid conformations, whilst allowing all bonds, angles, and torsion angles to vary during minimisation (flexible geometry) increases the area of conformational space accessible to a given glycosidic linkage (Homans *et al.*, 1987; Ha *et al.*, 1988b; Scarsdale *et al.*, 1988; French, 1989; Imberty *et al.*, 1989; Yan and Bush, 1990), resulting in a shallower topography which often exhibit minor minima that are not observed on rigid surfaces (Imberty *et al.*, 1989). Relaxed potential energy surfaces (French, 1989) in which ϕ_H and ψ_H are systematically varied in small steps (10° or 15°) and the geometry optimised for this value of the glycosidic angles may be presented as an iso-energy contour plot (Ramachandran plots), in which occupation is temperature dependent and governed by the Boltzmann law. Calculation of relaxed maps is preferable to the use of rigid-residue approach, since bad contacts may be avoided by relatively small deviations of the internal co-ordinates (Goebel *et al.*, 1970; French, 1988; Ha *et al.*, 1988b). Clearly this becomes impractical for larger molecules, since the number of degrees of freedom rapidly increases both the number of calculations and therefore the computational time. Additionally, the problem of false or multiple minima is accentuated since it cannot be ensured that at each ϕ/ψ point the molecule is at the global minimum energy.

An alternative approach for the determination of accessible conformational space is the calculation of molecular dynamics simulations, and studies on the behaviour of model saccharides during molecular dynamics simulations has highlighted several important points. First, whilst structures may be restricted to low-energy regions of conformational space, they exhibit some degree of conformational flexibility, with a number of conformations consistent

with experimental data. Second, internal motions occur on the time-scale of picoseconds, substantially faster than the rate of overall tumbling for even moderately sized molecules.

An additional advantage of MD simulations is that NMR parameters, such as NOEs and spin-coupling constants, may be back-calculated and compared with those measured experimentally. Significant improvement in the back-calculated data in comparison to the experimental data may be achieved with using experimentally derived distance restraints, r_{NOE} introduced into the force-field as 'pseudo energy' functions (Holak *et al.*, 1987). In conventional MD based NMR refinement (Nilges *et al.*, 1988) these distances are applied on the model structures using a harmonic potential term of the form:

$$\begin{aligned} V_{NOE} &= K_l(r_{model}(t) - r_l)^2 \qquad r_{model}(t) < r_l \\ V_{NOE} &= 0 \qquad\qquad\qquad\quad r_l \le r_{model}(t) \le r_u \\ V_{NOE} &= K_u(r_{model}(t) - r_u)^2 \qquad r_u < r_{model}(t) \end{aligned} \qquad [1.17]$$

where $r_{model}(t)$ is the instantaneous distance in the model molecule at time t. K_l and K_u are weak force constants (20kJmol^{-1}), and the NMR derived distance, r_{NOE}, typically lies in the middle of the range (r_l, r_u). The flat bottom region between r_l and r_u, where the penalty function is zero regardless of $r_{model}(t)$ accounts for the uncertainty of the NOE derived distances and because it is not possible to distinguish between a fixed internuclear distance and a variable internuclear distance cause by motional averaging. In the MD simulation these distance restraints are included as a penalty function which along with the analytic function (the potential energy of the system) gives the total energy of the molecule as a function of conformation.

The distance restraints serve to restrict the motion of the MD simulation to areas of the potential energy surface which are well parametrised (*i.e.* around the global energy minimum), and represent the *minimum* extent of torsional variation consistent with the experimental data. Unrestrained MD simulations in comparison represent the *maximum* torsional freedom consistent with the force-field which often takes the molecules into regions of the potential energy surface divorced from the global energy region which are poorly parametrised.

The problem with this approach is that the energy of the system is derived from snapshots along the MD simulation which comprise of static structures. Obviously the distance, r_{NOE}, derived from an NMR experiment represents as ensemble of the distance over the time-scale of the cross-relaxation period during the experiment, and it is therefore more appropriate to use $\langle r_{model(t)}^{-6} \rangle^{-1/6}$ in equation, where $\langle r_{model} \rangle$ is a time-averaged value (Torda *et al.*, 1989). For practical reasons the time-averaged distance is taken over a memory time τ, so that an effective NMR distance might by given by:

$$r_{eff}(t)^{-6} = \frac{1}{t}\int_0^{\tau} e^{-\frac{t'}{\tau}} \left[r(t-t')\right]^{-6} dt' \qquad [1.18]$$

where r and r_{eff} are the distance and time-averaged distance respectively, and t is time. Since only the average (and not instantaneous) distances need to satisfy the restraints, the restrictions on the conformational space sampled are generally less severe than for "conventionally" restrained MD simulations. This becomes important as the number of NMR derived restraints increases which may provide sets of conflicting distance restraints which can only be modelled well by time-averaged restraints.

Determination of the minimum energy structure may be reached by means of restrained simulated annealing, where convergence upon a similar final conformation from a number of different staring geometries ensures that a larger proportion of conformational space has been sampled compared to minimisation by differentiation of the energy function.

1.6 Outline of Investigation

In this investigation, the development of methodology for conformational analysis of oligosaccharides is discussed. The additional restraints, obtained by use of ^{13}C-enriched oligosaccharides and low temperature studies, are applied to a series of carbohydrates including the biologically important sialyl Lewis^x antigen.

Chapter 2 details the chemo-enzymatic synthesis of carbon-13 labelled sialyl Lewis^x and its precursor molecules.

In chapter 3 the theoretical and practical aspects of obtaining additional distance and angular restraints using NMR is detailed.

Chapter 4 describes the measurement of additional restraints through heteronuclear NMR experiments applied to the model system of *N*-acetyllactosamine.

In chapter 5 high resolution multidimensional NMR experiments are used to determine the three-dimensional structure and dynamics of ^{13}C-enriched sialylα2,3-*N*-acetyllactosamine.

Chapter 6 investigates the three dimensional structure and dynamics of sialyl Lewis^x in free solution and a preliminary study of the conformation of sialyl Lewis^x when bound to E-selectin.

Chapter 2

Synthesis of ^{13}C-labelled carbohydrates

Abstract

The synthesis of isotopically (^{13}C, and ^{15}N) enriched samples has allowed the application of multi-dimensional heteronuclear NMR to the structure determination of proteins and nucleic acids. The uniform ^{13}C-enrichment of oligosaccharides has, so far, been limited to polysaccharides and more recently glycoprotein glycans, with heteronuclear NMR experiments used in the assignment and conformational analysis of these carbohydrate moieties. The synthesis of biologically important oligosaccharides in carbon-13 enriched form allows the conformation of larger oligosaccharides in free solution to be determined (often difficult for homonuclear investigations because of the severe resonance overlap in the ^{1}H dimension), and when bound to proteins, by heteronuclear filtration experiments. In this present chapter the chemo-enzymatic synthesis of sialyl Lewis^{x} from [U-^{13}C] Glc and [U-^{13}C] Gal is described.

2.1 Introduction

2.1.1 NMR investigations of ^{13}C enriched Oligosaccharides

Multidimensional heteronuclear NMR has revolutionised the assignment and structure determination of proteins, DNA, and RNA since the introduction of methods to obtain isotopically ^{13}C and ^{15}N labelled material (reviewed by Pardi, 1992; Dieckmann and Feignon, 1994). It is, therefore, expected that similar benefits would be obtained from ^{13}C enriched oligosaccharides, in fact, Yu and co-workers have shown the application of two and three dimensional heteronuclear experiments to obtain the assignments of the carbon and proton resonances in [U-^{13}C] β-glucans extracted from yeast grown on [U-^{13}C] glucose (Yu *et al.*, 1993).

Historically there are many examples of NMR investigations of ^{13}C-labelled carbohydrates reviewed by Barker *et al.* (1982), including highly enriched labelled monosaccharides, 50%-^{13}C glucose (Perlin and Casu, 1969) . Other examples include monosaccharides with a single carbon uniformly labelled, used for measuring heteronuclear coupling constants to derive a Karplus relationship (Wu *et al.*, 1992), and determination of thermodynamic parameters of carbohydrates involved in protein binding (Swift and Connick, 1962; reviewed by Amin and Chatterjee, 1995). Partially enriched carbohydrate moieties have been used to determine conformation and dynamics, for example [U-1-^{13}C] galactose labelled sialyl Lewis^x was used to determine the torsion angle ψ of the Gal-GlcNAc linkage (Ichikawa *et al.*, 1992), and trans-glycosidic ^{13}C-^{13}C spin couplings were measured on a [U-1-^{13}C] galactose labelled Galβ1-4GlcNAc allowing an insight into the glycosidic torsion angles (Nunez and Barker, 1980). Work performed by the Homans' group using [U-^{13}C] carbohydrate moieties demonstrated the application of heteronuclear NMR experiments, initially derived for use with proteins, to study carbohydrate conformation in free solution (Harris *et al.*, 1997; Milton, 1997), bound to proteins (Low, 1996), and as glycoprotein glycans (Weller *et al.*, 1996).

Apart from obvious examples where oligosaccharides have been labelled through feeding bacteria and algae labelled monosaccharides (London *et al.*, 1975; Yu *et al.*, 1993; Weller *et al.*, 1996), there are limited examples of isotopically ^{13}C-enriched oligosaccharides, with the main drawback being the lack of commercially available monosaccharides. This problem is

being addressed at present with [U-^{13}C] monosaccharides becoming commercially available (Martek Biosciences), although limited at present to glucose and galactose. The synthesis of biologically interesting carbohydrates with a high degree of uniform enrichment is now a possibility, and as a test of the applicability of using fully ^{13}C labelled oligosaccharides in conformational analysis, the carbohydrate sialyl Lewis^x has been synthesised (Probert *et al.*, 1997).

2.2.2 Synthesis of sialyl Lewis^x

Since the discovery that the carbohydrate moiety involved in the adhesion process of inflammatory response is based upon the sialyl Lewis^x antigen, a large amount of effort has been invested in first synthesising sialyl Lewis^x for biochemical and conformational studies and later mimics of sialyl Lewis^x as potential inhibitors (reviewed by Sears and Wong, 1996; McGarvey and Wong, 1997). Initially sialyl Lewis^x was chemically synthesised (Nicolaou *et al.*, 1991) but major drawbacks involve the need to protect the sugar's functional groups, and the difficulty in obtaining high distereo- and regioselectivity.

The enzymatic synthesis of *N*-acetyllactosamine using β(1,4)galactosyltransferase (Nunez and Barker, 1980), opened up a new area in oligosaccharide synthesis. The development of enzymes for the synthesis of complex carbohydrates are particularly useful because, in contrast to chemical syntheses, enzymes show high diastereo and regioselectivity without the need for protecting groups. The use of enzymes in the synthesis of oligosaccharides has recently been reviewed (Ichikawa, 1997).

There are four types of enzymes known to catalyse glycosidic bond formation, (1) phosphorylases - these use a sugar 1-phosphate as a donor for transfer to an acceptor molecule. (2) glycosidases - these enzymes normally catalyse the hydrolysis of the glycosidic bond, although, under the correct conditions, they can be used to catalyse the formation of a glycosidic bond. Glycosidases are easy to obtain but, although the formation of the glycosidic bond proceeds stereo-selectively, it does not proceed efficiently with respect to regio-selectivity. (3) transglycosidases - these are a unique class of enzymes in that they transfer a particular carbohydrate moiety from one oligosaccharide to a donor oligosaccharide. One such enzyme, *trans*-sialidase, which transfers the sialic acid moiety from one carbohydrate to another, has been recently isolated from *Trypanosoma cruzi* and is

utilised in the present synthesis of sialyl Lewis^x. (4) glycosyltransferases - these enzymes require a sugar-nucleotide as donor substrate, and owing to the high regio and stereoselectivity of the reactions, are the enzymes most used for glycosidic bond formation.

Obviously, for a carbohydrate moiety to be synthesised *in vivo*, the requisite enzymes must be present and available. Therefore, assuming that the enzymes can be obtained, sialyl Lewis^x could be totally enzymatically synthesised. The first initial enzymatic syntheses of sialyl Lewis^x utilised the enzymes for the difficult chemical coupling reactions, and more recently, multi-enzymatic approaches have been used for the total synthesis of sialyl Lewis^x in kilogram quantities (Ichikawa *et al.*, 1992).

Scheme 1 shows the route used for the synthesis of uniformly ^{13}C-labelled sialyl Lewis^x. Although multi-enzymatic synthesis of sialyl Lewis^x is possible, the lack of commercial availability of some enzymes means this approach, at present, is limited. In the present synthesis a chemo-enzymatic approach has been used, with the coupling reactions achieved enzymatically and the preparation of the donor molecules via chemical synthesis.

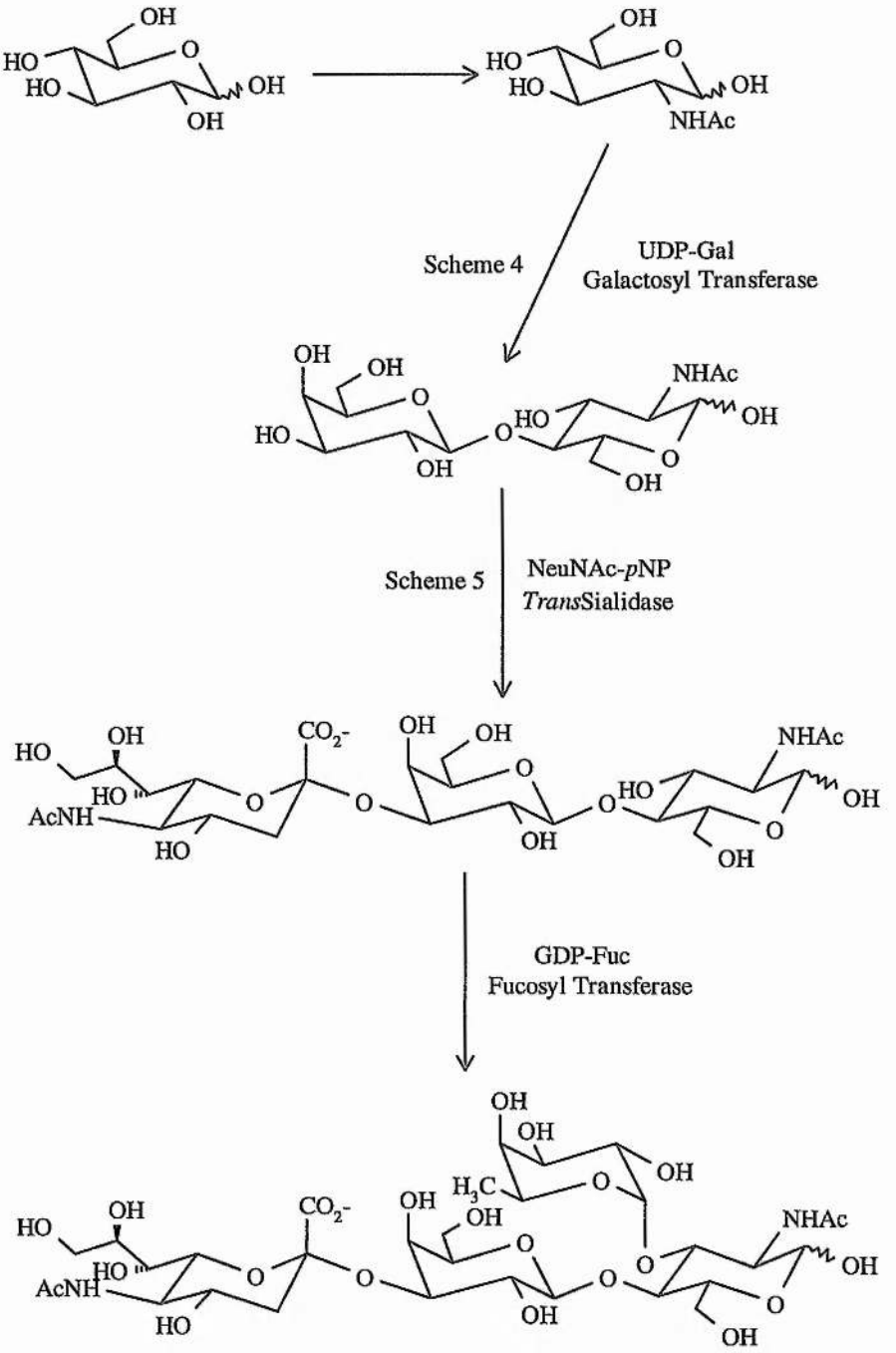

Scheme 1 - Schematic representation of the chemo-enzymatic synthesis of sialyl Lewis^x, the synthesis of the compounds shown in blue are described elsewhere in this chapter. The chemical synthesis involved in preparation of the donor molecules GDP-Fuc and Neu5Ac-*p*-NP was performed by Dr. M. A. Probert. Synthesis of GlcNAc was achieved using an enzymatic route performed by Dr. M. J. Milton (Milton, 1997), UDP-Gal was enzymatically produced *in situ* for production of *N*-acetyllactosamine. All of the coupling reactions were enzymatic, with the galactosyltransferase commercially available, the *trans*-sialidase was prepared by J. A. Harrison (Harrison *et al.*, 1997), and the fucosyltransferase was kindly donated by Prof. M. M. Palcic (Palcic and Hindsgaul, 1996).

2.2 Material and Methods

Conventions: In order to simplify the text the following nomenclature will be used when describing labelled compounds; the prefix [U-^{13}C] will be used to describe mono or oligosaccharides which are carbon-13 enriched to >99% at every carbon position except the carbon atoms of an *N*-acetyl moiety.

All chemicals were purchased from Sigma unless otherwise indicated. All enzymatic reactions were incubated at 37°C unless otherwise stated.

2.2.1 Synthesis of N-*acetyl [U-^{13}C] neuraminic acid (Scheme 3)*

Chemically synthesised [U-^{13}C]-*N*-acetylmannosamine (~300mg, Dr. M. A. Probert, *Scheme 2*), and [U-^{13}C] sodium pyruvate (1.1g, Martek Biosciences) were dissolved in 3.0mL of 20mM potassium phosphate buffer pH 7.5, and filtered through a 2 micron filter. Neuraminic acid aldolase (E.C 4.1.3.3)(2U) was added and the solution stirred at 37°C. A 500μL aliquot of the reaction mixture was transferred to a 5mm NMR tube containing 200μL D_2O. The reaction was followed by ^{13}C NMR.

[U-^{13}C] Neu5Ac was purified using ion-exchange chromatography (AG 1X8, 200 mesh, formate form) eluting with 2M formic acid. The presence of carbohydrate was tested using the sulfuric oricinol method (Lee, 1972). The proton and carbon chemical shifts of [U-^{13}C]-Neu5Ac synthesised matched those of a commercially unlabelled sample (Aldrich, *figure 2.1*).

2.2.2 Multi-enzymatic synthesis of N-*acetyl [U-^{13}C] lactosamine, Galβ1-4GlcNAc (Scheme 4)*

[U-^{13}C] galactose (75mg, 40% D-isomer, Martek Biosciences), $MgCl_2$ (11.2mg), ATP (139.2 mg) and UDP-glucose (157.5mg) were dissolved in 10mL of 50mM TRIS-HCl buffer, pH7.4. The pH was then re-adjusted to pH7.4 with 1M NaOH. Galactokinase (5U)(E.C. 2.7.1.6) and galactose-1-phosphate uridyl transferase (5U)(E.C. 2.7.7.12) were added to the reaction mixture. The reaction was completed by the addition of [U-^{13}C] GlcNAc [~30mg, Dr. M. J. Milton (Milton, 1997; Harris *et al.*, 1997)], 5mM $MnCl_2$, and

galactosyltransferase (8U)(lactose synthase, E.C. 2.4.1.22). The pH of the reaction mixture was maintained by periodic addition of 0.2M NaOH. The mixture was incubated for 18 hours and was then desalted (Chelex 100 over Dowex AG50 X12 over Dowex AG3 X4) and purified on Bio-gel P2. Synthesis of [U-^{13}C] *N*-acetyllactosamine was confirmed by ^{1}H NMR (*figure 2.2*) by comparison to a standard unlabelled sample (Aldrich).

2.2.3 Multi-enzymatic synthesis of lactose, Galβ1-4[U-^{13}C, 50%-^{2}H]Glc (Scheme 4)

Galβ1-4[U-^{13}C, 50%-^{2}H]Glc was made in an analogous method to [U-^{13}C] *N*-acetyllactosamine except GlcNAc was replaced with [U-^{13}C, 50%-^{2}H] Glc (Martek Biosciences) and α-lactalbumin (0.25 mg mL^{-1}). Synthesis of lactose was confirmed by ^{1}H, and ^{13}C NMR (data not shown).

2.2.4 Enzymatic synthesis of [U-^{13}C] sialylα2,3-N-acetyllactosamine (Scheme 5)

[U-^{13}C] *N*-acetyllactosamine (10mg) and p-NP [U-^{13}C] Neu5Ac (~5mg) were dissolved in 200μL of 50mM TRIS-HCl pH7.4 containing 0.05% NaN_3. The pH of the reaction mixture was maintained at 7.4 by the addition of 0.2M HCl. A 50μL aliquot of *trans*-sialidase enzyme [*E.coli* lysate (Harrison *et al.*, 1997)] was added. p-NP-[U-^{13}C]-Neu5Ac was found to be light sensitive, so the reaction was incubated in a light-tight container at room temperature and monitored by TLC (30cm plate, pyridine/butan-1-ol/H_2O/ethanol/acetic acid, 1:1:3:10:0.3). Production of sialylα2,3-*N*-acetyllactosamine (R_f 0.63) could be seen after two hours. Additional aliquots of *p*-NP [U-^{13}C] Neu5Ac (~5mg) were dissolved in 50μL buffer and the pH adjusted to 7.4 by step-wise addition of 0.2M HCl and transferred to the reaction mixture, followed by addition of 50μL of *E.coli* lysate. This procedure was repeated in 12 hour intervals until all of the *N*-acetyllactosamine (R_f 0.6) had been consumed (typically after 60 hours).

Purification was achieved by passing the reaction mixture through a Bio-gel P2 column, running 0.1M NH_4HCO_3 as eluant. The NH_4HCO_3 was removed by repeated freeze-drying, where the sample was obtained as the ammonium salts. Sialylα2,3-*N*-acetyllactosamine was obtained in ~75% yield, and confirmed by ^{1}H NMR (*figure 2.3*) with comparison to a commercially available unlabelled sample (Dextra).

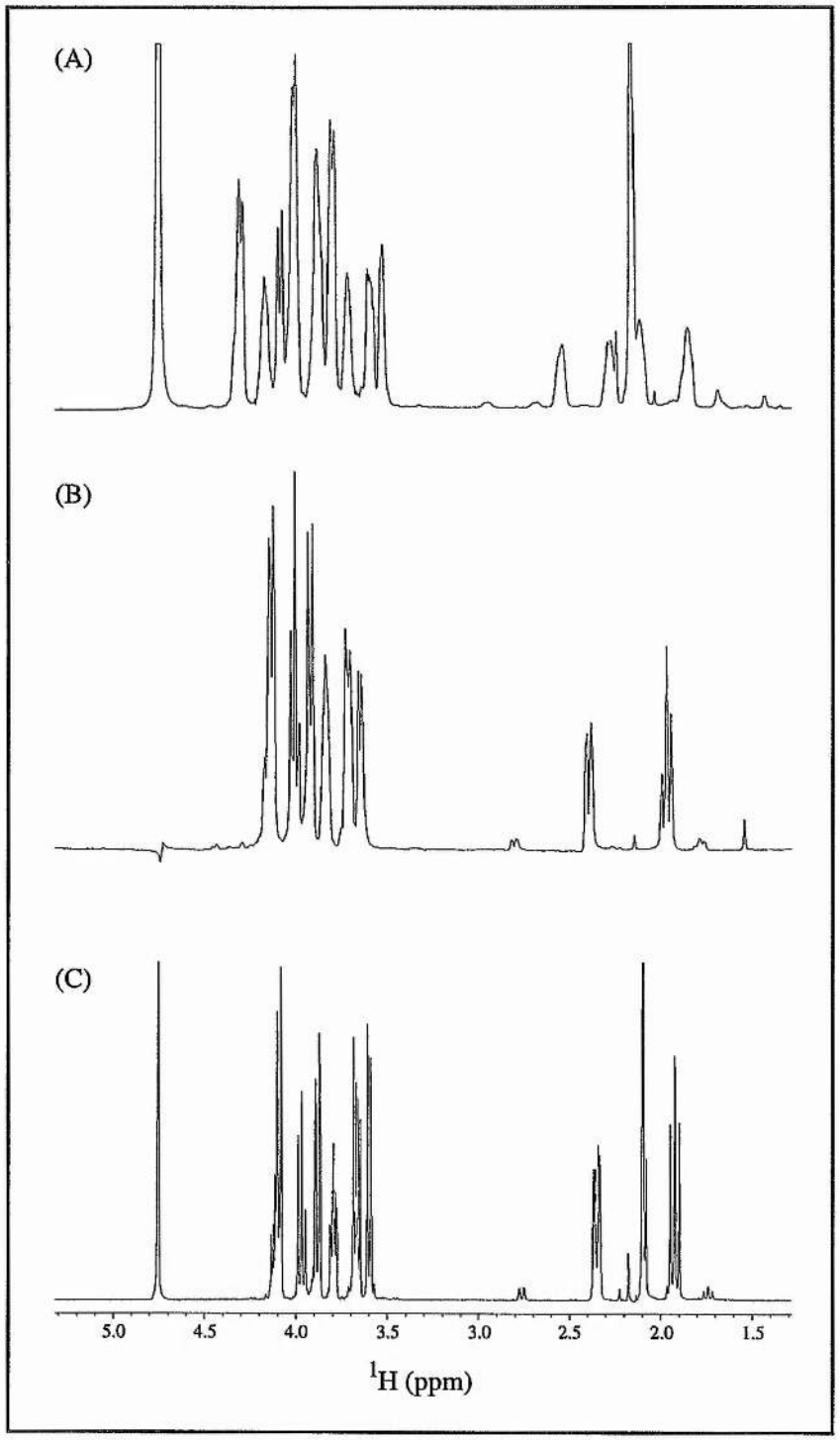

Figure 2.1 - (A) ^{1}H spectrum of [U-^{13}C] Neu5Ac. (B) 1D ^{1}H-^{13}C HSQC spectrum of [U-^{13}C] Neu5Ac (^{13}C-decoupled ^{1}H spectrum). (C) ^{1}H spectrum of standard unlabelled Neu5Ac (α-glycoside, Glaxo).

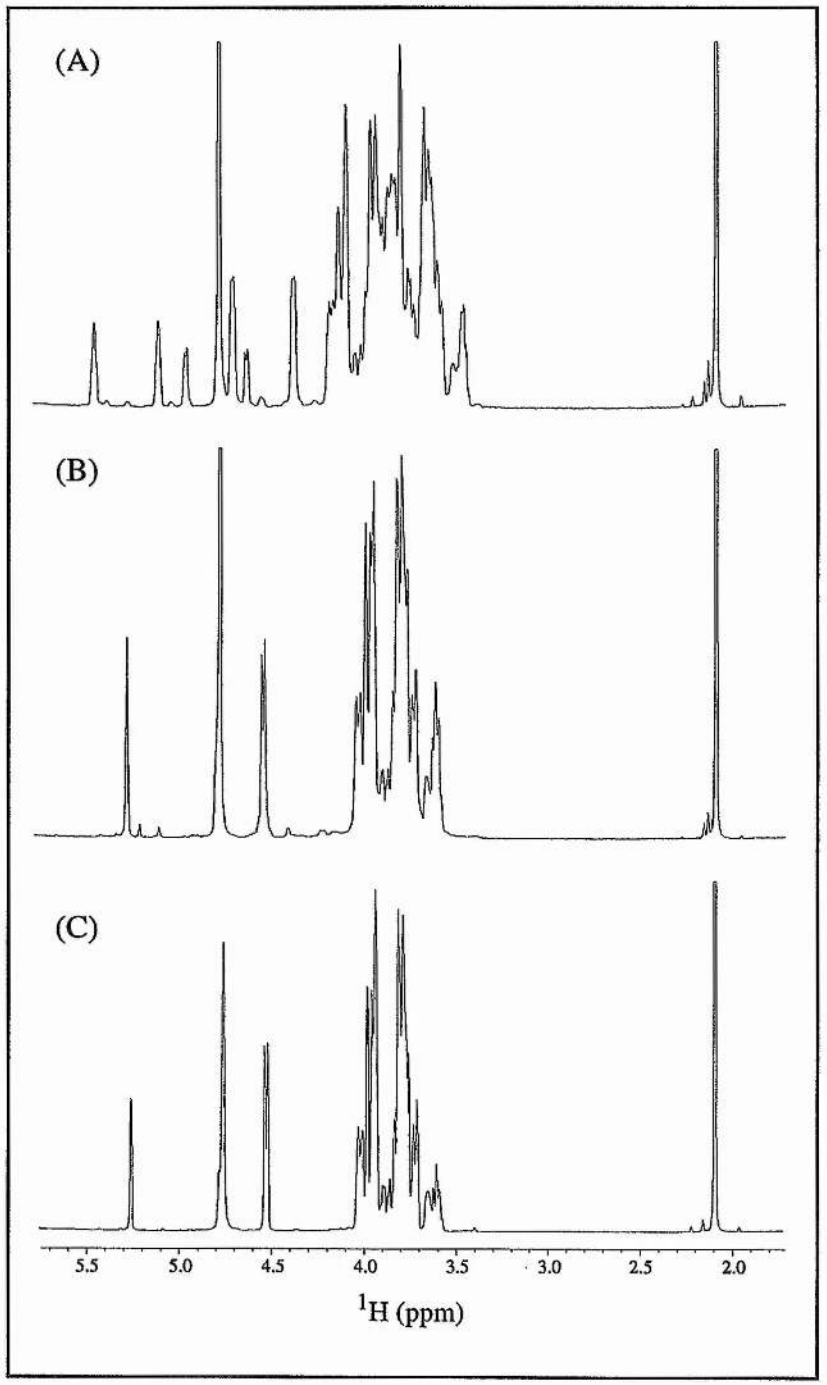

Figure 2.2 - (A) ^{1}H spectrum of *N*-acetyl-[U-^{13}C]-lactosamine. (B) ^{13}C-decoupled ^{1}H spectrum of *N*-acetyl-[U-^{13}C]-lactosamine. (C) ^{1}H spectrum of standard unlabelled *N*-acetyllactosamine (Aldrich).

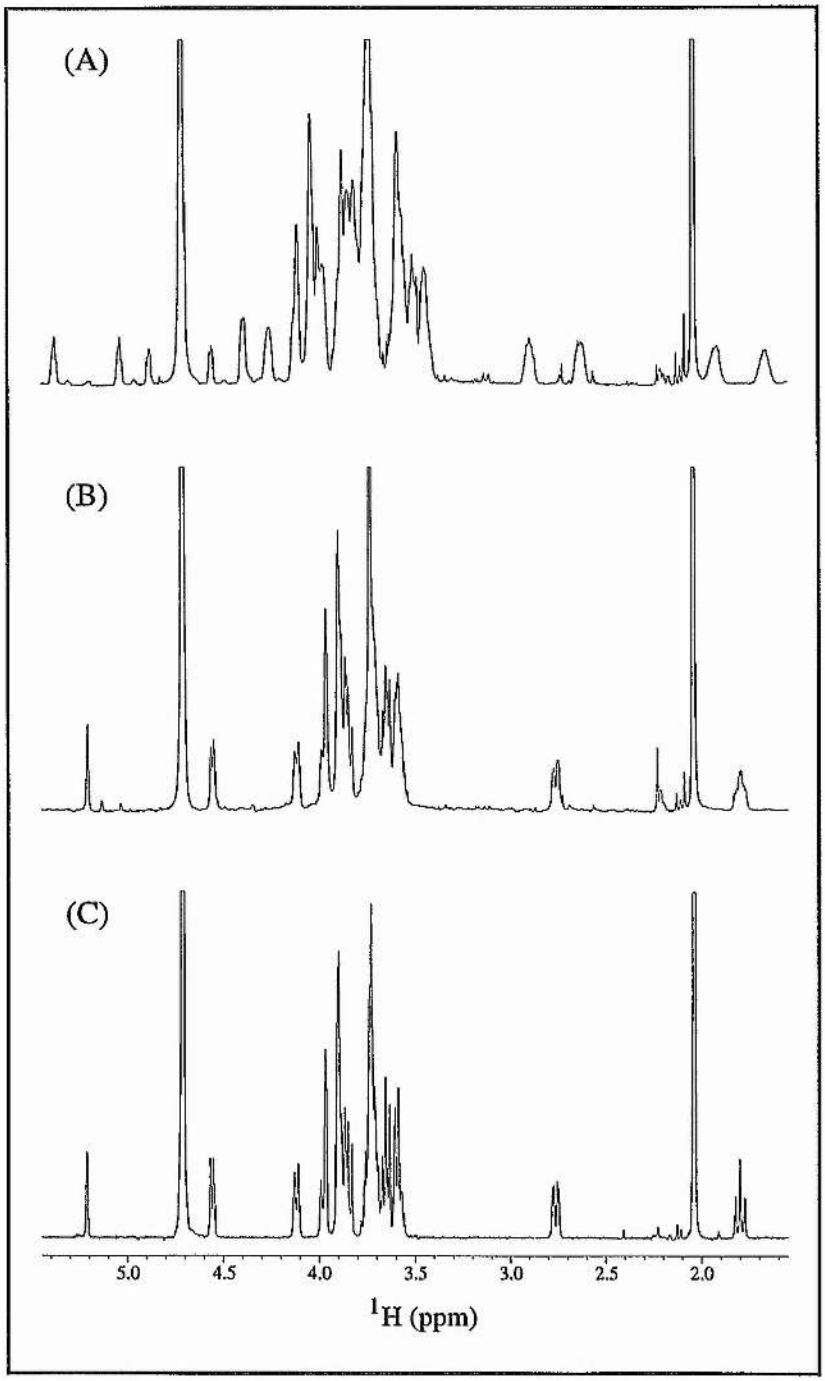

Figure 2.3 - (A) ^{1}H spectrum of [U-^{13}C]-sialylα2,3-*N*-acetyllactosamine. (B) ^{13}C-decoupled ^{1}H spectrum of [U-^{13}C]-sialylα2,3-*N*-acetyllactosamine. (C) ^{1}H spectrum of standard unlabelled sialylα2,3-*N*-acetyllactosamine (Aldrich).

2.2.5 Enzymatic synthesis of [U-^{13}C] Lewis^x and [U-^{13}C] sialyl Lewis^x (Scheme 1)

[U-^{13}C] *N*-acetyllactosamine (5mg) or [U-^{13}C] sialylα2,3-*N*-acetyllactosamine (5mg), GDP-β-L-[U-^{13}C] fucose (~2.5mg, Dr. M. A. Probert, *Scheme 6*), and 10mM $MnCl_2$ were dissolved in 100μL 100mM HEPES pH7.0 containing 0.05% NaN3. A 50μL aliquot of human milk fucosyltransferase preparation (Palcic and Hindsgaul, 1996) was added. The reaction was followed by TLC (30cm plate, propan-2-ol/H_2O/acetic acid, 2:1:2). Production of Lewis^x (R_f 0.31) or sialyl Lewis^x (R_f 0.31) could be seen after 6 hours. Additional aliquots of GDP-β-[U-^{13}C]-L-fucose (~2.5mg) were dissolved in 50μL buffer and added to the reaction mixture, with every other addition a further aliquot of 50μL of the fucosyltransferase. This procedure was repeated in 12 hour intervals until all the *N*-acetyllactosamine (R_f 0.43) or sialylα2,3-*N*-acetyllactosamine (R_f 0.39) had been consumed (typically after 96 hours).

Purification was achieved by passing the reaction mixture through a Bio-gel P2 column at a temperature of 25°C, running 0.1M NH_4HCO_3 as eluant. The samples were extracted from the NH_4HCO_3 through repeated freeze-drying. The sialyl Lewis^x was obtained as the ammonium salt, and the Lewis^x and sialyl Lewis^x was confirmed by ^{1}H NMR (*figures 2.4 and 2.5* respectively) and mass spectrometry (data not shown).

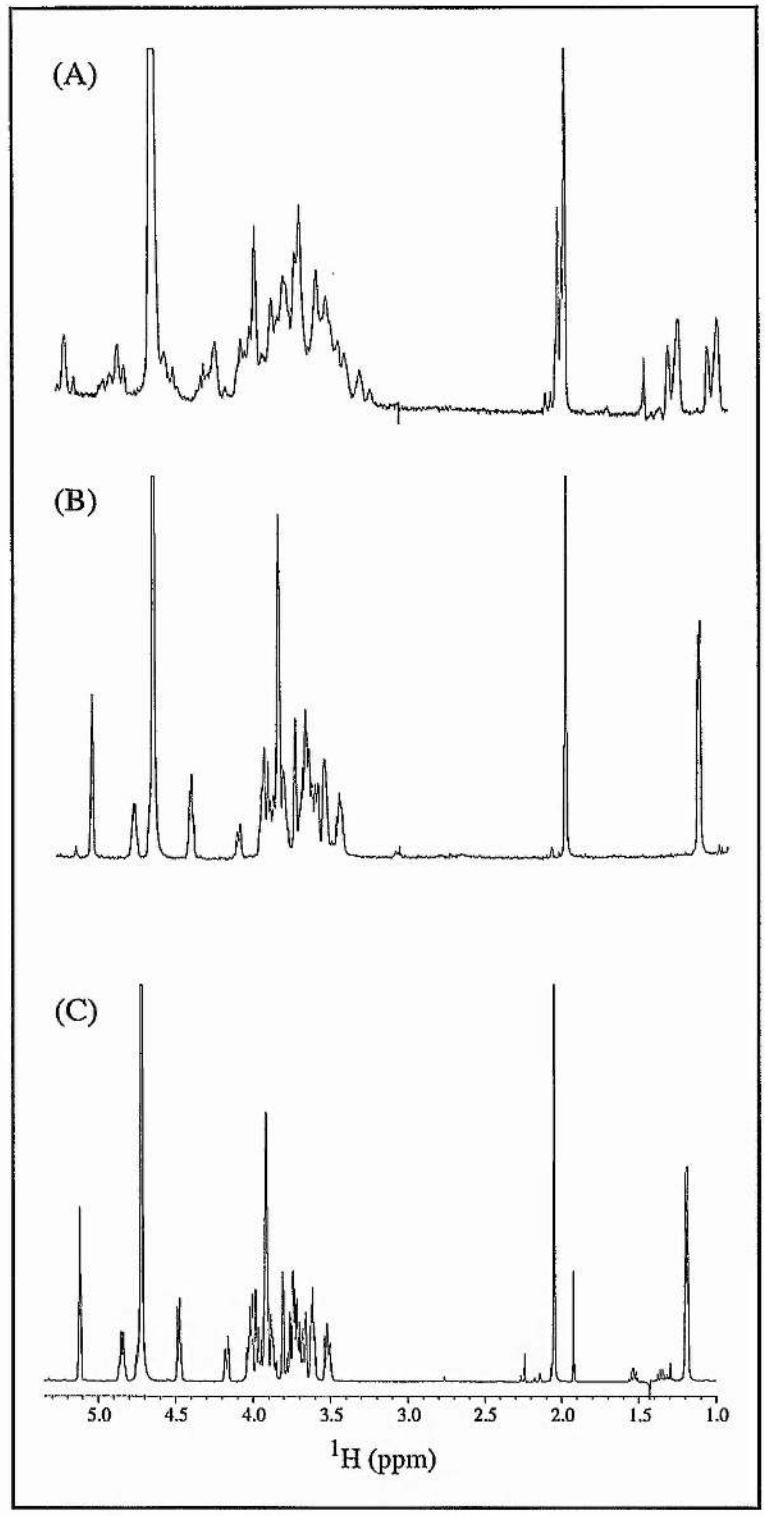

Figure 2.4 - (A) ^{1}H spectrum of [U-^{13}C]-Lewis^x. (B) ^{13}C-decoupled ^{1}H spectrum of [U-^{13}C]-Lewis^x. (C) ^{1}H spectrum of standard unlabelled Lewis^x (Dextra Labs.).

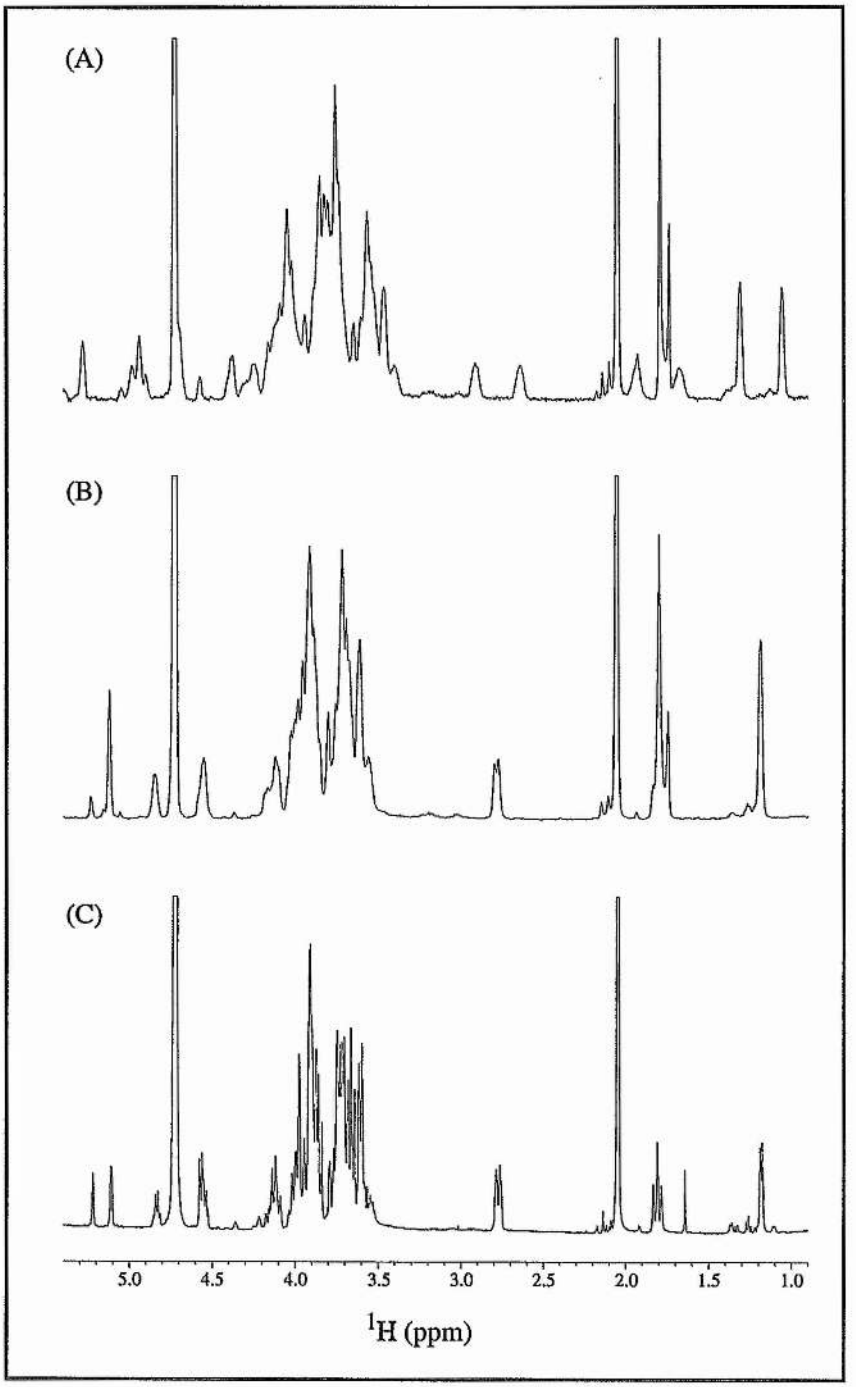

Figure 2.5 - (A) ^{1}H spectrum of [U-^{13}C]-sialyl Lewis^x. (B) ^{13}C-decoupled ^{1}H spectrum of [U-^{13}C]-sialyl Lewis^x. (C) ^{1}H spectrum of standard unlabelled sialyl Lewis^x (Dextra Labs.).

2.3 Results and Discussion

2.3.1 Chemical Synthesis of N-*acetyl [U-^{13}C] mannosamine*

The primary drawback in the chemo-enzymatic synthesis of [U-^{13}C] Neu5Ac is the poor yield and difficulties encountered in the purification of *N*-acetylmannosamine (ManNAc) from the base epimerisation of *N*-acetylglucosamine (GlcNAc). In order to circumvent these problems, an alternative chemical synthesis of [U-^{13}C] ManNAc (*Scheme 2*, performed by Dr. M. A. Probert) was employed (Probert *et al.*, 1997). Briefly, in the first step the α-methyl glucoside was converted from [U-^{13}C] glucose using methanol and Dowex AG-50-X8(H^+) followed by fractional crystallisation to separate anomers. The 4 and 6 hydroxyl groups were selectively protected by reacting II with benzaldehyde. The 2 position of III was activated by triflation (promoted by the favourable position of the 1-O-methyl group) followed by S_N2 displacement of the activated 2-OTf group with sodium azide to yield IV. Normally, the azide would be reduced followed by acid hydrolyses of the methyl mannoside to remove the methyl group, which also partially removes the *N*-acetyl group. Re-*N*-acetylated is achieved by acetylated all positions and then base hydrolyses of the *O*-acetyl groups. However, in this last step the ManNAc is base epimerised to GlcNAc. Therefore, an alternative strategy is required (*Scheme 2*), where methyl α-ManN_3 (IV) was converted to the benzyl α-ManNAc (VI). Upon hydrogenation both the glycoside and azide are reduced in one pot, with *N*-acetylation of resulting aminosugar, yields [U-^{13}C] ManNAc, avoiding the problems of above.

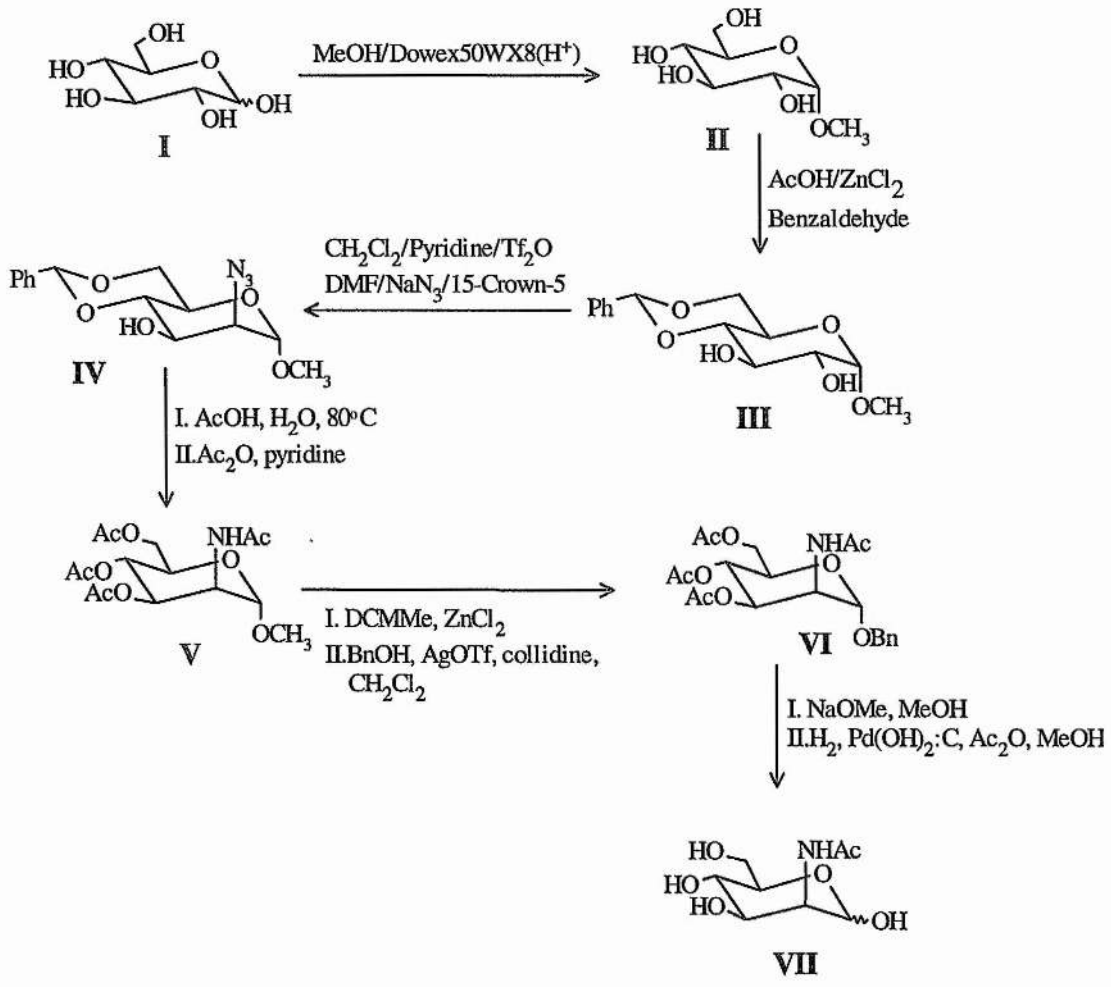

Scheme 2 - Chemical synthesis of *N*-acetylmannosamine (performed by Dr. M. A. Probert).

2.3.2 Enzymatic Synthesis of N-*Acetyl [U-^{13}C] neuraminic acid*

[U-^{13}C] Neu5Ac was produced using a simplified version of Whitesides' method (Simon *et al.*, 1988) for the production of CMP-Neu5Ac (*Scheme 3*). The equilibrium for this reaction lies with the reactants, so an eight-fold increase in pyruvic acid is required to push the reaction to completion. Unreacted ManNAc/GlcNAc was easily separated from the Neu5Ac by ion-exchange chromatography, however, unreacted [U-^{13}C] pyruvic acid could not be eluted off the column. The loss of [U-^{13}C] pyruvic acid is not prohibitive for the synthesis of milligram quantities of Neu5Ac, although alternative methods (Kragl, 1990) would be more applicable for large scale enzymatic synthesis of [U-^{13}C] Neu5Ac.

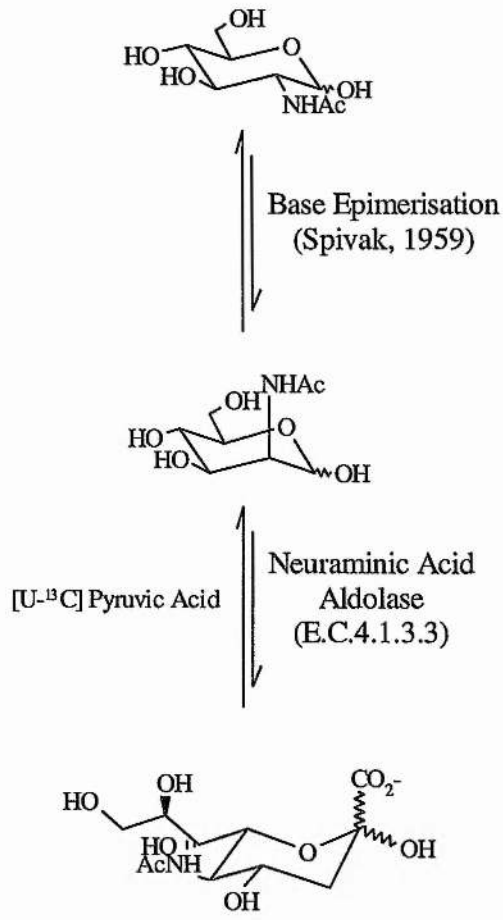

Scheme 3 - Base epimerisation of *N*-acetylglucosamine to *N*-acetylmannosamine followed by the enzymatic conversion to neuraminic acid.

2.3.3 Enzymatic Synthesis of N-*Acetyl [U-^{13}C] lactosamine*

Published methods for the synthesis of *N*-acetyllactosamine require nucleotide-sugar donor (UDP-galactose) and acceptor (GlcNAc) (Nunez and Barker, 1980). Using a method first described by Heidlas and co-workers (1992) and modified by Homans and co-workers (Gilhespy-Muskett *et al.*, 1994), UDP-[U-^{13}C]-Gal was synthesised very efficiently (*Scheme 4*). [U-^{13}C] Gal and ATP are enzymatically catalysed by galactokinase to yield galactose 1-phosphate and ADP, where the equilibrium lies strongly to the products. The galactose 1-phosphate is then converted to UDP [U-^{13}C] Gal by galactose-1-phosphate-uridyl transferase utilising UDP-glucose. Although, the formation of UDP [U-^{13}C] Gal is only about 50%, the equilibrium is driven over to the products by the addition of galactosyltransferase and [U-^{13}C]-GlcNAc, which employs the UDP [U^{13}C] Gal in the

production of *N*-acetyllactosamine. Galβ1-4[U-^{13}C, 50%-^{2}H]Glc was made in an analogous way except that unlabelled UDP-Gal (Sigma) was used, and the regulatory protein α-lactalbumin was required for the reaction to proceed quickly and to completion. Purification of *N*-acetyllactosamine from GlcNAc was achieved by using Bio-gel P2 gel filtration resin.

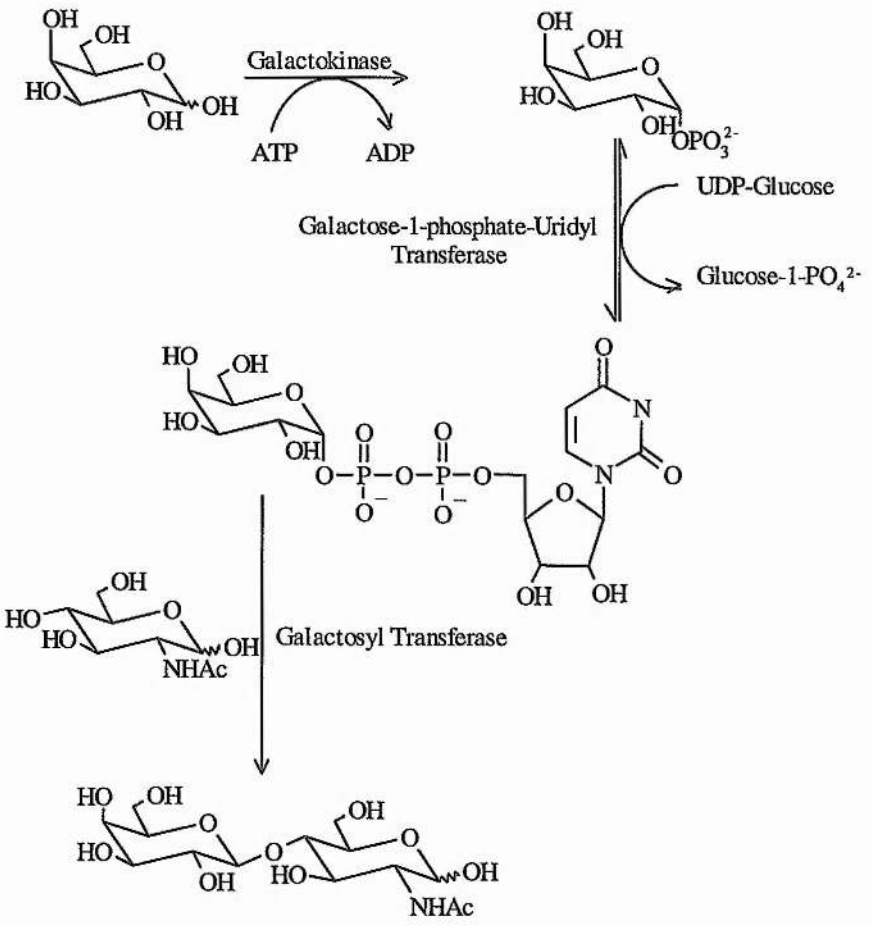

Scheme 4 - Schematic representation of the enzymatic synthesis of *N*-acetyllactosamine. UDP-Gal is made *in situ* and is driven to completion by the transferring of Gal to GlcNAc to synthesise *N*-acetyllactosamine.

2.3.4 Enzymatic Synthesis of Sialylα2,3-N-Acetyllactosamine

Enzymatic sialylation using sialyltransferases, which catalyse the transfer of sialic acid from CMP-Neu5Ac to an acceptor, have been employed to produce sialylated oligosaccharides (Ichikawa *et al.*, 1992; Kittelmann *et al.*, 1992; Lin-Chun Liu *et al.*, 1992). However, the use of sialyltransferases requires a stoichiometric reaction of sugar-nucleotide and acceptor, requiring separate preparation of the sugar-nucleotide and suffers from inhibition by the nucleotide mono-phosphate released. This was overcome by Wong and co-workers, who developed an efficient *in situ* regeneration system (Ichikawa *et al.*, 1992; Kittelmann *et al.*, 1992; Lin-Chun Liu *et al.*, 1992), allowing sialylα2,3-*N*-acetyllactosamine to be synthesised, although in relatively poor yield (<20%). An alternative strategy is to use *trans*-sialidases which transfer Neu5Ac from an α2,3-sialylated oligosaccharide and not the normal donor, CMP-Neu5Ac. Scudder *et al.* (1993) showed that the enzyme could transfer Neu5Ac from synthetic α-sialosides, such as 2-O-(*p*-nitrophenyl)-Neu5Ac. Despite *p*-NP-Neu5Ac being a rather kinetically poor substrate for *trans*-sialidase, it is easily chemically synthesised in high yield (*Scheme 5*, performed by Dr. M. A. Probert). The enzyme *trans*-sialidase has been expressed in *E. coli* (Harrison *et al.*, 1997) and the crude cell lysate coupled with the substrate *p*-NP-Neu5Ac was sufficiently active for the enzymatic synthesis of sialylα2,3-*N*-acetyllactosamine on the milligram scale in high yield (~75%).

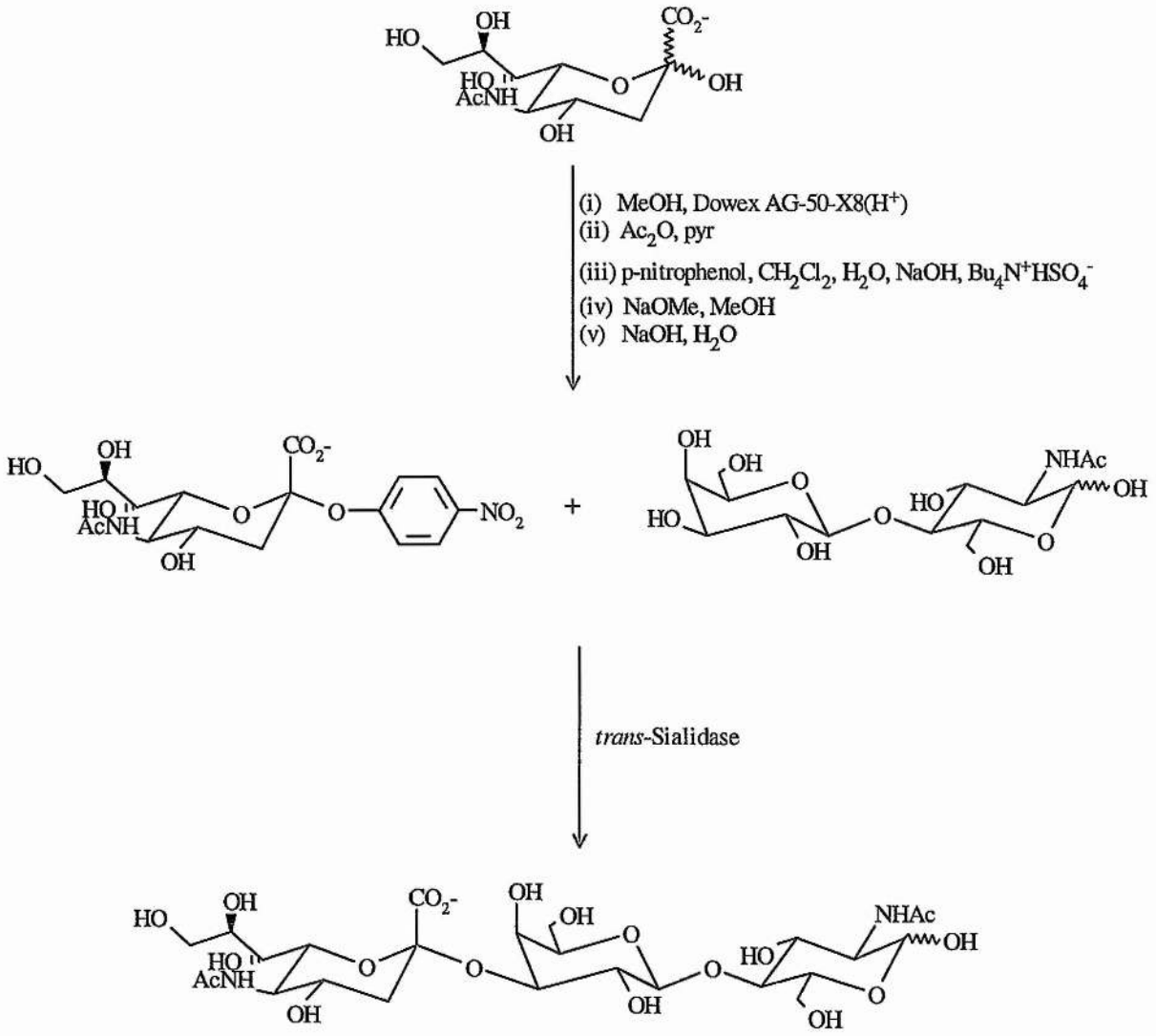

Scheme 5 - Chemo-enzymatic preparation of sialylα2,3-*N*-acetyllactosamine. The chemical synthesis of *p*-NP-Neu5Ac from Neu5Ac was performed by Dr. M. A. Probert.

2.3.5 Enzymatic Fucosylation

Fucosylation is often the final step in the biosynthetic pathway of oligosaccharides, and it has been proposed that the levels of fucosyltransferase activity plays an important role in intracellular recognition (Varki, 1993). Fucosyltransferases catalyse the transfer of L-fucose to an acceptor form guanidine 5'-diphospho-β-L-fucose (GDP-Fucose). Two enzymatic regeneration schemes for the synthesis of GDP-fucose have been proposed (Ichikawa *et al.*, 1992). One involving the natural biosynthetic pathway (where GDP-mannose is converted into GDP-Fuc), and the other based on a salvage route where the levels of GDP-Man are too low and involve conversion of Fuc to GDP-Fuc. However, all of the enzymes required for these synthesis are not commercially available therefore a chemical synthesis of GDP-Fuc has been utilised which is based largely upon literature methods (*Scheme 6*).

Essentially L-galactose is protected to allow selective bromination of the six position, which can be catalytically hydrogenation to yield protected L-fucose. Fucose-1 phosphate is then produced by bromination of the 1 position followed by substituting the bromine by phosphate activated by silver carbonate. The coupling of fucose 1-phosphate with an activated guanosine 5'-monophosphate derivative, GMP-morpholidate, yields GDP-β-L-fucose (*Scheme 6*, Dr. M. A. Probert).

Enzymatic transfer of fucose to both Galβ1-4GlcNAc and Neu5Acα2-3Galβ1-4GlcNAc using Lewis α(1,3/4)fucosyltransferase from human milk, kindly provided by Palcic and co-workers (Palcic and Hindsgaul, 1996), yielded milligram quantities of both Lewis^x and sialyl Lewis^x, respectively. The purification step by gel permeation chromatography was carried out at 25°C with degradation of products at higher column temperatures. The yields for these reactions were relatively low (~5% and 25% for synthesis of Lewis^x and sialyl Lewis^x, respectively), with the fucosylation of *N*-acetyllactosamine proceeding at a slower rate than the fucosylation of sialylα2,3-*N*-acetyllactosamine as expected (Johnson *et al.*, 1992).

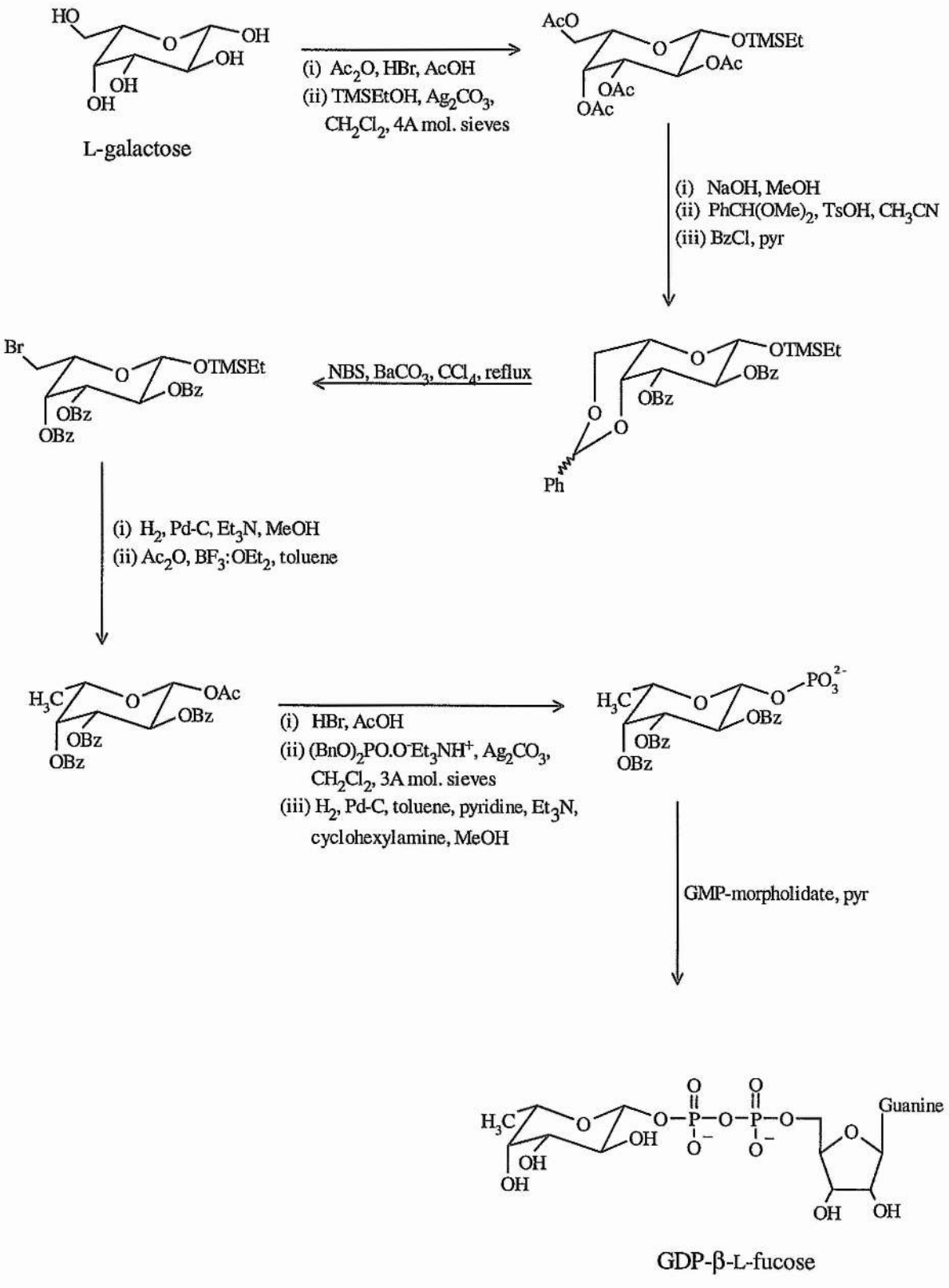

Scheme 6 - Chemical synthesis of GDP-β-L-fucose performed by Dr. M. A. Probert.

2.4 Conclusions

Uniformly carbon-13 labelled Neu5Ac has been synthesised using a predominately enzymatic route from [U-^{13}C] D-glucose via the chemically synthesised intermediate compound, *N*-acetylmannosamine. [U-^{13}C] GlcNAc and [U-^{13}C, 50%-^{2}H] glucose have been coupled to galactose in high yields via a one pot enzymatic synthesis to yield *N*-acetyllactosamine and lactose. Sialylα2,3-*N*-acetyllactosamine were produced by employing a novel enzymatic synthetic route utilising the enzyme *trans*-sialidase, which does not require the traditional sugar-nucleotide donor (CMP-Neu5Ac), but accepts a synthetic α-sialoside (*p*-NP-[U-^{13}C] Neu5Ac) as a substrate. Enzymatic fucosylation of both sialylα2,3-*N*-acetyllactosamine and *N*-acetyllactosamine yielded milligram quantities of both sialyl Lewis^{x} and Lewis^{x} oligosaccharides, respectively, allowing heteronuclear NMR investigations of the conformation and dynamics of these carbohydrates in free solution.

Chapter 3

Theoretical and Practical Aspects of Gaining Additional NMR Derived Restraints for Modelling of Oligosaccharides.

3.1 Introduction

Carbohydrates are now recognised as an important class of biological molecules which have diverse biological functions (reviewed by Varki, 1993), although knowledge of the primary structure of carbohydrates that produce specific functions is not well described. To understand the processes in which carbohydrates are involved the three dimensional structure of both the carbohydrate free in solution and when bound to its receptor, as well as the structure of the receptor is required. To date the most powerful methods in determining three dimensional structures are x-ray crystallography and NMR spectroscopy. X-ray crystallography is a powerful approach for the determination of the three-dimensional structure of the receptors, mainly proteins, but with regards to the carbohydrate conformations, it has proven to be less useful with few examples of crystal structures of either oligosaccharides free in solution or glycoproteins glycans. This limitation is presumably a product of the flexibility that carbohydrates exhibit in solution, with the examples of carbohydrate crystal structures limited to those that are bound to receptors, *e.g.*, proteins (for recent reviews of the literature see Vyas, 1991; Bundle and Young, 1992; Bourne *et al.*, 1993; Rice *et al.*, 1993; Woods, 1995; Weis, 1997), where the conformations are often 'frozen' out, or alternatively, oligosaccharides that are proposed to be rigid in solution *e.g.*, Lewis^x (Yvelin *et al.*, 1996). In contrast NMR is a useful complementary tool to X-ray crystallography because of the possibility to study oligosaccharides in solution (for recent reviews see Homans, 1990b; van Halbeek, 1994; Woods, 1995; Peters and Pinto, 1996; Imberty, 1997) and when bound to proteins (for review of current literature see Peters and Pinto, 1996; and for some examples see Cooke *et al.*, 1994; Scheffler *et al.*, 1995, 1997), whilst it is limited in the size of receptor that can be studied.

In solution, the individual monosaccharide rings of an oligosaccharide are essentially rigid and as such the three dimensional structure of oligosaccharides is defined in terms of the dihedral angles ϕ and ψ about the glycosidic linkages (*figure 3.1*). Therefore, the determination of the solution structure by NMR relies primarily on distance and angular restraints between contiguous monosaccharide units, derived from ^{1}H nuclear Overhauser effect (NOE) and three bond ^{1}H-^{13}C heteronuclear coupling constant measurements, respectively (reviewed in Homans, 1990b; van Halbeek, 1994).

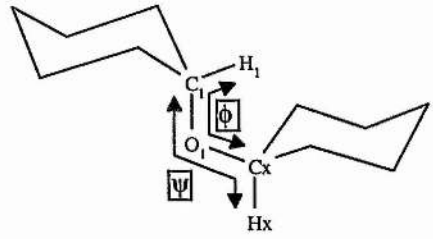

Figure 3.1 - Definition of ϕ and ψ for a generalised oligosaccharide linkage, such that ϕ = H1-C1-O1-Cx, and ψ = C1-O1-Cx-Hx.

NOE data are used in restrained molecular mechanics simulations to restrict the conformational space available to the dihedral angles, with back-calculation of the NOE data used to assess the proposed models. Unfortunately, the number of distance restraints is severely limited; typically it is possible to measure few NOEs, rarely exceeding three, and it can readily be shown that this is insufficient to distinguish between a model involving complete rigidity about the glycosidic linkage, and a model involving substantial torsional fluctuation (Rutherford *et al.*, 1993).

Extra restraints may be obtained in the form of heteronuclear coupling constants across the glycosidic linkage. The inclusion of these angular restraints in simulations would be of benefit. However, although appropriate parametrisations for the inclusion of angular restraints are appearing (Clore *et al.*, 1986; de Vlieg *et al.*, 1986; Kim and Prestegard, 1990; Torda *et al.*, 1993), they have yet to meet widespread acceptance. Therefore, like in the refinement of structures obtained by crystallographic methods, where 10% of the data is not used so as to assess the accuracy of the model, angular data is often used in assessing NMR derived structures as it is independent of the NOE data. This overcomes the often held criticism that the NOE data back-calculated from restrained models should inevitably agree with the experimental data, since the models are biased by the experimental data during the simulation, although owing to the r^{-6} dependence of the NOE, even with the tightest constraints there is considerable variation in the possible back-calculated NOE values.

As a model system to assess the impact of additional restraints derived in the present study, the sialyl Lewis^x antigen and the precursor carbohydrates in the synthesis of sialyl Lewis^x are used. Although the solution conformation of the sialyl Lewis^x antigen has been extensively

studied by a number of groups (Ball *et al.*, 1992; Ichikawa *et al.*, 1992; Lin *et al.*, 1992; Rutherford *et al.*, 1994; Poppe *et al.*, 1997) only nine inter-glycosidic distance restraints involving non-exchangeable protons (*figure 3.2A*), and three distance restraints involving exchangeable protons (*figure 3.2B*) (Poppe *et al.*, 1997), have been obtained, averaging to four restraints per linkage. Considering that a number of these NOEs about the Neu5Ac-Gal linkage are conflicting, suggesting a high degree of flexibility, with only one long range carbon-proton coupling constant available to assess the quality of any proposed models, it is apparent that this present situation is insufficient to describe the solution conformation of sialyl Lewis^x with any degree of confidence.

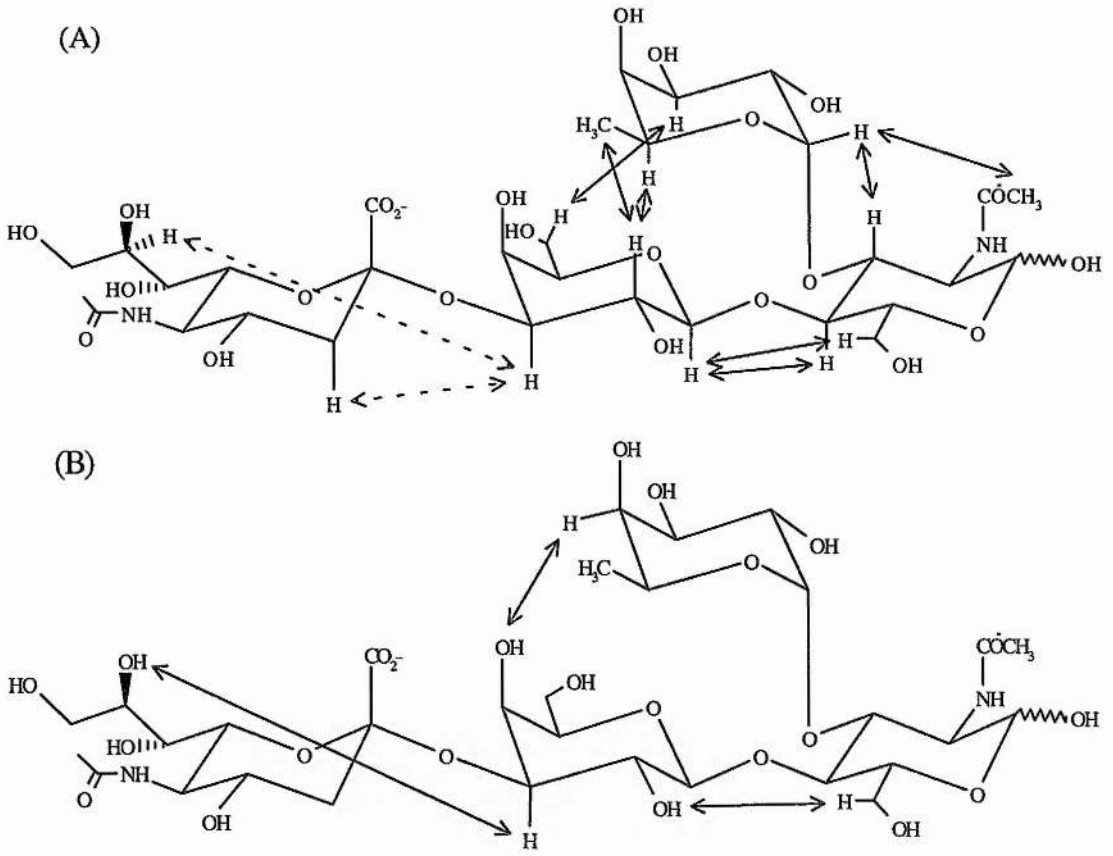

Figure 3.2 - Schematic representation of the NOEs observed in solution for sialyl Lewis^x between (A) non-exchangeable protons, and (B) exchangeable - non-exchangeable protons.

The application of ^{13}C labelling to assignment and conformational analysis is well documented for proteins and molecules involving nucleic acids. Similarly, for

oligosaccharides the incorporation of a ^{13}C label can be applied in the following manner. First, editing of homonuclear spectra into a third heteronucleus dimension resulting in an increased spectral dispersion allowing assignment of proton and carbon resonances, and more importantly, the unambiguous assignment of NOEs. Second, measurement of distance and angular data which directly involve the ^{13}C label, for example the measurement of heteronuclear NOEs and scalar carbon-carbon coupling constants, both of which are effectively impossible to measure without the high degree of ^{13}C enrichment.

In this present chapter theoretical and practical aspects of gaining extra restraints through ^{13}C labelled oligosaccharides and low temperature studies involving exchangeable protons are discussed with examples on the carbohydrates Galβ1-4Glc(NAc) (lactose, and *N*-acetyllactosamine).

3.2 Distance Restraints

The determination of the three-dimensional structure of carbohydrates has relied heavily upon the ^{1}H-^{1}H NOEs, because it is the primary method available in NMR to derive information about the distance between two nuclei. Recent advances in NMR experiments have allowed smaller NOEs to be measured accurately (Stonehouse *et al.*, 1994; Stott *et al.*, 1997), but only nuclei less than ~5Å apart will produce an enhancement large enough for observation. In general, the only measurable inter-glycosidic NOEs involve the anomeric proton of the preceding residue, and with fluctuating inter-nuclear distances resulting in a time-averaged distance most appropriately assigned to a range of distances for the NOEs measured, it has often lead to ambiguity over the flexibility of carbohydrates. Therefore, any additional distance restraints that can be measured will be of value in determining the structure and dynamics of oligosaccharides in solution.

3.2.1 ^{13}C-Edited ^{1}H-^{1}H NOEs

Structural studies on oligosaccharides using high resolution ^{1}H NMR are plagued by the severe overlap of the majority of proton resonances (Vliegenthart *et al.*, 1983). Apart from rendering complete resonance assignment difficult if not impossible, there remains the problem of accurate quantitation of cross-peak intensities in experiments such as NOESY or ROESY (Bothner-by *et al.*, 1984; Bax and Davis, 1985) for use as structural restraints.

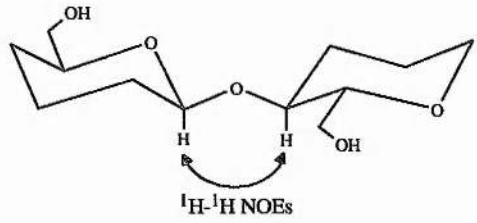

As a solution to this a number of homonuclear three-dimensional (3D) experiments have been proposed, where the NOE experiment (either ROESY or NOESY) is edited by a homonuclear through bond correlation dimension, *e.g.* COSY or HOHAHA, giving rise to experiments such as HOHAHA-NOESY (Vuister *et al.*, 1989) and ROESY-COSY (Homans, 1992). This approach is analogous to the methods applied to the resonance assignment of large proteins (Marion *et al.*, 1989), with the extension of the number of frequency dimensions from two to three, giving rise to increased spectral dispersion with respect to conventional two-dimensional NMR. However, even homonuclear 3D NMR experiments can suffer from spectral overlap, where two proton resonances reside at a single proton frequency, and a high digital resolution is still required because of this limited spectral dispersion. As an alternative, resonance overlap can in principle be overcome by application of heteronuclear 3D NMR methods, which offer improved spectral dispersion in comparison with their homonuclear counterparts in view of the fact that one or more dimensions in the 3D spectrum can represent the chemical shift of the heteronucleus. In the case of carbohydrates, although two or more proton resonances may overlap, it is often found that the carbons they are attached to have significantly dispersed chemical shifts. Therefore, heteronuclear 2D experiments, such as HSQC and HMQC, are an invaluable tool for deriving spectral assignments for carbohydrates.

^{13}C-edited NOESY experiments, for example NOESY-HSQC (Vuister *et al.*, 1989) and NOESY-HMQC (de Waard *et al.*, 1992) experiments, are potentially a rich source of

resolving additional information from NOE experiments, however the limitation up to now has been the low natural abundance of the carbon-13 nuclei rendering the experiments as only qualitative because of poor sensitivity (de Waard *et al.*, 1990).

In previous studies on sialyl Lewis^x at 500 MHz, cross-peak intensities in NOESY experiments are small or zero (Ichikawa *et al.*, 1992; Lin *et al.*, 1992), indicating that the condition $\omega\tau_c \sim 1$ is met, but can be overcome by using the rotating frame version, ROESY. In an analogous manner to that for editing the homonuclear NOEs into a third heteronuclear dimension, a ^{1}H-^{13}C ROESY-HMQC experiment has been proposed (Clore and Gronenborn, 1991). Surprisingly an equivalent experiment utilising the HSQC sequence has not been incorporated, and the 3D ^{1}H-^{13}C ROESY-HMQC experiment has been rarely used except for the stereospecific assignment of β-methylene protons and for measurement of NOEs to bound water.

The pulse sequence for the 3D ^{1}H-^{13}C ROESY-HSQC experiment, which is based on the ^{1}H,^{15}N ROESY-HSQC experiment, is shown (*figure 3.3*). Transverse ^{1}H magnetisation is initially generated which is modulated by the proton chemical shifts (t_1), whilst during the spin-lock period these transverse components cross relax. Transfer of this magnetisation to anti-phase transverse ^{13}C magnetisation via the INEPT sequence followed by mapping of the ^{13}C chemical shifts (t_2) and reverse INEPT sequence transferring magnetisation to observable ^{1}H magnetisation (t_3) gives rise to the 3D ROESY-HSQC sequence. During the reverse INEPT a gradient z-pulse, acting as a z-filter, is applied whilst the magnetisation of interest is of the form I_ZS_Z removing all magnetisation not aligned along the z-axis, such as any proton magnetisation not directly attached to a carbon (*e.g.* residual water).

Three-dimensional ^{1}H-^{13}C NOESY-HSQC and ROESY-HSQC experiments have been applied to edit the standard two-dimensional (R)NOESY spectra into a third ^{13}C dimension. As an example the ^{13}C-^{1}H (*F2F3*) HSQC plane from a three-dimensional NOESY-HSQC spectrum on [U-^{13}C] Galβ1-4Glc (lactose) at the proton chemical shift of Gal-H1 (*F1*) is shown (*figure 3.4*). In this plane, the diagonal peak observed in the NOESY experiment, appears as the one bond correlation between Gal H1 - Gal C1, and is of the opposite phase to a number of intra- and inter-residue correlations observed.

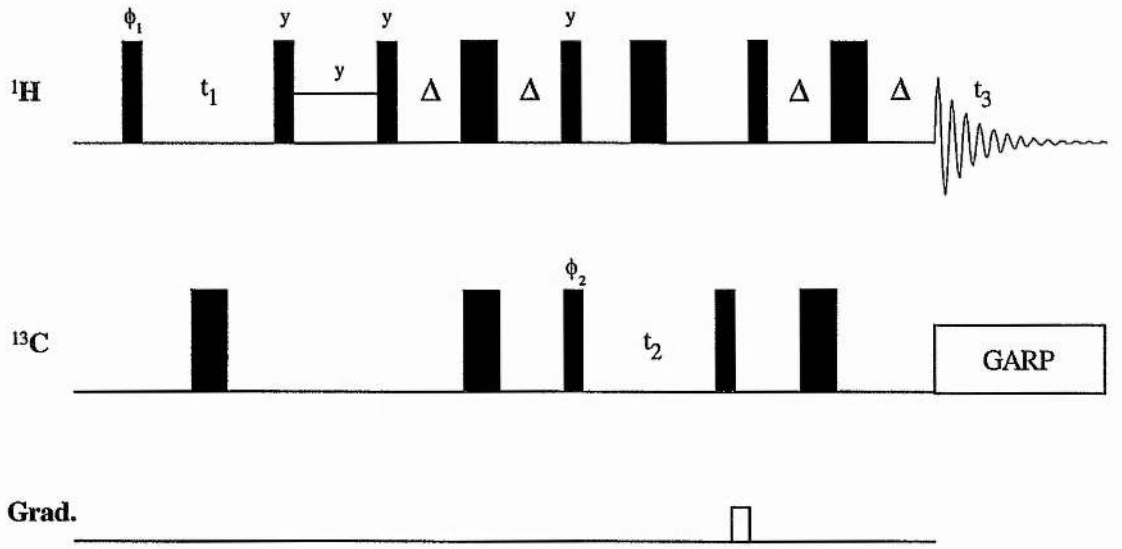

Figure 3.3 - 3D ROESY-HSQC pulse sequence. Narrow and wide bars represent 90° and 180° pulses respectively. Pulse phases are along x unless indicated otherwise. The spin-lock period is of the offset-compensated type to remove the offset dependence of the intensity of the ROE. The delay Δ is set to $1/4J_{CH}$, 1.65ms in practice. The gradient is applied to reduce artefacts derived from proton signals not directly attached to a carbon nuclei and is applied for 2ms at 9G/cm. Phase cycling is as follows: $\phi1$ = -x,-x,x,x; $\phi2$ = x,-x,x,-x, -x,x,-x,x; acq = x,-x,-x,x, -x,x,x,-x. These phase are incremented by 90° in the normal manner for quadrature detection in the *F1* and *F2* dimensions.

In the two-dimensional NOESY experiment the proton chemical shifts of Gal-H3 and GlcNAc-H4 are coincident which hinders the assignment and quantitation of the inter-glycosidic Gal-H1 - GlcNAc-H4 NOE. However, as can be seen in this HSQC plane, their respective carbons are sufficiently well resolved so that the contribution of each NOE to that observed in the 2D NOESY experiment can be determined by taking an *F1F3* NOESY slices through this HSQC plane editing out each NOE by its attached carbon chemical shift.

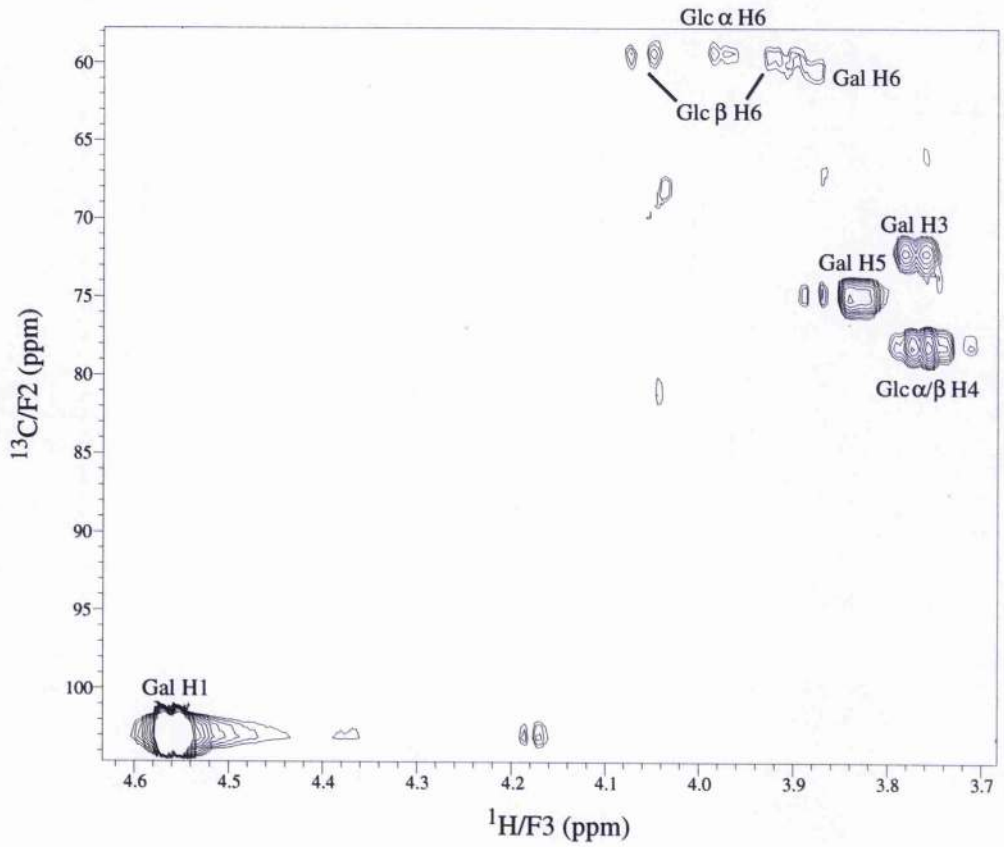

Figure 3.4 ^{13}C-^{1}H (*F2F3*) HSQC plane at the ^{1}H chemical frequency of Gal-H1 from a three dimensional NOESY-HSQC spectrum on [U-^{13}C] Galβ1-4Glc. Cross peaks are assigned.

3.2.2 ^{13}C-^{1}H NOEs

The enhancement of ^{13}C resonance intensities in small molecules on saturation of ^{1}H is well known. In the case of directly attached ^{13}C-^{1}H pairs, the enhancement is substantial and can reach the theoretical maximum of ~200%, resulting in a three-fold increase in ^{13}C resonance intensity (Neuhaus and Williamson, 1989). It has been successfully demonstrated in small molecules that heteronuclear Overhauser effects can in principle be measured for distances in the range of 0.1-0.4nm in a variety of ways (Kover *et al.*, 1980; Rinaldi, 1983; Yu and Levy, 1984; Kover and Batta, 1988; Neuhaus and Williamson, 1989; Neuhaus and van Mierlo, 1992; Stott and Keeler, 1996, and reviewed by Batta and Kover, 1987).

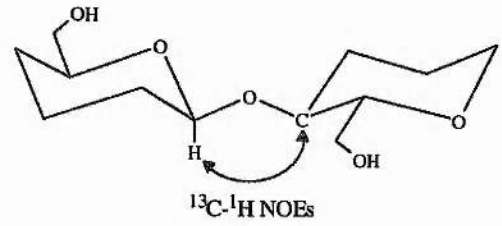

The inherent problem with the measurement of heteronuclear NOEs is that carbons with attached protons are efficiently relaxed by the proton, whilst three-spin effects arising from spin diffusion are of opposite sign to the direct NOEs. In a proton detected HOESY experiment on unlabelled lactose (*figure 3.5*), the heteronuclear NOEs observed at the carbon and proton chemical shift of Gal C1/H1 are of opposite phase to the direct one-bond heteronuclear NOE (Gal C1 - H1). These derive from a large direct homonuclear ^{1}H-^{1}H NOE (*e.g.* Gal H1 - Glc H4) followed by magnetisation transfer by the one bond heteronuclear NOE (*e.g.* Glc H4 - Glc C4). Simulations on lactose have shown that these three-spin effects have essentially identical fluctional dependence to the direct homonuclear NOE (Kiddle *et al.*, 1998), and therefore have no use in the conformational analysis of carbohydrates in this particular case, although these indirect effects in other cases have been utilised (Batta *et al.*, 1997). Therefore, the application of heteronuclear NOEs has been limited to one-bond NOEs for assignment (Rinaldi, 1983), for use in studying the dynamics of proteins, and measurement of long range NOEs to quaternary carbons (Poppe *et al.*, 1992).

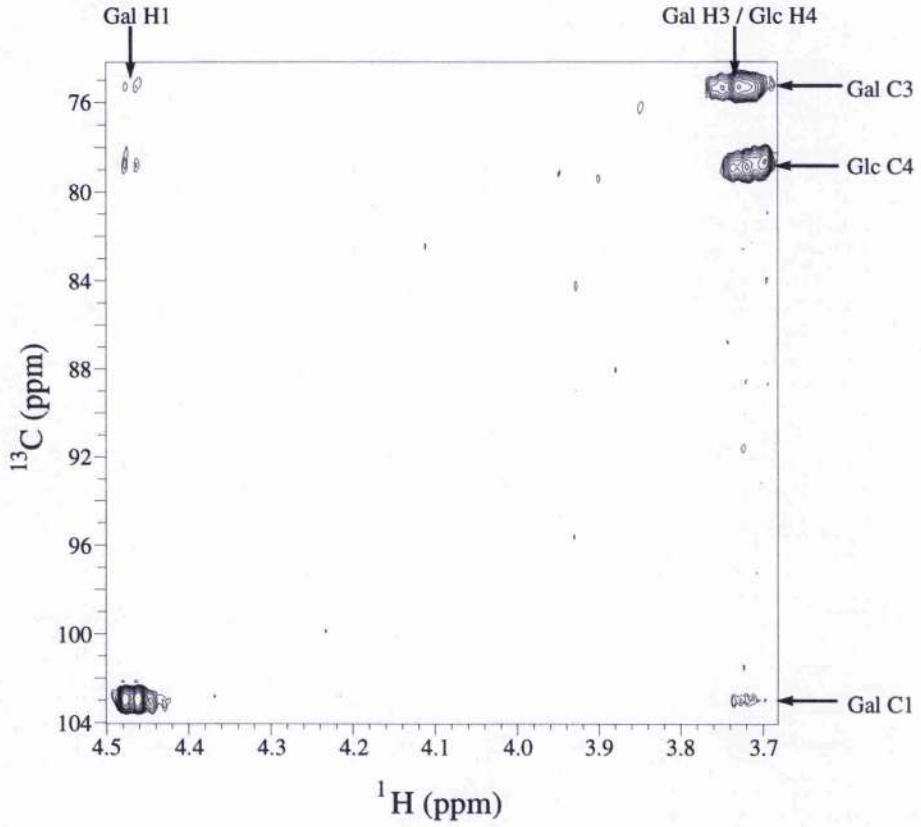

Figure 3.5 - Region of a two dimensional proton detected HOESY on unlabelled Galβ1-4Glc.

Considering that heteronuclear NOEs to carbons without directly attached protons are observable, it follows that a mechanism for improving this situation is by deuteration of one monosaccharide residue in an oligosaccharide. The advantage of deuteration is twofold, first, deuterons are less efficient than protons at relaxing the carbons they are attached to, and second, the homonuclear NOE and thus the three spin effects are removed. Hence it should be possible to measure inter-glycosidic heteronuclear NOEs. Owing to the difficulties in producing ^{13}C and ^{2}H labelled oligosaccharides, only [100%^{13}C, 50%^{2}H] Glc was available in this study. Although 100%^{13}C, 100%^{2}H labelled oligosaccharides would be ideal for testing the applicability of measuring heteronuclear NOEs, the present case is more practically applicable for the future. 50%^{2}H labelled samples allow the measurement of these heteronuclear NOEs and the acquisition of standard ^{1}H detected experiments on the one sample, thus avoiding the requirement of multiple samples of the same oligosaccharide but with different residues appropriately labelled. In the present case the labelled glucose can be incorporated into Galβ1-4Glc, and for the heteronuclear NOEs it is therefore only feasible to saturate protons in the galactose moiety and observe the ^{13}C spins in the Glc moiety.

Simulations of $^{13}C\{^{1}H\}$ steady state and reverse HOESY intensities with various mixing times for Glc-C4{Gal-H1} (*figure 3.6*) indicate that analogous to homonuclear ^{1}H systems (Neuhaus and Williamson, 1989), the 2D HOESY intensities are substantially smaller (<20 fold) than for the 1D steady state intensities, and reach maxima at times substantially shorter than steady-state measurements, suggesting that the 1D steady state NOE is the experiment of choice on grounds of sensitivity.

As discussed elsewhere (Stott and Keeler, 1996; Kiddle *et al.*, 1998), although the $^{13}C\{^{1}H\}$ steady state experiment provides a greater NOE the fact of ^{13}C detection means that the HOESY experiment with proton detection (inverse-HOESY) becomes more feasible on sensitivity grounds. However, a practical problem in the present case with the 50% ^{2}H enrichment is that direct heteronuclear NOEs and indirect NOEs (three spin effect) are of opposite sign and approximate magnitude (*see figure 3.7*) resulting in cancellation. Therefore, the following discussions are based upon the $^{13}C\{^{1}H\}$ steady-state experiment.

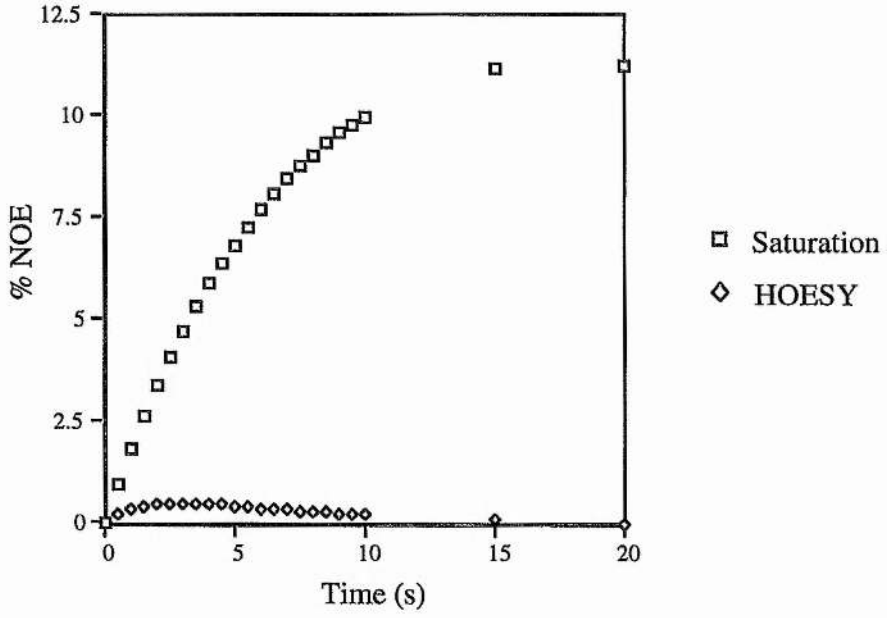

Figure 3.6 - Full relaxation matrix simulation of the Gal-H1 - Glc-C4 inter-glycosidic heteronuclear NOE in Galβ1-4[U-^{13}C,U-^{2}H]Glc. Time dependence of the steady-state (■) and transient HOESY (◆) NOE intensities experienced by Glc-C4 on saturation of Gal-H1.

Using a molecular dynamics simulation of 500ps and a rotational correlation time appropriate for a disaccharide (0.1ns), full relaxation matrix simulations accounting for the effect of only 50% ^{2}H labelling on the theoretical HOEs were preformed (*figure 3.7*). Although the deuteration of the detected carbon is necessary for the observation of a positive NOE, the size of the NOE is often also dependent on the deuteration of neighbouring carbons. Simulations for the observation of the heteronuclear NOE to Glc-C5, predict a small but practically unobservable NOE, whilst deuteration of C4 this NOE becomes experimentally measurable. Substantial trans-glycosidic NOEs are therefore, predicted between Gal-H1 and Glc-C3, C4, C5, and C6 under the appropriate conditions.

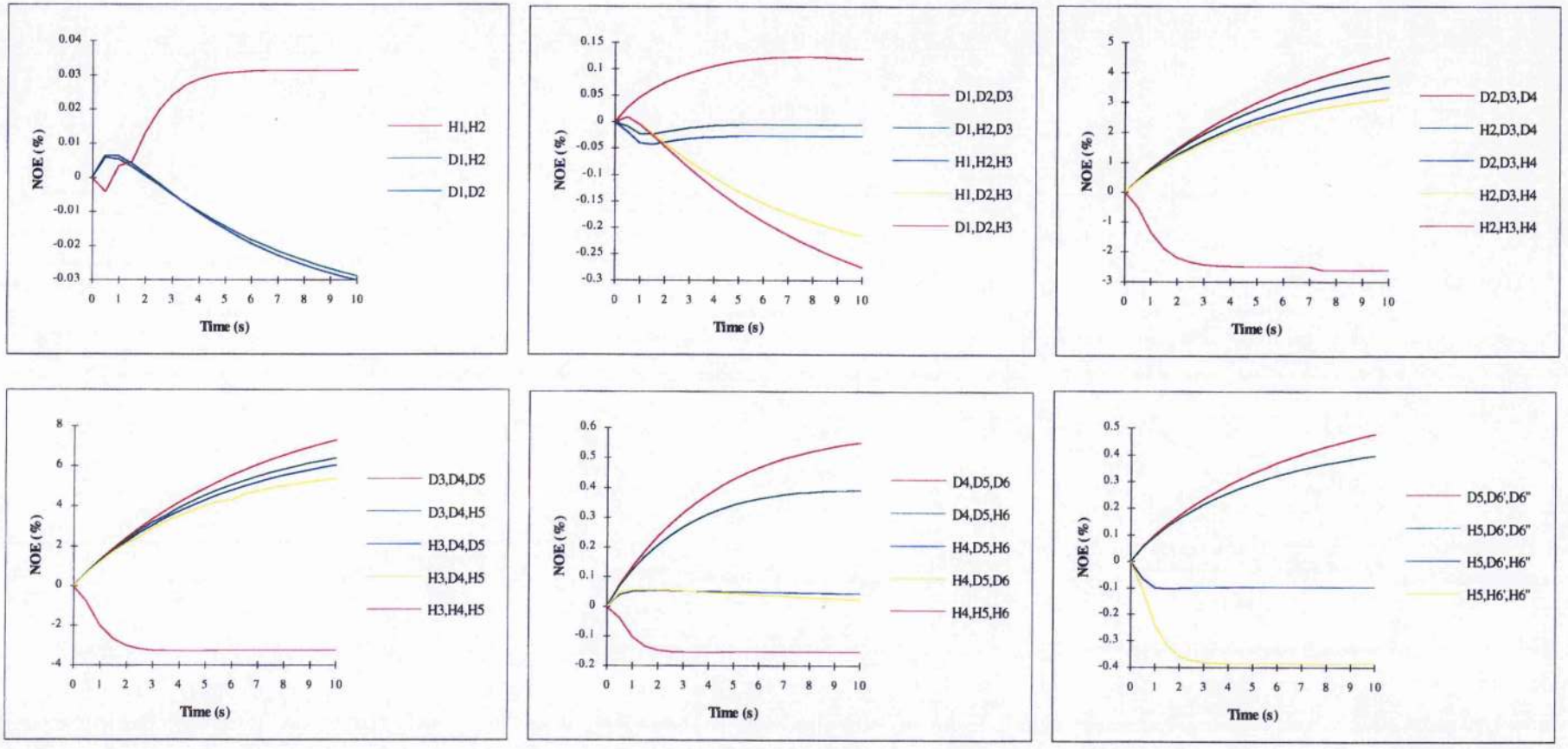

Figure 3.7 - Full relaxation matrix simulations of trans-glycosidic heteronuclear NOEs in Galβ1-4[50%^{2}H,100%^{13}C]Glc. Time dependence of the steady-state NOE intensities experienced by (a) Glc-C1, (b) Glc-C2, (c) Glc-C3, (d) Glc-C4, (e) Glc-C5, (f) Glc-C6 with deuteration/protonation of the carbon of interest and neighbouring carbons, on saturation of Gal-H1, based on molecular dynamics simulation of 510ps. A rotational correlation time of 0.1ns was used in all simulations using a proton resonance frequency of 500MHz.

Heteronuclear NOEs on Galβ1-4[100%^{13}C, 50%^{2}H]Glc were measured using the 1D steady state experiment with saturation of Gal-H1 during a 15s relaxation delay. The 1D ^{13}C NMR spectrum (*figure 3.8A*), ^{13}C difference spectrum without deuterium decoupling (*figure 3.8B*), and ^{13}C difference spectrum with deuterium decoupling (*figure 3.8*C) are shown for comparison. The line-widths in the deuterium decoupled spectrum are decreased in comparison to the difference spectrum without deuterium decoupling, owing to the removal of the ^{13}C-^{2}H couplings, and therefore is more practical for the measurement of any heteronuclear NOEs. The observation of an NOE to Glcβ-C1, which is not predicted, is an artefact of the saturation of Gal-H1, where Glcβ-H1 is also being partially saturated giving rise to a large one-bond heteronuclear NOE. The NOE to Glc-C4, predicted to be most intense, is observed, but is negative suggesting it is derived from the three spin effect. However, the fact that the line-widths are sharpened upon deuterium decoupling would suggest that this signal is derived from a carbon with an attached deuterium. The possibility that saturation of Glcβ-H1 contributes to a negative NOE can be ignored, with simulations (data not shown) showing that under every condition Glc-C4(D4) experiences a positive NOE. In contrast, a positive NOE is observed to Glcα/β-C6 which is surprising in light of the negative NOE to C4, as both H6's need to be deuterated to observe a positive NOE (*figure 3.7*). These conflicting results may be due to the problem of subtraction which plagues steady-state NOE experiments, although exactly the same results have been repeated. With this ambiguity over the results in using 50% ^{2}H labelled samples, the ideal situation for testing the applicability of measuring heteronuclear NOEs in carbohydrates is for all the carbons to be deuterated. Recently in this group Galβ1-4[~100%^{2}H,~100%^{13}C]Glc has been synthesised and a HOESY (Rinaldi, 1983) with proton detection was used to measure heteronuclear NOEs (Kiddle *et al.*, 1998) and as predicted by these simulations, NOEs to Glc-C3, C4, C5, and C6 were observed.

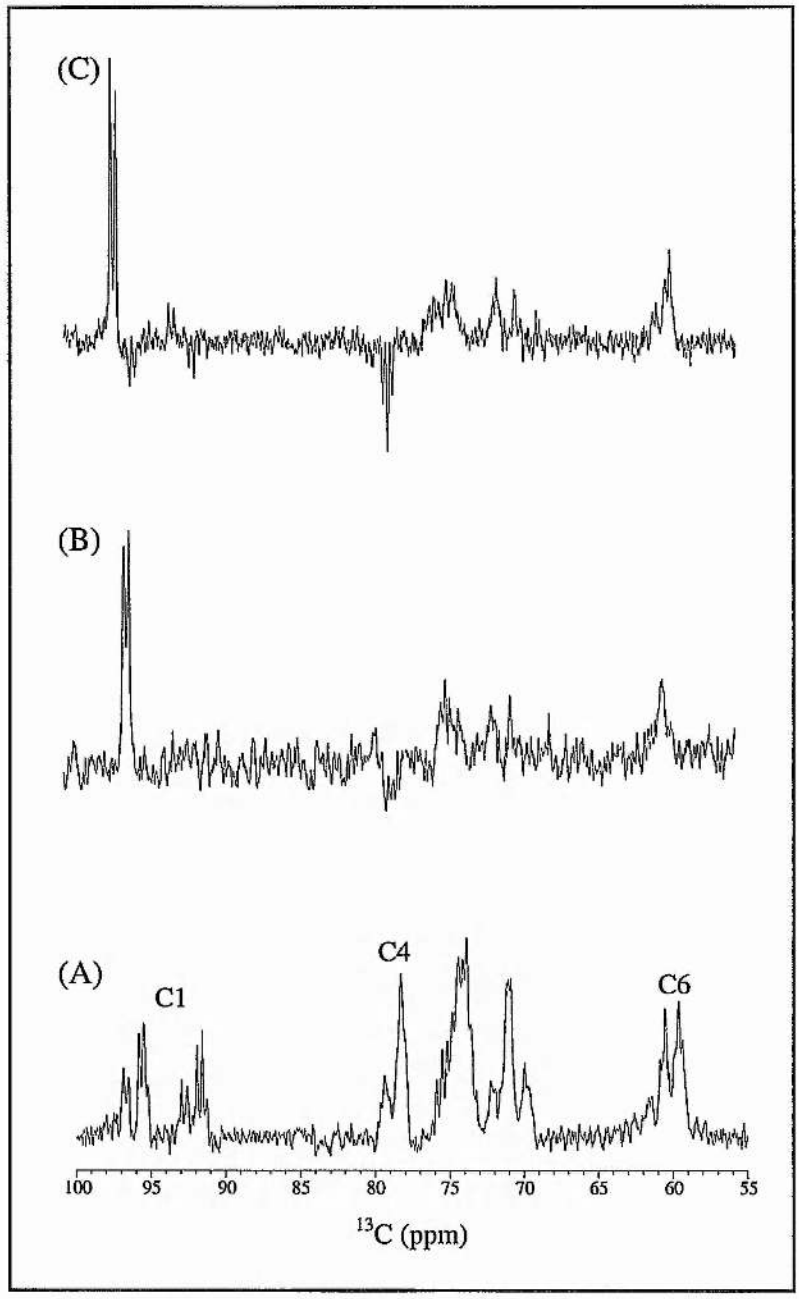

Figure 3.8 - (A) ^{13}C spectrum of Galβ1-4[50%^{2}H, 100%^{13}C]Glc. (B) ^{13}C difference spectrum upon saturation of Gal-H1 in Galβ1-4[50%^{2}H, 100%^{13}C]Glc without deuterium decoupling. (C) ^{13}C difference spectrum upon saturation of Gal-H1 in Galβ1-4[50%^{2}H, 100%^{13}C]Glc with deuterium decoupling.

3.2.3 NOEs to exchangeable protons

The application of exchangeable protons to assignment and conformational studies in carbohydrates is well documented (Dabrowski and Poppe, 1989; Acquotti *et al.*, 1990; Poppe and van Halbeek, 1991b; Poppe *et al.*, 1992; Sicinska *et al.*, 1993; Poppe and van Halbeek, 1994; Lynch *et al.*, 1996), with labile NH protons in aqueous solutions of proteins and nucleic acids being widely used (Wuthrich, 1986). Unfortunately, at room temperature in aqueous solutions of carbohydrates, the hydroxyl protons are in fast exchange, resulting in the hydroxyl proton signals resonating under the water resonance.

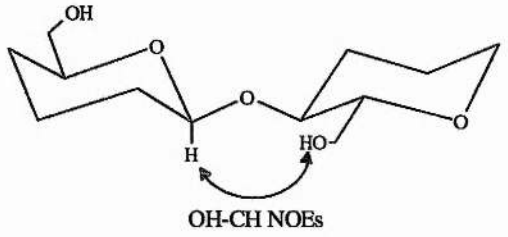

The utility of the hydroxyl protons in carbohydrates has been shown by the work in the Dabrowski group, where DMSO-d_6 has been used as solvent (Dabrowski and Poppe, 1989; Acquotti *et al.*, 1990; Poppe *et al.*, 1990a; Ejchart and von der Lieth, 1992; Dabrowski *et al.*, 1993), which allows the hydroxyl protons resonances to be readily observable at room temperature. The hydroxyl proton resonances are used as conformational probes, and allow additional inter-glycosidic NOE restraints to be derived for molecular modelling. However, there are major drawbacks with using DMSO-d_6. First, DMSO-d_6 is well known for assisting in the formation of hydrogen bonds, which can yield conformations about the glycosidic linkage not seen in aqueous solutions. For example, in Galβ1-3GlcOMe a hydrogen bond is observed between Gal-OH2 and Glc-OH4 which helps to drive the conformation into the anti-configuration about the glycosidic linkage, *i.e.* where the two glycosidic C-H bonds are turned from each other by 180° (Dabrowski *et al.*, 1995). Second, only small oligosaccharides are soluble in DMSO-d_6 limiting the use of this approach.

Work pioneered by Poppe and van Halbeek, initially in mixed solvent of H_2O and acetone (Poppe and van Halbeek, 1991b), and more recently pure water (Poppe and van Halbeek, 1994), overcame the fast exchange of the hydroxyl protons with water by cooling the solution to around 255K. At this temperature, the hydroxyl proton resonances are readily

observable with exchange rates around $10s^{-1}$ or less, which is sufficiently slow that narrow line-widths are obtained.

3.2.3.1 Sample Preparation

Recently an elaborate method for sample preparation has been published (Adams and Lerner, 1992) which, although allowing hydroxyl proton resonances to be observed, is very prohibitive for routine use. Using this as a starting point and working backwards to eliminate any steps which are not required, the following protocol was arrived at:

1) Dissolve the sample in water (this does not need to be distilled or de-ionised).
2) Adjustment of the pH to be in the range of 5-7.
3) Transfer to NMR tube/capillary and add any acetone as required.
4) Sonication for about 1 minute (this is used as a method for degassing).

This is the minimum amount of sample preparation required, although additional steps of cleaning NMR tubes and filtering samples to remove any particulate matter are advisable. The use of buffers would be preferable to allow accurate pH determination of the samples, however, with any significant salt content present in a sample the hydroxyl proton resonances were not observed. Even a small addition of TSP, for referencing of proton resonances obliterated all observation of the hydroxyl proton resonances, presumably by providing nucleation sites for catalysing exchange.

3.2.3.2 Variable temperature study of ^{13}C chemical shifts

For low temperatures to become applicable, the conformation adopted by the oligosaccharides cannot be different to those at physiological temperatures, otherwise this would render the determination of the conformation as irrelevant for biological situations. The effect of low temperature on the conformation of uniformly labelled ^{13}C Galβ1-4GlcNAc was investigated by the variation of ^{13}C chemical shifts, which are sensitive to changes in the 'virtual' conformation of oligosaccharides. ^{13}C chemical shifts were measured over a temperature range between 263 and 303K on a 100mM sample in water in a 1.7 o.d. capillary (which was inserted into a 5mm NMR tube with $CDCl_3$ acting as a lock solvent), where most resonances showed small, approximately linear, reversibly shift variations over this temperature range (*figure 3.9*), although the direction of change varied. Only the glycosylated carbon resonance had chemical shift differences ≥0.5ppm (down-field with

increasing temperature). Anomeric carbon resonances were generally insensitive to temperature.

Several groups have proposed correlations between glycosidic angles and ^{13}C chemical shifts. Bock proposed a linear relationship between the glycosidic dihedral angle ψ, and glycosylation shifts of both anomeric and aglyconic resonances in disaccharides containing α-Glc or α-Gal at the non-reducing terminus (Bock *et al.*, 1986). In general, for an aglyconic glycosylation shift of 1ppm there is a 5-10° shift in torsion angle, ψ.

In this study, the maximum variation of the ^{13}C chemical shifts for the aglyconic carbon was found to be 0.77ppm, indicating that although there is some small variation (<5°) in the torsion angle, ψ, measuring the conformation at low temperature is applicable to the physiological conformation of Galβ1-4GlcNAc.

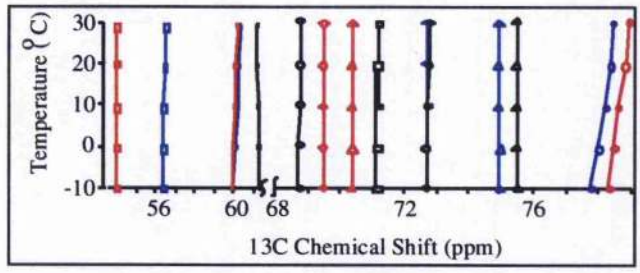

Figure 3.9 - ^{13}C Chemical Shift dependence on temperature (anomeric carbons not included). Red line represent GlcNAcα carbons; blue line represent GlcNAcβ carbons; and black lines represent Gal carbons. □ = C2, ◊ = C3, O = C4s, ∇ = C5, and × = C6

The measurement of ^{13}C chemical shifts over the same temperature range was repeated for a 100mM sample of Galβ1-4GlcNAc dissolved in H_2O/acetone-d_6 (85:15 v/v) in a 5mm NMR tube. Most resonances showed small, approximately linear, reversibly shift variations over this temperature range (data not shown), with only the glycosylated carbon resonances having chemical shift differences ≥0.5ppm (down-field with increasing temperature), but less than 1ppm. HSQC spectra for Galβ1-4GlcNAc in pure H_2O and H_2O/acetone, showed that the only significance difference (≥0.2ppm) in the chemical shifts between the two systems is restricted to 0.5 ppm for GlcNAcβ-C4, indicating that there is no significant difference in conformation in these two solvent systems (data not shown).

Due to the ease in sample preparation, and sensitivity of the experiments, the solvent mixture of H_2O/acetone (85:15) was chosen for all the following work in this study.

3.2.3.3 Optimisation of pH

One key aspect in the observation of the hydroxyl proton resonances is the pH of the sample. Previous studies have always used a pH of about 6.5 - 7, mimicking the physiological pH, however, Wuthrich *et al.* showed for low temperature studies on amino acids containing hydroxyl protons that the pH is critical on the exchange rate (Liepinsh *et al.*, 1992). Therefore, samples of lactose were made up according to the protocol described above except that the pH's were varied between 4.5 - 7.5. The exchange rates were measured at 268K and 256K, although at the latter temperature the variation of the exchange rates with pH is not so apparent as at the former temperature.

The variation of exchange rates with pH for a selection of the hydroxyl protons in lactose shows a general trend for the majority of the hydroxyl protons is for a minimum to be obtained in the exchange rates around pH 5.5 - 6 (*figure 3.10*). Exceptions to this are the hydroxyl protons at the reducing terminus of the glucose residue, which have a lower exchange rates at lower pHs around pH4. In light of this, the pH of the samples used for the low temperature studies were adjusted to around pH5.5 - 6.

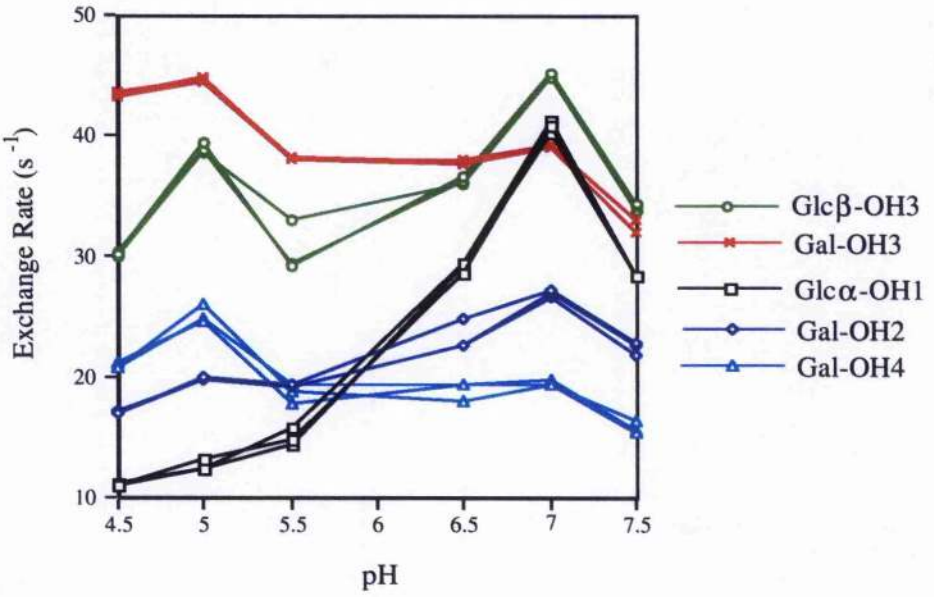

Figure 3.10 - Exchange Rates vs. pH for selected hydroxyl protons in lactose (measured three times) measured at 268K.

3.2.3.4 Water Suppression

A pre-requisite for the observation of the exchangeable proton resonances is an efficient method of suppressing the water signal. Water suppression in protein NMR is usually achieved by pre-irradiation of the water signal, however, saturation occurs resulting in transference to any protons in exchange with the water leading to a loss in sensitivity. Consequently, methods like jump return (Plateau and Gueron, 1982) and 1-1 echo (Sklenar and Bax, 1987b) have been used in previous studies on the hydroxyl protons of carbohydrates in aqueous solutions since they are frequency selective, and do not excite the water signal, resulting in no saturation transfer. Although these methods give good accumulated water suppression with phase cycling, in a single scan the water suppression is poor and the water signal amplitude restricts the receiver gain and the attainable S/N ratio.

Technical advances in probe design have introduced pulsed field gradients which can be used to dephase unwanted signals, and hence water suppression techniques using pulsed field gradients have been proposed, and among the most successful is the WATERGATE sequence (Sklenar *et al.*, 1993). In this method, a selective ^1H refocusing pulse which excites the region of interest, but not the water signal, is applied at the end of the pulse sequence. The insertion of gradients flanking this pulse ensures that the water signal is completely dephased while the signals excited by the selected pulse are unaffected. A more general approach to water suppression, termed Excitation Sculpting (ES), has been proposed by Hwang and Shaka (1995). Using a pulse scheme denoted by $A=G_1\text{-}S\text{-}G_1\text{-}G_2\text{-}S\text{-}G_2$, where S is any pulse sequence and G_1 and G_2 are gradients satisfying the condition that the application of G_2 does not refocus the magnetisation dephased by G_1, transverse magnetisation is returned to its original position by A. However, the amplitude of the signal is attenuated by a factor, P^2, where P is the probability that a spin is flipped by S ($P^2=0$ corresponds to the elimination of signal). Using S=(soft-180°x) - (hard-180°-x), the authors have demonstrated water suppression levels of >30,000-fold, where the soft 180°x pulse is selective for water.

An alternative approach in using pulse field gradients in water suppression is the selection of a particular coherence-transfer pathway, where the solvent signal is suppressed as it cannot undergo the selected pathway. Methods based on pulse field gradients in heteronuclear experiments are particular useful as the water can be purged by B_0 and gradient pulses whilst

the magnetisation lies on the heteronucleus, thus giving a high degree of water suppression and zero phase errors. This method is of particular use in protein NMR where the exchangeable protons (amides) are directly attached to an NMR active spin (*i.e.* ^{15}N). In the study of hydroxyl proton resonances this method of water suppression is less applicable because it does not allow for the hydroxyl resonances to be observed directly. However, in the correlation of non-exchangeables to exchangeable proton resonances (*e.g.* through space, or through bond), water suppression through coherence de-selection can be incorporated into three dimensional experiments necessary for the spectral editing of the non-exchangeable proton resonances, resulting in ^{13}C and -OH frequencies mapped in the indirect detected dimensions.

Although gradient methods that dephase water, or are used as purge pulses, result in a high degree of suppression, it has recently been shown that these methods allow magnetisation transfer between the dephased water and exchangeable protons, which decrease the intensity of the exchangeable proton resonances. Furthermore, saturation transfer can result in a significant decrease of the non-exchangeable proton resonances as well (Grzesiek and Bax, 1993; Li and Montelione, 1993; Stonehouse *et al.*, 1994b). During an experiment once the water protons become saturated (dephased) they will remain in this state because the repetition rate between scans is much more rapid than the longitudinal relaxation rate of the water ^{1}H spins. Consequently, it is important that gradient pulse that act as 'homospoils' be applied only when the water magnetisation is along the z axis, and that the magnetisation is returned to the +z axis before detection. Significant improvements in the S/N ratio of spectra that include such 'water flip-back methods' have been reported (Grzesiek and Bax, 1993).

So far these methods are limited to HSQC and NOESY-HSQC experiments, with HOHAHA and ROESY versions not being applicable because of the problem of attaining z magnetisation for water before the HSQC portion of the sequence. For smaller oligosaccharides at low temperatures where ROESY experiments are more applicable than NOESY experiments, it is impossible to circumvent the problem of saturation of the water resonance. Also, the gradient methods for homonuclear methods offer greater water suppression per single scan allowing better S/N ratios to be attained, which offsets the loss

by saturation transfer. So saturation of the water resonance is unavoidable in the present studies, and so needs to be considered in modelling NOEs to exchangeable protons.

3.2.3.5 Pulse sequences for the observation and measurement of NOEs to hydroxyl protons

With the possibility of observing hydroxyls protons in aqueous solutions appropriate NMR pulse sequences are required for the assignment an measurement of NOEs to these protons. Although homonuclear methods with 1-1 echo or jump return water suppression have been used, the relatively poor water suppression per single acquisition compared to the gradient techniques, means that pulse sequences incorporating these water techniques are needed. Whilst homonuclear sequences may be useful for smaller oligosaccharides, as the size increases so the severity of overlap in the non-exchangeable protons may result in ambiguity in assignment. With the availability of ^{13}C enriched carbohydrates editing 2D homonuclear NMR experiments into a third dimension to relieve this overlap is a possibility. Therefore, not only appropriate homonuclear techniques, but also heteronuclear pulse sequences are proposed for the observation and measurement of NOEs to exchangeable protons.

Homonuclear methods

Using the Excitation Sculpting water suppression technique, versions of the 2D experiments COSY, HOHAHA, NOESY and ROESY are proposed and illustrated (*figure 3.11*). Each sequence is identical to its respective conventional experiment, except the magnitude mode COSY experiment which incorporates soft 90° pulses on water of opposite phase to the following hard 90° pulse to keep the majority of the water signal along the z-axis throughout the sequence.

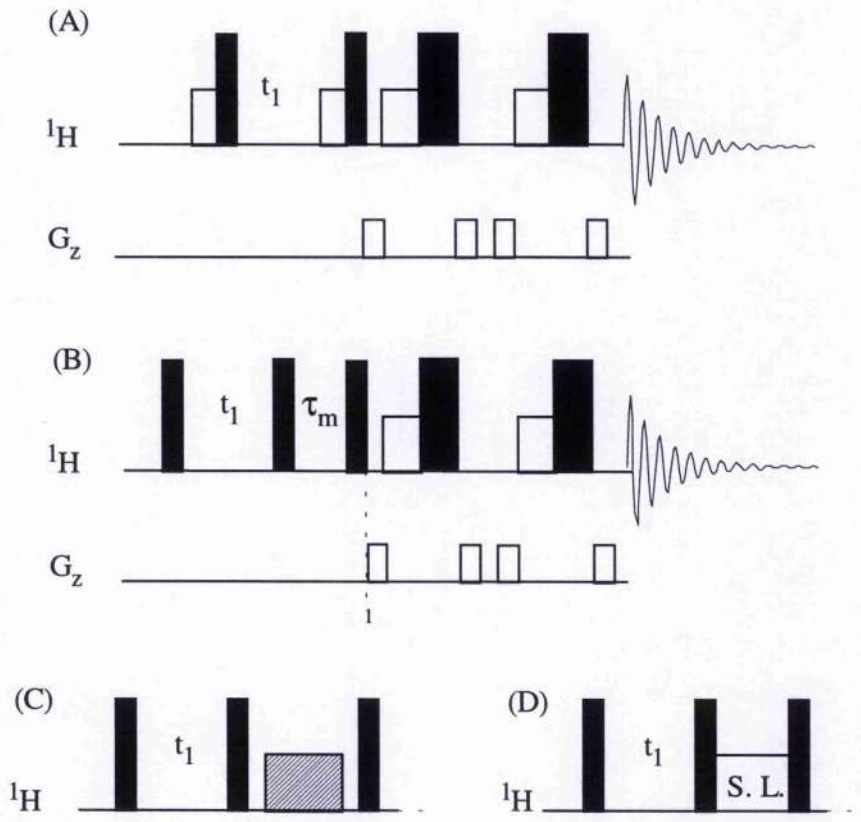

Figure 3.11 - Pulse sequences for the assignment and measurement of NOE/ROEs to exchangeable protons; (A) ES-COSY, (B) ES-NOESY, (C) ES-TOCSY, and (D) ES-ROESY. In (C) and (D) only the first part of the sequence is shown (upto point 1); the remainder is identical to (B). Filled narrow bars indicate 90° pulses and filled wide bars indicate 180° pulses, with open narrow bars representing soft selective 90° and wide open bars indicate selective 180° pulses on water. The spin-lock period in sequence (D) is of the offset-compensated type to remove offset dependence of the intensity of the ROE. The gradient duration and strengths are as follows: g1 = 500μs, 9G/cm; g2 = 800μs, 9G/cm. All pulse phases are the same as in standard sequences with the phases for the soft and hard π pulses being -x and x, respectively.

Heteronuclear methods

The pulse sequences proposed are illustrated, with each sequence identical to the conventional NOESY-HSQC (*figure 3.12A*), HOHAHA-HSQC (*figure 3.12B*), and ROESY-HSQC (*figure 3.12C*) sequences as far as point 1, and subsequently follow a common pathway. Transverse ^{13}C magnetisation ($2I_ZS_Y$) which is anti-phase with respect to the attached proton is refocused during the following interval 2δ, whose length is chosen to ensure refocusing of magnetisation from both methylene(C6) and methine(C1-C5) carbons. In-phase carbon magnetisation (S_x) is then rotated into the z axis by the first 90° ^{13}C pulse of phase y. During the time that the carbon magnetisation is along the z-axis, solvent suppression takes place using a proton purge pair which dephases the solvent signal due to the inhomogeneity of the B_1 field, together with a B_0 field gradient pulse g5, as originally described by Kay *et al.* (1993). Residual solvent magnetisations which is along the z-axis and unaffected by g5 is rotated into the transverse plane by the 90° ^1H pulse following the purge pulse pair, and is then dephased by g6. Longitudinal ^{13}C magnetisation is then rotated into the transverse plane by the second 90° ^{13}C pulse of phase y, followed by a dephasing period 2δ and finally reverse INEPT transfer to the directly attached proton.

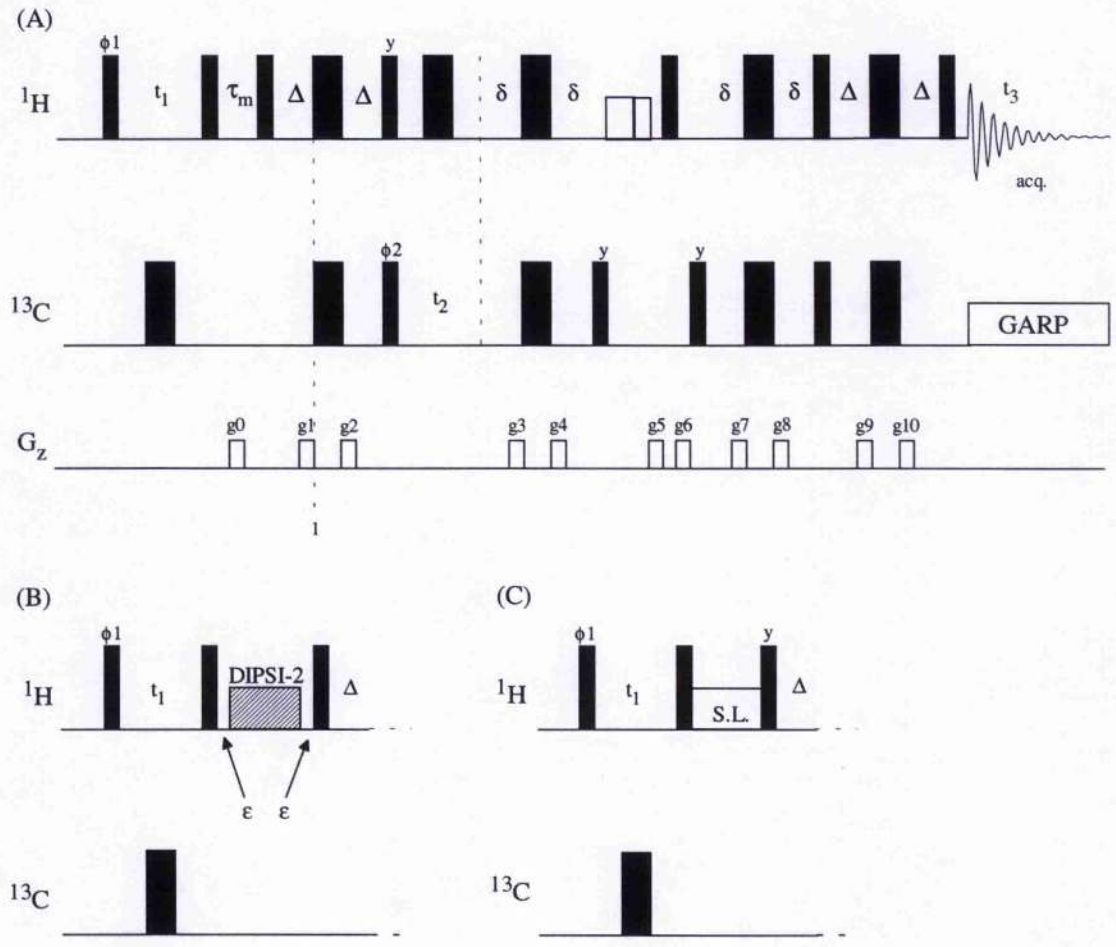

Figure 3.12 - Pulse sequences for (A) gd-NOESY-HSQC, (B) gd-HOHAHA-HSQC, (C) gd-ROESY-HSQC techniques described in the text. In (B) and (C) only the first part of the pulse sequences is shown; the remainder is identical to (A). Filled narrow bars indicate 90° pulse and filled wide bars indicate 180° pulses. Pulses are along the x-axis unless otherwise indicated. The spin-lock period in (C) is of the offset -compensated type (Griesinger and Ernst, 1987) to remove the offset dependence of the intensity of the ROE. The delay Δ is set to 1/4JCH, 1.65ms in practice, and δ=Δ/2 to insure efficient transfer for both methylene and methine protons, or δ=Δ to suppress signals corresponding to methylene protons in *F2*. The delay ε = 200μs. The proton purge pair (open bars) comprises 10kHz x and y pulses of duration 7ms and 4.3ms respectively. The gradient durations and strengths are as follows: g0 = 2ms, 8G/cm; g1 = g2 = g9 = g10 = 1ms, 8G/cm; g3 = g4 = g7 = g8 = 0.5ms, 8G/cm; g5 = 7ms, 12G/cm; g6 = 4.4ms, 12G/cm. Phase cycling for all experiments is as follows: ϕ1 = -x,x; ϕ2 = x,x,-x,-x; acq. = x,-x,-x,x. For quadrature detection in *F1* and *F2* incrementation by 90° of phases ϕ1 and ϕ2 respectively.

3.2.3.6 Quantification of NOEs

For the applicability of measuring NOEs to the hydroxyl protons at low temperatures, a method to quantify the NOEs and thus back calculate expected NOEs for possible conformations has to be developed. To predict the NOEs to exchangeable protons, two factors need to be considered other than the distance between the protons. First, the exchange rate of the exchangeable protons with the bulk water, and second, saturation of the exchangeable protons due to the water suppression technique.

Determination of the degree of saturation

The effect of exchange may be quantified by considering a two site exchange between protons I and S (Stonehouse, 1994), the forward and reverse exchange rates are denoted k_1 and k_{-1}, and the longitudinal relaxation rates of I and S are given the symbols R_I and R_S respectively. I_Z and S_Z represent the z-magnetisation of the OH protons and water, respectively, at a given time t. The water and the OH protons are assumed to be in equilibrium, such that $[I]k_1 = [S]k_{-1}$ and $k_1 \neq k_{-1}$, and the system may be summarised as:

$$I_0 \xleftarrow{R_I} I_Z \underset{K_{-1}}{\overset{K_1}{\rightleftharpoons}} S_Z \xrightarrow{R_S} S_0 \qquad [3.1]$$

where I_0 and S_0 represent the equilibrium Z-magnetisation of the OH protons and water respectively. The pair of coupled differential equations representing the above system was solved numerically using standard eigenvalue methods in order to simulate the recovery of I_Z under various conditions (Stonehouse, 1994). In summary, the longitudinal relaxation of the amide magnetisation no longer just depends on its own longitudinal relaxation rate but also depends on the rate of chemical exchange, the state of the water magnetisation and, if the water is not in equilibrium, on the longitudinal relaxation rate of the water. Therefore, for back calculation of the degree of saturation, the exchange rates and T_1's of the hydroxyl proton resonances is required.

The measurement of the hydroxyl proton exchange rates and T_1's can be measured or estimated fairly simply (see below), however, determination of the longitudinal relaxation rate of water is not so simple. Inversion recovery measurements of the T_1 of water is fraught with problems such as radiation damping which results in lower value of T_1 than

expected. As a solution, measurement of the 'effective' T_1 of water was achieved using a modified version of the gd-ROESY-HSQC sequence, where the final $\pi/2$ proton pulse was followed by a variable delay and additional $\pi/2$ proton read pulse to monitor the z component of the water magnetisation.

Determination of hydroxyl proton exchange rates and T_1's in water

The measurement of exchange rates for hydroxyl protons in carbohydrates is important not only in being able to quantify NOEs to hydroxyl protons, but also as an indication of possible involvement in intra-molecular hydrogen bonds. Chemical exchange is measured by saturation transfer, where irradiation of resonance A, involved in chemical exchange, causes a change in intensity of resonances B, because of transfer of saturation as a result of exchange. This is exactly analogous to the NOE, and chemical exchange rates have been measured using the NOESY pulse sequence, although in this context the experiment is called EXSY (for EXchange SpectroscopY). A simple ratio of the diagonal and off-diagonal peaks whilst varying the mixing time can give rise to the exchange rates.

Recently, an elegant 1D method based on the saturation experiment has been proposed for accurate measurement of proton exchange rates in aqueous solutions, where the exchange is purely with water molecules (Adams and Lerner, 1992). By the application of a 90° pulse, to equalise the water proton spin populations, followed by applying a spin lock pulse to maintain the equal populations, both selective on water, a pre-steady state saturation transfer experiment is obtained.

The major difference between this experiment and the standard truncated magnetisation transfer experiment (Wagner and Wuthrich, 1979) is the initial application of a rf-field pulse along x occurs when the water resides along the z-axis in the original experiment, but along the x-axis with the new experiment. The approach to steady state depends upon this initial state and has several important consequences (Johnstone and Little Jnr, 1995). First, the destruction of water magnetisation along both the z- and y-axes requires a finite time. Second, the water magnetisation is distributed between the z-axis and the spin lock axis, y, by differing amounts depending upon the irradiation time, making solvent suppression difficult. Third, the oscillatory behaviour of the water magnetisation is transferred to the hydroxyl protons. All of these difficulties are absent in the Adams and Lerner experiment.

Using this method, the exchange rate may be obtained by varying the length of the spin-lock time, with the decay time constant, τ_1, relating to the exchange rate, k, by:

$$\frac{1}{\tau_1} = \frac{1}{T_1} + k \qquad [3.2]$$

where T_1 is the spin-lattice relaxation time for the hydroxyl protons.

However, as the hydroxyl magnetisation does not decay to zero, but to a steady state value given by:

$$\frac{M_{zB}(ss)}{M_B^0} = \frac{\tau_1}{T_1} \qquad [3.3]$$

the exchange rate, k, and T_1's can be easily determined, although the values for the T_1's should only be taken as an estimate. In fact it was found that as $k \gg T_1$ as such it was impossible to gain an accurate measurement of the hydroxyl proton T_1's. As an estimate, these were determined by conventional T_1 measurements for the ^{13}C-enriched disaccharide in dimethylsulfoxide solution.

The exchange rates for the hydroxyl proton resonances in *N*-acetyllactosamine (pH 6.75) were measured with the original Adams and Lerner sequence incorporating the 1-1echo scheme for water suppression, and a modified version with the excitation sculpting water suppression method. Plots of ln(peak intensity) vs. spin lock time for two hydroxyl protons, GlcNAcα-OH3 and Gal-OH4, are shown for comparison of the raw data from both pulse sequences (*figure 3.14A*). Although the best fit line for both data give approximately the same gradient, and hence the same exchange rates, the data acquired with excitation sculpting as the water suppression technique gives a better fit to the line, as a result of the higher water suppression per single scan. The exchange rates measured at 256K using both methods (*figure 3.14B*), shows that the modified sequence has significantly more consistent values for the exchange rates, and as the values from both methods being of comparable magnitude indicating that the excitation sculpting method does not affect the size of the exchange rates, the exchange rates in the subsequent studies have been measured using the modified Adams and Lerner experiment.

(A)

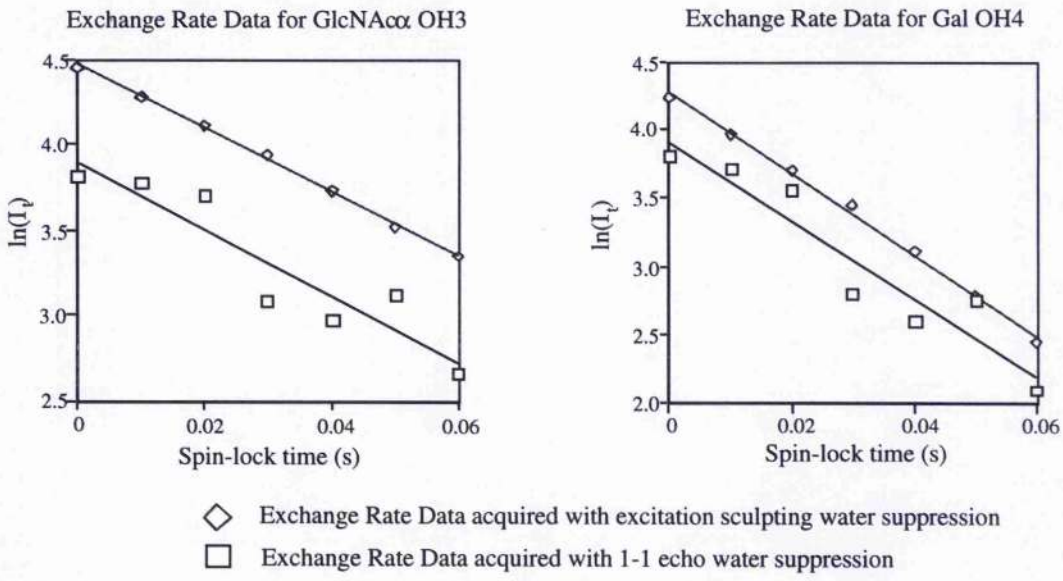

(B)

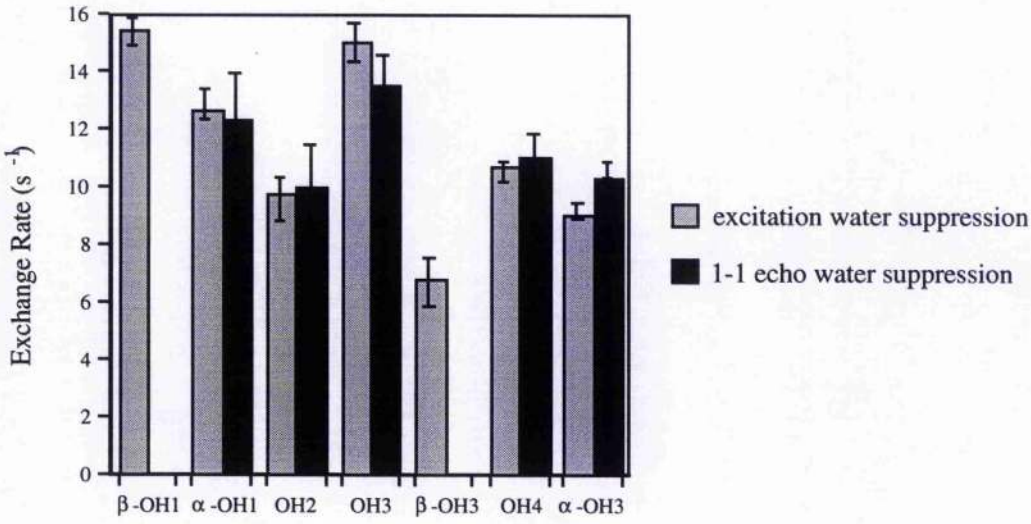

Figure 3.13 - (A) Plot of ln(peak intensity) vs. spin lock time for hydroxyl protons GlcNAcα OH3 and Gal OH4, with the gradient of the slope giving rise to the value of the decay time constant, τ_1.

(B) Exchange rates for the exchangeable protons in Galβ1-4GlcNAc measured with the Adams and Lerner approach with water suppression using excitation sculpting, and 1-1echo at 256K. Error bars are derived from measuring the exchange rates three times.

3.3 Angular Restraints

The measurement of three-bond or vicinal coupling constants can provide conformational information about the ring conformations and the glycosidic link in carbohydrates. Three-bond proton-proton coupling constants provide an insight into the ring conformation of furanosides, which are in conformational equilibria in solution, and have also been used to show that the glycerol side chain of *N*-acetyl neuraminic acid is in the extended conformation (Poppe and van Halbeek, 1991a; Poppe *et al.*, 1992; Siebert *et al.*, 1992). For 1-6 glycosidic linkages, $^{3}J_{HH}$ can give information about the important dihedral angle, ω, that describes the conformation about the C5-C6 bond. However, although $^{3}J_{HH}$ can provide some conformational information, it is limited to few cases for pyranoses, so heteronuclear $^{n}J_{CH}$ and homonuclear carbon-carbon couplings are of particular interest. Three-bond proton-carbon coupling constants directly define an average value for ϕ_H and ψ_H torsion angles, whilst the application of $^{1}J_{CH}$ values have been shown to be conformationally dependent upon these glycosidic torsion angles (Tvaroska and Taravel, 1995), and the measurement of $^{n}J_{CC}$ values across the glycosidic linkage has also been used to provide information regarding the glycosidic linkage. These data are of particular importance because of their independence of NOEs, and so represent data which can be used to assess models describing the conformations of carbohydrates.

3.3.1 One Bond ^{1}H-^{13}C Coupling Constants

Early interest in $^{1}J_{CH}$ couplings focused upon the structural factors that affect the magnitude of the coupling, such as hybridisation, bond length, angle *etc.* In carbohydrates it was noted that an approximately 10Hz difference in the magnitude of the $^{1}J_{CH}$ for the anomeric proton-carbon in α and β anomers, providing a quantitative basis for determining the anomeric configuration of carbohydrates and for calculating the percentage of $^{1}C_4$ ring conformation present in solution for a particular pyranoside. Recently, the glycosidic conformation has been shown to dependent upon the value of $^{1}J_{CH}$ for both the anomeric and aglyconic carbon-proton couplings through theoretical calculations and a relationship has been proposed for each anomer (Tvaroska, 1991; Tvaroska and Taravel, 1995).

For the α linkage:

$$^{1}J_{C1H1} = 1.32\cos2\phi - 3.38\cos\phi - 1.05\sin2\phi + 1.27\sin\phi + 168.9 + 0.0390\varepsilon$$

$$^{1}J_{CxHx} = 1.02\cos2\psi - 1.81\cos\psi - 0.19\sin2\psi + 0.41\sin\psi + 145.4 + 0.0294\varepsilon$$

For the β linkage:

$$^{1}J_{C1H1} = 0.57\cos2\phi - 3.46\cos\phi + 1.63\sin2\phi - 1.53\sin\phi + 161.5 + 0.0390\varepsilon$$

$$^{1}J_{CxHx} = 0.01\cos2\psi - 1.08\cos\psi + 0.51\sin2\psi - 1.01\sin\psi + 145.1 + 0.0294\varepsilon$$

where ε is the dielectric constant for the solvent.

3.3.2 Three Bond ^{1}H-^{13}C Coupling Constants

Among the earliest methods to determine long range coupling constants, was that of Bax and Freeman (1982), who proposed a carbon detected variant of the 2D heteronuclear J-resolved experiment which employs a selective 180° proton pulse. Variations on this basic experiment have been introduced, including the use of DEPT to excite the carbons(Uhrin *et al.*, 1989) and the exploitation of the differences in the proton T_1 values for spectral simplification (Hricovini and Liptaj, 1989). More recently, Sklenar and Bax (1987a), have proposed modifications, which still use selective proton pulses, but allow for proton detection. Additional 1D experiments have been introduced, where the spectral dispersion of the second dimension is not required, based upon the semi-selective INEPT sequence, which uses heteronuclear detection (Uhrin and Liptaj, 1989).

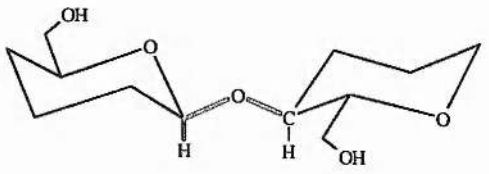

Long range correlation of chemical shifts depends upon the scalar coupling between correlated nuclei, thus, coupling constant data may be extracted directly from these experiments, for example, Bauer *et al* (1984). Crouch and Martin (1991) have developed a related method, by replacing the final carbon pulse in the HMBC experiment with a selective pulse, resulting in a 1D spectrum which is equivalent to a trace of the HMBC spectrum, which allows $^{3}J_{CH}$ involving quaternary carbons to be measured. Multiple bond

experiments have been used to measure the long range carbon-proton coupling constant directly from the long range correlation cross-peak (Rutherford *et al.*, 1994). In this experiment the active heteronuclear coupling is anti-phase in *F2*, whilst homonuclear couplings appear in-phase. This often leads to cancellation of the inner lines of the cross-peaks, but $^{3}J_{CH}$ values may be obtained if the homonuclear coupling constants are known.

Poppe and van Halbeek (1991a) have introduced a selective 1D method, which employs a selective excitation of a proton resonance well separated from other resonances, followed by transfer of magnetisation via isotropic mixing to the proton of interest. As a modification of this experiment, Adams and Lerner (1993) introduced selective carbon excitation for when the proton resonances occur in regions of overlap in the proton spectrum, as in the case of protons attached to glycosylated carbons in oligosaccharides. A further modification achieved elimination of the $^{1}J_{CH}$ and passive $^{n}J_{CH}$ couplings yielding a 1D spectrum with just the proton resonance of interest split by the specific $^{n}J_{CH}$ coupling and also $^{n}J_{HH}$ (Uhrin *et al.*, 1994).

Recently, many of the proposed experiments rely on the E.COSY approach (Griesinger *et al.*, 1986), where the coupling of interest to spin I is measured from the relative displacements of cross-peaks between two other spins both coupled to I. Long range couplings were determined by using the large one-bond proton carbon couplings to resolve what would otherwise be overlapped peaks (Montelione and Wagner, 1989). This has been extended to three- and four-dimensions (Sorensen, 1990), and this is most applicable to large molecules, such as proteins. The drawback of the E.COSY approach for carbohydrates is that unlike proteins, there are often many couplings to any particular carbon which over-complicates the analysis of the E.COSY multiplets.

Bax has developed an alternative approach, quantitative J correlation, which is based on the COSY principle (Bax *et al.*, 1994a). The value of the coupling constant is derived from the fraction of the magnetisation transferred "out and back" to its coupled partner, relative to the fraction that does not get transferred. This approach has been successfully used on proteins to determine a wide range of long range couplings (Bax *et al.*, 1992; Vuister *et al.*, 1993; Vuister and Bax, 1993), as well as on sialyl lactose to determine the $^{3}J_{CH}$ values (Zhu *et al.*, 1994).

Titman *et al.* (1989) used a fitting approach which compares two spectra, one where the active ^{1}H-^{13}C coupling is anti-phase (so called COSY-type peak) and the other where the active coupling is in-phase (so called TOCSY-type peak). Practically, two separate spectra have to be measured where care must be taken to acquire each spectrum in exactly the same way so as to assure that the couplings involved are identical in each spectra. As an improvement of this method, Ionides *et al.* (1995) have proposed a constant time heteronuclear COSY experiment for [U-^{13}C] labelled samples (*figure 3.14*) which allows acquisition of both type of cross-peaks in the one experiment, overcoming previous experimental problems, and this is the approach used in the present study.

A section of the 2D constant time long range carbon-proton (CT-LRCH) correlation experiment on [U-^{13}C] Galβ1-4Glc is shown with the two 1D slices through the areas boxed corresponding to the one bond correlation Gal-C1 - H1 and the long range correlation Gal-H1 - Glcα/β-C4 (*figure 3.15*). The one bond correlation corresponds to the TOCSY-like cross-peak with the three bond coupling in-phase, whilst the long range correlation corresponds to the COSY-like cross-peak with the three bond coupling anti-phase. Obviously, in this particular example, the $^{3}J_{CH}$ coupling can be easily measured straight from the spectrum, however even in this simple example the judgement of where to measure the coupling is subjective, and in the case where $^{3}J_{HH} \approx {}^{3}J_{CH}$ such that the inner multiplets are absent, the better approach is to use a data fitting method. In the present case, the appropriate data fitting approach is that described by Titman *et al.* (1990) where the 1D spectrum corresponding to the TOCSY-type is multiplied by an anti-phase coupling, and the COSY-type peak multiplied by an in-phase coupling. Subsequent comparison of the two resulting spectra followed, if necessary, by remultiplication with a different coupling is repeated until a suitable match is obtained, with the final value representing the experimental $^{3}J_{CH}$ value.

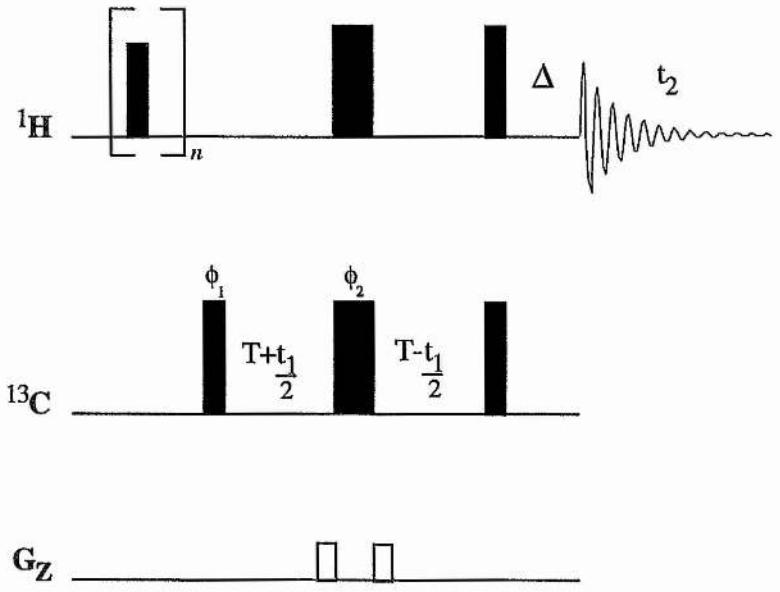

Figure 3.14 - Pulse sequence for the constant time heteronuclear COSY experiment (CT-LRCH) for measuring long range carbon-proton couplings. Narrow and wide bars represent 90° and 180° respectively. The initial proton train separated by a 100μs delay was used to build up an NOE to the carbons to increase the sensitivity of the experiment. The constant time period (2T) was set to $1/4J_{CC} \approx 1/J_{CH}$, where in practice T = 13.13ms, and the delay $\Delta = 1/4J_{CH}$, 1.65ms in practice. Gradients were applied either side of the central simultaneous 180° pulse to reduce the effects of imperfect pulse lengths, and were set to 100μs, 9G/cm. All pulse phases were x unless otherwise indicated and were as follows: $\phi1$ = x,-x; $\phi2$ = x,x,y,y,-x,-x,-y,-y; acq = 2(x,-x,-x,x) (Ionides *et al.*, 1995).

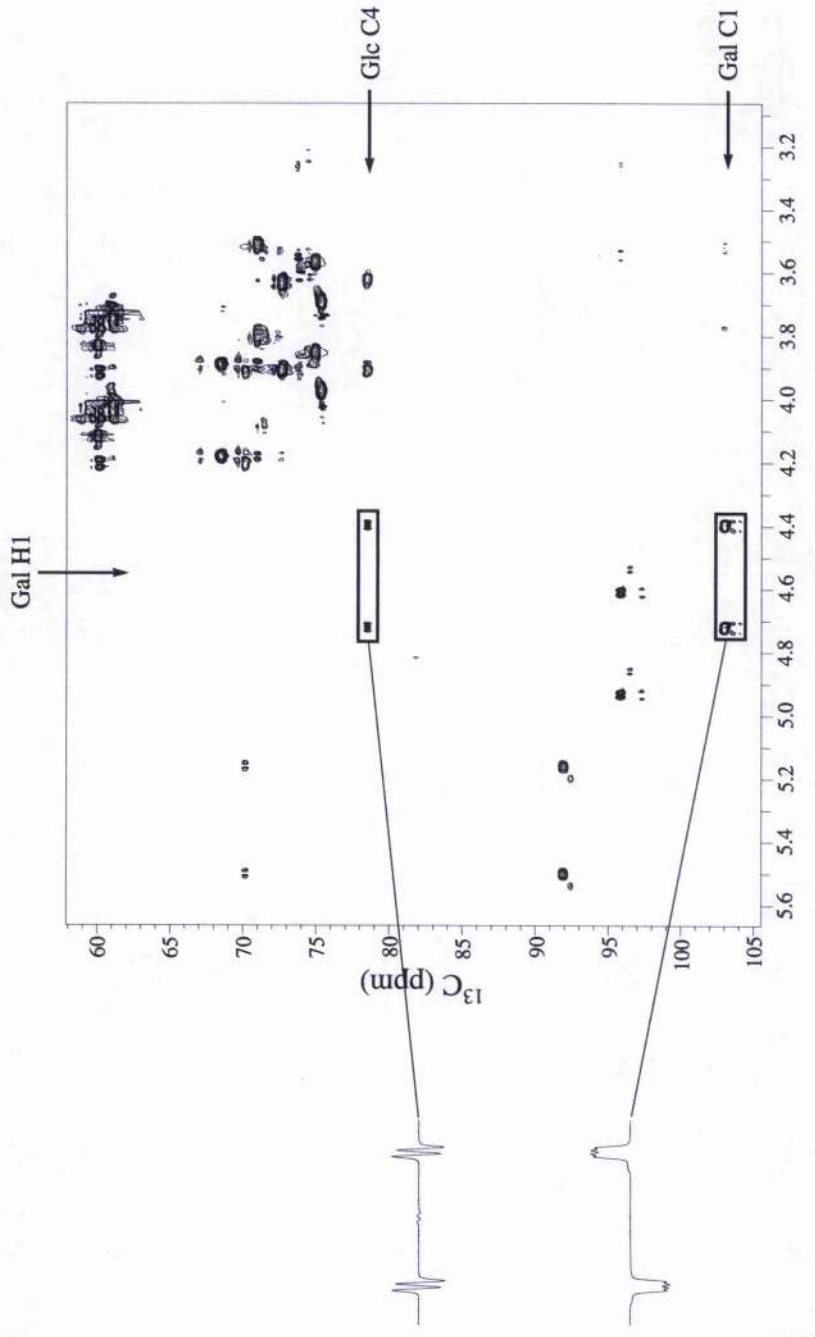

Figure 3.16 - Heteronuclear ^{1}H-^{13}C long range carbon-proton correlation (LRCH) spectrum for the measurement of long-range carbon-proton coupling constants. Three-bond trans-glycosidic correlations are assigned. 1D traces of the boxed sections of the two dimensional spectrum show the COSY-type cross-peak, with the long range carbon-proton coupling anti-phase (upper trace, Gal H1 - Glcα/βC4) and the one-bond correlation with the carbon-proton coupling in-phase, TOCSY-like cross-peak (lower trace, Gal H1 - Gal C1).

3.3.3 ^{13}C-^{13}C Coupling Constants

The enrichment of oligosaccharides with ^{13}C was initially used as a method for verifying ^{13}C chemical shifts, with early work by Walker *et al.* (1976), Gorin and co-workers (1973; 1974; 1975), Bundle *et al.* (1973), and Koch and Perlin (1970), demonstrating the utility of isotopically labelled compounds in making unambiguous assignments, which had previously been difficult. Interestingly ^{13}C NMR on 50% fully enriched glucose was performed in 1969 (Perlin, 1969), however, no long range carbon-carbon couplings were resolved due to the significant broadening.

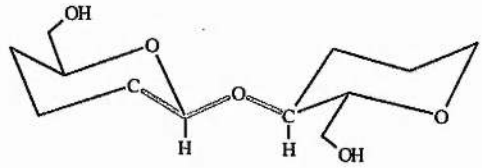

With relatively easy incorporation of a single ^{13}C label at C1 of monosaccharides, by the cyanohydrin reaction, interest in accurate measurement of carbon-carbon couplings was initiated, because, in contrast to the fully labelled monosaccharides, these long range couplings are directly resolvable in ^{13}C NMR spectra (data reviewed by Krivdin and Della, 1991).

Marshall and Miller showed that three bond C-C-C-C couplings in a variety of aliphatic carboxylic acids follow a modified Karplus relationship (Marshall and Miller, 1973). However, although C-O-C-C couplings are believed to follow a Karplus relationship, no actual parametrisation has been possible, limiting the analysis of inter-glycosidic couplings to a qualitative approach.

Since the introduction of the single ^{13}C-label, NMR methods of determining J_{CC} have been proposed for natural abundance samples. The earliest of these methods used the INADEQUATE pulse sequence (Bax *et al.*, 1981), in which the undesirable "parent" signal arising from molecules containing only a single isolated carbon-13 spin are suppressed, in order to reveal the pure ^{13}C satellite spectrum. The inherent low sensitivity of this method is due to only one molecule in 10^4 having the requisite isotopic composition in natural abundance samples. Transfer of proton magnetisation to carbons via INEPT/DEPT sequences increase sensitivity of the INADEQUATE experiment resulting in a threefold

increase in signal to noise ratios (Sorensen*et al.*, 1982; Kessler*et al.*, 1985; Lee and Morris, 1986; Podkorytov, 1990), whilst measurement of carbon-carbon splittings to quaternary carbons have been proposed by utilising relayed experiments, such as C-relayed HC INEPT (Kessler *et al.*, 1985) and DEPT C-C relay (Kawabata and Fukushi, 1994). Keller and Vogele (1986) developed a proton detected variant of the INADEQUATE experiment, allowing measurement of $^{1}J_{CC}$ values.

These proposed methods are relatively insensitive and require large quantities of material, which is obviously unfeasible for complex carbohydrates. However, now that fully labelled proteins/peptides are being produced, there has been a resurgence in interest in $^{3}J_{CC}$. Measurement of these long range carbon-carbon coupling constants from 1D spectra is obviously impracticable for proteins, due to the large number of signals and complexity of each resonance by multiple carbon-carbon couplings. Therefore, a variety of new experiments have been proposed for use with uniformly labelled samples, including the 2D and 3D quantitative J correlation method (Bax *et al.*, 1992; Bax *et al.*, 1994a; Bax *et al.*, 1994b), and the 3D HCCC-ECOSY method (Schwalbe *et al.*, 1993).

Work by the Serriani group has concentrated on the measurement of $^{2}J_{COC}$ couplings, with the prediction of the magnitude of the values due to conformation of the electronegative groups about a given carbon (Serianni *et al.*, 1996; Church, *et al.* 1996). This method known as the "sum projection rule" comes from a non Karplus relationship between the magnitude of the coupling constant and angle, and is based on the observations made from the measurements of $^{2}J_{CH}$. Unfortunately this only allows information about the angle ϕ to be determined, as by definition of the sum projection rule (*figure 3.16*) the angle ψ cannot affect the magnitude of the inter-glycosidic $^{2}J_{COC}$, but Serianni and co-workers have been able to give an insight into the conformation about the glycosidic linkage (Duker and Serianni, 1993), and furanose conformations (Wu *et al.*, 1992; Church *et al.*, 1997). This approach, however, is limited by the fact that the sugars are only singly labelled, and are only concerned with $^{2}J_{COC}$ which can only be estimated by an empirical rule. In contrast, measurement of $^{3}J_{COCC}$ with an appropriate Karplus curve would give a more practical approach in estimating the torsion angles ϕ and ψ.

For the general application of inter-glycosidic $^{3}J_{COCC}$ values to the conformation of oligosaccharides, there are two basic requirements. First, a Karplus equation is required, and second, fully labelled oligosaccharides need to be generally available. The latter problem is being addressed with the commercial availability of fully labelled monosaccharides, which can be used to chemically and enzymatically synthesise oligosaccharides. The problem at present is that there are limited Karplus relationships parametrised for carbon-carbon coupling constants.

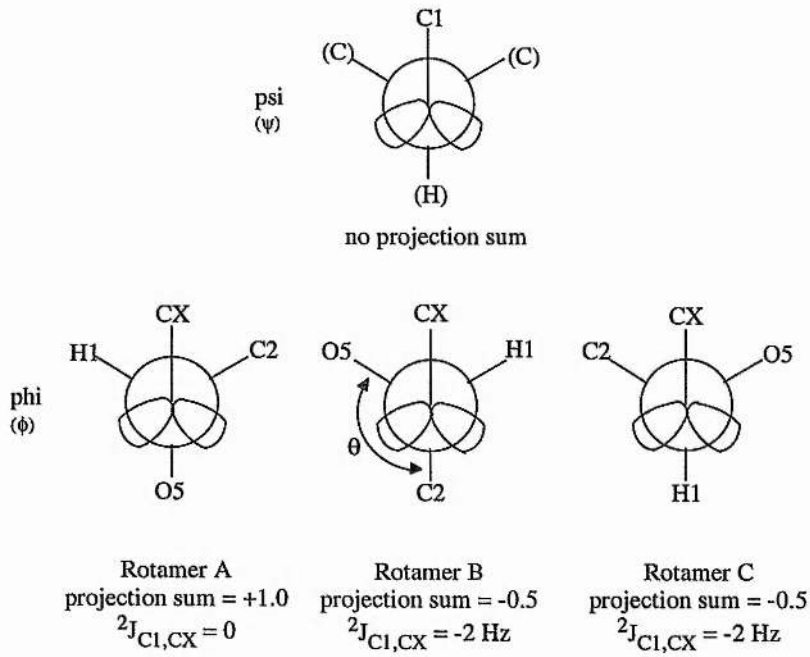

Figure 3.16 - Sum projection rule for $^{2}J_{COC}$ about oligosaccharide linkages. The sum projection rule involves an inspection of the angles each electronegative group on the C-O-C pathway makes with an axis trans to the O-C bond (θ). The value of the projection sum is then a summation of cos(θ) over all contributions. Hence, in the case for ψ, there are no electronegative groups, therefore no projection sum.

3.3.3.1 Karplus parametrisation

Parametrisation of a Karplus relationship for use with carbohydrates ideally requires experimental $^3J_{CC}$ values distributed over a wide range of C-O-C-C dihedral angles. On grounds of sensitivity such coupling constants must be determined for compounds with a high degree of ^{13}C enrichment, and in this regard the information that can be obtained from readily available compounds is limited. In monosaccharides only two dihedral angles are available, 180° for C1-O-C5-C6, and 60° for C1-O-C5-C4. The measurement of the latter coupling constant is hampered by a simultaneous and opposite coupling pathway, C1-C2-C3-C4, and the two contributions can not be readily separated resulting in a zero coupling (Krivdin and Della, 1991).

Dihedral angles of +60°/-60°, 180°, and 109° in C-O-C-C fragments can be obtained in two simple sugar derivatives, namely methyl 4,6-O-(1-methylbenzylidene)-α-D-glucopyranoside (I) and 2,3-O-isopropylidene-1,6-anhydro-D-mannopyranose (II), see Table 3.1. Compound I allows measurement of $^3J_{CC}$ values for +60°, -60° from C4 and C6 to the methyl carbon of the methylbenzylidene protecting group, respectively. The value of the dihedral angle, ~110°, between C1 and the central carbon of the isopropylidene protecting group in compound II, was confirmed by x-ray crystallography (Dr. P. Lightfoot, 1997).

Measurement of the $^3J_{CC}$ values were obtained from the 1D carbon spectra with selective carbon decoupling. From the data collated on monosaccharides (reviewed by Krivden and Della, 1991) it is apparent that the magnitude of the three bond coupling constant between C1 and C6 is dependent on the anomeric configuration, as is seen for glucose (Table 3.1). It is therefore important to realise that any Karplus parametrisation will only be appropriate to a particular linkage type. Using the data obtained from the spectra, the $^3J_{CC}$ values listed in Table 3.1 were fitted to a Karplus relation of the form $^3J_{CC}=A\cos^2\theta + B\cos\theta + C$, giving rise to curves appropriate for α and β linked carbohydrates (*figure 3.17*). It is appreciated that with the limited experimental data used in fitting, this parametrisation is at best a semi-quantitative, and is probably unreliable in the region $0°<\theta>60°$. However, it is worthy of note that the predicted average $^3J_{CC}$ value over 360° rotation (2.55Hz) is in reasonable agreement with the measured $^3J_{CC}$ value for the freely rotating dihedral angle C2-C1-O-Me in methyl-4,6-O-(1-methylbenzylidene)-α-D-glucopyranoside (Table 3.1). In any event, the

experimental data-points lie within the region of the curve that is likely to be populated by trans-glycosidic $^3J_{CC}$ values, and thus should predict these values with reasonable accuracy.

Table 3.1 - Three-bond ^{13}C-^{13}C coupling constants measured in ^{13}C model compounds and utilised for the parametrisation of a Karplus curve for the C-O-C-C fragment.

Compound	Coupling	Angle (deg.)	$^3J_{CC}$ (Hz)
α-D-Glucose	$^3J_{C1\text{-}O\text{-}C5\text{-}C6}$	180	3.3
β-D-Glucose	$^3J_{C1\text{-}O\text{-}C5\text{-}C6}$	180	3.8
● = ^{13}C			
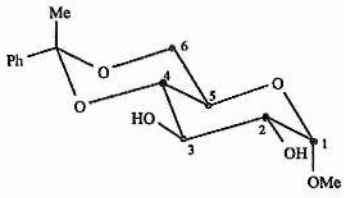 (I)	$^3J_{C1\text{-}O\text{-}C5\text{-}C6}$	180	3.1
	$^3J_{Me\text{-}C\text{-}O4\text{-}C4}$	60	2.4
	$^3J_{Me\text{-}C\text{-}O6\text{-}C6}$	60	1.9
	$^3J_{C2\text{-}C1\text{-}O1\text{-}Me}$	Av.[1]	2.8
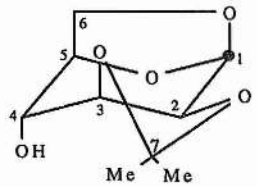 (II)	$^3J_{C1\text{-}C2\text{-}O2\text{-}C7}$	109[2]	0.6

1 Averaging over 360°
2 Value determined from crystal structure (Lightfoot, 1997, unpublished data)

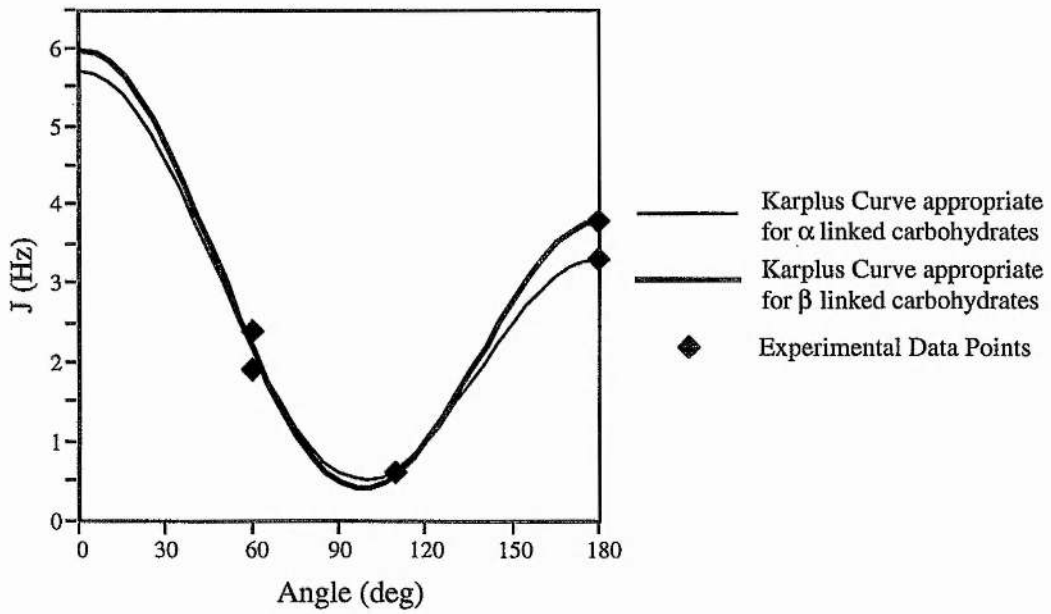

Figure 3.17 - Karplus Curve for $^{3}J_{COCC}$, parametrised using the data in Table 3.1. Experimental data-points (♦) were fitted to the function $^{3}J_{CC} = A\cos^2\theta + B\cos\theta + C$, giving rise to the constants A = 3.9, B = 1.2, and C = 0.6 for α-linked carbohydrates, and A = 4 .4, B = 1.1, and C = 0.5 for β-linked carbohydrates.

Measurement of long range $^{3}J_{COCC}$ in 1D ^{13}C spectra with selective decoupling in uniformly labelled oligosaccharides is not practical because of the number of carbon-carbon couplings experienced by each carbon. Therefore, measurement of inter-glycosidic $^{3}J_{CC}$ values in uniformly labelled oligosaccharides have been measured using the 2D (Bax *et al.*, 1992) and 3D LRCC experiments (Bax *et al.*, 1994a,b). The long range coupling constant is derived by a ratio of the volumes of these cross-peaks and the "reference" HSQC-type correlations in the following manner:

$$^{n}J_{CC} = \frac{1}{2\pi T}\tan^{-1}\left(\sqrt{\frac{V_{lr}}{V_{ref}}}\right)$$

where V_{lr} is the volume of the long range (H_a,C_{a+n}) cross-peak, V_{ref} is the reference cross-peak (H_a,C_a) volume, and T is a delay tuned to evolve $^{n}J_{CC}$ whilst refocusing $^{1}J_{CC}$.

Chapter 4

Three Dimensional Structure and Dynamics of the disaccharide N-*acetyllactosamine*

Abstract

The three-dimensional structure and dynamics of *N*-acetyllactosamine are investigated with the additional NMR-derived restraints discussed in the previous chapter. Heteronuclear NMR experiments on the ^{13}C-enriched carbohydrate have allowed additional structural information to be obtained, namely ^{13}C-^{13}C coupling constants, and using ^{13}C-edited NOESY unambiguous measurement of inter-glycosidic NOEs, which were overlapped in the homonuclear 2D spectrum. Low temperature studies in a mixed solvent system have allowed NOEs to exchangeable protons to be measured, and using these extra restraints it is shown that the conformation cannot be described by a single static structure, but is best represented by a dynamical model with significant torsional fluctuations confirming the flexibility of carbohydrates in solution.

4.1 Introduction

Although the disaccharide *N*-acetyllactosamine, Galβ1-4GlcNAc (*figure 4.1*) has no specific defined biological function, it forms the core structure of the type 2 oligosaccharides, including many blood group antigens, and arms on the tri-mannose core of *N*-linked oligosaccharides. The three-dimensional structure has been determined using x-ray crystallography (Longchambon *et al.*, 1981), and by NMR and modelling (Nunez and Barker, 1980; and reviewed by Imberty, 1997). With a well defined structure, Galβ1-4GlcNAc represents a good model system for testing the new additional NMR derived restraints discussed in the previous chapter.

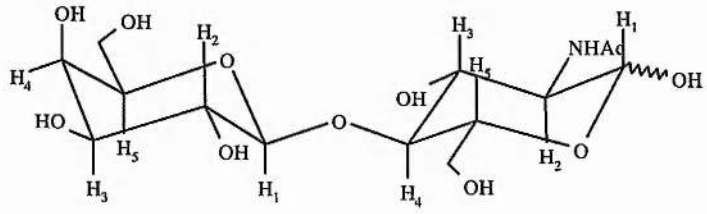

Figure 4.1 - Schematic representation of *N*-Acetyllactosamine, including numbering scheme used in the text.

In NMR experiments, the ^{13}C-labelled sample is enriched <95% at all carbons except the *N*-acetyl group.

4.2 Materials and Methods

4.2.1 Sample preparation

10mg of Galβ1-4GlcNAc (Aldrich) and *N*-acetyl [U-^{13}C] Galβ1-4GlcNAc (~18mg) were dissolved and lyophilised into 99.96% D_2O three times followed by dissolution in 750μL D_2O. For the observation of the exchangeable protons samples of the natural abundance and ^{13}C-labelled Galβ1-4GlcNAc were dissolved 750μL of H_2O containing 15% 99.96% acetone-d_6 (Cambridge Isotopes). The pH was adjusted to 5.5 to 6.0 by careful step-wise addition of dilute HCl or NaOH and transferred to a 5mm NMR tube. The sample was degassed by sonication for about 1 minute.

4.2.2 NMR Experiments

NMR spectra were obtained at 303K and 258K with a reference frequency of 500MHz on a Varian Unity$^+$ spectrometer equipped with a self shielded z gradient triple resonance probe. All spectra recorded in the phase sensitive mode using the States method for quadrature detection (States *et al.*, 1982).

Homonuclear ^{13}C (^1H decoupled) two dimensional correlated spectroscopy experiment (COSY) was recorded in magnitude mode with a spectral width of 6.5 kHz, with 256 complex points in t_1, using scans per increment and 8K points in t_2, resulting in a total acquisition time of ~15 hours.

2D HCCH-TOCSY experiments were recorded using the three-dimensional pulse scheme of Bax and co-workers (Bax *et al.*, 1990; Yu *et al.*, 1993). A total of 128 and 1K complex points was acquired in the t_1 and t_2 dimensions respectively, with spectral widths of 1kHz and 7.5kHz. Two dimensional long range carbon-carbon J correlation (LRCC) experiments (Bax, 1992) were recorded with a proton sweep width of 1.2kHz, consisting 2048 complex points and a ^{13}C sweep width of 7.2kHz in t_1 (512 complex points), with a total of 32 scans acquired per increment. ^{13}C-^{13}C couplings evolve and are refocused during the delay (2T) of 22.2ms. Total acquisition time for the 2D experiment was ~16 hours. The values of the long range coupling constants are derived from the ratios of the cross-peaks obtained in the spectrum in the manner as described previously (Bax *et al.*, 1992).

Trans-glycosidic carbon-proton coupling constants were measured using the 2D constant-time pulse sequence, CT-LRCH (Ionides *et al.*, 1995). Proton and carbon sweep-widths were 1.9kHz and 7.5kHz, respectively, with 4096 complex points in t_2 and 512 t_1 increments consisting of 24 scans per increment, resulting in a total acquisition time of ~15 hours.

The three dimensional ^{13}C-edited NOESY experiment was acquired with the conventional pulse sequence with spectral widths of 1.1kHz, 3.5kHz, and 1.1kHz and 128, 32, and 512 complex points in t_1, t_2, and t_3 respectively. The NOESY mixing time was 800ms. Prior to Fourier transformation, data were apodised with cosine-bell functions, and t_1, and t_2 dimensions were zero filled to 256 and 64 complex points, respectively. Total acquisition time for the 3D experiment was ~40 hours.

Two dimensional ES-TOCSY and ES-ROESY spectra were acquired at 258K with spectral widths of 4.2kHz, 256 t_1 increments, 16 scans per increment with 2K complex points in t_2. ES-TOCSY spectra were acquired with a 100ms spin-lock period using a DIPSI-2 with a 7.6kHz rf field whose carrier was located at the residual water signal (5.14ppm). The ES-ROESY was acquired under identical conditions except the spin-lock period was a weak (~3kHz) continuous-wave rf field. Before two dimensional Fourier transformation data were apodised using cosine-bell functions, and total acquisition times were 4 hours for each experiment. Hydroxyl exchange rates were measured using the method described by Adams and Lerner (1992) incorporating excitation sculpting water suppression (Hwang and Shaka, 1995). Spectra were acquired with 32 scans, 4K complex points, a sweep width of 4kHz and were recorded with saturation times varying from 0 to 1s. ES-1D ^{1}H spectra were acquired with a proton sweep width of 3.5kHz and 8K points. Temperature coefficients were acquired from ES-1D ^{1}H spectra acquired between 255K and 265K, and exchangeable spin couplings were measured from the ES-1D ^{1}H spectrum acquired at 258K.

Two dimensional gradient-ROESY-HSQC spectra (gd-ROESY-HSQC) were acquired with spectral widths of 1000Hz in *F2* and 3450Hz in *F1*, with 1024 and 256 complex points, respectively. Sixteen transients were acquired per t_1 increment, giving a total acquisition time of ~4 hours. The spin-lock time was 100ms using a weak (~3kHz) continuous-wave rf field. Three dimensional gd-ROESY-HSQC spectra were acquired with spectral widths 1000 Hz in *F3*(^{1}H), 3450 Hz in *F1*(^{1}H) and 3600 Hz in *F2*(^{13}C) and with 512, 128, and 32 complex points per increment. Four transients were acquired per increment giving a total acquisition time of ~24 hours. Prior to three-dimensional Fourier transformation, data were apodised with cosine-bell functions, followed by zero filling once in each dimension. The recycle delay in all experiments was 1s.

The rotational correlation time of the disaccharide was measured by ^{13}C T_1 relaxation measurements at 258K, and was also calibrated independently from diagonal versus cross-peaks volumes for fixed internuclear distances using a full relaxation matrix analysis. The value obtained (2.5 ± 0.2 ns) reflects the high viscosity of the disaccharide solution at low temperature.

4.2.3 Molecular Modelling

Computer models were assembled using Biosym's Insight II molecular graphics package running on a Silicon Graphics Indigo 2 Challenge. Random structures were generated by dynamical quenching. An initial structure was built with pyranose rings in the $^4C_1$ chair conformation with trial values of phi (ϕ) and psi (ψ), and subjected to 200ps of unrestrained molecular dynamics at 750K, during which the torsional terms are scaled by a factor of 7 to prevent excessive ring puckering. A random structure was saved every 10ps. Energy minimisation by restrained simulated annealing was achieved as follows: models were equilibrated for 10ps with a thermal bath at temperatures 500K, 450K, 350K, 300K, and then successively for 1ps in decreasing steps of 10K, followed by a further 1ps at 5K. The system was minimised using steepest descents algorithm until the maximum derivative was less than 0.04kJmol^{-1}Å^{-1}. Restraints were applied as a biharmonic function. NOE contacts were arbitrarily assigned as strong (1.8Å - 2.7Å), medium (1.8Å - 3.3Å), and weak (1.8Å - 5.00Å). The dihedral angle ω about the C5-C6 bond was weakly constrained to two values (180°, and -60°) using a force constant of 10kcal/Å^2.

All dynamics simulations were performed *in vacuo* with a dielectric constant (ε) of 80.0. The AMBER force-field (Weiner *et al.*, 1984; Weiner *et al.*, 1986) with a carbohydrate parameter set developed by Homans (1990a) was used with the exo-anomeric potentials set to zero. Simulations lasted 510ps with the last 500ps used in further analysis.

4.3 Results and Discussion

4.3.1 Spectral Assignments

4.3.1.1 Non-exchangeables protons and carbons

Spectral assignments for the non-exchangeable protons and carbons of Galβ1-4GlcNAc (*N*-acetyllactosamine) are given in Table 4.1, whilst assignments, exchange rates, and temperature coefficients for the exchangeable protons are compiled in Table 4.2. These data agree with previous assignments for the non-exchangeable protons (Nunez and Barker, 1980; Breg *et al.*, 1989) and comparable exchangeable proton assignments to *N*-acetyllactosamine (Poppe and van Halbeek, 1994).

Initial assignments of the carbon resonances were made for [U-^{13}C] Galβ1-4GlcNAc using ^{13}C-^{13}C COSY (*figure 4.2A*), from which all but one of the carbon chemical shifts (GlcNAc-C3β) could be assigned. The combination of a HSQC experiment (*figure 4.3A*), which correlates carbons with their attached protons, and a 2D version (^{1}H, ^{13}C) of the 3D HCCH-TOCSY experiment (*figure 4.2B*), which allows the correlation of a proton resonance to the carbon its attached to, and depending on the length of the carbon spin-lock period to the neighbouring carbons up to every carbon within each monosaccharide ring, the complete assignment of both proton and chemical shifts was possible. The HCCH based experiments use the uniformly large one bond carbon-proton (~150Hz) and carbon-carbon (~40Hz) coupling constants. Therefore, unlike the standard through-bond correlation experiments, such as ^{1}H,^{1}H HOHAHA where transfer is dependent on small $^{3}J_{H,H}$ couplings, which can in some cases (galactose and sialic acid) fail to correlate all the protons in each monosaccharide ring, the HCCH based methods do not suffer from this problem. For example, in the 2D ^{1}H/^{13}C (*F2F3*) version of the 3D HCCH-TOCSY experiment, the proton resonance for Gal H1 is correlated to carbons C2 to C5, producing a distinctive 'ladder' effect for the carbon resonances of galactose allowing the other proton chemical shifts of the galactose residue to be easily identified (*figure 4.2B*).

Homonuclear ^{1}H-^{1}H spin couplings were obtained from a COSY experiment on unlabelled samples and confirm the ring structures of GlcNac and Gal ($^{4}C_{1}$). Using this experiment and ^{1}H-^{13}C HSQC experiments, the $^{3}J_{H5,H6}$ coupling constants were measured allowing the

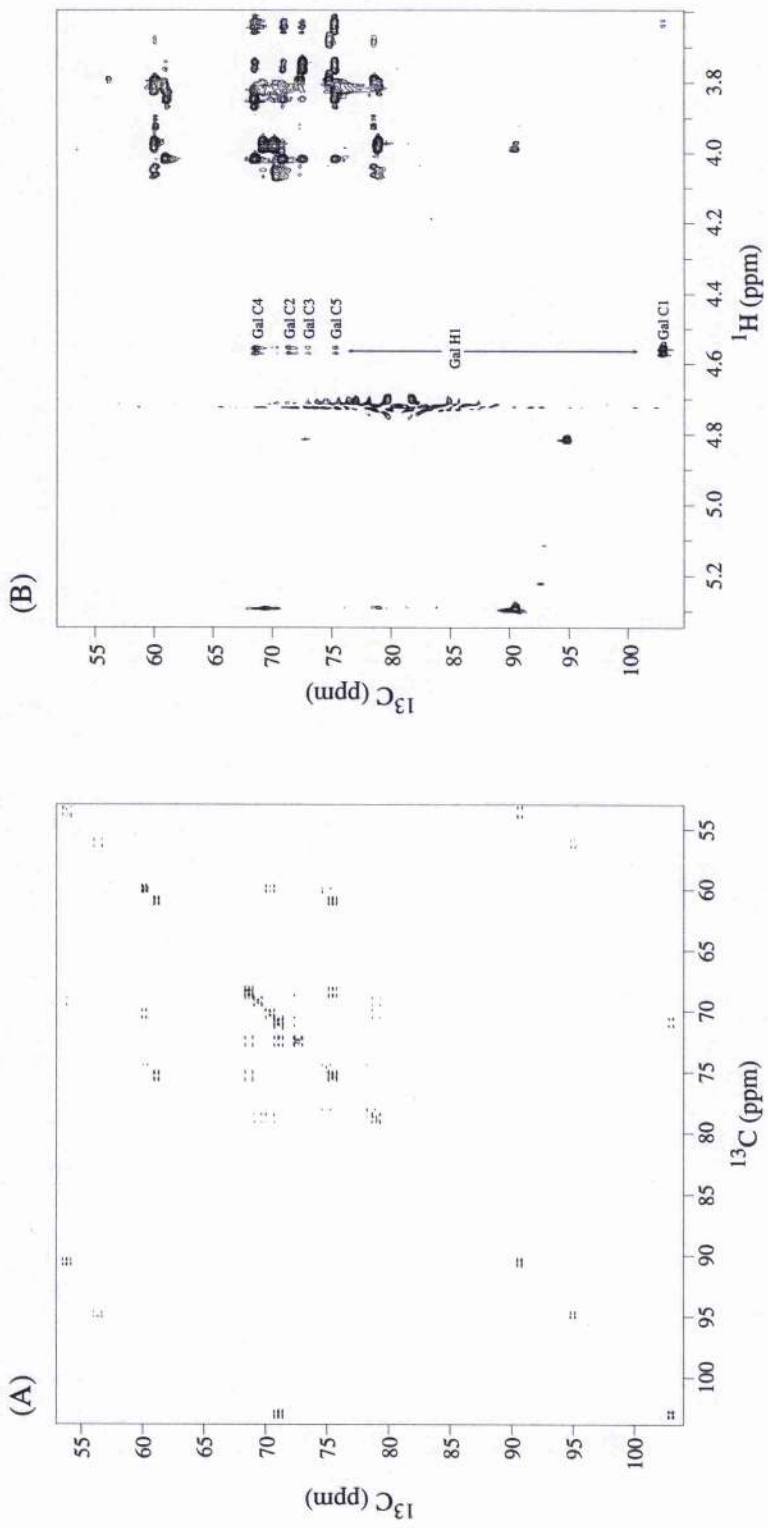

Figure 4.2 - (A) Two dimensional ^{13}C-^{13}C COSY spectrum and (B) two dimensional ^{1}H-^{13}C HCCH-TOCSY spectrum of [U-^{13}C] *N*-acetyllactosamine at 303K.

hydroxymethyl group relative populations to be estimated using the method by Wu *et al.* (1983), as gg 66%, tg 0%, and gt 34%.

4.3.1.2 Exchangeable Protons

The assignment of the exchangeable protons was based upon homonuclear experiments with excitation sculpting for water suppression which requires the assignment of the non-exchangeable protons. These were obtained using the gd-NOESY-HSQC (with mixing time set to zero). Similar to the lack of variation in the ^{13}C chemical shifts of lactose (chapter 3) at the low temperatures, the ^{13}C chemical shifts of *N*-acetyllactosamine were not observed to vary >0.5Hz between 303K and 258K (except for the aglyconic carbons), suggesting that there is no drastic change in conformation between temperatures. A two dimensional ^{1}H-^{1}H ES-HOHAHA spectrum of ~200mM Galβ1-4GlcNAc at pH5.75 was used to assign the exchangeable protons (*figure 4.3B*). At this mixing time (100ms) a number of cross-peaks corresponding to single-bond and relayed coherence transfers between the non-exchangeable and exchangeable protons are observable, as well as cross-peaks between exchangeable protons. Of particular note are the cross-peaks between the exchangeable protons and GlcNAcα-H1, which resonates ~40 Hz from the residual solvent water resonance.

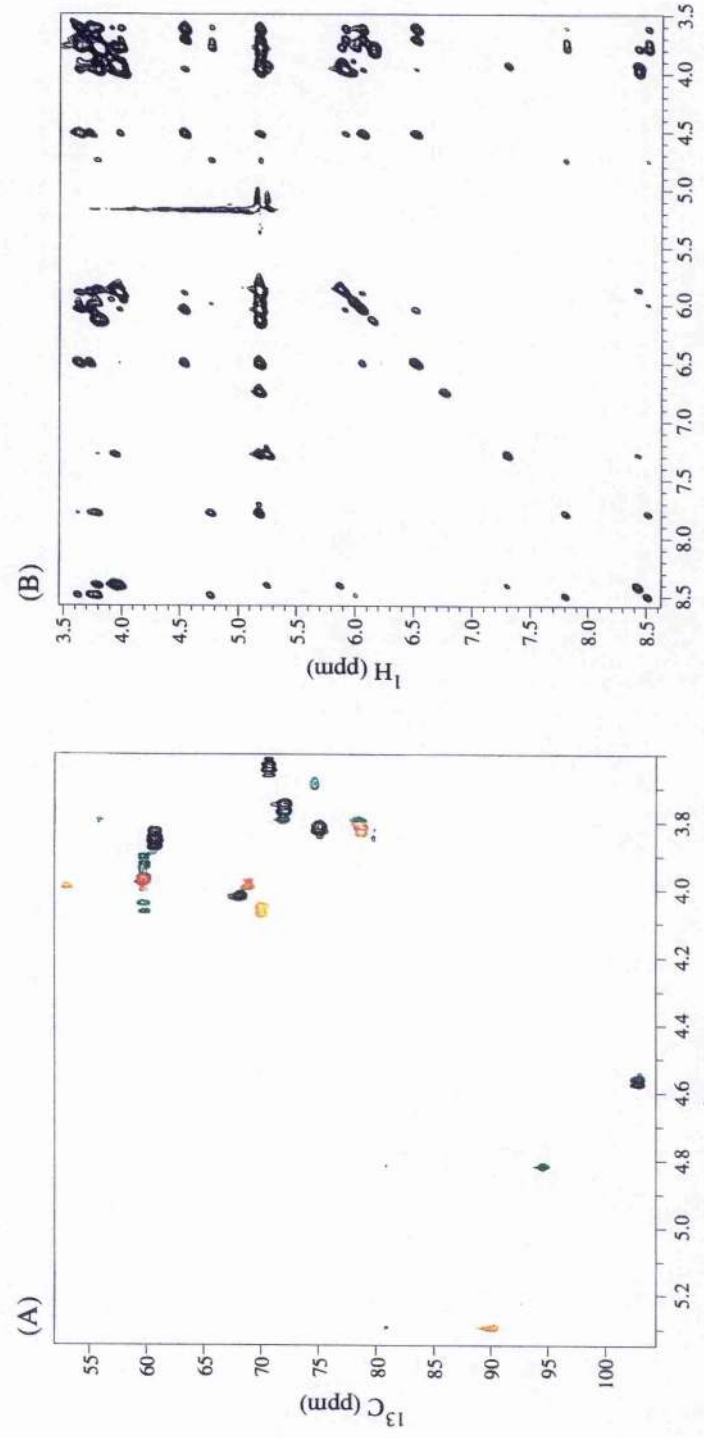

Figure 4.3 - (A) Two dimensional ^{1}H-^{13}C HSQC spectrum of *N*-acetyllactosamine at 303K.
Peaks in Black = Gal, Red = GlcNAcα, and Green = GlcNAcβ.
(B) Two dimensional ^{1}H- ^{1}H ES-HOHAHA spectrum showing through space correlations (mixing time = 100ms).

Table 4.1 - ^{1}H and ^{13}C chemical shift assignments for *N*-acetyllactosamine at 303K.

	Galactose		GlcNAc-α		GlcNAc-β	
	^{1}H	^{13}C	^{1}H	^{13}C	^{1}H	^{13}C
1	4.58	103.0	5.31	90.8	4.83	95.1
2	3.64	71.2	4.00	53.9	3.80	56.5
3	3.76	72.9	3.99	69.4	3.80	72.3
4	4.04	68.8	3.83	79.0	3.80	78.7
5	3.83	75.5	4.08	70.4	3.69	74.9
6	3.86	61.2	3.98	60.4	4.06, 3.93	60.3
NAc			2.14		2.14	

Chemical shifts are referenced to $\delta_{TSP} = 0.00$ppm

Table 4.2 - NMR data for the exchangeable protons of *N*-acetyllactosamine in H_2O/acetone-d_6 (85:15) at 258K.

Proton	Chemical Shift (ppm)[a]	Exchange Rate (s^{-1})[b]	Temperature Coefficient (ppb/K)[c]	Coupling $^{3}J_{HH}$ (Hz)
Gal-OH2	6.54	9.7	104	5.9
Gal-OH3	6.09	15.1	10.4	5.4
Gal-OH4	5.94	10.7	10.5	6.1
Gal-OH6	6.14	n.d.	n.d.	6.2
GlcNAcα-OH1	7.28	12.5	6.9	2.9
GlcNAcα-OH3	5.89	8.9	11.3	~2.4
GlcNAcα-OH6	5.89	n.d.	n.d.	n.d.
GlcNAcα-NH2	8.48	–	7.7	7.7
GlcNAcβ-OH1	7.83	15.1	9.8	7.5
GlcNAcβ-OH3	6.03	6.5	12.2	4.1
GlcNAcβ-OH6	5.99	n.d.	n.d.	n.d.
GlcNAcβ-NH2	8.43	–	9.9	6.6

(a) Chemical shifts referenced to $\delta_{TSP} = 0.00$ ppm (by setting residual acetone to 2.19 ppm).
(b) Exchange rates measured at 258K.
(c) Temperature coefficients measured over a 10K range between 258K - 268K.
n.d. = not determined.

4.3.2 Inter-glycosidic NOEs

4.3.2.1 Non-exchangeable ^{1}H-^{1}H Homonuclear NOEs

It is clear from Table 4.1 that even for this simple disaccharide there is substantial spectral overlap in both proton and carbon dimensions. This is a particular problem in the proton dimension in interpreting homonuclear ^{1}H-^{1}H NOE spectra. From the NOESY spectrum for unlabelled *N*-acetyllactosamine (*figure 4.4*), unambiguous inter-glycosidic NOE assignments could be ascertained between Gal-H1 and GlcNAcα/β-H6 (indicated on the spectrum). The expected inter-residue NOE between Gal-H1 and GlcNAcα/β-H4, however, cannot be resolved due to the overlap with the intra-residue NOE to Gal-H5. Owing to the chemical shift similarity between GlcNAcα/β-H4 and Gal-H5, their respective NOE contributions to the cross-peak could not be assessed using homonuclear methods. With the availability of the ^{13}C-labelled *N*-acetyllactosamine, the homonuclear NOESY experiment can be edited by the ^{13}C nucleus, resulting in the 3D ^{13}C-^{1}H NOESY-HSQC experiment. Using two *F1F3* planes from the 3D experiment at the *F2* carbon chemical shifts of Gal-C5 (*figure 4.5A*) and GlcNAcα/β-C4 (*figure 4.5B*), the contributions of each NOE to the cross-peak in the 2D NOESY spectrum could be determined. The two inter-glycosidic NOEs observed were normalised to an intra-residue cross-peak volume, and were used in molecular modelling simulations (Table 4.4).

The measurement of only two inter-glycosidic NOEs is representative of the problem in determining the solution conformation of oligosaccharides. Since the linkages are the primary source of conformational flexibility, the overall three-dimensional structure is under defined by these NOEs alone. This results in a reliance on molecular mechanics calculations to restrict the number of possible conformations that are consistent with the NMR data, and it has been shown that this can result in models of the solution behaviour described by a single conformation or alternatively multiple conformations (Rutherford *et al.*, 1993). Additional restraints may be obtained from long-range heteronuclear (^{13}C-^{1}H) trans-glycosidic coupling constants, however have not been used in restrained molecular mechanics simulation due to lack of appropriate modelling protocols. In this study NOEs to exchangeable protons are investigated which are potentially a further rich source of distance restraints.

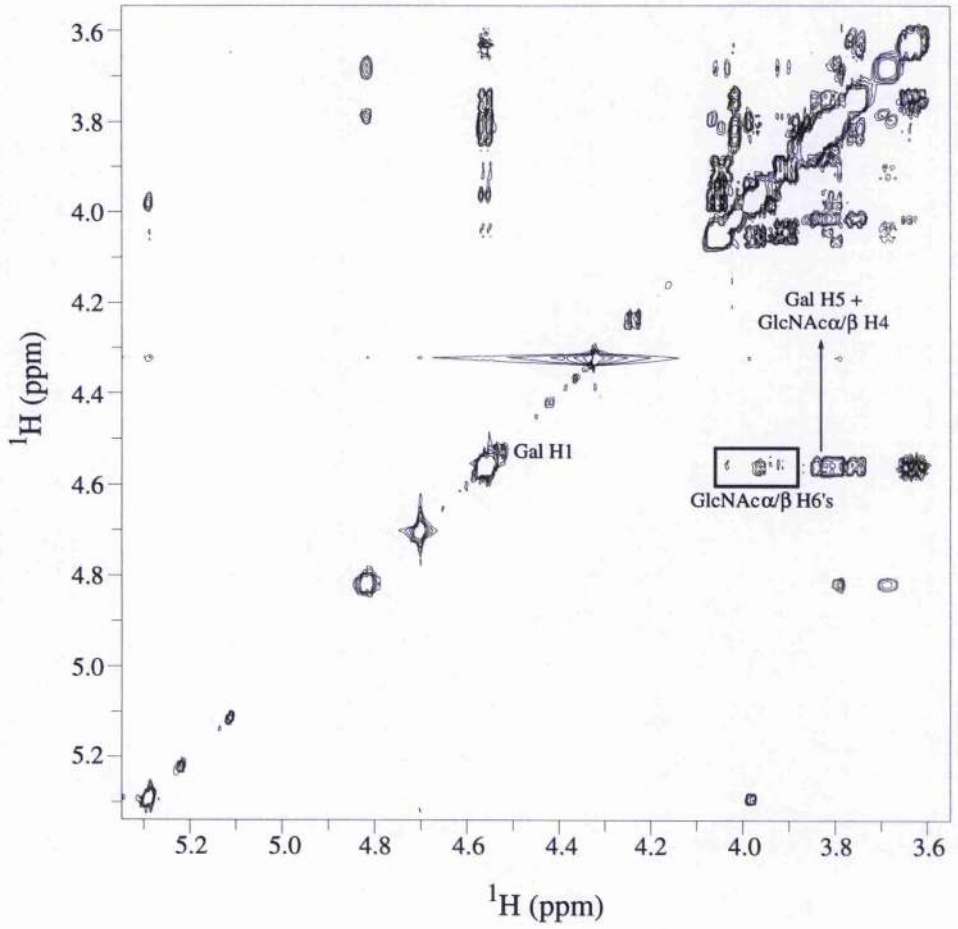

Figure 4.4 - 2D ^{1}H-^{1}H NOESY spectrum of unlabelled *N*-acetyllactosamine. Inter-glycosidic NOEs are assigned.

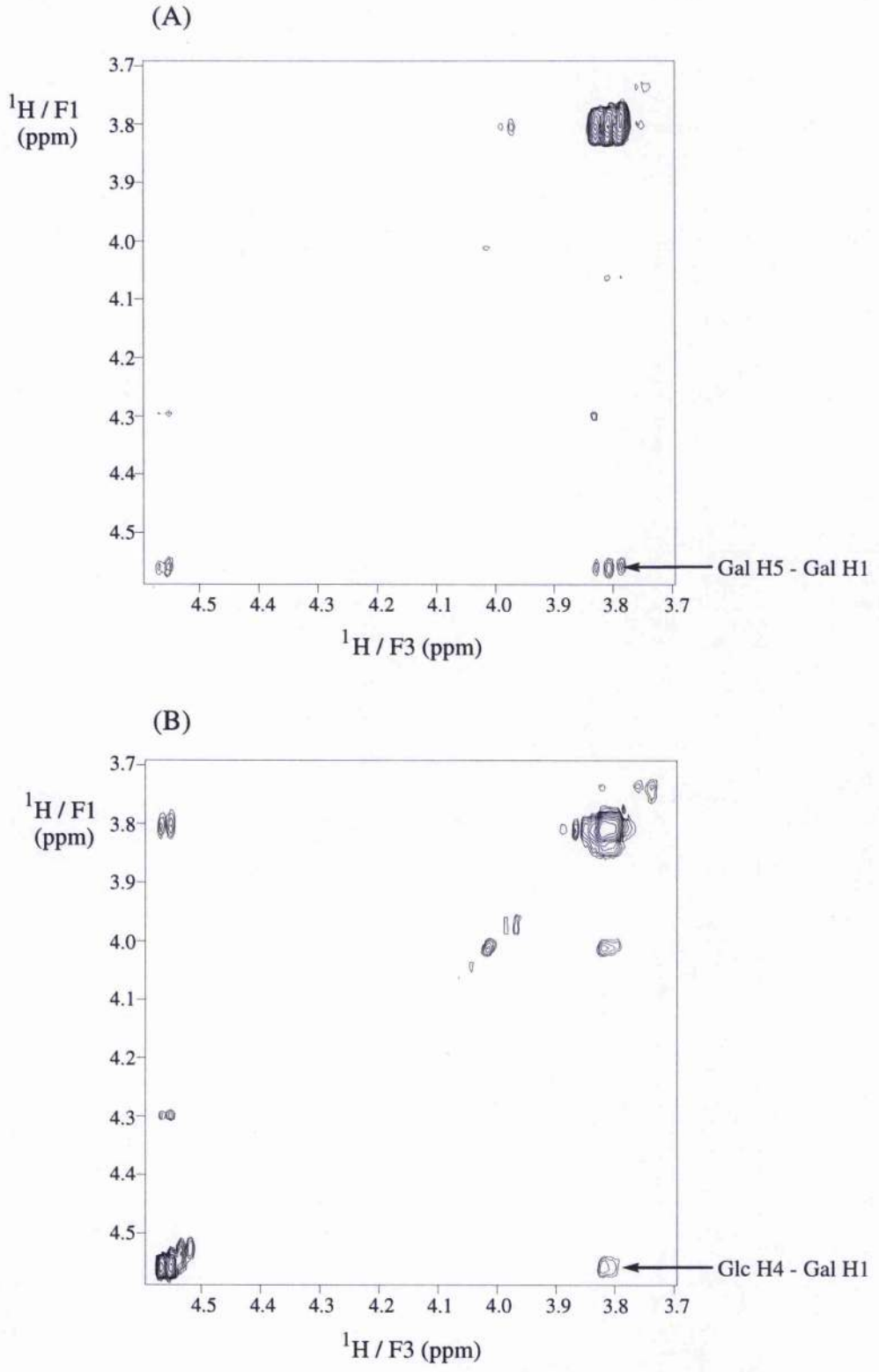

Figure 4.5 - *F1F3* planes from the three dimensional NOESY-HSQC spectrum of [U-^{13}C] *N*-acetyllactosamine at 303K at the ^{1}H chemical frequencies of (A) Gal-C5, and (B) GlcNAcα/β-C4.

4.3.3 Exchangeable Protons

Exchangeable protons in carbohydrates have been observed and used in conformational analysis for a long time. The majority of this work has been in the solvent DMSO-d_6, in which the exchangeable (OHs and NHs) protons do not exchange with the bulk solvent and therefore are observable at ambient temperature. Recently, work pioneered by Poppe and van Halbeek (1991b), and Adams and Lerner (1992), have allowed hydroxyl protons to be observed in, originally a mixture of water and acetone-d_6, and later supercooled water (Poppe and van Halbeek, 1994).

4.3.3.1 ROEs involving exchangeable protons

A section of the two dimensional ROESY spectrum of ~200mM Galβ1-4GlcNAc at pH5.75 corresponding to the non-exchangeable region in *F2* and the exchangeable proton resonances in *F1*, acquired using the excitation sculpting ROESY sequence, is shown (*figure 4.6A*). At this mixing time (100ms) a number of cross-peaks are observed to both hydroxyl and amide protons, together with intense correlations to the solvent water resonance. Of interest are the correlations between exchangeable protons, which are consigned to ROEs between the amide proton and the hydroxyl protons (data not shown). This suggests that although the rate of exchange for hydroxyl protons have been considerable lowered, it is still insufficiently slow to allow NOEs to be observed between two hydroxyl protons.

Whilst the majority of these ROEs are readily assignable, the resonance overlap in the region *F2* ~3.7ppm/*F1* ~6.0ppm is sufficiently severe to prevent unambiguous assignment of all the cross-peaks. This problem of overlap in the non-exchangeable resonances could be overcome by editing the spectrum in a third ^{13}C frequency dimension in the conventional manner. An example from the 3D gd-ROESY-HSQC spectrum (*figure 4.6B*), illustrates an *F1F3* slice at the ^{13}C resonance frequency (*F2*) of GlcNAcα/β-C6 (identical shift for each anomer). Apart from the intra-residue connectivities between the H6 protons of GlcNAcα and GlcNAcβ and the corresponding OH6 resonances, an inter-residue connectivity can be readily detected between the H6 protons of each anomer and Gal-OH2. From this experiment three inter-glycosidic NOEs were observed but before these could be utilised in

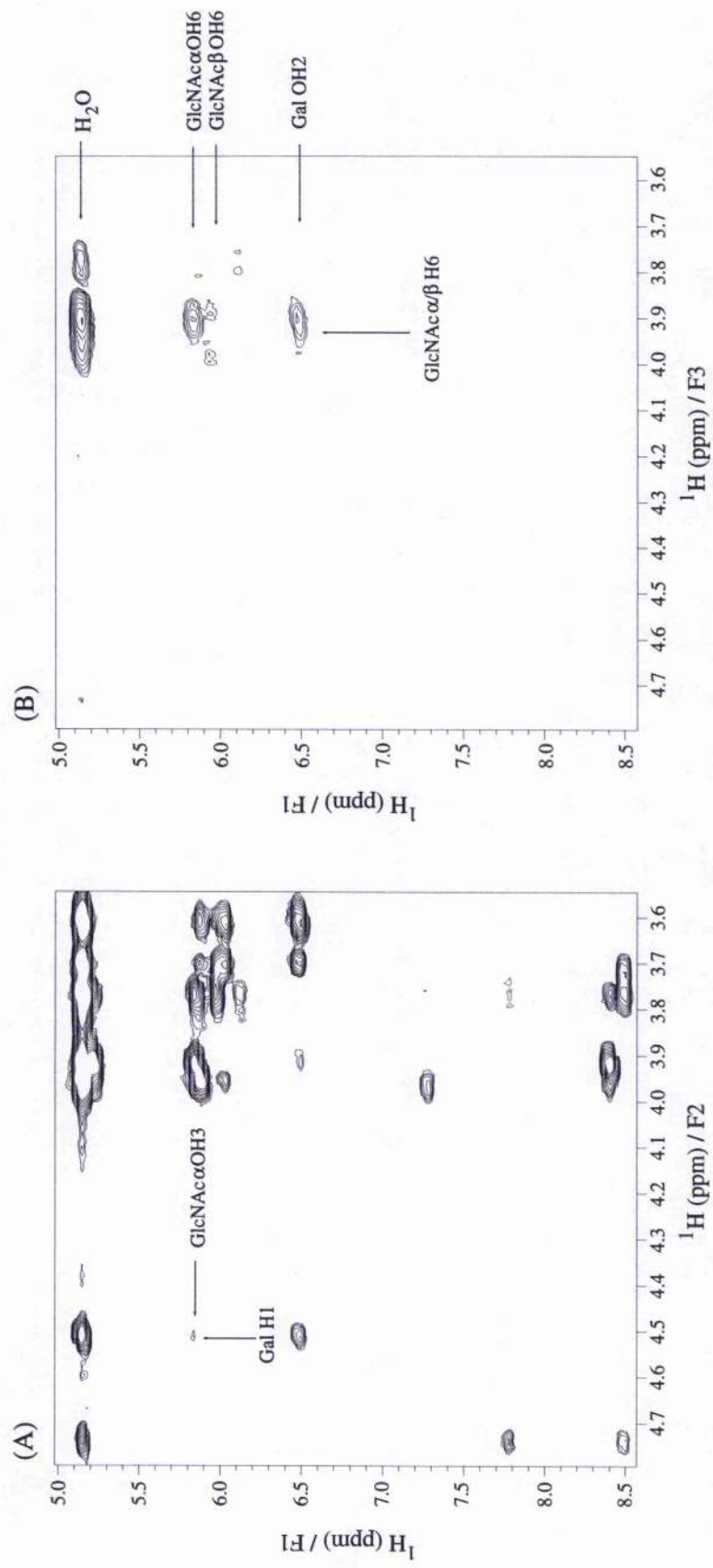

Figure 4.5 - (A) Region of the two dimensional ES-ROESY spectrum (mixing time = 100ms) showing through space connectivities to exchangeable protons. An inter-glycosidic connectivity is shown.
(B) Plane from the three dimensional gd-ROESY-HSQC spectrum at the ^{13}C chemical frequency of GlcNAcα/β -C6 (identical for exch monomer) showing the much improved resolution in comparison to the ES-ROESY spectrum. The delay $\delta = \Delta/2$ to ensure efficient transfer to both methylene and methine protons. Cross-peaks are assigned.

modelling studies to investigate the importance of these extra restraints, accurate quantitation is required.

4.3.3.2 Quantitation of ROE data involving exchangeable protons

The extraction of quantitative distance information from cross-peak intensities is not straightforward. First, as discussed by James and co-workers (Liu *et al.*, 1993), a loss of cross-peak intensity arises from exchange of magnetisation with solvent water. This is effectively a leakage process that affects only the diagonal elements of the relaxation matrix, and can be accounted for in a full relaxation matrix calculation of NOESY or ROESY intensities. A second problem concerns the saturation of the water magnetisation. If the water magnetisation is saturated prior to acquisition, substantial saturation transfer can occur from bulk solvent (which is in vast excess) to the solute during the acquisition period and relaxation delay, and can result in a substantial reduction in resonance intensity of exchangeable protons (Grzesiek and Bax, 1993; Li *et al.*, 1993; Stonehouse *et al.*, 1994a).

As discussed in the previous chapter, to estimate the degree of saturation, the 'effective' longitudinal relaxation of water, the longitudinal relaxation rate of the hydroxyl protons, and the exchange rate must be known. The exchange rates are easily measured using the modified Adams and Lerner pulse sequence, and have been measured for *N*-acetyllactosamine (Table 4.2). The longitudinal relaxation rate of the hydroxyl protons can only be estimated since it cannot be readily separated from the exchange rate, which is usually much larger. Conventional T_1 measurements for the ^{13}C enriched disaccharide in dimethylsulfoxide suggest that the relaxation rate is in the region 1.3 - 1.6s^{-1} for all the hydroxyl protons. That this is a reasonable estimate for the relaxation rate of the exchangeable protons in H_2O solution at 256K, is in evidence from the fact that the non-exchangeable proton T_1's are within 20% in the two solvents.

For these simulations a value for the longitudinal relaxation rate of water was estimated using a modified sequence of the gd-ROESY-HSQC sequence where the final $\pi/2$ pulse was followed by a variable delay and an additional $\pi/2$ read pulse. The plot of recovery of water magnetisation during the acquisition and relaxation delay of the gd-ROESY-HSQC pulse sequence (*figure 4.7*), allows the longitudinal relaxation rate of water magnetisation to be measured, which at 256K is 2.5s^{-1}.

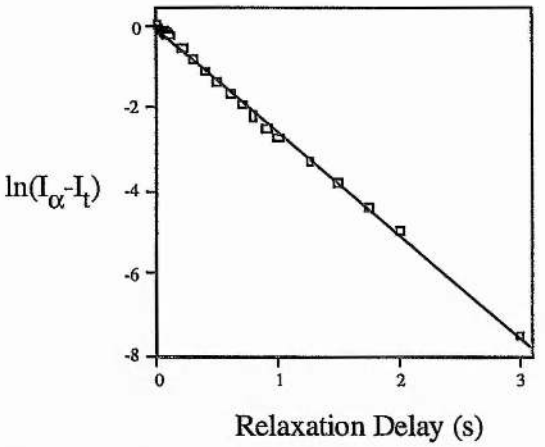

Figure 4.7 - Plot of recovery of water magnetisation during the acquisition period and delay of the gd-ROESY-HSQC pulse sequence. The recovery of the water magnetisation was measured using a simple modification of the gd-ROESY-HSQC sequence where the final $\pi/2$ pulse was followed by a variable delay and an additional $\pi/2$ read pulse to monitor the z component of the water magnetisation. The measured longitudinal relaxation rate of the water magnetisation at 256K is $2.5s^{-1}$.

Simulations of the recovery of I_Z using a variety of values centred around the value of the relaxation rate of the hydroxyl protons and the measured exchange rates shows that the recovery of I_Z is complete to ~90% after 1 second, and is virtually independent of $5<K<25s^{-1}$, and $0.07<R_I<7s^{-1}$ (*figure 4.8A-C*). Therefore no correction of cross-peak intensities is required for a combined acquisition time and relaxation delay greater than 1 second.

The essential independence of the recovery with respect to R_I is very useful in view of the difficulty in measuring this value accurately, and arises from the rapid recovery of the solvent magnetisation at low temperatures necessary for the observation of the exchangeable protons. The experimentally determined recovery of the magnetisation of GlcNAcβ-OH1 (▩) measured using the modified sequence, is also plotted (*figure 4.8A-C*), and is seen to recover at a rate similar to that predicted. The poor fit of these data to an exponential recovery derives from the difficulty in integrating the peak area in the presence of the intense solvent water resonance.

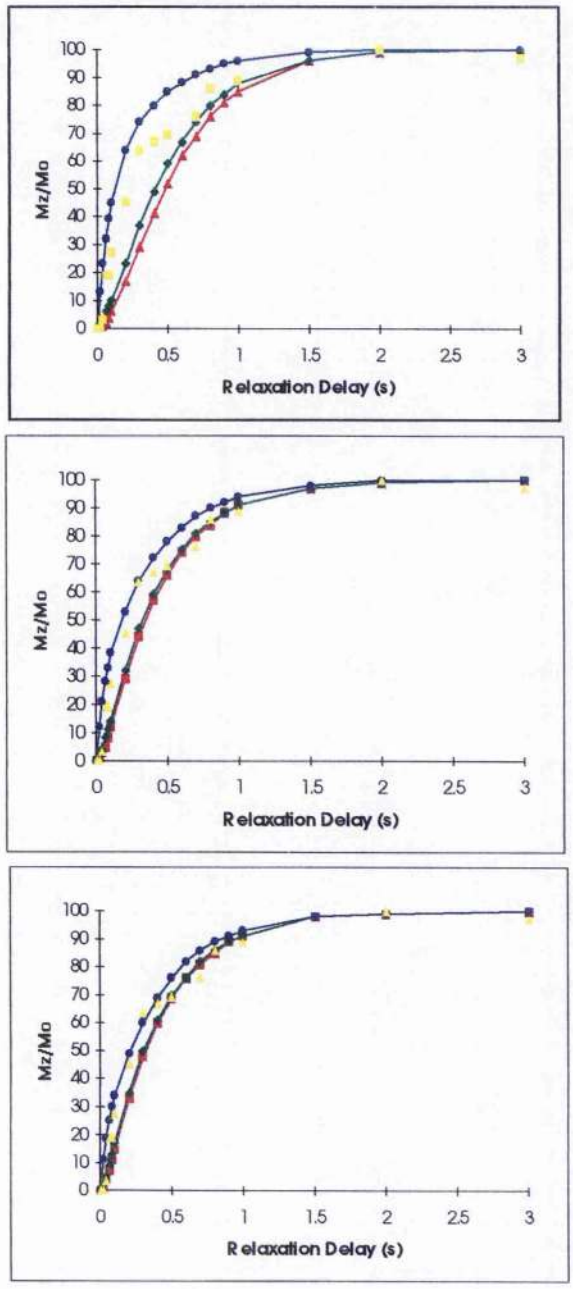

Figure 4.8 - Simulations of the rate of recovery of exchangeable proton magnetisation during the acquisition and relaxation delay of the pulse sequences in figure 3.12 (Chapter 3), assuming complete saturation of the water immediately before the acquisition period. Each plot shows the recovery of magnetisation for longitudinal rates of $7.0s^{-1}$ (•), $0.7s^{-1}$ (•) and $0.07s^{-1}$ (•), and exchange rates K1 of (A) $5s^{-1}$, (B) $15s^{-1}$, and (C) $25s^{-1}$. The experimentally determined recovery of the z magnetisation of GlcNAcβ-OH1 is shown (■) in each plot.

4.3.3.3 Evidence of Hydrogen Bonds

Poppe and van Halbeek have proposed that a hydrogen bond exists in solution for Galβ1-4Glc between Glc-OH3:::Gal-O5 (Poppe and van Halbeek, 1994). The evidence for this is based upon the dramatic up-field shift upon galactosylation of Glc-OH3, the exchange rate and chemical shift temperature coefficients of this hydroxyl proton. The simple modification of Glc to *N*-acetylglucosamine would not be expected to alter the hydrogen bond.

Figure 4.9 shows the proton spectra of the exchangeable proton region for Galβ1-OMe, GlcNAc, and *N*-acetyllactosamine. Upon galactosylation GlcNAc-OH3 experiences a large up-field shift of approximately 0.5ppm, as expected (Poppe and van Halbeek, 1994). From the HO-CH coupling constant data (Table 4.2), a hydroxyl group that is freely rotating has a coupling constant of about 5.5 - 6 Hz. GlcNAc-OH3 in *N*-acetyllactosamine has a significantly smaller coupling constant, and the exchange rate measured is also smaller than the exchange rates for the other hydroxyls which is suggestive of a hydrogen bond involving this hydroxyl. In contrast the chemical shift temperature coefficients, which in previous studies have reported smaller temperature coefficients for hydroxyls involved in hydrogen bonds, are in the present study larger than the other hydroxyl protons. This conflicting evidence suggests that a hydrogen bond may exist in aqueous solution, however, it is probably not long lived.

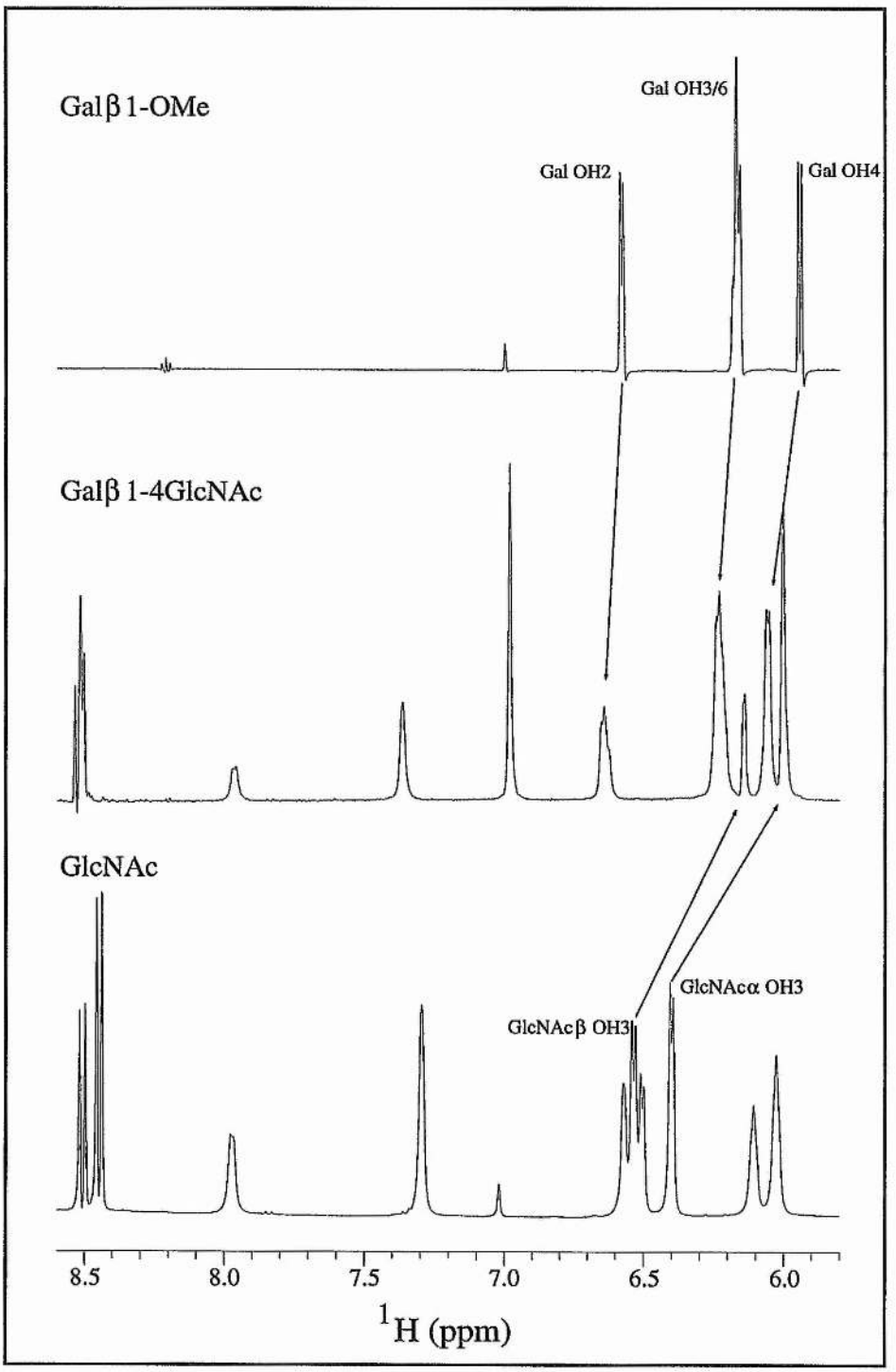

Figure 4.9 - 1D ES-^{1}H spectra of (A) Galβ1-OMe, (B) Galβ1-4GlcNAc, and (C) GlcNAc in H_2O/acetone-d_6 (85:15) at 258K.

4.3.4 Trans-glycosidic Coupling Constants

In every oligosaccharide there are five three bond trans-glycosidic coupling constants that can be measured (generally, two $^3J_{CH}$, and three $^3J_{CC}$). For Galβ1-4Glc(NAc) linkage, both of the two $^3J_{CH}$ values, Gal-C1 - GlcNAc-H4 and Gal-H1 - GlcNAc-C4 (Barker *et al.*, 1982; Rosevear *et al.*, 1982), and two of the $^3J_{CC}$ values, GalC1-GlcNAcC5 and GalC1-GlcNAcC3 (Nunez and Barker, 1980), have been previously determined. Using methods applicable to fully ^{13}C-labelled materials, four of these five coupling constants have been determined (Table 4.5).

4.3.4.1 ^{13}C-^{13}C Coupling Constants

The carbon-carbon coupling constants have been measured by the quantitative J correlation method described by (Bax *et al.*, 1992). *F1* strips of the LRCC spectrum corresponding to the proton chemical frequencies of Gal-H1 and Gal-H2, with the one-bond correlations (reference peaks) and long range correlations corresponding to trans-glycosidic couplings indicated (*figure 4.10*). The measurement of the coupling constants is simply a ratio of the long range correlation (H_X, C_Y) and the "one bond" correlation (H_X,C_X), and the values obtained from this method are complied in Table 4.5. Interestingly, the trans-glycosidic coupling constant between Gal-C1 and GlcNAc-C3 does not give rise to a correlation in this spectrum indicating a coupling below the threshold of detection (~<1.0 Hz). The apparent zero value for this coupling constant and the value for $^3J_{\text{Gal-C1, GlcNAc-C5}}$ compare favourable with those values measured on [1-^{13}C] Galβ1-4GlcNAc (Nunez and Barker, 1980).

The error in the coupling constants measured via this approach can be estimated as the apparent one bond carbon-carbon coupling constants are the difference between the actual value and the "tuned" value of 45Hz, giving rise to cross-peaks with a value equivalent to the difference. Table 4.3 summarises the one-bond carbon-carbon coupling constants from this LRCC experiment, the one bond carbon-carbon coupling constant values from the ^{13}C,^{13}C COSY spectrum, and the error between these values.

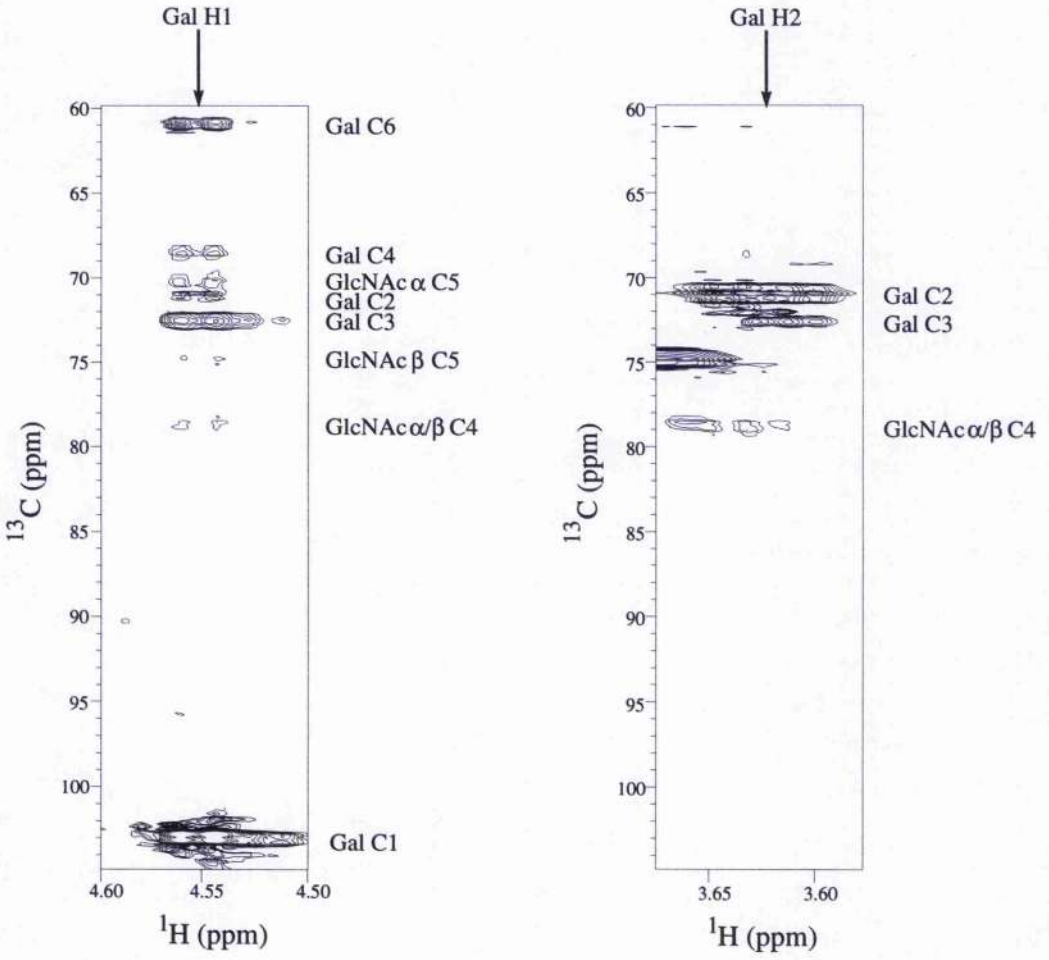

Figure 4.10 - *F1* strips of the 2D ^{1}H-^{13}C LRCC spectrum at the ^{1}H chemical frequencies of (A) Gal-H1, and (B) Gal-H2.

Table 4.3 - Values of the apparent $^{1}J_{CC}$ from the LRCC experiment compared with $^{1}J_{CC}$ values obtained from a 1D ^{13}C spectrum, allowing estimations of the errors in the coupling constants derived from the quantitative J correlation method.

Coupling	J_{CC}[a] (Hz)	Equivalent $^{1}J_{CC}$	$^{1}J_{CC}$[b]	Error[c] (%)
Gal				
C1 - C2	2.0	47.0	46.5	25%
C2 - C3	3.9	41.1	42.2	29%
C3 - C4	7.7	37.3	38.4	21%
C4 - C5	6.9	38.1	38.4	5%
GlcNAc				
C3 - C4	7.2	37.8	38.2	6%
C4 - C5	3.2	41.8	42.5	23%

(a) Value derived from the LRCC experiment
(b) $^{1}J_{CC}$ values from a 1D ^{13}C spectrum
(c) Error calculated as follows:

$$\%Error = \left[\frac{^{1}J_{CC}(LRCC) - {}^{1}J_{CC}(1D)}{^{1}J_{CC}(LRCC)}\right]\times 100$$

where the $^{1}J_{CC}(1D)$ represent the values that should be obtained in the LRCC experiment (i.e., 45Hz - $^{1}J_{CC}$)

4.3.4.2 ^{13}C-^{1}H Coupling Constants

Measurement of the carbon-proton coupling constants (Table 4.5) was by the constant time heteronuclear COSY experiment for ^{13}C labelled samples, proposed by Ionides *et al.* (1995) and fitting procedure described by Titman *et al.* (1990). This method simultaneously allows the COSY-type peak, with the active carbon-proton coupling in anti-phase, and the HOHAHA-type peak, where the active carbon-proton coupling is in-phase, in the one experiment. Unfortunately, similar to the case for lactose, the proton resonances for Gal-H5 and GlcNAc-H4 are coincidental, and therefore in this heteronuclear COSY spectrum the long range correlations to Gal-C1 overlap which does not allow these long range correlations to measured. With selective decoupling during acquisition of the Gal-C5 to collapse the relevant cross-peaks, a further complication arising for the determination of this Gal-C1, Glc-H4 coupling was encountered. In *N*-acetyllactosamine the proton H4 is strongly coupled, and determination by the fitting procedure is not possible. Unfortunately, due to the strongly coupled nature of this resonance no applicable method has been found to

measure this coupling constant. The value of this coupling constant has been previously determined as $^{3}J_{Gal\text{-}C1,\ GlcNAc\text{-}H4} = 4.9$ Hz (Barker *et al.*, 1982).

4.3.5 Modelling

4.3.5.1 Structural implications of ROE data for exchangeable protons

Only two trans-glycosidic NOEs are observed in *N*-acetyllactosamine that do not involve exchangeable protons. In order to assess the impact of the additional restraints obtained, it is necessary to take into account the very rapid (picosecond) motional averaging of the hydroxyl groups about their respective C-O bond, which gives rise to fluctuating internuclear distances. A convenient method for achieving this is by simulation of the molecular dynamics trajectory of the glycan *in vacuo* for a period of time that is longer than the timescale of the internal motions. In this present study a 500ps restrained MD simulation was computed, with restraints derived from the inter-glycosidic NOEs involving non-exchangeable protons. These restraints were applied as 'fixed' distances, corresponding with the 'single conformation' model involving limited torsional fluctuations about the glycosidic linkage. The time averaged inter-glycosidic NOEs involving exchangeable protons were then calculated over the timecourse of the simulation, using a full relaxation matrix analysis using a formalism appropriate for fluctuating inter-nuclear distances due to internal motions which are rapid with respect to overall isotropic tumbling (Tropp, 1980; Homans and Forster, 1992). One of these NOEs involves GlcNAc-OH6, which forms part of the pendent hydroxymethyl group whose internal rotation about the C5-C6 bond is slow with respect to overall tumbling. It is therefore necessary to compute two MD simulations with the dihedral angle ω about the C5-C6 bond weakly constrained to two conformations (gg and gt) observed to exist in the disaccharide on the basis of homonuclear spin-coupling constant measurements. A weighted average [gg (66%) and gt (34%)] was then taken over the two simulations. Results for the relevant trans-glycosidic ROEs involving exchangeable protons are given in Table 4.4, where it can be seen in particular the ROE between Gal-H1 and GlcNAc-OH3 is severely underestimated in these simulations. This immediately suggests that substantial torsional fluctuations exist in the disaccharide in free solution, and indeed the experimental ROEs compare more favourably with predicted values when the restraint bounds corresponding to the two original NOEs are relaxed (Table 4.4). The resulting torsional fluctuations about φ and ψ lie within the global minimum energy region of

the glycan, and offer a plausible model for the dynamic behaviour of the glycan in solution (*figure 4.11*).

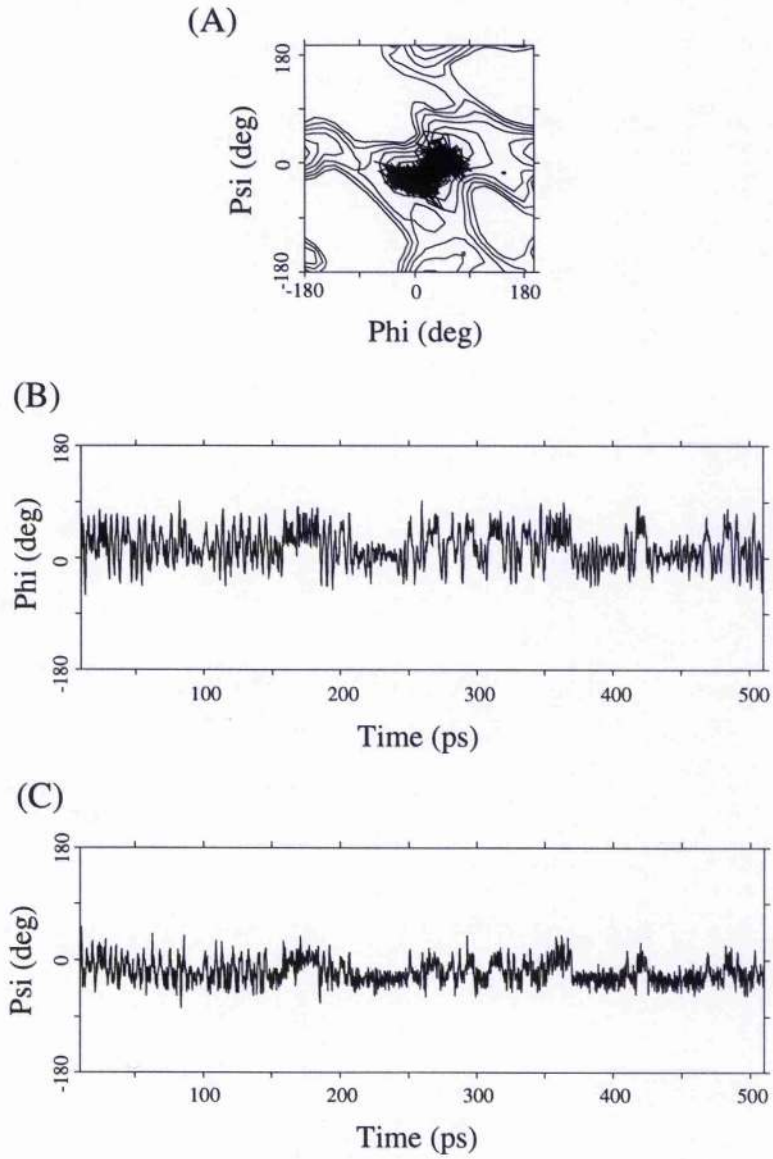

Figure 4.11 - (A) Instantaneous values of the glycosidic torsion angles ϕ and ψ over the 500ps restrained MD simulation *in vacuo* for Galβ1-4GlcNAc. (B) Instantaneous values of the glycosidic torsion angles ϕ vs. time over the 500ps restrained MD simulation. (C) Instantaneous values of the glycosidic torsion angles ψ vs. time over the 500ps restrained MD simulation.

4.3.5.2 Assessment of model

Long range spin-coupling constants are important NOE-independent data which can be used to assess the models proposed by restrained molecular dynamics simulations. Theoretical coupling constants were computed from a two 500ps dynamics simulation, one with the two inter-glycosidic non-exchangeable restraints as fixed distances and the other with all the non-exchangeable and exchangeable NOE restraints, with in-house written software 'MDPROCESS' with a trans-glycosidic $^3J_{CH}$ Karplus relationship derived by Tvaroska *et al.* (1989) and the trans-glycosidic $^3J_{CC}$ Karplus relationship derived in this present study (see chapter 3). Table 4.5 lists these theoretical data, with the back-calculated values from the model with 'fixed' restraints showing poor agreement with the experimental values, especially the $^3J_{Gal\text{-}C1,\ GlcNAc\text{-}C5}$, and $^3J_{Gal\text{-}H1,\ GlcNAc\text{-}C4}$ values. This is in agreement with the NOEs to the hydroxyl protons where they could not be accurately simulated using a model with limited torsional fluctuations. In comparison, the model where these restraints are relaxed, and the hydroxyl proton restraints included, are in good agreement with those measured experimentally, and this suggests that this model of increased torsional fluctuation is a reasonable representation of the dynamics of *N*-acetyllactosamine in solution.

Table 4.4 - Experimental ROEs involving exchangeable protons compared with theoretical values derived from two 500ps restrained MD simulations *in vacuo* for Galβ1-4GlcNAc.

ROE Connectivity	ROE Intensities (%)		
	Experimental[c]	Theoretical	
		'Fixed' restraints[a]	'Relaxed' restraints[b]
Gal H1 - GlcNAc OH3	0.7	0.1	1.2
Gal H1 - GlcNAc OH6*	0.5[d]	1.0	0.2
Gal OH2 - GlcNAc H6*[e]	2.0	1.0	2.3

(a) Restraints: Gal H1 -GlcNAc H4: 2.34Å<r<2.54Å; Gal H1 - GlcNAc H6: 2.92Å<r<3.12Å; force constant = 10 kcal/Å^2.
(b) Restraints: Gal H1 - GlcNAc H4: 1.8Å<r<2.7Å; Gal H1 - GlcNAc H6: 1.8Å<r<5.0Å; force constant = 10 kcal/Å^2.
(c) Experimental values (±10%) expressed as the sum of intensities of α and β anomers.
(d) Estimated error ±25% due to low cross-peak intensity.
(e) Theoretical value computed as the sum of the ROEs to each hydroxymethyl proton.
*: treated as a pseudoatom.

Table 4.5 - Comparison of experimental trans-glycosidic coupling constants vs. theoretically computed values derived from a 510ps *in vacuo* molecular dynamics simulation.

Trans-glycosidic Coupling	Experimental[a] (Hz)	Theoretical Value(Hz)	
		'Fixed' Restraints	'Relaxed' Restraints
$^3J_{CC}$			
Gal C2 - GlcNAc C4	2.9	3.3	2.3
Gal C1 - GlcNAc C3	< 1.0	1.0	0.6
Gal C1 - GlcNAc C5	1.6	0.8	1.6
$^3J_{CH}$			
Gal H1 - GlcNAc C4	4.4	3.1	4.0
Gal C1 - GlcNAc H4	n.d[b]	5.2	4.7

(a) Errors in these measurements estimated as ±0.5 Hz.
(b) Literature value for this coupling is 4.9 Hz (Barker *et al.*, 1982).

4.4 Conclusions

The accurate quantitation of an inter-glycosidic NOE coincident with an intra-residue NOE was obtained by the application of heteronuclear NMR experiments on a carbon-13 enriched oligosaccharide. To supplement the two inter-glycosidic NOEs to C-linked protons, low temperature studies allowing observation of the exchangeable protons, have provided an additional three ROEs. Unlike NOEs involving non-exchangeable protons, which tend by nature to involve protons close to the glycosidic linkage, and therefore are not very sensitive to torsional fluctuations about the glycosidic linkage, NOEs involving OH and NH protons in oligosaccharides are not necessarily proximal to the glycosidic linkage, and hence are much more sensitive to conformation. In this example, sufficient ROEs to exchangeable protons have been observed to confirm that substantial torsional fluctuations exist about the glycosidic linkage, a result that in the past has not been obvious without recourse to detailed relaxation-time measurements.

Using all of the distance restraints in a restrained molecular dynamics simulations, the resulting torsional fluctuations predicted lie within the global minimum energy region of the glycan, and the back-calculated NOE and spin coupling constants (carbon-carbon and carbon-proton) are within reasonable agreement suggesting that this flexible model is consistent with the experimental data.

Chapter 5

Heteronuclear NMR Investigation of the Solution Structure and Dynamics of the carbohydrate moiety sialylα2,3-N-acetyllactosamine

Abstract

Heteronuclear NMR experiments were performed to study the structure and dynamics of a carbon-13 enriched carbohydrate, sialylα2,3-*N*-acetyllactosamine (Neu5Acα2-3Galβ1-4GlcNAc) in free solution. Structural information was obtained using multidimensional heteronuclear NMR experiments, namely, ^{13}C-edited ROESY, measurement of long range carbon-proton, and carbon-carbon spin coupling constants. 3D ROESY-HSQC experiments provided unambiguous assignment of all ROESY cross-peaks, proved that one ROE reported in the literature was assigned incorrectly, and revealed two additional ROEs across the Galβ1-4GlcNAc linkage. Additional structural information was obtained from low temperature studies which allowed observation of the hydroxyl proton resonances, and assignment of three additional inter-glycosidic NOEs. The increase in the number of observable restraints has allowed time-averaged restrained molecular dynamics to be employed to study the dynamics of this carbohydrate in solution.

5.1 Introduction

The structural element Neu5Acα2-3Galβ1-4GlcNAc is a prominent part of many sialyl oligosaccharides of glycoproteins, with complex type saccharides normally terminating with this or the closely related Neu5Acα2-6Galβ1-4GlcNAc moiety. Sialic terminating oligosaccharides are known to be involved in many biological functions (reviewed by Varki, 1993), with the negative charge of the sialic acid being important. Sialylα2,3-*N*-acetyllactosamine is a known ligand for two of the sialoadhesions, a family of sialic acid dependent recognition molecules within the immunoglobulin superfamily. Both Sn and CD33 recognise sialylα2,3-*N*-acetyllactosamine, although specific biological functions have yet to be demonstrated for these proteins.

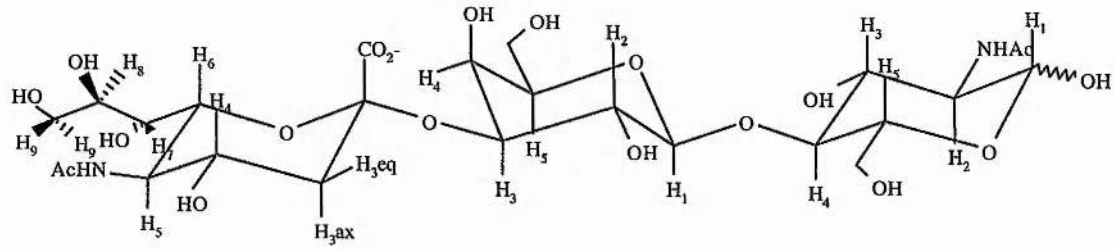

Figure 4.1 - Schematic representation of sialylα2,3-*N*-acetyllactosamine with numbering scheme used in the text.

The three dimensional conformation of sialylα2,3-*N*-acetyllactosamine and the structure and dynamics of a closely related oligosaccharide, G_{M3} (sialylα2,3-lactose), have been studied using various high resolution NMR techniques (Breg *et al.*, 1989; Siebert *et al.*, 1992). A heteronuclear NMR study of G_{M3} in which the neuraminic acid was ^{13}C-enriched in the 1, 2, and 3 positions, was studied on the surface of a magnetically oriented membrane by measurement of ^{13}C-^{13}C and ^{1}H-^{13}C dipolar splittings (Aubin and Prestegard, 1993). The information obtained, however, was limited to the orientation of the Neu5Ac pyranose ring relative to the membrane surface. With recent advances in heteronuclear NMR experiments and the synthesis of highly ^{13}C-enriched sialylα2,3-*N*-acetyllactosamine, a rigorous investigation of the conformation and dynamics is now possible.

5.2 Materials and Methods

5.2.1 Sample preparation

5mg of Neu5Acα2-3Galβ1-4GlcNAc (Aldrich) and *N*-acetyl-[U-^{13}C]-Neu5Acα2-3Galβ1-4GlcNAc (~7mg) were dissolved and lyophilised into 99.96% D_2O three times followed by dissolution into 750μL D_2O. For the observation of the exchangeable protons the natural abundance Neu5Acα2-3Galβ1-4GlcNAc was dissolved in 750μL of H_2O containing 15% 99.96% acetone-d_6 (Cambridge Isotopes). The pH was adjusted to 5.5 to 6.0 by careful step-wise addition of dilute HCl or NaOH and transferred to a 5mm NMR tube. The sample was degassed by sonication for about 1 minute.

5.2.2 NMR Experiments

NMR spectra were obtained at 303K and 258K with a reference frequency of 500MHz on a Varian Unity$^+$ spectrometer equipped with a self shielded z gradient triple resonance probe. All spectra were recorded in the phase sensitive mode (except the ES-COSY spectra which were acquired in absolute intensity mode) with use of the States method for quadrature detection (States *et al.*, 1982).

2D HSQC experiments were recorded with a total of 512 complex and 2K complex points in the t_1 and t_2 dimensions respectively, with spectral widths of 9.3kHz and 2kHz. Four scans were acquired per t_1 increment, with a total acquisition of 3 hours.

2D HCCH-COSY and HCCH-TOCSY experiments were recorded using the three-dimensional pulse scheme (Bax *et al.*, 1990; Yu *et al.*, 1993). A total of 256 complex and 2K complex points were acquired in the t_1 and t_2 dimensions respectively, with spectral widths of 9.3kHz and 2kHz. Two and three dimensional gradient enhanced long range carbon-carbon J correlation (LRCC) experiments (Bax *et al.*, 1992; Bax *et al.*, 1994a,) were recorded with a proton sweep width of 2.1kHz, consisting 1K complex points and a ^{13}C sweep width of 9.6kHz in t_1 (256 complex points) and a 9.6kHz (32 complex points) in t_2 for the 3D experiment. A total of 256 scans and 8 scans were acquired per increment for the 2D and 3D experiments respectively. ^{13}C-^{13}C couplings evolve and are refocused during the delay (2T) of 22.2ms. Total acquisition times for the 2D and 3D experiments were ~60

hours and ~48 hours, respectively. The values of the long range coupling constants are derived from the ratios of the cross-peaks obtained in the spectrum in the manner as described by Bax *et al.* (1992).

Trans-glycosidic carbon-proton coupling constants were measured using the 2D constant-time pulse sequence (CT-LRCH) of Ionides *et al.* (1995). The constant time period was 13.13ms to allow evolution of the ^{13}C-^{1}H couplings whilst refocusing the ^{13}C-^{13}C couplings. Proton and carbon sweep-widths were identical to those used in the 2D LRCC experiment with 4096 complex points in t_2 and 256 t_1 increments consisting of 64 scans per increment, yielding a total acquisition time of ~20 hours.

Three dimensional ^{13}C-edited ROESY (Bothner-by *et al.*, 1984; Bax and Davis, 1985) experiments were acquired with the pulse sequence described in chapter 3, which includes offset compensation (Griesinger and Ernst, 1987) and with spectral widths of 1.9kHz, 7kHz, and 1.9kHz and 128, 32, and 1024 complex points in t_1, t_2, and t_3 respectively. The proton offset was placed 200Hz up-field of the highest field resonance during the spin-lock period to minimise coherence effects. To optimise digital resolution the Neu5Ac-C3 resonances were folded-in once, with the incremental delay at time zero in t_2 calculated (Edison *et al.*, 1994) to give a processed spectrum where the folded peaks have an opposite phase to non-folded peaks when zero and first order phases are set to 90° and -180°, respectively. The effective field for spin locking was 2kHz and was applied for 250ms. Prior to Fourier transformation, data were apodised with cosine-bell functions, and t_1, and t_2 dimensions were zero-filled to 256 and 64 complex points, respectively. Total acquisition time for the 3D experiment was ~55 hours.

Two dimensional ES-COSY and ES-NOESY spectra were acquired at 258K with the pulse sequences described in chapter 3, and spectral widths of 3.8 kHz, 512 t_1 increments, 32 scans per increment with 4K complex points in t_2. ES-COSY spectra were acquired in magnitude mode. The ES-NOESY spectrum was acquired with a spin-lock period of 100ms using a weak (~3kHz) continuous-wave rf field. Prior to two dimensional Fourier transformation data were apodised using cosine-bell functions. Hydroxyl exchange rates were measured using the method described by Adams and Lerner (1992) incorporating excitation sculpting water suppression (Hwang and Shaka, 1995). Spectra were acquired

with 16 scans, 4K complex points, a sweep width of 3.8 kHz and were recorded with saturation times varying from 0 to 1s. ES-1D ^{1}H spectra were acquired with a proton sweep width of 4 kHz and 8K points. Temperature coefficients were acquired from ES-1D ^{1}H spectra acquired between 255K and 265K, and exchangeable spin couplings were measured from the ES-1D ^{1}H spectrum acquired at 258K with resolution enhancement via selection of appropriate window functions prior to Fourier transformation.

5.2.3 Molecular Modelling

Computer models were assembled using Biosym's Insight II molecular graphics package running on a Silicon Graphics Indigo 2 Challenge. Random structures were generated by dynamical quenching. An initial structure was built with pyranose rings in the $^4C_1$ chair conformation with trial values of phi (ϕ) and psi (ψ), and were subjected to 200ps of unrestrained molecular dynamics at 750K, during which the torsional terms are scaled by a factor of 7 to prevent excessive ring puckering. A random structure was saved every 10ps. Energy minimisation by restrained simulated annealing was achieved as follows: models were equilibrated for 10ps with a thermal bath at temperatures 500K, 450K, 350K, 300K, and then successively for 1ps in decreasing steps of 10K, followed by a further 1ps at 5K. The system was minimised using steepest descents algorithm until the maximum derivative was less than 0.04kJmol^{-1}Å^{-1}. Restraints were applied as a biharmonic function (discussed in Chapter 1).

All molecular dynamics simulations were performed *in vacuo* with a dielectric constant (ε) of 80.0. The AMBER force-field (Weiner *et al.*, 1984; Weiner *et al.*, 1986) with a carbohydrate parameter set developed by Homans (1990a) was used with the exo-anomeric potentials set to zero. Simulations using Discover lasted 1.01ns and 5.01ns with the last 1ns and 5ns, respectively, used in further analysis. Simulations using time-averaged restraints were performed with XPLOR (Brunger, 1987) where an initial 50ps of "conventional" restrained dynamics was used to equilibrate the system and then 1ns and 5ns time-averaged restrained trajectories were performed.

5.3 Results and Discussion

5.3.1 Spectral Assignments

Spectral assignments for the non-exchangeable protons and carbons of Neu5Acα2-3Galβ1-4GlcNAc (sialylα2,3-*N*-acetyllactosamine) are given in Table 5.1, whilst assignments, exchange rates, and temperature coefficients for the exchangeable protons are compiled in Table 5.2. These data are in agreement with previous assignments for the non-exchangeable protons and carbons (Breg *et al.*, 1989; Ichikawa *et al.*, 1992) except for the assignments of the GlcNAcβ H1, H2, and H3 due to both previous studies involved GlcNAcβ-O-glycosides of sialylα2,3-*N*-acetyllactosamine.

Complete assignments of the proton and carbon chemical shifts were obtained from 2D ^{1}H-^{1}H COSY, TOCSY, and 2D ^{1}H-^{13}C HSQC (*figure 5.2A*) experiments. The exchangeable proton chemical shifts were obtained from 2D ^{1}H-^{1}H ES-COSY (*figure 5.2B*), and ES-TOCSY experiments.

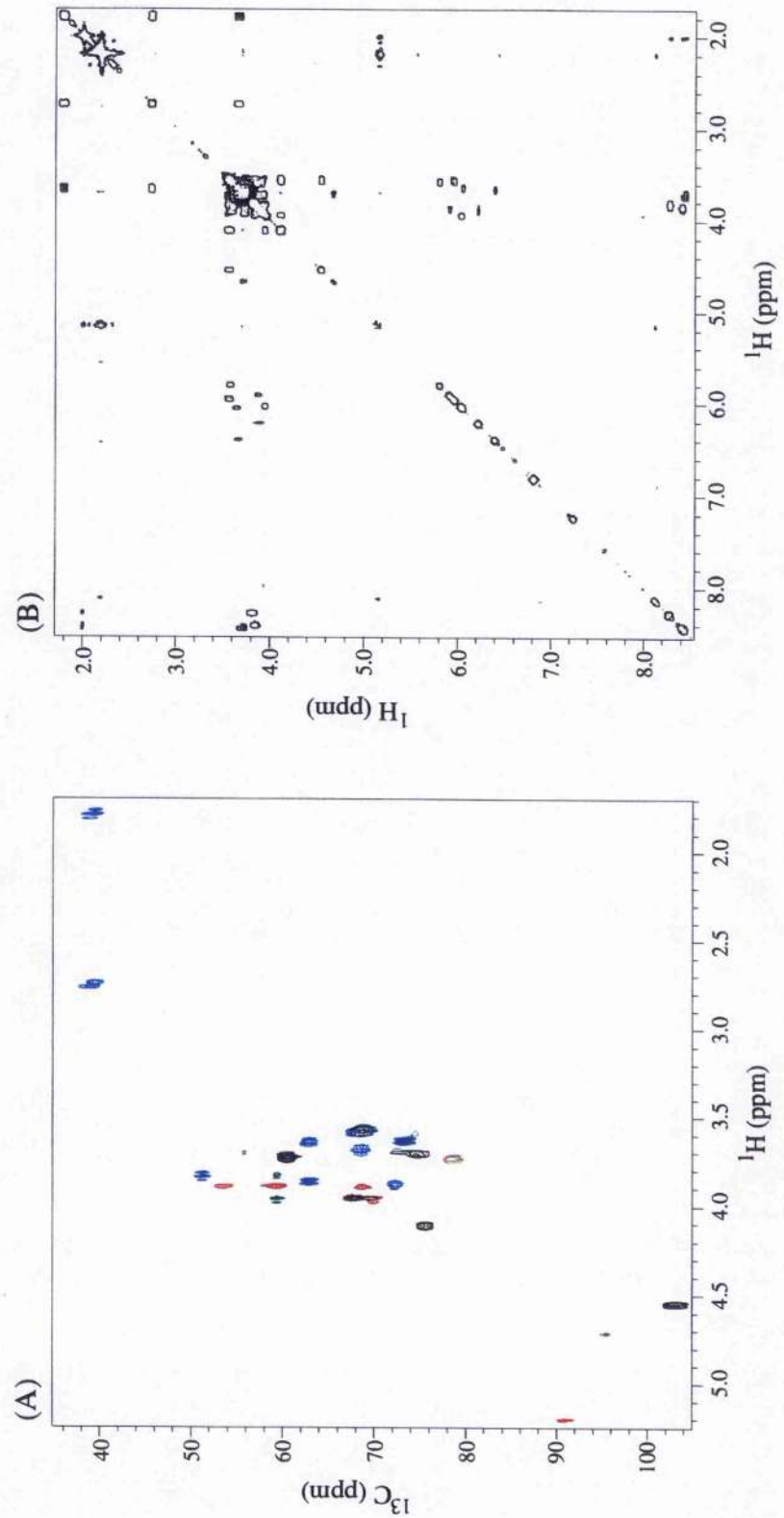

Figure 5.2 - (A) Heteronuclear ^{1}H-^{13}C HSQC spectrum of [U-^{13}C] sialylα2,3-N-acetyllactosamine at 303K in D_2O. Peaks shown in Black = Gal, Red = GlcNAcα, Green = GlcNAcβ, and Light Blue = Neu5Ac. (B) Two dimensional magnitude mode ^{1}H-^{1}H ES-COSY spectrum of sialylα2,3-N-acetyllactosamine at 258K in H_2O/acetone-d_6 (85:15) showing through-bond connectivities to exchangeable protons.

Table 5.1 - ^{1}H and ^{13}C Chemical Shift Assignments for sialylα2,3-*N*-acetyllactosamine in D_2O at 303K.

	Neu5Acα		Galβ		GlcNAcα		GlcNAcβ	
	^{1}H	^{13}C	^{1}H	^{13}C	^{1}H	^{13}C	^{1}H	^{13}C
1		174.2	4.57	103.0	5.22	90.9	4.73	95.2
2		100.2	3.60	69.6	3.91	54.0	3.72	56.5
3	2.77 eq	39.9	4.13	75.8	3.91	69.5	3.72	72.9
	1.81 ax							
4	3.71	68.6	3.97	67.9	3.76	79.1	3.75	78.7
5	3.86	52.0	3.73	75.5	3.99	70.5	3.61	75.1
6	3.65	73.2	3.75	61.3	3.91	60.2	3.99	60.4
							3.86	
7	3.71	68.4						
8	3.90	72.1						
9	3.88	63.0						
	3.66							
NAc	2.05				2.05		2.05	

Chemical shifts are referenced to $\delta_{TSP} = 0.00$ppm (^{1}H and ^{13}C).

Table 5.2 - NMR data for the exchangeable protons from sialylα2,3-*N*-acetyllactosamine in H_2O/acetone-d_6 (85:15) at 258K.

Proton	Chemical Shift (ppm)[a]	Exchange Rate (s^{-1})[b]	Temperature Coefficient (ppb/K)[c]	Coupling $^3J_{HH}$ (Hz)
Neu5Ac-OH4	6.46	31.2 (57.7)	9.5	~3.5
Neu5Ac-OH7	5.87	24.5 (40.3)	10.5	6.9
Neu5Ac-OH8	6.28	24.1 (51.1)	4.2	broad
Neu5Ac-OH9	~5.87	n.d.	n.d.	n.d.
Neu5Ac-NH5	8.34	–	5.5	9.5
Gal-OH2	6.03	15.5 (23.3)	12.2	3.5
Gal-OH4	6.10	15.8 (30.1)	10.7	3.4
Gal-OH6	6.16	n.d.	11.9	n.d.
GlcNAcα-OH1	7.30	24.1 (45.8)	6.6	broad
GlcNAcα-OH3	5.97	21.2	10.5	broad
GlcNAcα-OH6	5.95	n.d.	n.d.	n.d.
GlcNAcα-NH2	8.51	–	9.1	9.6
GlcNAcβ-OH1	7.88	27.6	9.8	broad
GlcNAcβ-OH3	6.11	15.8 (31.8)	n.d.	~2.6
GlcNAcβ-OH6	6.01	19.8	11.8	n.d.
GlcNAcβ-NH2	8.47	–	7.2	7.8

(a) Chemical shifts referenced to $\delta_{TSP} = 0.00$ ppm (by setting residual acetone to 2.19 ppm).
(b) Exchange rates measured at 258K and 268K (figure in brackets).
(c) Temperature coefficients measured over a 10K range between 258K - 268K.
n.d. = not determined.

5.3.2 ^{1}H-^{1}H Homonuclear NOEs

Spectral overlap in the ^{1}H dimension is sufficiently severe that analysis of the conventional two-dimensional ^{1}H-^{1}H ROESY spectrum is not straightforward. To illustrate this point, a small section of the 2D ROESY spectrum centred at Gal-H1 (*F1*) is shown (*figure 5.3A*). A few cross-peaks may be unequivocally assigned, but severe overlap prevents both unambiguous identification and quantition of certain resonances. By contrast, the observed cross-peaks were readily dispersed by their ^{13}C chemical shift in a two-dimensional *F2F3* (^{13}C/^{1}H) slice from the 3D ROESY-HSQC spectrum at the *F1* (^{1}H) resonance frequency of Gal-H1 (*figure 5.3B*), and all the ROE connectivities from Gal-H1 can clearly be assigned. In particular, the connectivity proposed by Siebert *et al.* (1992) (for Neu5Acα2-3Galβ1-4Glc) between Gal-H1 and Neu5Ac-H8 (^{1}H 3.89 ppm, ^{13}C 72.1 ppm) could not be observed in this 2D slice, instead an ROE connectivity to GlcNAc-H6α (^{1}H 3.90 ppm, ^{13}C 60.2 ppm) was observed which is of similar size to the proposed ROE (Siebert *et al.*, 1992). The ROE between Gal-H3 and Neu5Ac-H8 is observed however, which is consistent with the orientation of the glycerol side chain of Neu5Ac (θ_1=-60°, θ_2=180°) suggested by previous work (Poppe and van Halbeek, 1991; Siebert *et al.*, 1992), and is similarly supported by ^{1}H-^{1}H coupling constants in this present study (data not shown). An intriguing aspect of the data shown is the presence of weak cross-peaks from Gal-H1 to GlcNAcα/β-H3 and H5 (*figure 5.3B*), which have not been seen previously because of the essentially complete overlap with other resonances. The observation of these ROE connectivities must be interpreted with care, since these can arise from a strong ROE connectivity (in this case Gal-H1 to GlcNAc-H4) followed by relayed coherence transfer to other coupled protons (GlcNAc-H3 and GlcNAc-H5) via a HOHAHA mechanism (Neuhaus and Keeler, 1986). However, these cross-peaks were found to be independent of the position of the spin-lock carrier, confirming that they correspond to direct connectivities. In fact, similar ROE connectivities have been observed for the nearly identical oligosaccharide, oligo-GM3 (Neu5Acα2-3Galβ1-4Glc) (Milton, 1997). The implication of these ROE connectivities is that the Gal-GlcNAc linkage is adopting the 'anti-conformer' in aqueous solution, a phenomenon only recently observed in either DMSO-d_6 or water (Lipkind *et al.*, 1985; Lipkind *et al.*, 1987; Poppe *et al.*, 1990b; Bock *et al.*, 1994; Dabrowski *et al.*, 1995; Espinosa *et al.*, 1996).

In total seven inter-glycosidic ROEs were observed in the 3D experiment, with no evidence of the ROE reported by Siebert *et al.* (1992) between Gal-H4 and Neu5Ac-H8, with all of these utilised in restrained molecular modelling simulations (Table 5.3).

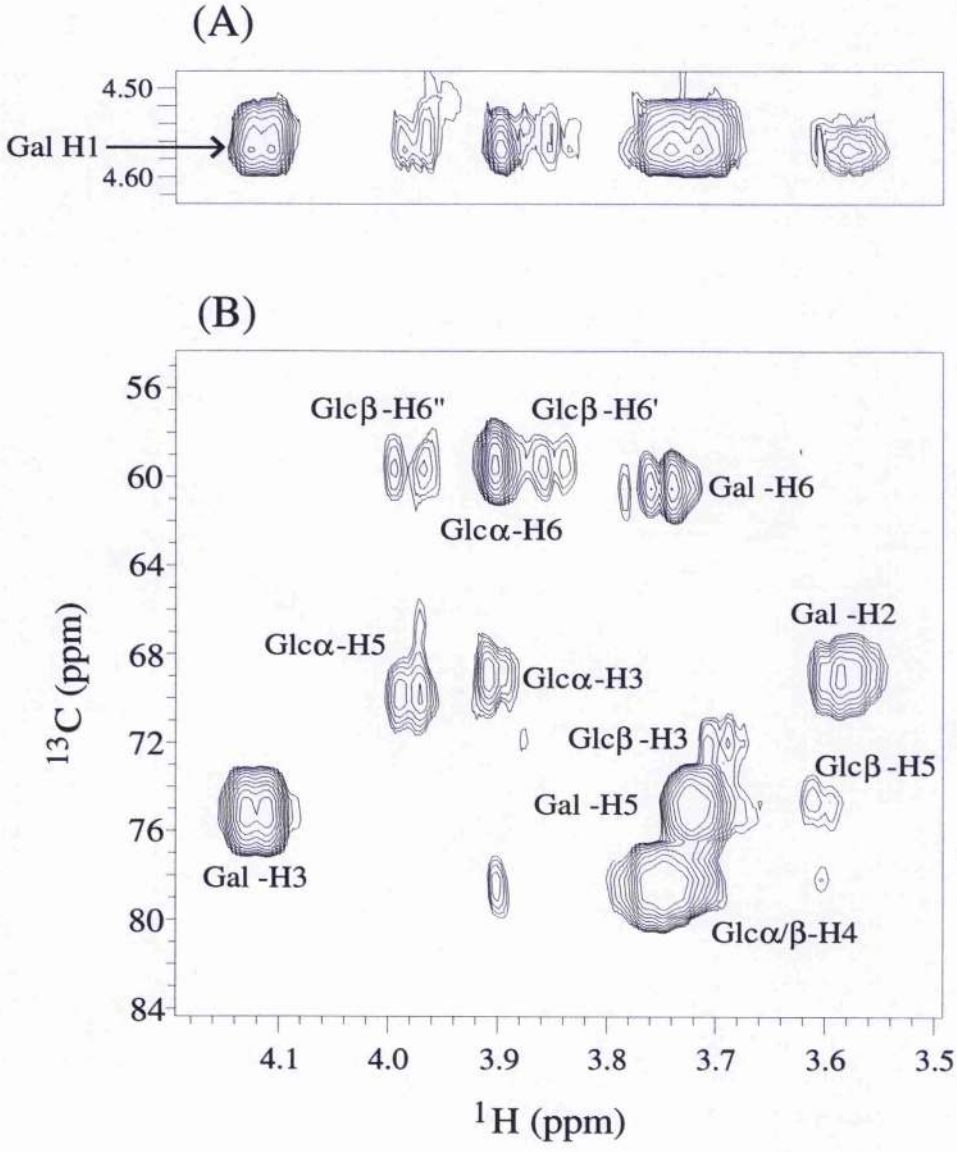

Figure 5.3 - (A) A section of the 2D ROESY spectrum of sialylα2,3-*N*-acetyllactosamine centred at Gal-H1 (*F1*). (B) An *F2F3* plane from the 3D ROESY-HSQC spectrum at the proton chemical frequency of Gal-H1.

5.3.3 Exchangeable Protons

5.3.3.1 Evidence of Hydrogen Bonding

Recently a number of hydrogen bonds occurring in the sialylα2,3-*N*-acetyllactosamine moiety in sialyl Lewis^x have been proposed, namely Neu5Ac-COOH:::Neu5Ac-OH8, Gal-OH2:::Neu5Ac-O6, and Neu5Ac-COOH:::Gal-OH4 (Poppe *et al.*, 1997). The existing proposed hydrogen bond in the Galβ1-4GlcNAc moiety should not be perturbed upon sialylation of *N*-acetyllactosamine. The basis for the proposal of these hydrogen bonds is dramatic up-field shifts, small HO-CH coupling constants, low exchange rates and chemical shift temperature coefficients. From the comparison of the exchangeable regions of the 1D ES-^{1}H spectra for *N*-acetyllactosamine and sialylα2,3-*N*-acetyllactosamine (*figure 5.4*), the proton resonance of Gal-OH2 experiences an up-field shift of approximately 0.5ppm upon sialylation. Due to the significant broadening of the exchangeable resonances indicating high exchange rates, only an estimate for $^3J_{OH2\text{-}H2}$ could be made (Table 5.2) which is comparable to the values obtained for the other hydroxyl proton resonances. The observation of an NOE between Gal-OH2 and GlcNAc-H6's [not observed in sialyl Lewis^x (Poppe *et al.*, 1997)] suggests that during a significant portion of the time, Gal-OH2 must be pointing away from the sialic acid moiety, and therefore not involved in a hydrogen bond. Both the exchange rates and temperature coefficients do not indicate that a strong hydrogen bond occurs in solution.

Previous studies, on sialyl Lewis^x and sialylα2,3-lactose, indicated that Neu5Ac-OH8 is involved in a hydrogen bond, based primarily on a significantly lower exchange rate. In this present study the evidence is again conflicting. The temperature coefficient for this hydroxyl proton resonance is significantly lower than other exchangeable protons indicating a possible involvement in hydrogen bonding. In comparison, unlike the data obtained by Poppe *et al.* (1997), the exchange rate was of the same order to the other values. In particular, the exchange rate at 268K was the greatest for those measured. For a hydroxyl proton involved in a hydrogen bond the resonance line-width would still be expected to be small at this temperature.

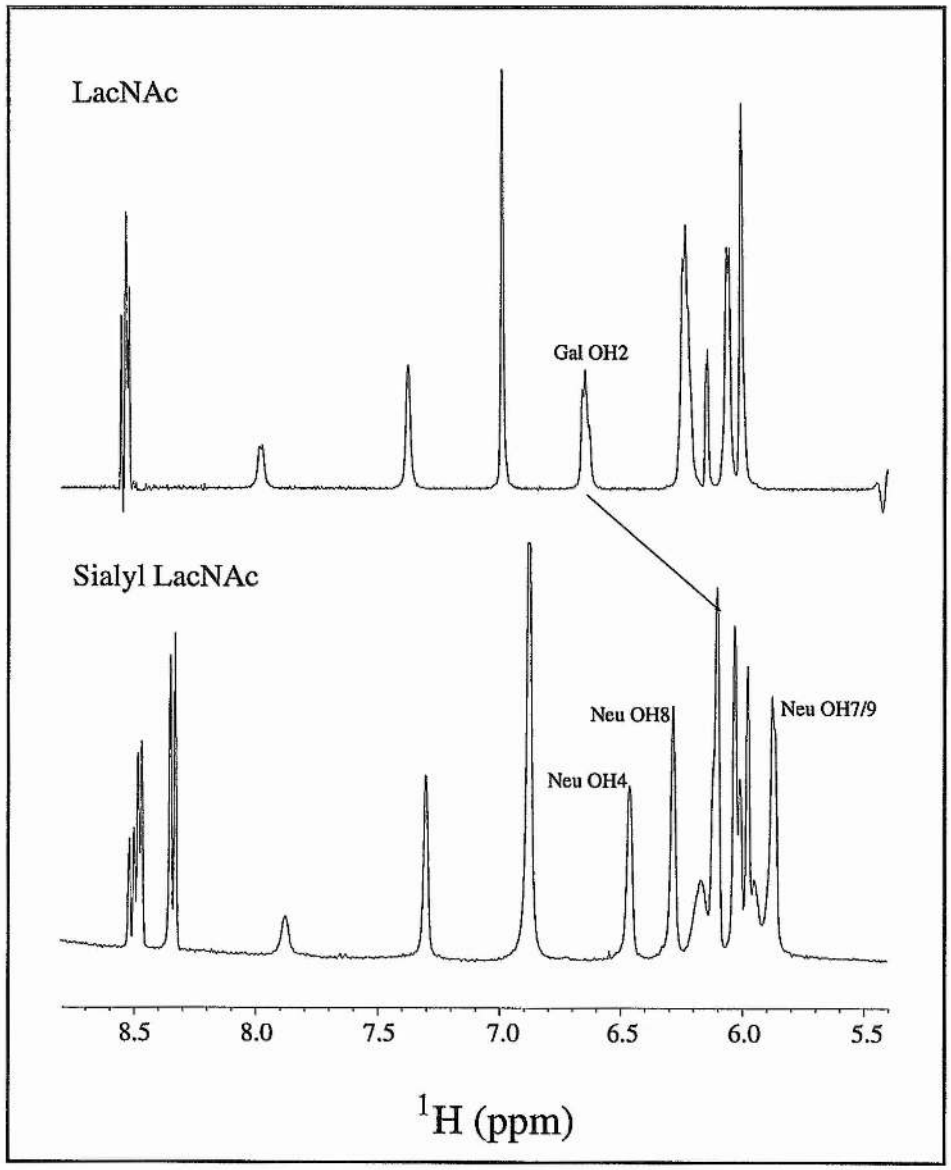

Figure 5.4 - 1D ES-^{1}H spectra of sialylα2,3-*N*-acetyllactosamine and *N*-acetyllactosamine in H_2O/acetone-*d*6 at 258K.

5.3.3.2 NOEs to hydroxyl protons

From the two dimensional ES-NOESY spectrum of sialylα2,3-*N*-acetyllactosamine at pH~6 at 258K (*figure 5.5*), corresponding to the cross-peaks between hydroxyl protons (*F2*) and non-exchangeable protons (*F1*), a number of inter-glycosidic NOEs are observable, and are indicated on the spectrum. Of particular interest are those NOEs about the Neu5Ac-Gal linkage due to the lack of and conflicting nature of the non-exchangeable/non-exchangeable NOEs observed. A further two inter-glycosidic NOEs are observed, between Gal-OH2 – Neu5Ac-H3ax and Gal-H3 – Neu5Ac-OH8, which confirms the flexibility of the Neu5Ac-Gal linkage even at low temperature. An NOE is also observed between Gal-OH2 – Neu5Ac-H3eq which arises through spin diffusion (confirmed by the lack of a cross-peak in the ES-ROESY spectrum, data not shown). One inter-glycosidic NOE is observed about the Gal-GlcNAc linkage between Gal-OH2 - GlcNAc-H6's.

A total of 3 inter-glycosidic NOEs involving exchangeable protons were observed, and these were utilised in the molecular modelling as 'weak' restraints because of the difficulty to accurately describe them as strong, medium, or weak (Table 5.3).

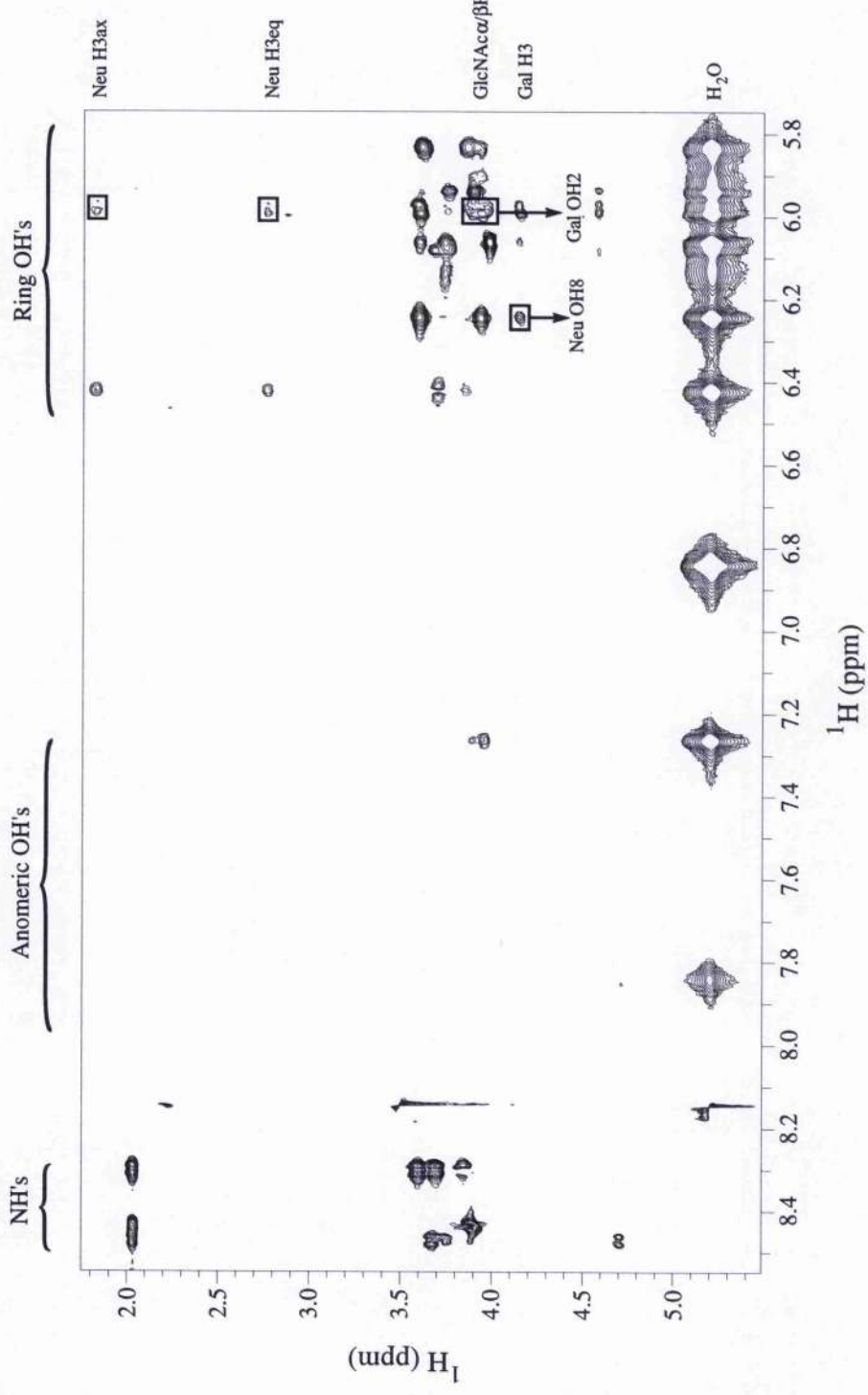

Figure 5.5 - Region of the two dimensional ^1H- ^1H ES-NOESY spectrum of sialylα2,3 - *N*-acetyllactosamine at 258K in H_2O/acetone-d_6(85:15), mixing time of 100ms, showing through-space connectivities from the exchangeable protons (*F2*) to the non-exchangeable protons (*F1*). Inter-glycosidic cross-peaks as shown.

Table 5.3 - Experimental ROEs (non-exchangeables) and NOEs (involving exchangeables).

(R)NOE Connectivity	Relative ROE[a]	r(Å)[b]	Constraint[c]
Neu5Ac-H3ax – Gal-H3	0.53	2.70	W[d]
Neu5Ac-H8 – Gal-H3	0.21	3.15	W[d]
Neu5Ac-HO8 – Gal-H3	0.15	3.33	W
Neu5Ac-H3ax – Gal-OH2	0.07	3.78	W
Gal-H1 – GlcNAc-H4	1.52	2.27	S/M
Gal-H1 – GlcNAc-$H6_{proR}$	0.11	3.51	W
Gal-H1 – GlcNAc-$H6_{proS}$	0.07	3.78	W
Gal-H1 – GlcNAc-H3	0.11	3.51	W
Gal-H1 – GlcNAc-H5	0.11	3.51	W
Gal-OH2 – GlcNAc-H6	0.34		W

(a) Reference ROE/NOE Gal H1 - H3, reference distance 2.43Å.
(b) Approximate effective ^1H-^1H distance , based upon a simple ROE ratio calculation which neglects the influence of internal motions and anistropic re-orientation.
(c) Restraints used in modelling studies; W = weak, 1.8Å<r<5.00Å; M = medium, 1.8Å<r<3.3Å; S = strong, 1.8Å<r<2.7Å
(d) Restraints applied as weak because of the conflicting nature of these NOEs, although the approximate effective distance would indicate medium restraints.

5.3.4 Trans-glycosidic Coupling Constants

Long range carbon-carbon coupling constants are potentially an important source of additional structural information for sialic acid containing oligosaccharides because, generally, only one proton-carbon coupling constant can be measured (except when there is a 2-6 linkage) and used for assessing potential models. Long range J_{CC} values may be measured from the 2D LRCC spectrum, however, sialylα2,3-*N*-acetyllactosamine suffers from poor dispersion in the ^{13}C chemical shift dimension. From a section of the 2D LRCC spectrum (*figure 5.6A*) two trans-glycosidic carbon-carbon coupling constants can be measured unequivocally between Gal-C3 and Neu5Ac-C3, and Gal-C2 and GlcNAcα/β-C4. However because of the spectral overlap in both dimensions none of the other three couplings could be measured unambiguously. In contrast, the three-dimensional experiment allows the unambiguous assignment of the trans-glycosidic correlations, and hence the measurement of all the conformationally important couplings. *F1* strips corresponding to the *F2F3* frequencies for Gal-C4/H4, Gal-C3/H3, Gal-C2/H2, GlcNAcα-C5/H5, and GlcNAcα-C3/H3, allow the trans-glycosidic correlations to be identified (*figure 5.6B*). Interestingly, no correlations were observed for $^{3}J_{Neu5Ac\text{-}C2,\ Gal\text{-}C4}$, and $^{3}J_{Gal\text{-}C1,\ GlcNAc\text{-}C3}$ indicating that both these couplings are small (<1.0), which is similar to the $^{3}J_{Gal\text{-}C1,GlcNAc\text{-}C3}$ coupling in *N*-acetyllactosamine. From this 3D experiment seven trans-glycosidic coupling constants were measured (Table 5.5). Additional three-bond carbon-carbon coupling constant were measured along the glycerol backbone of the sialic acid residue. Contrary to expectation, the measured values were not all indicative of a trans arrangement indicated by an extended formation of this tail previously proposed (Poppe and van Halbeek, 1991b; Siebert *et al.*, 1992). The values obtained indicate that the C5-C8 torsion angle is approximately ±130°, whilst the C6-C9 torsion angle is far from being a free rotor, and adopts an average conformation of approximately ±140°.

Long range proton-carbon coupling constants were measured using the 2D CT-LRCH experiment, Table 5.5. Unfortunately, as discussed previously, GlcNAc-H4 is strongly coupled and so measurement of the $^{3}J_{Gal\text{-}C1,\ GlcNAc\text{-}H4}$ value could not be determined, however the $^{3}J_{Neu5Ac\text{-}C2,\ Gal\text{-}H3}$, and $^{3}J_{Gal\text{-}H1,\ GlcNAc\text{-}C4}$ values were measured (data not shown).

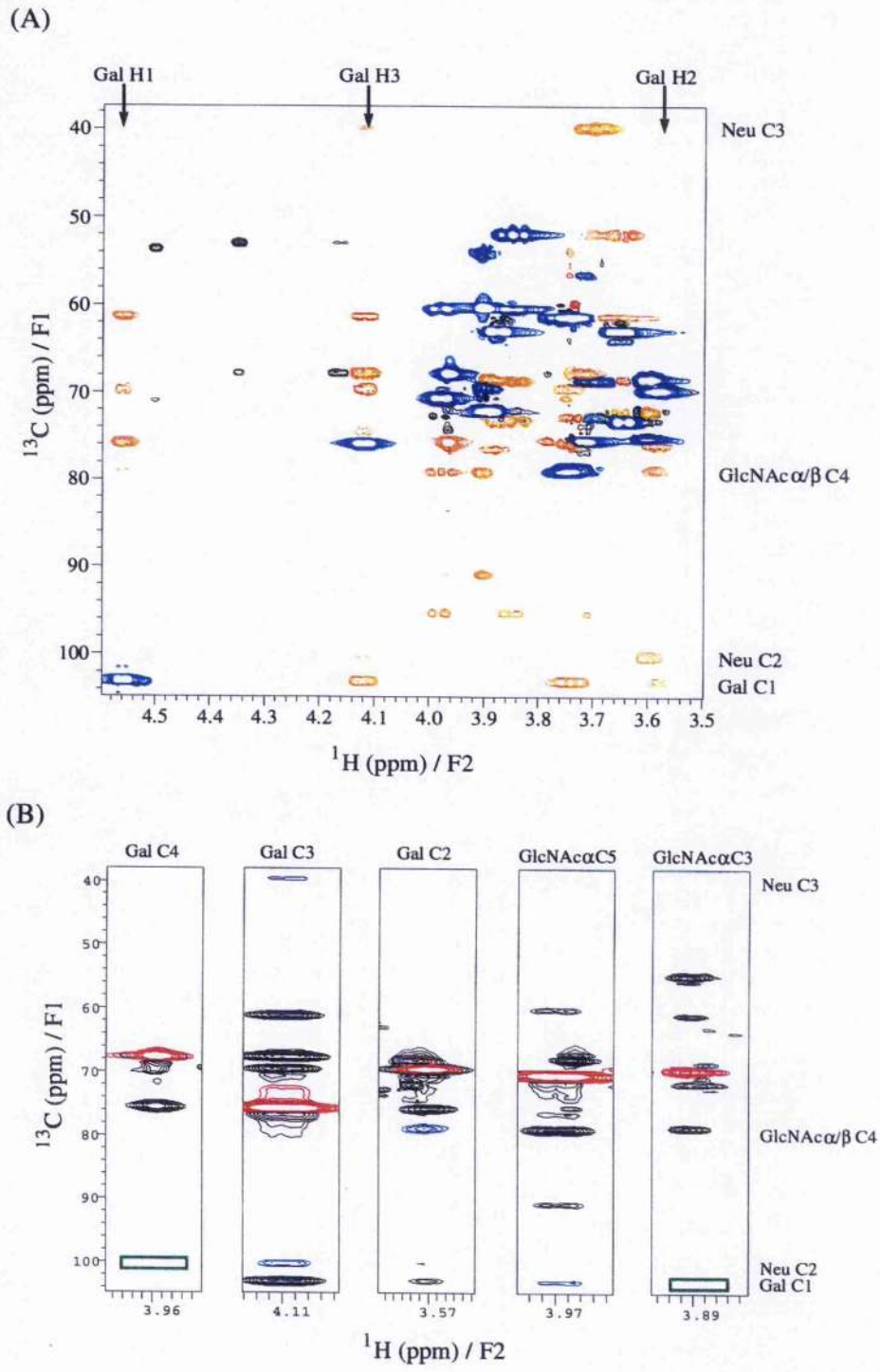

Figure 5.6 - (A) Section of the 2D LRCC spectrum of sialylα2,3-*N*-acetyllactosamine.

(B) *F1F3* strips from the 3D LRCC spectrum of sialylα2,3-*N*-acetyllactosamine.

5.3.5 Modelling

The solution dynamics of sialylα2,3-*N*-acetyllactosamine have been previously reported by Breg *et al.* (1989) using distance mapping procedures based on inter-residue ROE contacts. With the ROE contacts about the Gal-GlcNAc linkage (Gal-H1 to GlcNAcα/β-H3 and GlcNAcα/β-H5) indicating increased flexibility about this linkage, and with the addition of three NOEs to exchangeable protons, a new investigation into the solution structure and dynamics of this carbohydrate was undertaken.

5.3.5.1 Time-averaged vs. conventional restraints

In recent years a novel strategy has emerged for the refinement of structures from experimental data where distance restraints, and more recently angular restraints, incorporate time-averaged information (Torda and co-workers, 1989, 1990, 1993). The impetus for this new approach is the emergence of data which confirms that many molecules are best described in terms of a dynamical equilibrium of conformations instead of a single static picture. However, the use of time-averaged restraints has been limited in the field of glycoconjugates (Low, 1996), although it is clear that carbohydrates cannot be described in terms of a static structure, and therefore would be best described using time-averaged restraints.

In conventional refinement schemes, molecular dynamics simulations are used to sample the conformational space available in search of low energy conformations. In these simulations the agreement between experimentally derived data and instantaneous values, corresponding to snapshots along the dynamics trajectory, are optimised, and takes the form:

$$\sum_j k_j (r_{j,model} - r_{j,target}) \qquad [4.1]$$

where, $r_{j,model}$ is the inter-proton distance derived from the model structure, $r_{j,target}$ is the "observed" inter-proton distance from NOE data, and k_j is a force constant.

Obviously, the 'snapshots' are static structures which are being compared to data often derived from NOEs, which are time averaged values. It is therefore possible for a set of static structures to obey a distance restraint but be meaningless in terms of realistic conformations. Clearly a more appropriate approach would be to incorporate the time-

averaging of the distance restraints into account during the simulations, where the function to be optimised becomes:

$$\sum k_j \left(\left\langle r_{j,model} \right\rangle - r_{j,target} \right) \qquad [4.2]$$

where $\langle r_{j,model} \rangle$ now represents the time-averaged distance derived from the model.

Since only the average distance (and not the instantaneous value) needs to conform to the restraints, the conformational space sampled is generally about the same as unrestrained dynamics, and often an increase over the more restrictive conventionally "restrained" dynamics, resulting in increased information about dynamical properties of the system. However, the application of time-averaged restraints in modelling a system with few restraints results in a greater conformational flexibility than even in unrestrained dynamics, therefore, to extract information from time-averaged dynamics it is necessary to make sure that the system is sufficiently well described by the restraints (Pearlman *et al.*, 1991). It is this latter constraint which has probably limited the application to carbohydrate systems because of the few non-exchangeable/non-exchangeable NOE distance restraints obtainable.

Table 5.3 lists the distance restraints used in the restrained simulated annealing and MD simulations (conventional and time-averaged). The Neu5Acα2-3Gal linkage has been extensively studied, with Breg *et al.* (1989) first noting that the this linkage may adopt 3 different conformations in free aqueous solution (*figure 5.7*). Conformer 'A' ϕ,ψ -70°, 5°; Conformer 'B' ϕ,ψ -165°, -20°; Conformer 'C' ϕ,ψ -95°, -45°. Similar minima have been observed for the sialyl Lewis^x moiety (Rutherford *et al.*, 1994), oligo-G_{M3} (Siebert *et al.*, 1992; Milton, 1997). Conformers 'A' and 'B' are characterised by the conflicting ROEs between Gal-H3 to Neu5Ac-H3ax, and Gal-H3 to Neu5Ac-H8 respectively. ES-NOESY experiments performed on sialylα2,3-*N*-acetyllactosamine at 258K also generate conflicting NOE restraints between Gal-OH2 – Neu5Ac-H3ax, and Gal-H3 – Neu5Ac-OH8. The latter NOE has also been seen in sialyl Lewis^x (Poppe *et al.*, 1997). These conflicting ROEs indicate that sialylα2,3-*N*-acetyllactosamine must be in conformational exchange in free solution, and with the increased number of NOE restraints, it is therefore a suitable case to investigate the use of time-averaged restraints.

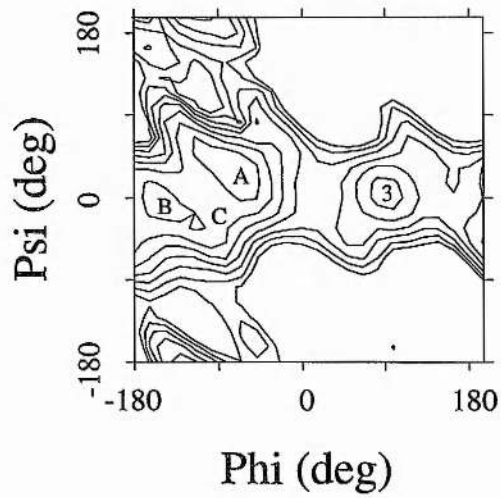

Figure 5.7 - Potential energy surface for the Neu5Acα2-3Gal linkage showing the solution conformers 'A' and 'B' predicted by Breg *et al.* (1989) and the additional solution minima predicted by Siebert *et al.* (1990). Contours are in steps of 4.2 $kJmol^{-1}$.

Although time-averaged restraints have been used in minimisation and simulated annealing, the approach used in this present study is to use conventional methods to obtain the low energy structures and compare molecular dynamics simulations with conventional and time-averaged restraints. Ten computer models of sialylα2,3-*N*-acetyllactosamine were generated from an unrestrained high-temperature (750K) MD simulation (with all torsion terms scaled by a factor of seven to prevent unrealistic ring distortions). Each of these pseudo-random structures were input into restrained simulated annealing protocol described previously. Five of the ten starting structures converged to conformer 'A' (including the global minimum structure), three annealed to conformer 'B', and one to conformer 'C' (*figure 5.8,* Table 5.4). The remaining structure violated the Gal-H1 – GlcNAc-H4 restraint and was discarded. The lowest energy structure of each family was input into a restrained MD simulation of length 1ns. Each of these three simulations gave similar results, therefore the global minimum structure was used as the input for 1ns trajectories of time-averaged restrained MD simulations with a variety of memory functions, τ, to discover the best choice of value. Previous restrained dynamics simulations performed on sialyl $Lewis^x$ antigen (Rutherford *et al.*, 1994) highlighted the requirement of long MD simulations (up to 5ns) as oscillations between conformers 'A' and 'B' are slow on the MD time-scale (≤ 12 per ns).

Therefore the lowest energy structure was subjected to two 5ns MD trajectories, one with 'conventional' restraints (Discover) and the other with time-averaged restraints (XPLOR) with the suitable value of τ

5.3.5.2 Conventionally Restrained Molecular Dynamics Simulations

In the 5ns conventionally restrained molecular dynamics trajectories for sialylα2,3-*N*-acetyllactosmine conformers 'A', 'B', and 'C' are sampled indicated by synchronous changes in ϕ and ψ values (*figure 5.8*). The back calculated ROEs and coupling constants are in poor agreement with experimental values (Tables 5.5 & 5.6), where values shown in bold in the table indicate that theoretical values significantly different to the experimental measurements. For this 'conventional' restrained simulation using Discover, the under-prediction of the Neu5Ac-H3ax – Gal-H3 NOE with the under-estimate for the $^{3}J_{Neu5Ac\text{-}C2,Gal\text{-}C2}$ value indicates that conformer A is under populated in this simulation. For the Gal-GlcNAc linkage at no time during the simulation does the ψ torsion angle adopt the 'anti-conformer', resulting in a complete under-estimate for the Gal-H1 – GlcNAc-H3&H5 ROEs where the theoretical ROEs are outside the factor of two agreement. In a second 5ns simulation with the Gal-H1/GlcNAc-H4 restraint relaxed to medium, similar results were obtained, with no observation of the 'anti-conformer' about the ψ torsion angle.

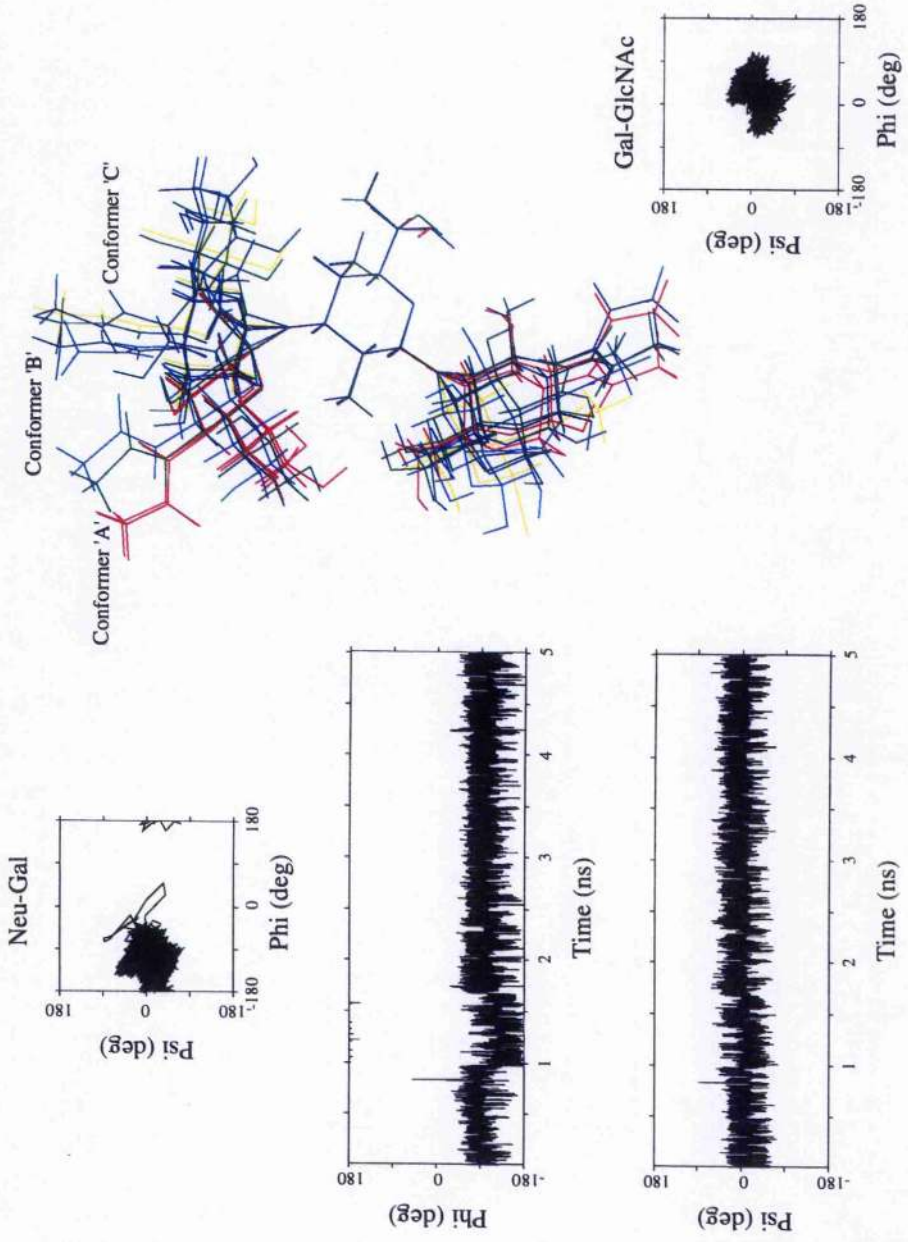

Figure 5.8 - Superposition of nine geometeries derived from the restrained dynamical simulated annealing calculations on sialylα 2,3-*N* -acetyllactosamine. Instantaneous values for ϕ vs.ψ for the Neu5Acα2-3Gal and Gal β1-4GlcNAc linkages, and the ϕ vs.ψ time plots for the Neu5Acα2-3Gal linkage from the 5ns conventionally restrained MD simulation.

Table 5.4 - Energies and torsion angles of structures from the simulated annealing process which satisfied the distance restraints obtained from ROESY data at 303K and NOESY data at 258K. The lowest energy structure for each conformer about the Neu5Ac-Gal linkage, highlighted in bold, was used in the molecular dynamics simulations.

Structure	Conformer	Neu5Ac-Gal Linkage		Gal-GlcNAc Linkage		Energy
		ϕ	ψ	ϕ	ψ	(kcal)
1	B	-156.63	-24.29	-16.81	-25.29	-1.602
2	B	-155.99	-22.21	50.38	1.66	-1.352
3	**B**	**-151.69**	**-18.97**	**0.00**	**-24.63**	**-2.424**
4	**C**	**-113.96**	**-40.52**	**47.47**	**-2.27**	**-3.235**
5	A	-81.92	14.12	32.14	3.59	-2.692
6	**A**	**-82.61**	**15.39**	**44.64**	**0.51**	**-4.053**
7	A	-77.33	14.97	0.54	-15.90	-3.256
8	A	-77.79	9.15	-26.33	-24.76	-2.828
9	B	-155.78	-16.64	35.00	-3.61	-1.993

5.3.5.3 Time-averaged Restrained Molecular Dynamics Simulations

An important technical point in the use of time-averaged restraints is the value of the exponential decay constant used in calculating the running average in time-averaged restrained simulations. An estimation of the value of the τ has been crudely set as an order of magnitude less than the total length of the simulation to allow reliable estimates of the time-averaged properties (Torda *et al.*, 1989). The main consideration is to set τ such that it is large enough to allow conformational variability in the molecule of interest. Obviously as $\tau \rightarrow 0$ so the simulation will become equivalent to the conventional restrained simulations, equally, excessively large values of τ are to be avoided because the conformational space available will be more equivalent to an unrestrained dynamics simulation which therefore defeats the use of restraints, and relies upon the accuracy of the force-field being used.

Time-averaged restrained molecular dynamics simulations were 1ns in length with varying values of τ (500ps, 50ps, 5ps and 0.05ps) and for comparison an unrestrained simulation. Figure 5.9 shows the phi vs. psi plots for the Neu5Ac-Gal linkage for each of these simulations. With longer values of τ there is an increase in conformational space

experienced in the simulation, with conformer '3' (*see figure 5.7*) populated for about half of the simulation time with τ = 500ps. Tables 5.5 & 5.6 gives back-calculated data from these simulations and with the observation of conformer '3' resulting in a significant NOE expected between Neu5Ac-H3eq and Gal-H3, not observed in solution. This increased flexibility is also observed for the Gal-GlcNAc linkage (*figure 5.10*) where the ψ torsion angle is flipped into the anti-conformer for about 250ps, and this results in an over-prediction of the Gal-H1 - GlcNAc-H3 NOE.

In contrast, the simulation with τ = 0.05ps (conventional-like restrained dynamics), does not sample conformer '3', but conformers 'A', 'B', and 'C' are sampled about the Neu5Ac-Gal linkage in this trajectory indicated by synchronous changes in ϕ and ψ values. As expected similar results to the Discover 'conventional' restrained simulation are obtained, with no 'anti-conformer' about the Gal-GlcNAc linkage predicted resulting in an under-prediction of the Gal-H1 - GlcNAc-H5 NOE.

For simulations with a value of 50 and 5ps for the memory function, the back-calculated data (NOEs and scalar coupling constants) prove to be in good agreement. The need for long simulation times is apparent, with fluctuations into the anti-conformer only occurring five times during the molecular dynamics simulation, and a 5ns restrained MD simulation with τ = 5ps was run with the resulting phi vs. psi, and phi/psi vs. time plots shown (*figure 5.11*). In this simulation the anti conformer is adopted for approximately 75ps of the time, and this is sufficient for back-calculated ROEs to be in good agreement with the experimental values.

The poor agreement in all simulations of the Gal-H3 - Neu5Ac-OH8 NOE are surprising because the other data about the Neu5Ac-Gal linkage is within acceptable agreement of the experimental data. This however may be rationalised when considering that Neu5Ac-OH8 has been proposed to be involved in a hydrogen bond, whilst within these *in vacuo* simulations the hydroxyl group is effectively a free rotor adopting the gg, gt, and tg conformers (data not shown). The NOEs between Gal-H3 and Neu5Ac-H8/-OH8 are in fact conflicting, and although not significantly higher, the Gal-H3 - Neu5Ac-H8 is slightly over predicted in the majority of the simulations. Upon inclusion of an extra distance restraint, based upon this proposed hydrogen bond between Neu5Ac-OH8 and Neu5Ac-COOH, the hydroxyl group no longer behaves as a free rotor and the predicted NOEs for both Gal-H3 -

Neu5Ac-H8/-OH8 are within experimental error, with the predicted Gal-H3 - Neu5Ac-H8 NOE decreased and the Gal-H3 - Neu5Ac-OH8 increased.

From this modelling study, time-averaged restraints are well suited to describing conformational flexibility about glycosidic linkages. The application of the time-averaged restraints until now has been limited by the requirement of a large number of restraints, which is a problem for carbohydrates. However, with the additional NOE restraints derived from exchangeable protons and extra NOEs through ^{13}C-edited spectra, it is apparent that modelling using time-averaged restraints is now a viable strategy for the conformational analysis of carbohydrates.

The apparent lack of discrimination between models on the basis of the carbon-carbon coupling constant data is unfortunately a product of the symmetric nature of the Karplus relationship proposed in this study. The torsion angle, ϕ, for conformers A/B/C and conformer 3 are approximately 180° apart, therefore in this particular case the theoretical coupling constants will be unable to discriminate between the flexible and more rigid models predicted from the time-averaged restrained molecular dynamics simulations.

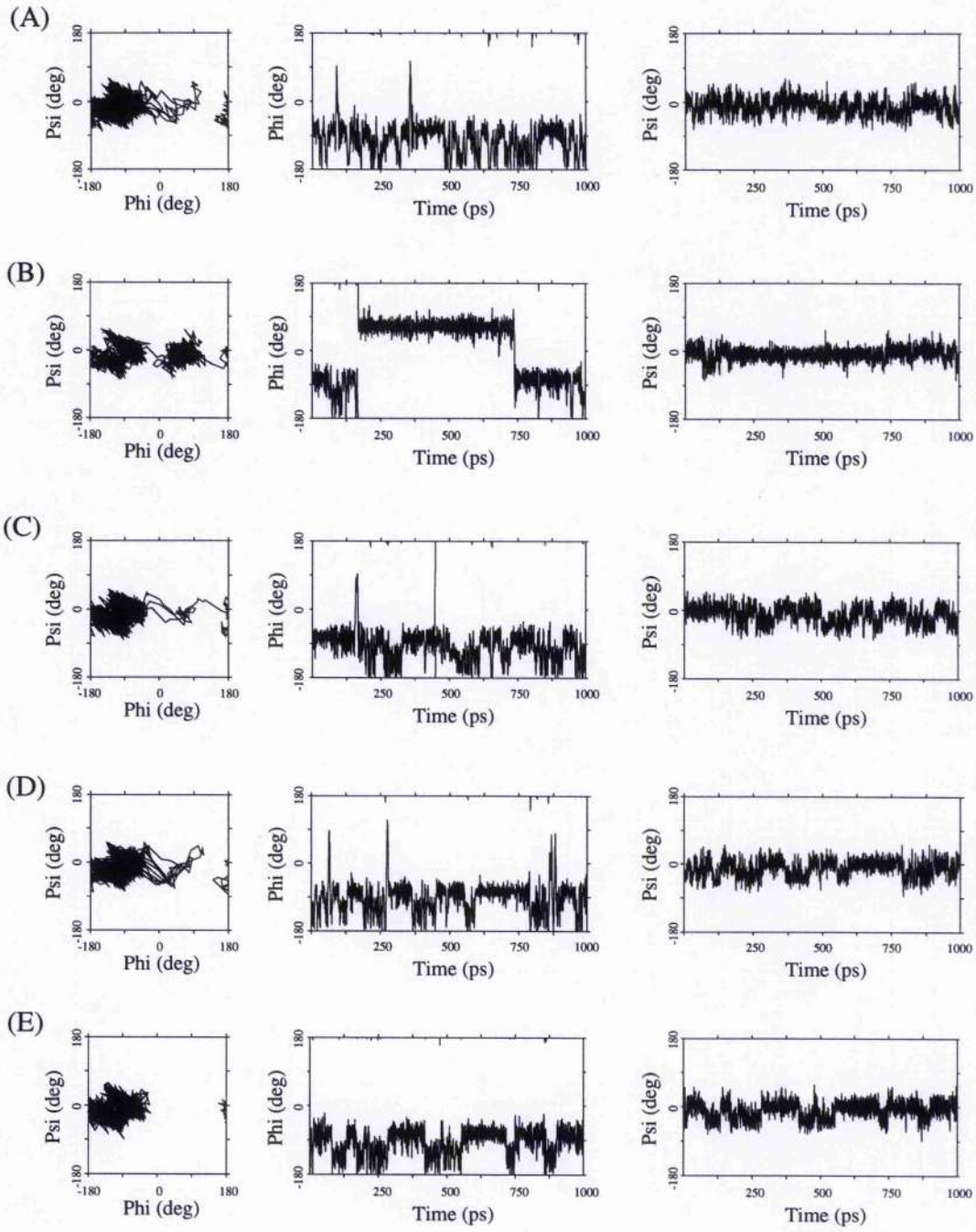

Figure 5.9 - Instantaneous values for ϕ vs. ψ, ϕ vs. time, and ψ vs. time plots for the Neu5Ac-Gal linkage from 1ns time-averaged MD simulations.

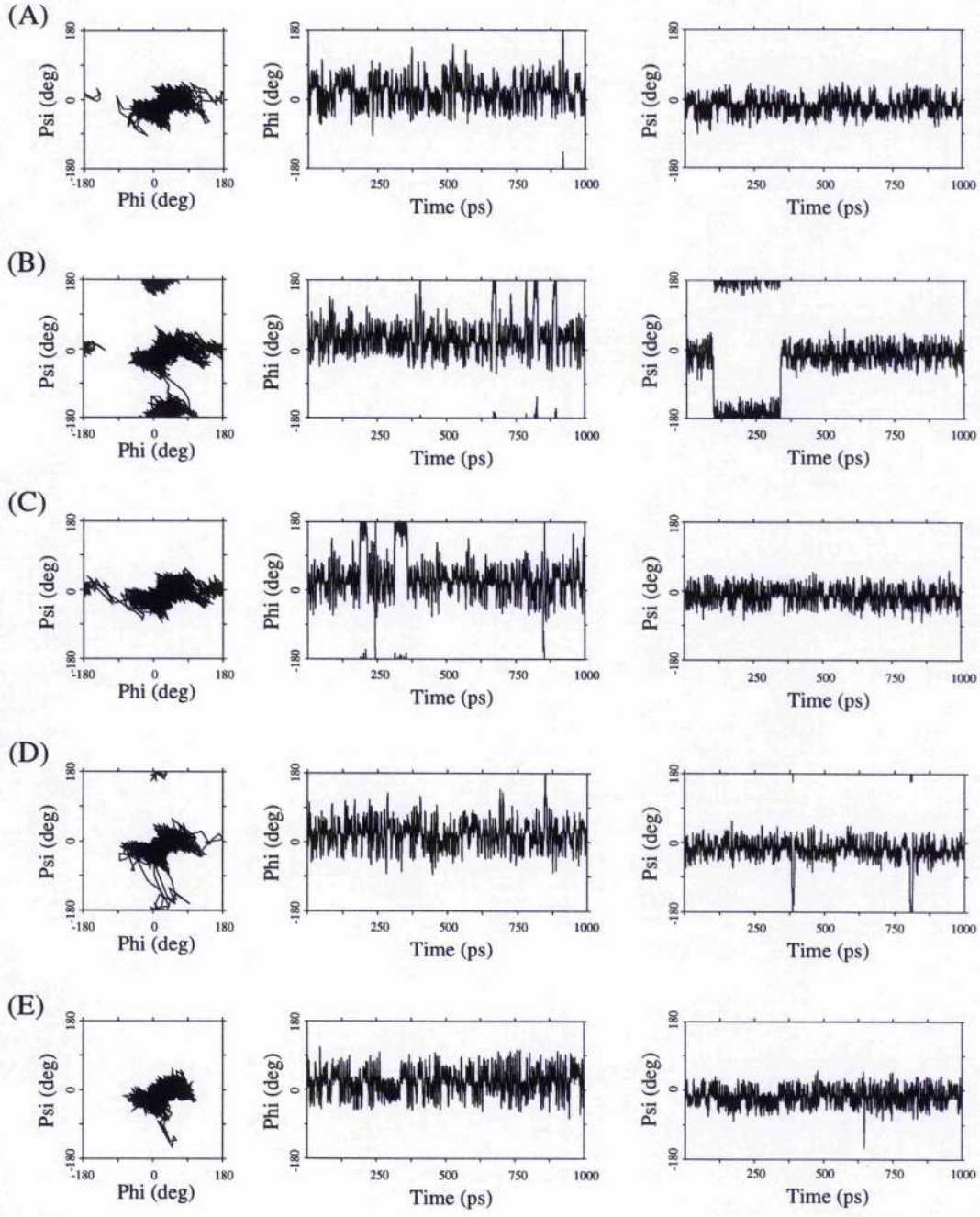

Figure 5.10 - Instantaneous values for ϕ vs. ψ, ϕ vs. time, and ψ vs. time plots for the Gal-GlcNAc linkage from 1ns time-averaged MD simulations.

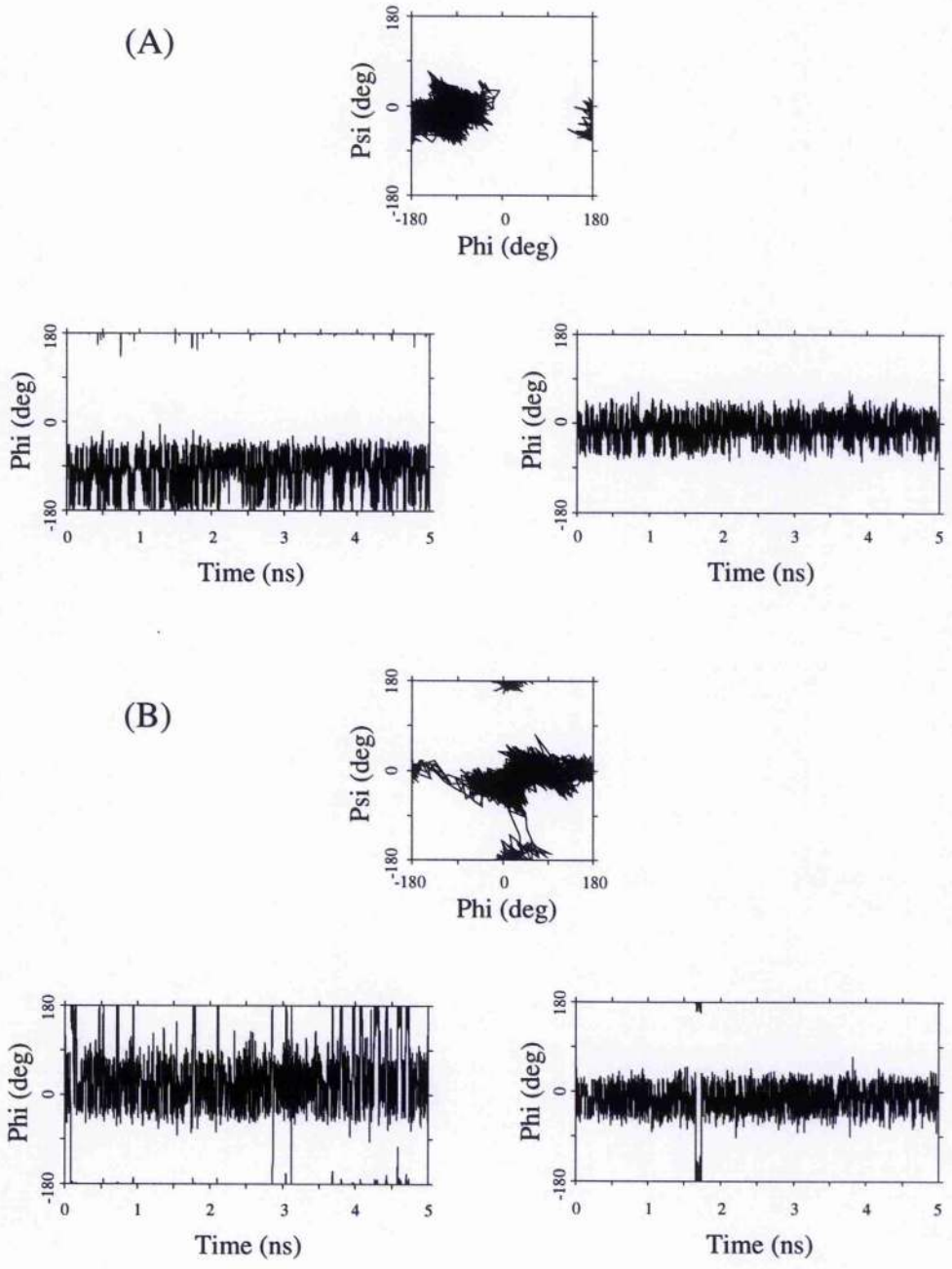

Figure 5.11 - Instantaneous values for glycosidic torsion angles ϕ and ψ for the Neu5Ac-Gal and Gal-GlcNAc linkages from a 5ns time-averaged MD simulation with τ = 5ps.

Table 5.5 - Experimental trans-glycosidic scalar coupling constants in sialylα2,3-*N*-acetyllactosamine vs. theoretical values computed from the 1ns MD simulations using 'conventional' and time-averaged restraints.

Scalar Coupled Nuclei	Restrained Molecular Dynamics Simulations[a]					Experiment[b]
	Conventional	Time Averaged Restraints				
		τ = 500ps	τ = 50ps	τ = 5ps	τ = 0.05ps	
$^3J_{CC}$						
Neu5Ac-C1 – Gal-C3	1.0	1.6	1.5	1.7	1.5	nd
Neu5Ac-C3 – Gal-C3	2.1	2.2	2.4	2.1	2.4	1.7
Neu5Ac-C2 – Gal-C2	1.1	1.0	1.1	1.0	1.1	<1.0
Neu5Ac-C2 – Gal-C4	**1.1**	1.8	1.7	1.9	1.7	1.7
Gal-C2 – GlcNAc-C4	2.5	2.3	2.2	2.2	2.3	3.3
Gal-C1 – GlcNAc-C3	0.7	1.1	0.9	1.0	0.9	<1.0
Gal-C1 – GlcNAc-C5	1.4	1.8	2.0	1.9	2.0	1.9
$^3J_{CH}$						
Neu5Ac-C2 – Gal-C3	4.7	4.5	4.6	4.5	4.6	5.0
Gal-C1 – GlcNAc-H4	4.8	4.8	4.6	4.6	4.6	
Gal-H1 – GlcNAc-C4	3.7	4.0	4.0	3.9	3.9	3.8

(a) Molecular dynamics calculations were of 1 ns length for the XPLOR based time-averaged restrained simulations, and 1.01 ns for the Discover based 'conventional' restrained simulation (where only the last 1ns were used for the calculations).

(b) Experimental values are ±0.5Hz for the $^3J_{CC}$ values and $^3J_{CH}$ values.

Figures highlighted in bold indicate theoretical values significantly different to the experimental values.

Table 5.6 - Experimental inter-glycosidic NOE(ROE)s in sialylα-2,3-*N*-acetyllactosamine vs. theoretical values computed from the 1ns MD simulations using 'conventional' and time-averaged restraints.

NOE Connectivity[b]	Restrained Molecular Dynamics Simulations[a]					Experiment
	Conventional	Time Averaged Restraints				
		τ = 500ps	τ = 50ps	τ = 5ps	τ = 0.05ps	
Gal-H3 – Neu5Ac-H3ax	**0.23**	0.41	0.40	0.58	0.36	0.53
Gal-OH2 – Neu5Ac-H3ax	0.09	0.09	0.23	0.22	0.24	0.12
Gal-H3 – Neu5Ac H3eq	0.0	**0.23**	-0.01	-0.04	-0.03	<0.05
Gal-OH2 – Neu5Ac-H3eq	0.03	0.05	0.08	0.08	0.09	0.01
Gal-H3 – Neu5Ac-H8	0.17	0.26	0.34	0.19	0.33	0.21
Gal-H3 – Neu5Ac-OH8	**0.09**	**0.02**	**0.03**	**0.03**	**0.03**	0.23
Gal-H1 – GlcNAc-H3	**0.04**	**0.38**	0.12	0.12	0.06	0.11
Gal-H1 – GlcNAc-OH3	0.21	0.28	0.32	0.38	0.38	0.25
Gal-H1 – GlcNAc-H4	1.95	1.92	2.11	2.11	2.28	1.52
Gal-H1 – GlcNAc-H5	**0.02**	0.17	0.05	0.05	**0.02**	0.11
Gal-H1 – GlcNAc-H6	0.48	0.34	0.36	0.38	0.38	0.40
Gal-OH2 – GlcNAc-H6	0.48	0.39	0.54	0.55	0.62	0.34

(a) Molecular dynamics calculations were of 1 ns length for the XPLOR based time-averaged restrained simulations, and 1.01 ns for the Discover based 'conventional' restrained simulation (where only the last 1ns were used for the calculations).

(b) The NOEs are relative to the Gal H1 - H3 inter-nuclear NOE, and the rotational correlation time used to back-calculate ROE data (0.25 ns) and NOE data (1.6 ns and 2.0 ns, for the Discover and XPLOR simulations respectively) was calibrated from diagonal versus cross-peak volumes for fixed inter-nuclear distances using a full relaxation matrix analysis.

Figures highlighted in bold indicate theoretical values significantly different to the experimental values.

5.4 Conclusions

Heteronuclear NMR investigations of the solution behaviour of the trisaccharide sialylα2,3-*N*-acetyllactosamine has distinct advantages over purely homonuclear methods. In particular complete unambiguous assignment of ROE cross-peaks were possible using a three-dimensional ROESY-HSQC experiment, which revealed two new ROE connectivities about the Galβ1-4GlcNAc linkage. The additional information on the relative orientation about the glycosidic linkages were made from long range carbon-carbon coupling constants, which were used to show that the application of time-averaged restraints in molecular dynamics simulations best represents the solution conformation of the sialylα2,3-*N*-acetyllactosamine. These modelling studies showed that there are two dominant conformations sampled about the Neu5Ac-Gal linkage which is consistent with previous studies on carbohydrates terminating in Neu5Acα2-3Gal.

NOEs involving exchangeable protons have been used to supplement the internuclear distance restraints obtained from heteronuclear NMR methods, and have led to the conclusion that one of these NOEs, namely Neu5Ac-OH8 - Gal-H3, can only be explained if Neu5Ac-OH8 is involved in a hydrogen bond. Evidence for the possible involvement in a hydrogen bond is conflicting with only the temperature coefficient being suggestive of this fact, however, previous studies on sialylα2,6-*N*-acetyllactosamine and sialylα2,3-*N*-acetyllactosamine have conclusively shown that Neu5Ac-OH8 is involved in a hydrogen bond, to either Neu5Ac-COOH, or to Neu5Ac-O6.

It has been shown in this study that both heteronuclear NMR and low temperature studies have an important future role in the determination of the solution conformation and dynamics of carbohydrates.

Chapter 6

Heteronuclear NMR Investigation of the three-dimensional conformation of sialyl Lewis^x in free solution and in complex with E-selectin

Abstract

Heteronuclear NMR experiments were employed to study the structure and dynamics of the carbon-13 enriched carbohydrate moiety sialyl Lewis^x (Neu5Acα2-3Galβ1-4[Fucα1-3]GlcNAc), in free solution and in complex with E-selectin. Structural information was obtained using multidimensional heteronuclear NMR experiments, namely, ^{13}C-edited ROESY, and measurement of long range carbon-carbon spin coupling constants. 3D ROESY-HSQC experiments provided unambiguous assignment of all ROESY cross-peaks. Additional structural information was obtained from low temperature studies which allowed observation of the hydroxyl proton resonances, and assignment of eight additional inter-glycosidic NOEs. The bound conformation of sialyl Lewis^x in complex with E-selectin was probed using 3D ^{13}C-edited transferred NOESY (TRNOESY-HSQC) experiments.

6.1 Introduction

Sialyl Lewis^x antigen is the core carbohydrate moiety which is involved in the recognition of leukocytes by the endothelial cell wall through the interaction with a family of proteins, namely the selectins. Although recent advances have shown that sialyl Lewis^x moiety (*figure 6.1*) is not the carbohydrate ligand presented *in vivo*, the actual ligands have structural variants of the sialyl Lewis^x core structure. For example, the P-selectin glycoprotein ligand, PSGL-1, incorporates the sialyl Lewis^x structure as, forming a part of the glycan portion of the ligand (Goetz *et al.*, 1997). Sialyl Lewis^x is also implicated in tumour metastasis, where expression of sialyl Lewis^x on the surface of cancer cells promotes metastasis by providing the means for adhesion and invasion points for the circulating metastatic cells. With the early implication that sialyl Lewis^x was the minimal ligand for the selectins, a vast amount of interest has been generated in the mechanism of recognition of the selectins, information on the three dimensional structure in free solution and when bound to the selectins, with implications on drug design.

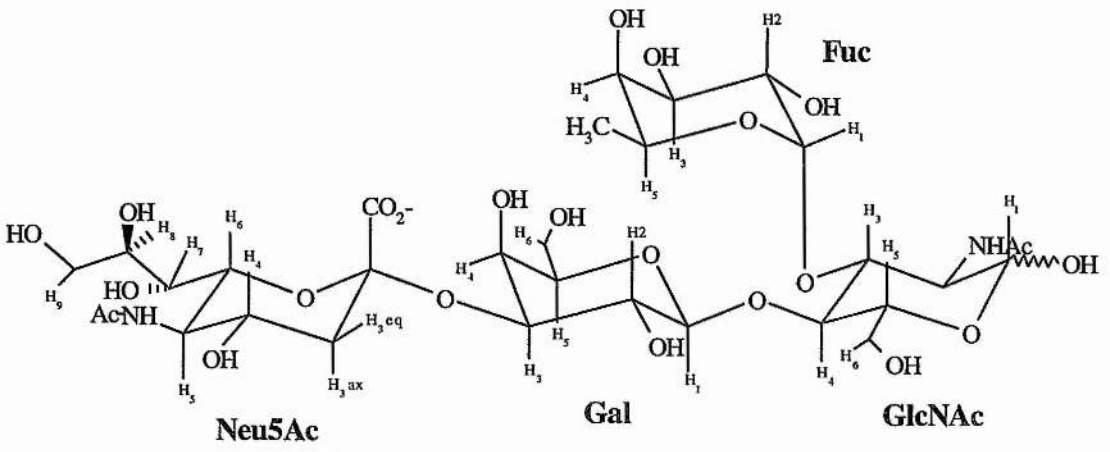

Figure 6.1 - Schematic representation of sialyl Lewis^x with numbering scheme used in the text.

Previous investigations on the solution conformation of sialyl Lewis^x have highlighted the fact that the intensities of cross-peaks in 2D ^{1}H-^{1}H NOESY experiments are small or zero indicating that the condition $\omega\tau_c \sim 1$ is met (Lin *et al.*, 1992; Ichikawa *et al.*, 1992), and to date all investigations have, therefore, used ROESY experiments for obtaining distance information. To obtain distance restraints for molecular dynamics (MD) simulations, unambiguous assignments of cross-peaks and accurate quantitation of these peaks is

required. Early investigations observed a number of inter-glycosidic ROEs, namely, Neu5Ac-H3ax - Gal-H3, Gal-H1 - GlcNAc-H4, Fuc-H1 - GlcNAc-H3, and Gal-H2 - Fuc-H5 &-H6 (Lin *et al.*, 1992; Ichikawa *et al.*, 1992; Ball *et al.*, 1992). It was noted that the accurate quantitation of the Fuc-H1 - GlcNAc-H3 ROE was difficult because of overlap, and these investigations failed to identify the characteristic Neu5Ac-H8 - Gal-H3 ROE, indicative of conformer 'B' about the Neu5Ac-Gal linkage, and therefore concluded that sialyl Lewis^x adopted a single rigid conformation in solution. Rutherford *et al.* (1994) assigned this ROE and identified a further ROE between Gal H1 and one of the GlcNAc H6's, whilst they were unable to unambiguously assign the NOE to the second GlcNAc H6 because of severe overlap at ~3.88ppm. They also concluded that the Lewis^x moiety was essentially rigid, but that there is conformational flexibility about the Neu5Ac-Gal linkage based upon the two conflicting ROEs observed, which had also been observed in the non-fucosylated material (Breg *et al.*, 1989).

In the most recent investigation of the solution conformation of sialyl Lewis^x, additional distance restraints were obtained using exchangeable protons (Poppe *et al.*, 1997). This provided further evidence that the Neu5Ac-Gal linkage is flexible through the observation of the NOE between Neu5Ac-OH8 and Gal-H3, along with the previously observed Neu5Ac-H3ax - Gal-H3 NOE. A further two NOEs to exchangeable protons were observed and were used as constraints to predict a low energy conformation of sialyl Lewis^x, rather than utilising them in MD simulations.

The aim of the current investigation is to describe the three-dimensional solution structure and dynamics of sialyl Lewis^x with the application of the methodology proposed and tested in the previous chapters, namely, the use of three-dimensional ROESY-HSQC experiments to unambiguously assign all ROE cross-peaks, the use of the exchangeable protons to increase the number of distance restraints provided for molecular modelling, and to record additional angular data, $^3J_{CC}$ coupling constants.

Similar to the investigation of the solution conformation, the bound conformation with E-selectin has equally been thoroughly investigated using homonuclear NMR experiments. However conflicting evidence has been observed in the conformation adopted upon binding. Hensley *et al.* (1994) studied the bound conformation at 278K, and observed similar NOEs

to those described for the Lewis^x moiety in solution, and observed only one NOE about the Gal - Neu5Ac linkage, between Gal-H3 and Neu5Ac-H3ax. The authors therefore concluded that there was no conformational change upon binding. Cooke *et al.* (1994), however, studied the bound conformation at 298K, and under these conditions observed that the Gal-H3 - Neu5Ac-H3ax NOE was absent, indicating that conformational change upon binding had occurred. They predicted that sialyl Lewis^x selects a single conformation upon binding, with the most likely conformation being GESA-C (after Ichikawa *et al.*, 1992), or conformer 'A', although they did not observe the characteristic NOE, Neu5Ac-H8 - Gal-H3. Recently Scheffler *et al.* (1995; 1997) studied the bound conformation of sialyl Lewis^x at 310K and observed a disappearance of the Neu5Ac-H3ax - Gal-H3 NOE whilst observing an enhancement of the Neu5Ac-H8 - Gal-H3, over the solution studies, and therefore concluded that conformer 'B' is adopted upon binding. Confirmation of this has come from Poppe *et al.* (1997) who studied the bound conformation at 300K, and observed significant NOEs in a NOESY experiment acquired at 285K.

The likely conclusion from the evidence at present is that upon binding sialyl Lewis^x selects a single conformation, conformer 'B', and the discrepancy with the earliest investigation (Hensley *et al.*, 1994) could be the temperature of the study, 278K, where significant NOEs have been observed for free sialyl Lewis^x at a similar temperature (Poppe *et al.*, 1997), coupled with the relatively high sialyl Lewis^x to E-selectin ratio (40:1) resulting in the free solution state NOEs being observed in the NOESY experiment instead of true TRNOEs.

The aim of the current investigation is to present preliminary data on the application of heteronuclear 3D carbon-edited transferred NOESY experiments on the bound conformation of sialyl Lewis^x.

6.2 Materials and Methods

6.2.1 Sample preparation

5mg of Neu5Acα2-3Galβ1-4[Fucα1-3]GlcNAc (Dextra) and *N*-acetyl [U-^{13}C] Neu5Acα2-3Galβ1-4[Fucα1-3]GlcNAc (~2mg) were dissolved and lyophilised into 99.96% D_2O three times followed by dissolution into 750μL D_2O. For the observation of the exchangeable protons the natural abundance sample of sialy Lewis^x was dissolved 750μL of H_2O containing 15% 99.96% acetone-d_6 (Cambridge Isotopes). The pH was adjusted to between 5.5 to 6.0 by careful step-wise addition of dilute HCl or NaOH and transferred to a 5mm NMR tube. The sample was degassed by sonication for about 1 minute.

6.2.2 NMR Experiments

6.2.2.1 Free Solution Studies

NMR spectra were obtained at 303K and 258K with a reference frequency of 500MHz on a Varian Unity$^+$ spectrometer equipped with a self shielded z gradient triple resonance probe. All spectra were recorded in the phase sensitive mode (except the ES-COSY spectra which were acquired in absolute intensity mode) with use of the States method for quadrature detection (States *et al.*, 1982).

2D HSQC experiments were recorded with a total of 512 complex and 2K complex points in the t_1 and t_2 dimensions respectively, with spectral widths of 9.3kHz and 2kHz. Four scans were acquired per t_1 increment, with a total acquisition of 3 hours.

2D HCCH-COSY experiments were recorded using the three-dimensional pulse scheme (Bax *et al.*, 1990; Yu *et al.*, 1993). A total of 256 complex and 2K complex points were acquired in the t_1 and t_2 dimensions respectively, with spectral widths of 9.3kHz and 2kHz. Two and three dimensional gradient enhanced long range carbon-carbon J correlation (LRCC) experiments (Bax *et al.*, 1992; Bax *et al.*, 1994a,b) were recorded with a proton sweep width of 2.1kHz, consisting 1K complex points and a ^{13}C sweep width of 9.6kHz in t_1 (256 complex points) and a 9.6kHz (32 complex points) in t_2 for the 3D experiment. ^{13}C-^{13}C couplings evolve and are refocused during the delay (4T) of 44.4ms. A total of 64 scans and 8 scans were acquired per increment for the 2D and 3D experiments with total acquisition

times of ~24 and ~48 hours, respectively. The values of the long range coupling constants are derived from the ratios of the cross-peaks obtained in the spectrum in the manner as described before (Bax *et al.*, 1992).

Three dimensional ^{13}C-edited ROESY (Bothner-By *et al.*, 1984; Davis and Bax, 1985) experiments were acquired with the pulse sequence described in chapter 3, which includes offset compensation (Griesinger and Ernst, 1987) and with spectral widths of 1.9kHz, 7kHz, and 1.9kHz and 128, 32, and 1024 complex points in t_1, t_2, and t_3, respectively. The proton offset was placed 200Hz up-field of the highest field resonance during the spin-lock period to minimise coherence effects. To optimise digital resolution the Fuc-C6 and Neu5Ac-C3 resonances were folded-in once, with the incremental delay at time zero in t_2 calculated (Edison et al, 1994) to give a processed spectrum where the folded peaks have an opposite phase to non-folded peaks when zero and first order phases are set to 90° and -180°, respectively. The effective field for spin locking was 2kHz and was applied for 250ms. Prior to Fourier transformation, data were apodised with cosine-bell functions, with t_1, and t_2 dimensions zero-filled to 256 and 64 complex points, respectively. Total acquisition time for the 3D experiment was ~55 hours.

Two dimensional ES-COSY, ES-NOESY, and ES-ROESY spectra were acquired at 258K with spectral widths of 3.8kHz, 512 t_1 increments, 32 scans per increment with 4K complex points in t_2. ES-COSY spectra were acquired in magnitude mode, and the lentgh of the mixing time in the ES-NOESY experiment was 100ms. The ES-ROESY spectrum was acquired with a spin-lock period of 100ms using a weak (~3kHz) continuous-wave rf field. Prior to two dimensional Fourier transformation data were apodised using cosine-bell functions. Hydroxyl exchange rates were measured using the method described by Adams and Lerner (1992) incorporating excitation sculpting water suppression (Hwang and Shaka, 1995). Spectra were acquired with 16 scans, 4K complex points, a sweep width of 3.8kHz and were recorded with saturation times varying from 0 to 1s. ES-1D ^{1}H spectra were acquired with a proton sweep width of 4kHz and 8K points. Temperature coefficients were measured from ES-1D ^{1}H spectra acquired between 255K and 265K, and exchangeable spin couplings were measured from the ES-1D ^{1}H spectrum acquired at 258K.

6.2.2.2 Bound State Conformational Studies

A chimeric molecule comprising an IgG and two E-selectin moieties was kindly provided by Beat Ernst (Novartis), and was concentrated for buffer exchange. The sample was repeatedly dissolved into a D_2O buffer containing imidazole-d_4 with 1mM $CaCl_2$ (and was left overnight to exchange the amide protons) followed by concentration, to remove any water present.

E-selectin (~6mg) was dissolved in imidazole-d_4 and was transferred to a 5mm NMR tube (Wilmad 528pp). [U-^{13}C] sialyl Lewis^x was added to the NMR tube until significant signal to noise ratio was obtained from a 2D ^{1}H-^{13}C HSQC experiment. 3D NOESY-HSQC experiments were acquired with a NOESY mixing time of 50ms. The ^{1}H sweep-width was 2.1kHz in t_1 and t_3, and the carbon sweep-width was set to 7kHz in t_2, to optimise digital resolution in the latter dimension, the Neu5Ac-C3 and Fuc-C6 resonances were folded in once. A total of 128, 32, and 1K complex points were acquired in t_1, t_2, and t_3, respectively, to give a total acquisition time of ~55 hours. Prior to Fourier transformation, data were apodised with cosine-bell functions, and each dimension was zero-filled to 256, 128, and 2K complex points in t_1, t_2, and t_3.

2D NOESY and ROESY peak volumes were measured using the 2D integration routine contained in the Varian VNMR software. 3D peak volumes were measured by summing the volume of cross-peaks over all 2D *F1F3* planes in which they appear.

6.2.3 Conventions

The torsion angles ϕ (phi) and ψ (psi) are analogous to ϕ_H and ψ_H in IUPAC convention, and are defined as H1-C1-O1-Cx and C1-O1-Cx-Hx, where Cx and Hx represent the aglyconic atoms. Neu5Ac torsion angles are defined as C1-C2-O2-Cx (ϕ) and C2-O2-Cx-Hx (ψ), and torsion angles around the glycerol side chain are defined as, ϕ_1: H6-C6-C7-H7, ϕ_2: H7-C7-C8-H8, and ϕ_3: H8-C8-C9-O9.

6.2.4 Molecular Modelling

Computer models were assembled using Biosym's Insight II molecular graphics package running on a Silicon Graphics Indigo 2 Challenge. Random structures were generated by dynamical quenching. An initial structure was built with pyranose rings in the $^4C_1$ chair conformation with trial values of phi (ϕ) and psi (ψ), and were subjected to 200ps of unrestrained molecular dynamics at 750K, during which the torsional terms are scaled by a factor of 7 to prevent excessive ring puckering. A random structure was saved every 10ps. Energy minimisation by restrained simulated annealing was achieved as follows: models were equilibrated for 10ps with a thermal bath at temperatures 500K, 450K, 350K, 300K, and then successively for 1ps in decreasing steps of 10K, followed by a further 1ps at 5K. The system was minimised using steepest descents algorithm until the maximum derivative was less than 0.04kJmol^{-1}Å^{-1}. Restraints listed in Tables 6.3 were applied as a biharmonic function. NOE contacts were arbitrarily assigned as strong (1.8Å - 2.7Å), medium (1.8Å - 3.3Å), and weak (1.8Å - 5.00Å).

All dynamics simulations were performed *in vacuo* with a dielectric constant (ε) of 80.0 and at a temperature of 300K, for simulations describing the dynamics of the free oligosaccharide. To mimic in part the micro-environment of the protein-binding site a dielectric constant of 4.0 was chosen for the dynamical simulated annealing simulations using TRNOE distance restraints. The amber force-field (Weiner *et al.*, 1984; Weiner *et al.*, 1986) with a carbohydrate parameter set developed by Homans (1990a) was used with the exo-anomeric potentials set to zero. Simulations using Discover (Biosym Technologies Inc.) lasted 1.01ns and 5.01ns with the last 1ns and 5ns, respectively, used in further analysis. Simulations using time-averaged restraints were performed with XPLOR (Brunger, 1987) where an initial 50ps of "conventional" restrained dynamics was used to equilibrate the system and then 1ns and 5ns time-averaged restrained trajectories were performed.

6.3 Results and Discussion

6.3.1 Spectral Assignments

Spectral assignments for the non-exchangeable protons and carbons for sialyl Lewis^x are given in Table 6.1, whilst assignments, exchange rates, and temperature coefficients for the exchangeable protons are compiled in Table 6.2. These data are in agreement with previous assignments for the non-exchangeable protons and carbons (Ball *et al.*, 1992; Ichikawa *et al.*, 1992) except for the assignments of the GlcNAcβ H1, H2, and H3 where both previous studies involved β-O-glycosides of sialyl Lewis^x. Complete assignments were obtained from 2D ^{1}H-^{13}C HCCH-COSY (*figure 6.2A*), and 2D ^{1}H-^{13}C HSQC experiments (*figure 6.3A*).

The exchangeable proton chemical shifts were obtained from 2D ^{1}H-^{1}H ES-COSY (*figure 6.2B*), and ES-TOCSY experiments, and are in good agreement with previous reported values of sialyl Lewis^x in super-cooled water (Poppe *et al.*, 1997).

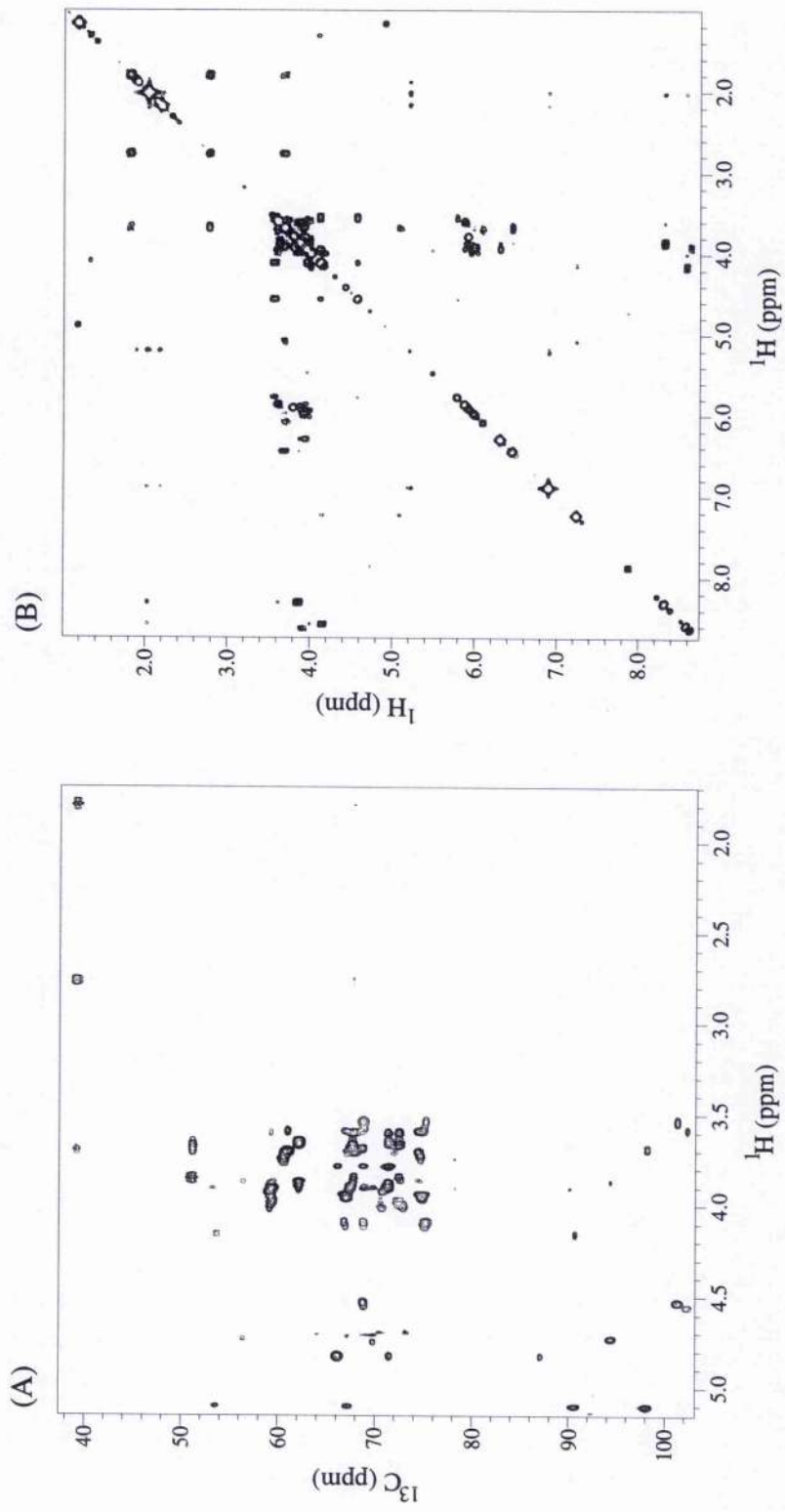

Figure 6.2 - (A) Two dimensional ^{1}H-^{13}C HCCH-COSY spectrum of [U-^{13}C] sialyl Lewis^x at 303K in D_2O.
(B) Two dimensional magnitude mode ^{1}H-^{1}H ES-COSY of sialyl Lewis^x at 258K in H_2O/acetone-d_6 showing through-bond connectivities to the exchangeable protons.

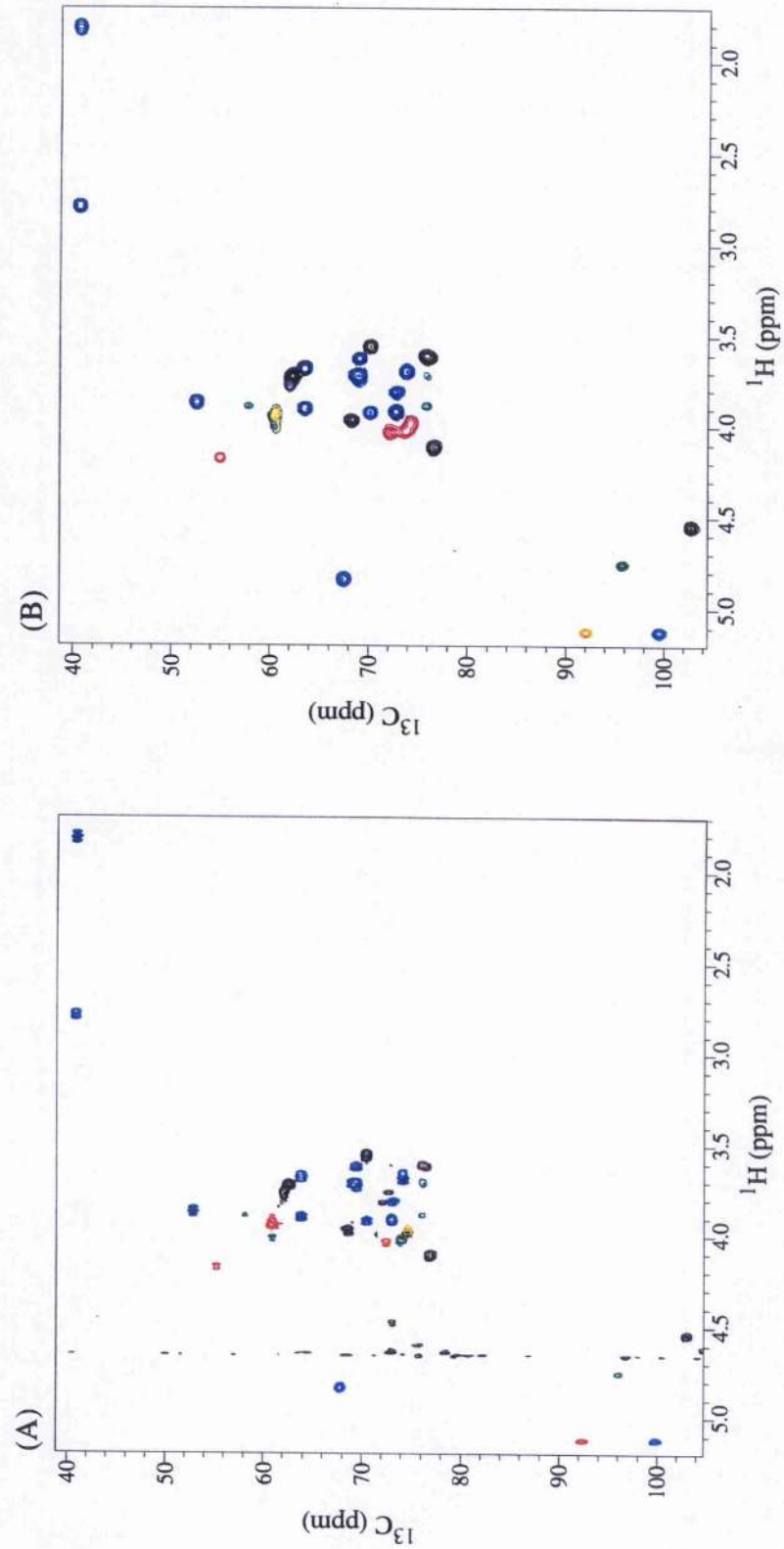

Figure 6.3 - Regions of the heteronuclear ^{1}H-^{13}C HSQC spectra of (A) [U-^{13}C] sialyl Lewis^x in free solution and, (B) [U-^{13}C] sialyl Lewis^x in the presence of E-selectin. Spectra recorded at 310K and in D_2O/Imidazole-d_4, peaks shown in Black = Gal, Red = GlcNAcα, Green = GlcNAcβ, Light Blue = Fuc, and Dark Blue = Neu5Ac (not shown are the correlations to Fuc-C6/H6).

Table 6.2 - ^1H and ^{13}C Chemical Shift Assignments for Sialyl-Lewis^x in D_2O at 303K.

	Neu5Acα		Galβ		Fucα		GlcNAcα		GlcNAcβ	
	^1H	^{13}C	^1H	^{13}C	^1H	^{13}C	^1H	^{13}C	^1H	^{13}C
1			4.53	101.5	5.10	98.4	5.10	90.9	4.72	94.6
2			3.53	69.2	3.68	68.0	4.15	53.8	3.87	56.6
3	1.79ax	39.4	4.10	75.3	3.89	69.1	3.96	72.7	3.86	74.8
	2.76eq									
4	3.68	68.0	3.95	67.4	3.78	72.0	4.00[a]	71.0[a]	3.96	73.1
5	3.85	51.4	3.59	74.8	4.82	66.4	3.98[a]	70.3[a]	3.60	74.8
6	3.65	72.6	3.70	61.2	1.17		3.91	59.4	3.98	59.5
7	3.60	68.0								
8	3.89	71.5								
9	3.65	62.4								
	3.87									

(a) Assignments interchangeable.

Chemical shifts are referenced to δ_{TSP} = 0.00ppm (^1H and ^{13}C).

Table 6.2 - NMR data for the exchangeable protons from sialyl Lewis^x in H_2O/acetone-d_6 (85:15) at 258K.

Proton	Chemical Shift (ppm)[a]	Exchange Rate (s^{-1})[b]	Temperature Coefficient (ppb/K)[c]	Coupling $^3J_{HH}$ (Hz)
Neu5Ac-OH4	6.45	8.7 (21.2)	9.5	5.4
Neu5Ac-OH7	5.87	4.7 (19.1)	11.0	6.9
Neu5Ac-OH8	6.30	7.4 (13.5)	5.6	~0
Neu5Ac-OH9	~5.87	n.d.	n.d.	n.d.
Neu5Ac-NH5	8.31	–	5.5	11.1
Gal-OH2	5.78	2.6 (6.3)	12.8	2.5 (anomeric effect of 6.3Hz)
Gal-OH4	5.48	n.d. (~5.5)	10.5	~2.4
Gal-OH6	6.09	14.3 (40.2)	10.9	5.3
Fuc-OH2	n.d	n.d.	n.d.	n.d.
Fuc-OH3	5.98	11.9 (31.8)	11.6	5.3
Fuc-OH4	5.91	11.0 (21.8)	12.8	5.7
GlcNAcα-OH1	7.23	7.6 (22.9)	6.1	3.8
GlcNAcα-OH6	5.95	13.1 (32.3)	10.8	~4.0
GlcNAcα-NH2	8.57	–	8.3	10.7
GlcNAcβ-OH1	7.87	10.3 (29.5)	9.6	7.0
GlcNAcβ-OH6	6.02	12.3 (34.2)	10.9	4.2
GlcNAcβ-NH2	8.63	–	6.7	10.2

(a) Chemical shifts referenced to $\delta_{TSP} = 0.00$ ppm (by setting residual acetone to 2.19 ppm).
(b) Exchange rates measured at 258K and 268K (figure in brackets).
(c) Temperature coefficients measured over a 10K range between 258K - 268K.
n.d. = not determined.

6.3.2 ^{1}H-^{1}H Homonuclear NOEs

In early investigations a key ROE describing the flexibility about the Neu5Ac-Gal linkage was not assigned, and later investigations have not been able to assign all ROEs unambigiously because of the severe overlap in the ^{1}H dimension. In contrast, the assignment of ROEs from a 3D ROESY-HSQC spectrum is relatively straightforward because the cross-peaks are dispersed by their ^{13}C chemical shifts. From two *F2F3* spectra at the proton chemical shifts of Gal-H1 (*figure 6.4A*), and Gal-H3 (*figure 6.4B*), four inter-glycosidic ROEs are observed, with both Gal-H3 - Neu5Ac-H3ax & -H8 NOEs (*figure 6.4b*), confirming the flexibility of the Neu5Ac-Gal linkage in solution. Similarly, a further five inter-glycosidic NOEs between Fuc-GlcNAc, and Fuc-Gal residues could be assigned, and these were normalised to an intra-residue cross-peak volume (Gal-H1 - Gal-H3), and used in restrained molecular modelling simulations (Table 6.3).

In contrast to the NOEs observed for sialylα2,3-*N*-acetyllactosamine, no evidence of the 'anti' conformer was observed about the Gal-GlcNAc in sialyl Lewis^x, which taken with the NOEs between the Gal-Fuc residues is indicative of a relatively rigid stacked conformation. The Gal-H2 - Fuc-H5 NOE observed was 87% of the intra-residue Gal-H1 - Gal-H3 and is comparable to previous studies on sialyl Lewis^x and Lewis^x, but in contrast to recent studies on Lewis^x derivatives, namely , GlcNAcβ1-4[Fucα1-3]GlcNAcβ1- and GalNAcβ1-4[Fucα1-3]GlcNAc, where the NOE observed was only 20 - 30% of that observed in Lewis^x (Lommerse *et al.*, 1995).

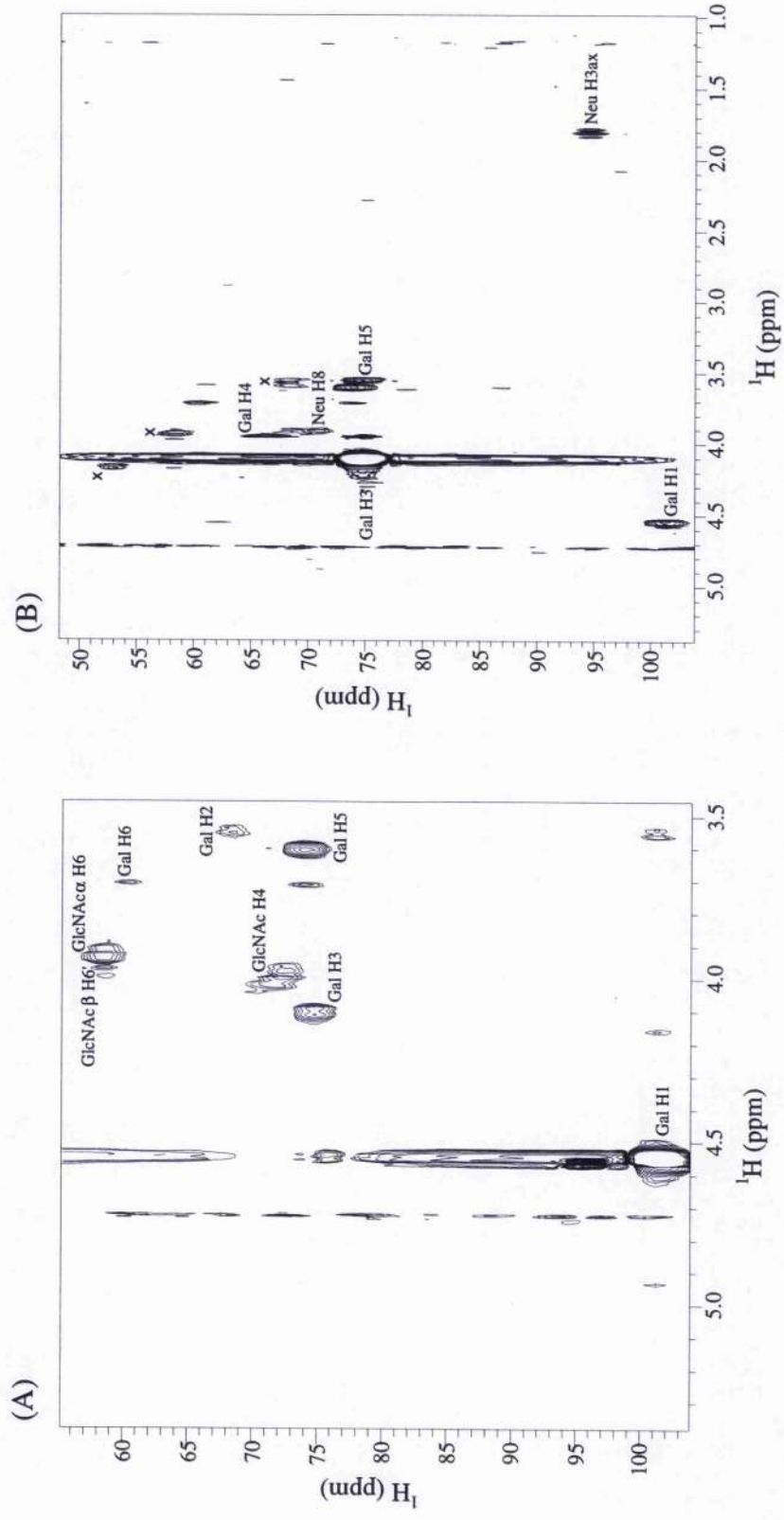

Figure 6.4 - ^{1}H-^{13}C (*F3F2*) planes from the three dimensional ROESY-HSQC spectrum of [U-^{13}C] sialyl Lewis^x at 303K (mixing time of 100ms) at the ^{1}H chemical frequencies of (A) Gal H1, and (B) Gal H3. Cross-peaks are assigned.

6.3.3 Exchangeable Protons

6.3.3.1 Evidence of Hydrogen Bonding

Recently a number of hydrogen bonds occurring in sialyl Lewis^x have been proposed (Poppe *et al.*, 1997), namely Neu5Ac-COOH:::Neu5Ac-OH8, Gal-OH2:::Neu5Ac-O6, and Neu5Ac-COOH:::Gal-OH4. The basis for the proposal of these hydrogenbonds is upon the dramatic up-field chemical shifts, smaller HO-CH coupling constants, lower exchange rates and lower chemical shift temperature coefficients, in comparison to the other hydroxyl protons. The 1D ES-^{1}H spectra for sialyl Lewis^x, Lewis^x, and sialylα2,3-*N*-acetyllactosamine corresponding to the exchangeable protons region is shown (*figure 6.5*). From comparison of these three spectra it is immediately apparent that Gal-OH4 experiences a dramatic up-field shift upon fucosylation of sialylα2,3-*N*-acetyllactosamine. Similarly, the proton resonance of Gal-OH2 experiences an up-field shift, of approximately 0.5ppm, upon sialylation of Lewis^x to sialyl Lewis^x, and this resonance is also shifted up-field in comparison between sialylα2,3-*N*-acetyllactosamine and sialyl Lewis^x. The coupling constants for these two hydroxyl protons and Neu5Ac-OH8 (Table 6.2) all show significantly smaller values than for the other hydroxyl protons, indicative of non free rotor behaviour in solution. The exchange rates for each of these three hydroxyl protons (Table 6.2) are of a significantly smaller value, especially at the higher temperature (268K). The chemical shift temperature coefficients, which are an indirect measure of an exchangeable protons involvement in a hydrogen bond, show no significant decreased values in comparison to the other hydroxyl protons except for Neu5Ac-OH8, which is of the same order as the NH's. Overall these data supports the suggestion that these three exchangeable protons are involved in hydrogen bonds in solution at this temperature.

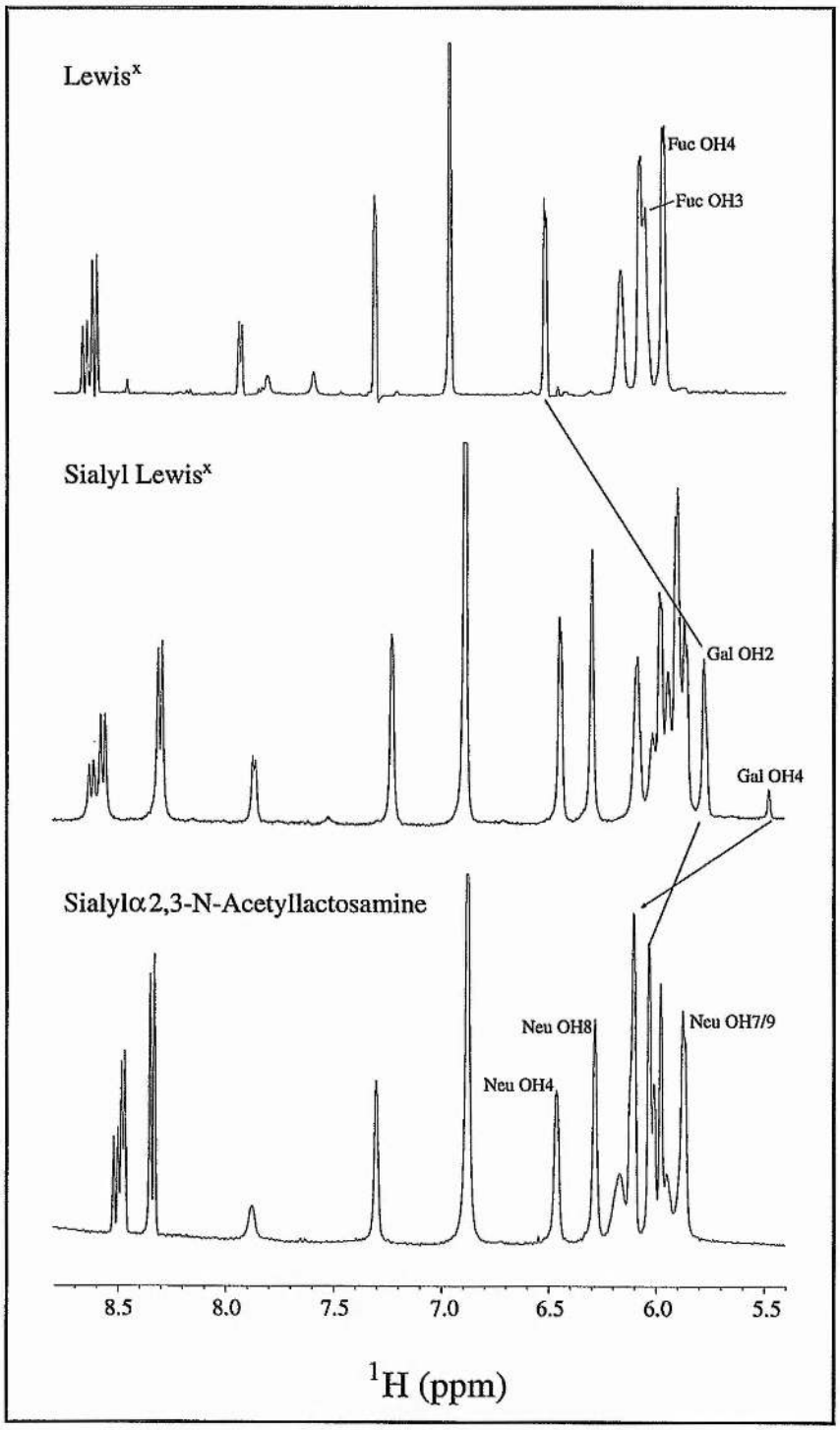

Figure 6.5 - 1D ES-^{1}H for sialyl Lewis^x, Lewis^x, and sialylα2,3-*N*-acetyllactosamine. Assignments of the sialic acid and fucose hydroxyl protons are annotated on the 1D spectra of sialylα2,3-*N*-acetyllactosamine, and Lewis^x, respectively. The dramatic up-field shifts of the Gal-OH2 and -OH4 resonances are also indicated.

6.3.3.2 NOEs to hydroxyl protons

A section of the two dimensional ES-NOESY spectrum of sialyl Lewis^x, pH~6, at 258K, corresponding to the cross-peaks between hydroxyl protons (*F1*) and non-exchangeable protons (*F2*) show a number of observable inter-glycosidic NOEs (*figure 6.6A*). Of particular interest are those NOEs about the Neu5Ac-Gal linkage due to the lack of, and conflicting nature of the non-exchangeable/non-exchangeable NOEs observed. Three inter-glycosidic NOEs could be unambiguously identified between Gal-OH2 - Neu5Ac-H3ax, Gal-OH4 - Neu5Ac-H3eq, and Gal-H3 - Neu5Ac-OH8, whilst a further NOE to Gal-OH2 (^{1}H 3.90ppm) could not be assigned unambiguously, but is probably a contribution of two NOEs, namely Gal-OH2 - Neu5Ac-H8, and Gal-OH2 - GlcNAc-H6's. These NOEs confirm the flexibility of the Neu5Ac-Gal linkage even at low temperature, whilst a further inter-glycosidic NOE is observed between the Neu5Ac and Gal resides, Gal-OH2 - Neu5Ac-H3eq, but arises through spin diffusion, and is confirmed by the lack of a cross-peak in the ES-ROESY spectrum (*figure 6.6B*). The ES-ROESY spectrum also confirms that the Gal-OH4 to NeuH3eq, not observed in sialylα2,3-*N*-acetyllactosamine, is not due to spin diffusion but is a direct NOE. In addition to the possible NOE between Gal-OH2 - GlcNAc-H6's a further inter-glycosidic (R)NOE is observed about the Gal-GlcNAc linkage, namely, Gal-H1 - GlcNAc-OH6, and another (R)NOE is observed about the Fuc-GlcNAc linkage, Fuc-H1 - GlcNAc-NH2. A further three NOE/ROEs were observed between Gal - Fuc, Gal-OH4 - Fuc-H4 & Fuc-H6, and Gal-OH2 - Fuc-H6 indicating the stacking arrangement of the fucose ring below the galactose.

In total, ten inter-glycosidic NOEs involving exchangeable protons were observed (Table 6.3), which were utilised in the molecular modelling as 'weak' restraints because of the difficulty to accurately describe them as strong, medium, or weak.

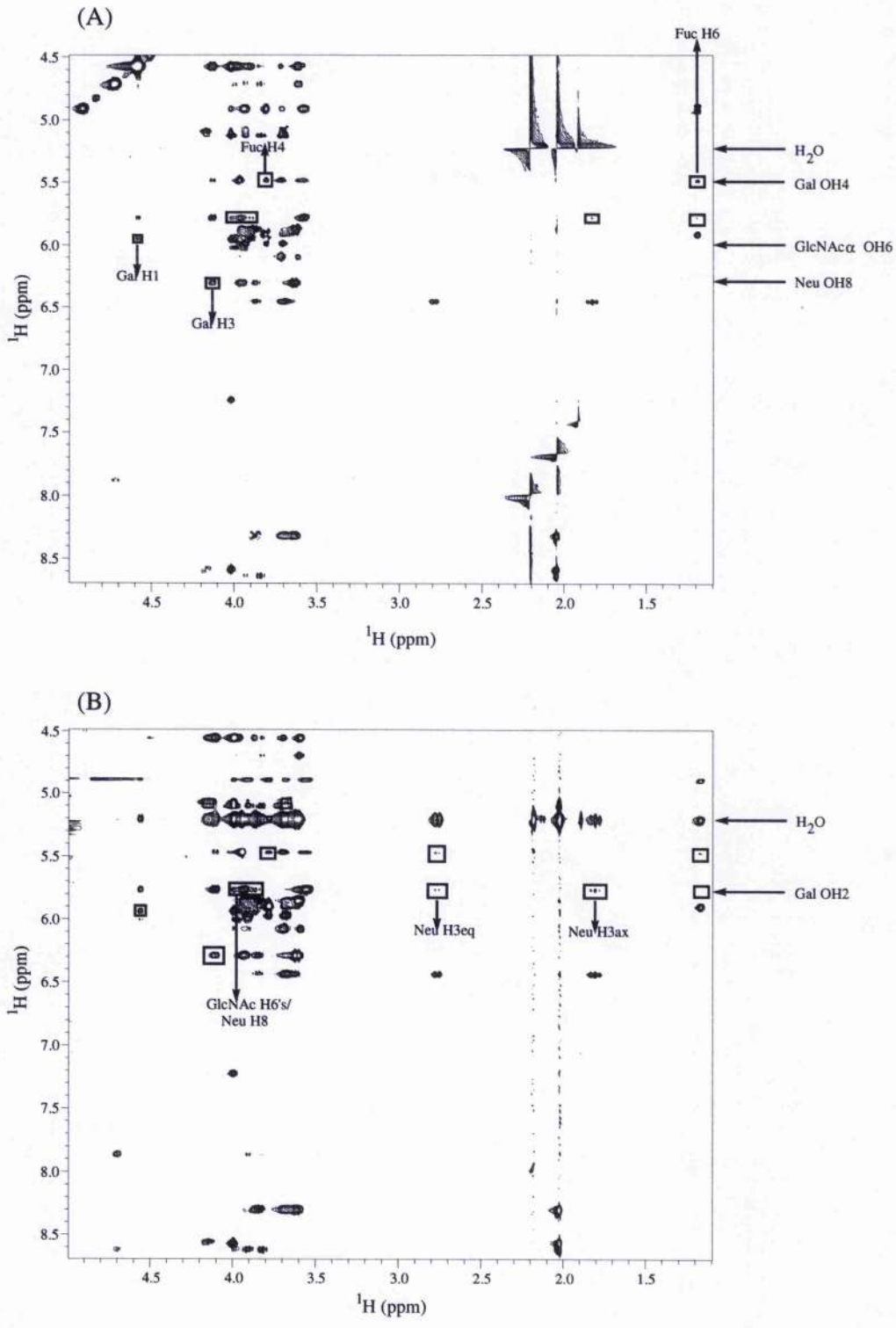

Figure 6.6 - (A) Region of the ^1H-^1H ES-NOESY spectrum of sialyl Lewis^x at 258K, showing the through space connectivities from the non-exchangeable (*F2*) to exchangeable protons (*F1*).

(B) Same region but from the ^1H-^1H ES-ROESY spectrum of sialyl Lewis^x at 258K. Inter-glycosidic NOEs are assigned.

Table 6.3 - Experimental ROEs (non-exchangeables) and NOEs (involving exchangeables).

(R)NOE Connectivity	Relative ROE[a]	r(Å)[b]	Constraint[c]
Neu5Ac-Gal			
Neu5Ac H3ax - Gal H3	0.59	2.65	W[d]
Neu5Ac H8 - Gal H3	0.54	2.69	W[d]
Neu5Ac HO8 - Gal H3	0.47	2.75	W
Neu5Ac H3ax - Gal OH2	0.87	2.48	W
Fuc-GlcNAc			
Fuc H1 - GlcNAc H3	0.60	2.65	M
Fuc H1 - GlcNAc H2	0.28	3.00	W
Fuc H1 - GlcNAc NH2	0.59	2.65	W
Gal-GlcNAc			
Gal H1 - GlcNAc H4	0.83	2.51	M
Gal H1 - GlcNAc H6*	1.23	2.35	W
Gal H1 - GlcNAc OH6	0.52	2.71	W
Gal OH2 - GlcNAc H6*	0.81	2.51	W
Fuc-Gal			
Fuc H5 - Gal H2	0.87	2.49	W
Fuc H3 - Gal H6	0.99	2.43	W
Fuc H6 - Gal H2	0.99	2.43	W
Fuc H4 - Gal OH4	0.33	2.92	W
Fuc H6 - Gal OH2	0.13	3.41	W
Fuc H6 - Gal OH4	0.18	3.23	W

(a) Reference ROE/NOE Gal H1 - H3, reference distance 2.43Å.
(b) Approximate effective ^{1}H-^{1}H distance , based upon a simple ROE ratio calculation which neglects the influence of internal motions and anistropic re-orientation.
(c) Restraints used in modelling studies; W = weak, 1.8Å<r<5.00Å; M = medium, 1.8Å<r<3.3Å; S = strong, 1.8Å<r<2.7Å
(d) Restraints applied as weak because of the conflicting nature of these NOEs, although the approximate effective distance would indicate medium restraints.

6.3.4 Trans-glycosidic Coupling Constants

The measured values of the trans-glycosidic carbon-proton coupling constants are documented in the literature (Tvaroska and Taravel, 1995), and so only the trans-glycosidic carbon-carbon coupling constants (Table 6.4), and the one bond carbon-proton coupling constants have been measured in the present study.

The long range carbon-carbon coupling constants may be measured from the 2D LRCC experiment, however due to the poor spectral dispersion in both ^{1}H and ^{13}C dimensions it is necessary to extend this into three dimensions using a further ^{13}C chemical shift frequency. For example, the *F1* strip corresponding to the conformatioanlly important long range correlations from Gal C1 to GlcNAcβ C3/C5 are overlapped with the intra-residue correlations to Gal C3/C5 (*figure 6.7A*). So from this trace it would not be possible to measure the long couplings. However, by taking a slice at this ^{13}C frequency (~75ppm) in the three dimensional spectrum, the correlations are edited out such that the Gal-C3 and GlcNAcβ-C3 are well resolved and the cross-peaks to Gal-C1 can be measured (*figure 6.7B*). In this spectrum the correlation between GlcNAcβ-C3 and Gal-C1 is shown at four times the height of the rest of the spectrum because of the weak nature of this coupling and because it is only from approximately half of the molecules. Interestingly, neither Gal-C5 or GlcNAcβ-C5 gives rise to a correlation to Gal-C1, indicating that both these couplings are small or zero. From this spectrum the three-bond correlation to Neu5Ac-C3 is also observed as well as the two bond correlation to Neu5Ac-C2. The *F1* slice centred at Gal H2 is also shown (*figure 6.7C*), with the correlations to both Neu5Ac and GlcNAcα/β C4. Figure 6.8 shows the correlations for the trans-glycosidic couplings for the Fuc-GlcNAc linkage, and the sialic acid glycerol side chain correlations which indicate the relative orientation of the side chain. From these strips, nine of the $^3J_{COCC}$ values could be measured, with three further couplings giving rise to no correlation indicating that the coupling is small and below the detectable threshold of the experiment (~<1Hz).

Of interest are those values defining the conformation of the sialic acid side chain (Table 6.4), which up to now has always been described as being in the elongated conformation, where the $^3J_{H7,H8}$ (9.5Hz) indicates that these protons are trans, and the small $^3J_{H6,H7}$

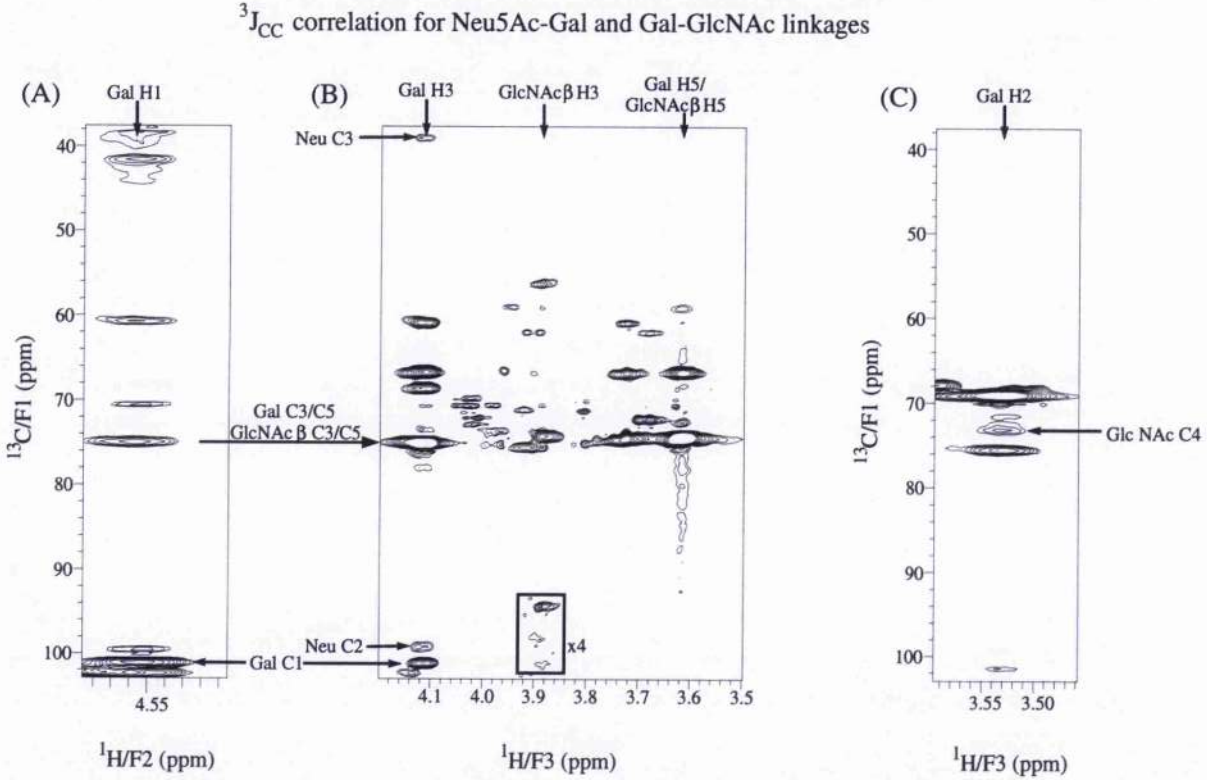

Figure 6.6 - (A) Region of the two dimensuional LRCC spectrum of [U-^{13}C] sialyl Lewis^x at 303K, corresponding to the long range correlations from Gal C1. Indicated is the overlap between the inter-glycosidic correlation to GlcNAc βC3/C5 and the intra-residue correlations to Gal C3/C5.
(B) Region of the three dimensional LRCC spectrum at the ^{13}C chemical frequencies of GlcNAc βC3/C5 and Gal C3/C5 showing the individual correlations to Gal C1, as assigned. The GlcNAc C3 - Gal C1 correlation is shown at four times the level of the rest of the spectrum.
(C) Region of the three dimensional LRCC spectrum, at the ^{13}C chemical frequency of Gal C2, showing the trans-glycosidic correlation to GlcNAc α/β C4.

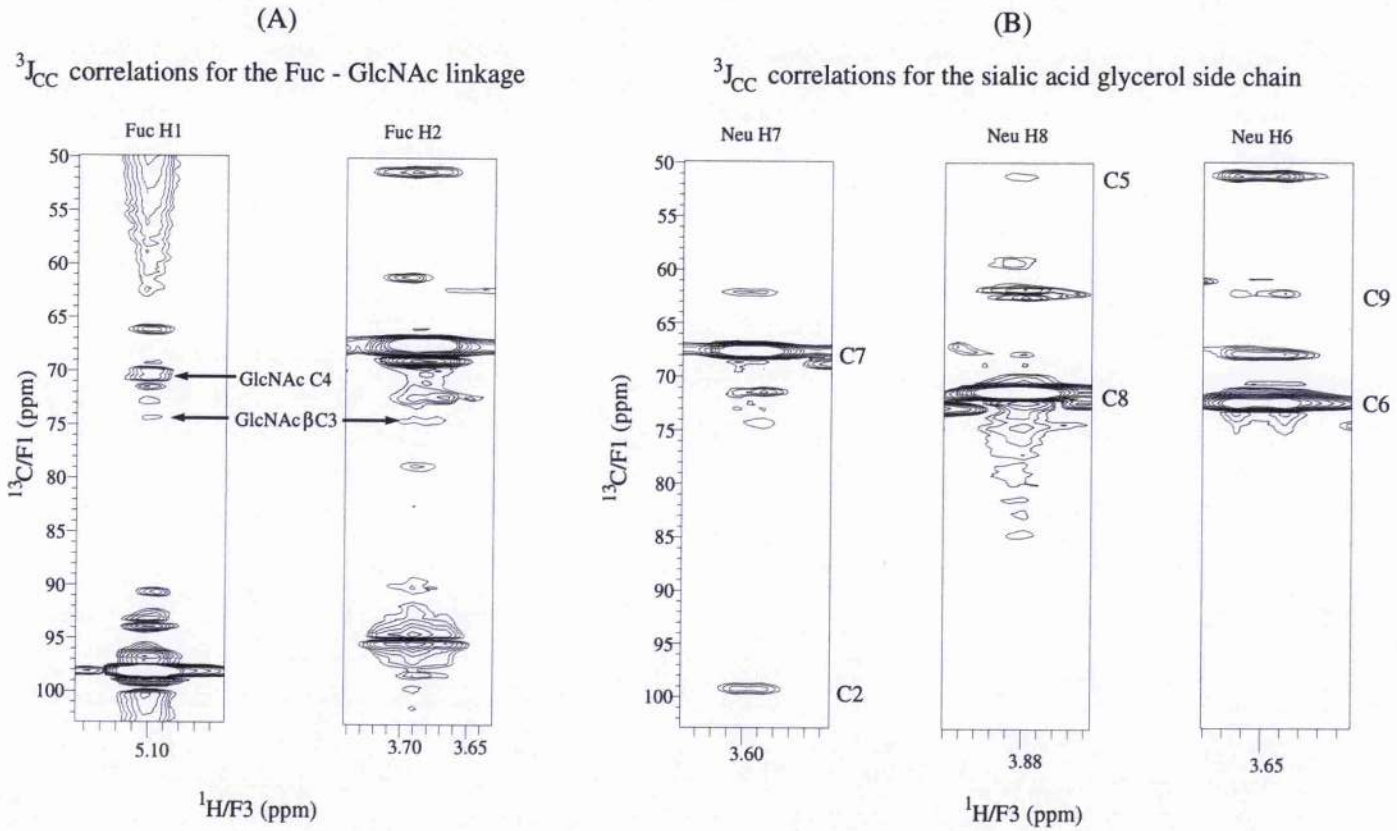

Figure 6.7 - (A) Regions of the three dimensional LRCC spectrum corresponding to the trans-glycosidic correlations for the Fuc-GlcNAc linkage at the ^{13}C chemical frequencies of Fuc H1 and Fuc H2.
(B) Regions of the three dimensional LRCC spectrum corresponding to the three-bond correlations along the Neu5Ac glycerol side chain at the ^{13}C chemical shifts of Neu5Ac C6, C7, and C8.

(1.7Hz) coupling indicating a dihedral angle of about 60°. The carbon-carbon coupling constants for $^3J_{C2,C7}$ (3.2Hz) and $^3J_{C6,C9}$ (3.6Hz) indicate an approximate 180° dihedral angle which supports the proposal. However, the value for the $^3J_{C5,C8}$ (2.1Hz) is not indicative of a trans coupling but of a dihedral angle in the range of 120° - 140°, this is based upon the Karplus type relationship derived for $^3J_{CCCC}$ fragments (Marshall and Miller, 1973). This suggests that in contrast to previous conclusions based upon the proton-proton coupling constants alone, the arrangement of the sialic acid glycerol tail is not extended but has an arrangement where the C5-C8 torsion angle is approximately ±130°.

The inter-glycosidic $^2J_{COC}$ values were also measured and the values obtained from the 3D LRCC spectrum are given in Table 6.4. The magnitude of the coupling constants can be estimated using the sum projection rule (Church *et al.*, 1996). By definition the dihedral angle, ψ, cannot give a sum projection, so the magnitude of the coupling constant is dominated by the sum projection about the torsion angle ϕ. Back-calculation of the dihedral angles (O5-C1-O1-Cx) for each of the glycosidic linkages from the a 5ns time average restrained molecular dynamics simulation (τ = 50ps) gave the following average values: Neu5Ac-Gal, ϕ = -60.1° ± 57.1°; Gal-GlcNAc, ϕ = -66.7° ± 14.4°; and Fuc-GlcNAc, ϕ = -70.3° ± 19.9°. From the sum projection rule, these would give resultant values of -0.5, -0.4, and -0.3, respectively. Therefore, $^2J_{COC}$ values would all be expected to be of the same magnitude and approximately 2Hz. However, the experimental values show significant discrepancies from these predicted values. For the $^3J_{Gal\text{-}C1,GlcNAc\text{-}C4}$ value obtained in this experiment, the resultant sum projection value would need to be of the order 3.0, to predict the experimental value. For a simple disaccharide this resultant sum projection value cannot be obtained. Therefore, whilst in some cases the sum projection rule has shown to be of value (Church *et al.*, 1996), in the present analysis of the conformation of sialyl Lewis^x it is of limited use.

One bond carbon-proton coupling constants were measured from a 2D ^1H-^{13}C HSQC spectrum without ^{13}C decoupling during acquisition. The one bond couplings of the anomeric carbon - proton, and the aglyconic carbon - proton are dependent upon the conformation of the dihedral torsion angles ϕ and ψ, respectively. Recently, Tvaroska and Taravel (1995) have used the derived relationships to back-calculate these values from

Table 6.4 - Experimental values for the inter-glycosidic $^{3}J_{COCC}$ and $^{1}J_{CH}$ couplings in sialyl Lewis^{x}

Inter-glycosidic $^{3}J_{COCC}$ Coupling	Experimental Value (Hz)[a]
Neu5Ac-C3 - Gal-C3	2.1
Neu5Ac-C2 - Gal-C2	1.3
Neu5Ac-C2 - Gal-C4	n.c.
Gal-C2 - GlcNAc-C4	2.9
Gal-C1 - GlcNAc-C3	~2.3
Gal-C1 - GlcNAc-C5	n.c.
Fuc-C2 - GlcNAc-C3	3.3
Fuc-C1 - GlcNAc-C2	n.c.
Fuc-C1 - GlcNAc-C4	2.2

Inter-glycosidic $^{1}J_{CH}$ Coupling	Experimental Value (Hz)[a]
Gal-C3 - Gal-H3	142.4
Gal-C1 - Gal-H1	162.3
Fuc-C1 - Fuc H1	172.4
GlcNAc C4 - GlcNAc-H4	~139.8
GlcNAc C3 - GlcNAc-H3	149.4

Inter-glycosidic $^{2}J_{COCC}$ Coupling	Experimental Value (Hz)[a]
Neu5Ac-C2 - Gal-C3	2.5
Gal-C1 - GlcNAc-C4	3.4
Fuc-C1 - GlcNAc-C3	1.7

(a) Experimental values are ±0.5Hz

molecular mechanics studies to give an insight into the flexibility of carbohydrates, including sialyl Lewis^x. However, these studies were based on static conformations and in the present study, the back-calculation of $^1J_{CH}$ values from modelling simulations have shown that these values are essentially independent of the amount of torsional variation (maximum variation in the values for different models is 0.8Hz). Therefore it appears that although theoretically the $^1J_{CH}$ values should be dependent upon the glycosidic torsion angles, they are not sufficiently sensitive to studying dynamical models.

6.3.5 Modelling

Recent studies on Lewis^x type structures have shown that the rigidity of the Fucα1-3GlcNAc in Lewis^x is not transposed to similar molecules. In a theoretical analysis for the Fucα1-3GlcNAc using the force-field CHEAT95 with specific inclusion of water, Kouwijzer *et al.* (1995) found four low energy minima. In a recent NMR derived structure on a bromelain glycan, containing the moiety GlcNAcβ1-4[Fucα1-3]GlcNAcβ1-, showed that whilst the GlcNAc - GlcNAc linkage was rigid, there was two stable conformations for the Fuc - GlcNAc linkage (Lommerse *et al.*, 1995). Interestingly, a GalNAcβ1-4[Fucα1-3]GlcNAc variation of Lewis^x gives similar conformations (Bergwerff *et al.*, 1993), suggesting that the *N*-acetyl group on the preceding residue to GlcNAc is important in this conformational flexibility. NMR relaxation measurements (cross-relaxation rates, ^{13}C T_1 and T_2 measurements, and heteronuclear NOEs) on GalNAcα1-3Galβ1-4[Fucα1-3]Glc1-OMe (Poveda *et al.*, 1996, 1997) indicate that the Fuc and GalNAc residues have smaller S^2 values compared to the Gal and Glc moieties (0.8 vs. 0.9, respectively), suggesting that the these residues are more flexible than the other two. The evidence of substituted Lewis^x derivatives suggests that there may be greater conformational flexibility about the Fucα1-3Glc(NAc) linkage for Lewis^x than previous modelling studies have suggested.

Table 6.3 lists the distance restraints used in the restrained simulated annealing and MD simulations (conventional and time-averaged). In sialyl Lewis^x previous modelling studies have proposed that the Lewis^x moiety, Galβ1-4[Fucα1-3]GlcNAc, has essentially a single low energy conformation with limited torsional fluctuations (Ichikawa *et al.*, 1992; Rutherford *et al.*, 1994). In contrast the Neu5Ac-Gal linkage is flexible and adopts one of three conformers, conformer 'A' ϕ,ψ -70°, 5°; conformer 'B' ϕ,ψ -165°, -20°; conformer

'C' ϕ,ψ -95°, -45°. Conformers 'A' and 'B' are characterised by the conflicting ROEs between Gal-H3 to Neu5Ac-H3ax, and Gal-H3 to Neu5Ac-H8, respectively. Previous modelling studies on sialyl Lewis^x from within this group (Rutherford *et al.*, 1994) have shown the problem of using conventional molecular dynamics simulations in studying sialyl Lewis^x because of the conflicting nature of the NOEs observed about the Neu5Ac-Gal linkage. With the application of medium restraints, for the Gal-H3 - Neu5Ac-H3ax & -H8 NOEs, the resulting conformations adopted in the MD simulations were not a transition between conformers 'A' and 'B', but yielded a compromise, conformer 'C'. Back-calculated coupling constant datum ($^3J_{Neu\text{-}C2,\ Gal\text{-}H3}$) indicated that this was not a good representation of the dynamics of sialyl Lewis^x in solution. This demonstrates the problem with conventional modelling where time-averaged values, NOEs, are applied to static structures, and in this case, resulting in a conformation that is not a true representation of the data because of the need to satisfy the two separate and conflicting restraints simultaneously. With the increased number of restraints derived from NOEs to exchangeable protons, a modelling study using time-averaged restraints has been implemented, as well as the standard "conventional" method for comparison.

Similar to the modelling of sialylα2,3-*N*-acetllactosamine, conventional methods were used to obtain the low energy structure for input into the molecular dynamics simulations. Ten computer models of sialyl Lewis^x were generated from an unrestrained high-temperature (750K) MD simulation (with all torsion terms scaled by a factor of seven to prevent unrealistic ring distortions). Each of these pseudo-random structures were input into restrained simulated annealing, with four of the ten starting structures converging to conformer 'A' (including the global minimum structure), two annealing to conformer 'B', and one to conformer 'C' (*figure 6.9,* table 6.5). The remaining structures violated the restraints and were discarded. The global minimum energy structure, corresponding to conformer 'A', had an unusual conformation about the sialic aid glycerol side chain, which during MD simulations either rotated to the usual conformation or stayed in its initial conformation resulting in substantial differences in certain back-calculated NOEs, whilst in other respects the simulations behaved as expected. Therefore, the next lowest energy structure (Table 6.5) was used as an input for trajectories of conventionally restrained and time-averaged restrained MD simulations.

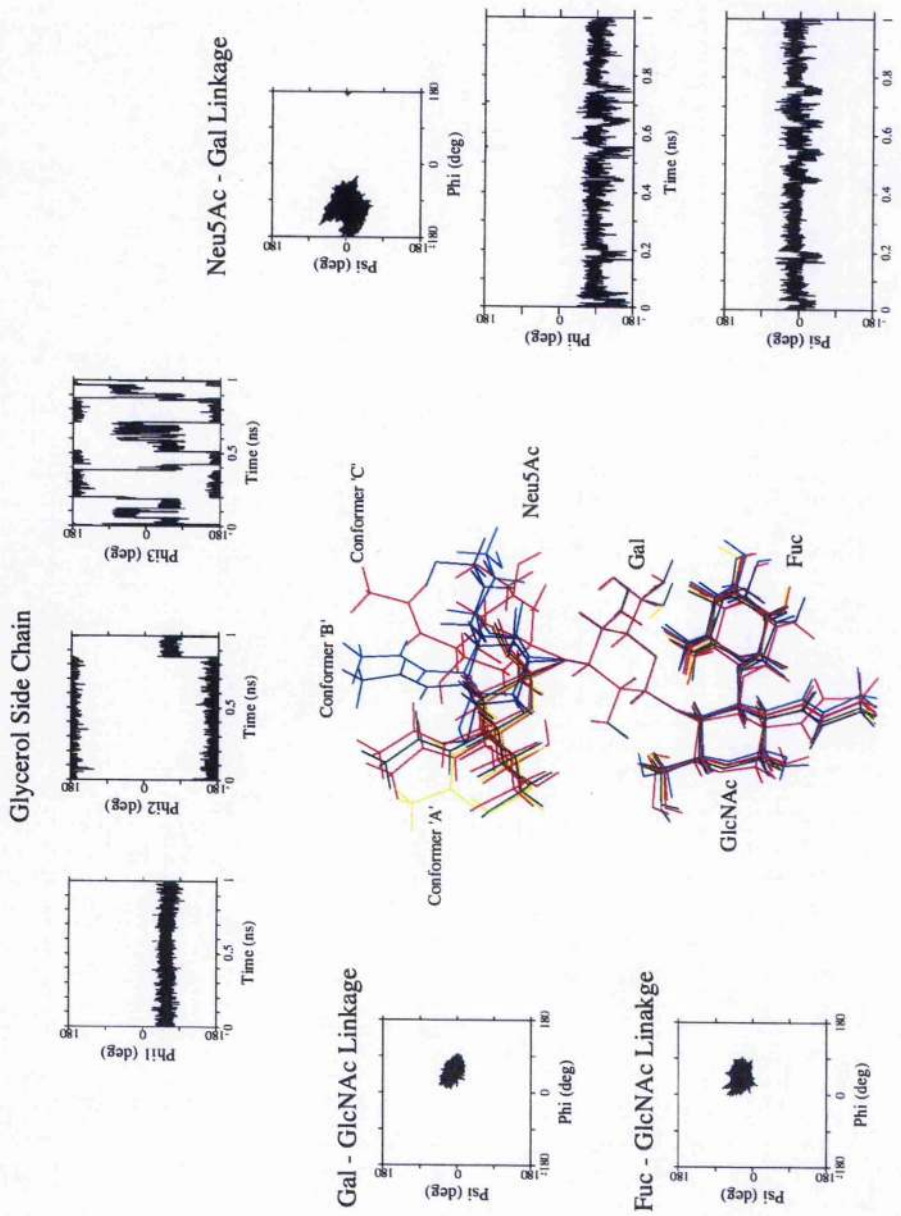

Figure 6.9 - Superimposition of seven geometries derived from the restrained dynamical simulated annealing calculations on sialyl Lewis^x. Instantaneous values of ϕ vs. ψ for the Neu5Acα2-3Gal, Galβ1-4GlcNAc, and Fucα1-3GlcNAc linkages, and the ϕ vs. time plots for the glycerol side chain from the 1ns conventionally restrained MD simulation.

Table 6.5 - Energies and torsion angles of structures from the simulated annealing process which satisfied the distance restraints obtained from ROESY data at 303K and NOESY data at 258K. The lowest energy structure for each conformer about the Neu5Ac-Gal linkage, highlighted in bold, was used in the molecular dynamics simulations.

Structure	Conformer	Neu5Ac-Gal		Gal-GlcNAc		Fuc-GlcNAc		Energy
		ϕ	ψ	ϕ	ψ	ϕ	ψ	(kcal)
1	A	**-79.4**	**12.9**	**46.3**	**15.1**	**41.7**	**21.0**	**-7.76**
2	C	-111.8	-47.6	53.3	8.5	34.1	24.1	-5.32
3	A	**-61.0**	**11.8**	**51.8**	**9.5**	**40.6**	**24.3**	**-6.64**
4	A	-78.9	9.4	50.3	8.5	43.2	24.5	-5.44
5	B	-151.0	-24.3	55.7	6.7	29.9	24.7	-5.40
6	B	-154.7	-16.7	52.8	12.0	30.3	23.8	-5.23
7	A	-76.1	5.1	52.4	8.3	36.7	24.4	-5.57

6.3.5.1 Conventionally Restrained Molecular Dynamics Simulations

Using a full relaxation matrix analysis, NOE data were back calculated from 1ns Discover-based simulations. The correlation times for the 3D ROESY-HSQC and low temperature studies were based upon the fitting of an intra-residue cross-peak and diagonal peak (Gal-H1 - Gal-H3, and Gal-H1 - Gal-H1 were chosen, respectively), and the values were calculated as 0.2ns and 1.2ns, respectively. The ϕ vs. ψ plots for each of the glycosidic linkages for the unrestrained and restrained simulations indicates the maximum extent of conformational mobility consistent with the force-field, and the minimum extent of conformational flexibility consistent with the restraints, respectively (*figure 6.9*).

The two molecular dynamics simulations employing conventional restraints are unable to predict the conflicting nature of the ROEs observed across the Neu5Ac-Gal linkage (Table 6.6). In both simulations there are significant torsional fluctuations with asynchronous changes in both ϕ and ψ indicating that both conformers 'A' and 'B' are explored. However, in the case of the unrestrained simulation the under prediction of the Gal-H3 - Neu5Ac-H8 ROE (outside a factor of two as compared to the experimental values) indicates that conformer 'B' is under populated in this simulation. In contrast, the restrained simulation is constrained to conformer 'A' with only five significant fluctuations into

conformer 'B' during the time course of the simulation. As a result of this conformational inflexibility two of the back-calculated three bond carbon-carbon coupling constants are significantly different to the experimental values.

The conformation of the Galβ1-4GlcNAc linkage has been well studied and in the unrestrained simulation the 'anti' conformer is populated for a significant length of time. However, the linkage appears to have a single low energy conformer, which it adopts for the rest of the time in this simulation and in the restrained simulation. The back-calculated data for this linkage (Tables 6.6 & 6.7) are in good agreement with experiment, except for one carbon-carbon coupling constant, which is probably as a result of the difficulty in measuring accurately the low intensity of the long range correlation observed in the LRCC spectra.

The prediction of increased flexibility of the Fucα1-3GlcNAc from a number of Lewis^x related oligosaccharides is observed in the unrestrained simulation. Significant torsional fluctuations occur with inter-conversion of two low energy structures. Owing to the population of the anti-conformer in the Galβ1-4GlcNAc linkage, which through necessity requires a conformational change in the orientation of the Fucα1-3GlcNAc, additional conformational space is sampled. In contrast in the restrained simulations this linkage only adopts one conformer, although significant torsional fluctuations are observed within the region of space around this low energy conformer. Back-calculation of long range coupling constant values reveal that one carbon-carbon, and one carbon-proton coupling constant are significantly different (>0.5Hz) from experimental values for the unrestrained simulation. Therefore, in solution the conformational flexibility of this linkage is best described in terms of a single conformer with some torsional fluctuations.

Table 6.6 - Back-calculated inter-glycosidic (R)NOEs for sialyl Lewis^x from the "conventionally" restrained MD simulations using DISCOVER.

NOE	Unrestrained	Restrained with OH restraints	Restrained with 'medium' restraints	Restrained with H-bonds	Experimental Values
Gal-H1 - GlcNAc-H4	1.00	1.21	1.30	1.31	0.83
Gal-H1 - GlcNAc-H61	1.27	1.18	2.30	1.49	1.23
Fuc-H1 - GlcNAc-H3	1.43	0.99	1.31	1.34	1.80(β)
Fuc-H1 - GlcNAc-H2	**0.15**	**0.13**	**0.18**	**0.13**	0.86(β)
Gal-H2 - Fuc-H5	0.73	1.23	1.34	1.47	0.87
Gal-H2 - Fuc-H61	0.69	0.89	**2.24**	1.40	0.99
Gal-H61 - Fuc-H3	0.66	1.25	1.49	1.48	0.99
Gal-H3 - Neu5Ac-H3ax	0.60	**0.14**	0.57	**0.05**	0.59
Gal-H3 - Neu5Ac-H8	**0.16**	0.33	0.46	0.38	0.54
Gal-H1 - GlcNAc-OH6	-0.39	-0.53	-0.45	-0.56	-0.52
Gal-OH2 - GlcNAc-H6	-0.65	-0.75	-0.58	-0.35	-0.81[a]
Gal-OH2 - Neu5Ac-H8	-0.14	-0.15	-0.05	-0.28	
Fuc-H1 - GlcNAc-NH2	**-0.62**	**-0.62**	**-0.74**	**-0.61**	-1.75(β)
Gal-OH2 - Fuc-H6	-0.21	-0.12	-0.24	-0.09	-0.13
Gal-OH4 - Fuc-H6	**-0.56**	**-0.60**	**-1.63**	-0.34	-0.18
Gal-OH4 - Fuc-H4	-0.31	**-0.80**	**-1.38**	-0.20	-0.33
Gal-OH4 - Neu5Ac-H3eq	**-0.02**	**-0.02**	**-0.02**	-0.08	-0.12
Gal-OH2 - Neu5Ac-H3ax	-0.61	**-0.26**	**-0.23**	**-0.34**	-0.87
Gal-H3 - Neu5Ac-HO8	**-0.21**	**-0.20**	-0.57	-0.34	-0.47
Gal-OH4 - Fuc-H3	**-0.31**	**-0.48**	**-0.34**	-0.04	<-0.04

(a) Cross-peaks overlapping.

Table 6.7 - Experimental vs. Back-calculated carbon-carbon and carbon-proton coupling constants from the 1ns MD simulation using DISCOVER.

Trans-glycosidic Coupling	Unrestrained	Restrained	Restrained - 'medium'	Experimental Values (Hz)[a]
Neu5Ac-C1 - Gal-C3	1.4	0.8	1.3	n.d.
Neu5Ac-C3 - Gal-C3	1.8	2.3	1.9	2.1
Neu5Ac-C2 - Gal-C2	1.2	**0.8**	1.2	1.3
Neu5Ac-C2 - Gal-C4	1.2	**1.4**	1.2	n.c.
Gal-C2 - GlcNAc-C4	3.1	3.5	2.8	2.9
Gal-C1 - GlcNAc-C3	**1.4**	**1.3**	**1.4**	~2.3
Gal-C1 - GlcNAc-C5	1.0	0.4	0.4	n.c.
Fuc-C2 - GlcNAc-C3	**2.5**	2.9	2.8	3.3
Fuc-C1 - GlcNAc-C2	0.9	0.6	0.7	n.c.
Fuc-C1 - GlcNAc-C4	2.1	2.2	2.3	2.2
Neu5Ac-C2 - Gal-H3	**4.5**	**4.8**	**4.6**	5.4
Gal-H1 - GlcNAc-C4	2.9	2.5	2.6	2.8
Gal-C1 - GlcNAc-H4	5.3	5.1	5.1	4.8
Fuc-H1 - GlcNAc-C3	**4.2**	**4.3**	**4.2**	5.0 - 5.2
Fuc-C1 - GlcNAc-H3	**3.4**	2.8	3.0	2.8

(a) Errors in these measurements estimated as ±0.5 Hz.

A second restrained simulation with the appropriate restraints increased to 'medium', improved the back-calculation of the NOEs about the Neu5Ac-Gal linkage, however, the resulting carbon-carbon coupling constants about this linkage were in poor agreement with the experimental data (Tables 6.6 & 6.7). Therefore, the conventional approach to modelling of sialyl Lewis^x results in a poor model for the dynamical behaviour in solution.

6.3.5.2 Time-averaged Restrained Molecular Dynamics Simulations

Time-averaged restrained molecular dynamics simulation using a variety of values for τ (0.05ps, 5ps, and 50ps) were used to assess the most appropriate value for the memory function. The phi vs. psi plots for each of the disaccharide linkages indicate that with increasing values of τ, the simulations become more unrestrained like (*figure 6.10*), for comparison an unrestrained MD simulation is also shown. Back-calculated NOEs and coupling constants for these simulations are given in Tables 6.8 & 6.9.

From these values it is clearly seen that for the unrestrained simulation a number of these data are outside the allowable experimental values. In particular the poor agreement for the data about the Gal-GlcNAc and Fuc-GlcNAc linkages (Tables 6.8 & 6.9) is as a result of substantial excursions into phi/psi space (*figure 6.10A*).

In the other extreme the simulation with τ = 0.05ps (conventionally restrained-like simulation, *figure 6.10B*), shows limited torsional fluctuations about the Gal-GlcNAc and Fuc-GlcNAc linkages, and back-calculated values agree reasonable well with experimental values (Tables 6.8 & 6.9). In contrast, the limited fluctuations about the Neu5Ac-Gal linkage (essentially locked into conformer 'B', except at the start of the simulation) results in an under prediction of the Neu5Ac-H3ax - Gal-H3 ROE, and the over prediction of $^3J_{\text{Neu5Ac-C3, Gal-C3}}$.

In the simulation with τ = 5ps, the phi/psi space for the Gal-GlcNAc and Fuc-GlcNAc linkages show essentially single conformations with minor excursions outside these low energy minima (*figure 6.10C*). During the simulation the Neu5Ac-Gal linkage adopts both conformer 'A' and 'B', however as in the case of the unrestrained Discover

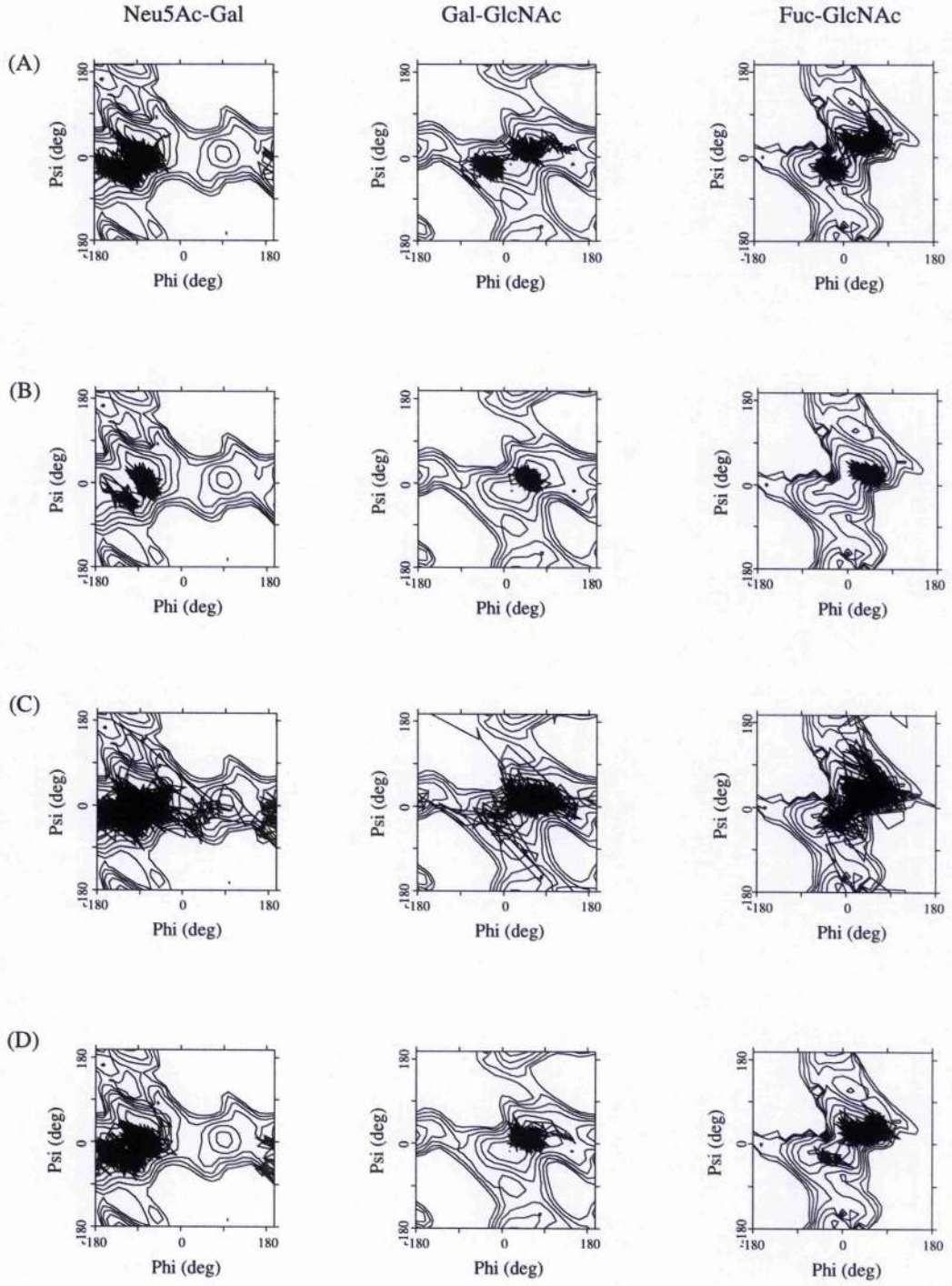

Figure 6.10 - Instantaneous values for ϕ vs. ψ for the Neu5Acα2-3Gal, Galβ1-4GlcNAc, and Fucα1-3GlcNAc linkages, from 1ns time-averaged restrained MD simulations for (A) unrestrained, (B) τ = 0.05ps, (C) τ = 5ps, and (D) τ = 50ps.

simulation, conformer 'A' is not sufficiently sampled for a significant build up of the ROE between Neu5Ac-H3ax and Gal-H3, resulting in the under prediction of this ROE.

In contrast, the simulation with τ = 50ps, gives good back-calculated values for nearly all of the experimental data (Tables 6.8 & 6.9). In this case the Gal-GlcNAc, and Fuc-GlcNAc are effectively restrained into a single conformation with minor excursions outside these areas in conformational phi/psi space (*figure 6.10D*), and the conflicting nature of the ROEs across the Neu5Ac-Gal linkage are well simulated.

From these studies the dynamics best describing the solution conformation of sialyl Lewis^x is the time-averaged restrained molecular dynamics simulation with τ = 50ps. This suggests that the Lewis^x moiety is relatively rigid within the bounds of allowing minor torsional fluctuations to occur about the linkages, and that the Neu5Ac-Gal linkage is relatively flexible.

Throughout these simulations, the back-calculation of the NOEs to Gal-OH4 observed in the low temperature ES-NOESY experiment have not been predicted at all well. In particular an NOE between Gal-OH4 and Fuc-H3 is predicted in all simulations, whereas no evidence for this NOE is observed. This can be rationalised in view of the fact that Gal-OH4 is proposed to be involved in a hydrogen to Neu5Ac-COOH in solution (and partially supported by the experimental data in this study), whereas in these simulations it behaves as if it is a free rotor (data not shown). Thus, if a hydrogen bond does exist, it would tie this hydroxyl group away from the fucose residue and hence reduce the NOE to Fuc-H3. A 500ps Discover simulation with this proposed hydrogen bond incorporated into the restraints (Gal-OH4:::Neu5Ac-COOH, set as 1.8Å<r<3.2Å) confirmed this hypothesis with NOEs to Fuc H4, H6 and H3 all agreeing with the experimental data (Table 6.6). Further evidence was obtained from studying the NOEs within the galactose residue. In particular, in the simulations without the hydrogen bond included, a large NOE is predicted to Gal-H2, whereas in solution only a small NOE is observed in the ES-NOESY spectra. In contrast, with the inclusion of the hydrogen bond, the restricted rotation of this hydroxyl group does not allow it to rotate under the galactose ring whereby producing a large NOE to Gal-H2, and back-calculated values produced are in good agreement with experimental data. The only drawback with these simulations with the inclusion of the hydrogen bond is that they

effectively fix the conformation about the Neu5Ac-Gal linkage into conformer 'A'. This suggests that whilst a hydrogen bond is likely to be present in solution it will be transitory in nature.

In contrast, NOEs to Gal-OH2, which has also been proposed to be involved in a hydrogen bond, are well modelled in the simulations without the inclusion of any hydrogen bond restraints. This essential free rotating behaviour of the hydroxyl group is necessary for the back-calculated to be within good agreement of the experimental data. With the inclusion of a hydrogen bond (Gal-OH2:::Neu5Ac-O6, set as 1.8Å<r<3.2Å) the value for the Gal-OH2 - Neu5Ac-H3ax NOE is over predicted, whilst the contribution to the NOE (^{1}H 3.80ppm) from the Gal-OH2 - GlcNAc-H6's is decreased (Table 6.5). Therefore, these simulations suggest that if a hydrogen bond involving Gal-OH2 does exist, it is not long lived in solution.

In a similar manner to those NOEs observed in low temperature studies of sialylα2,3-*N*-acetyllactosamine, the Gal-H3 - Neu5AC-H8/HO8 conflicting NOEs are only modelled well with an inclusion of the hydrogen bond Neu5Ac-HO8:::Neu5Ac-COOH (Table 6.5).

In this present study of the solution behaviour of sialyl Lewis^x, the inclusion of NOEs to exchangeable protons has doubled the number of distance restraints and has allowed time-averaged restrained molecular dynamics simulations to be used. The predicted dynamical properties from a time-averaged simulation with τ = 50ps is shown to provide the best agreement with experimental data. The observation of exchangeable proton NOEs has allowed for direct evidence in modelling studies for significant hydrogen bonding for two hydroxyl groups in sialyl Lewis^x, with back-calculated NOEs only consistent with the inclusion of hydrogen bonds.

Table 6.8 - Back-calculated inter-glycosidic (R)NOEs for sialyl Lewis^x from the time-averaged restrained MD simulations using XPLOR.

NOE	Unrestrained	Restrained τ = 0.05ps	Restrained τ = 5ps	Restrained τ = 50ps	Experimental Values (Hz)
Gal-H1 - GlcNAc-H4	**1.73**	1.34	1.33	1.41	0.83
Gal-H1 - GlcNAc-H61	0.72	1.43	1.45	1.46	1.23
Fuc-H1 - GlcNAc-H3	2.11	1.74	1.50	1.61	~1.80(β)
Fuc-H1 - GlcNAc-H2	**0.11**	**0.14**	**0.28**	**0.18**	~0.86(β)
Gal-H2 - Fuc-H5	**0.30**	**1.88**	1.20	1.27	0.87
Gal-H2 - Fuc-H61	**0.16**	1.21	0.54	0.67	0.99
Gal-H61 - Fuc-H3	**0.32**	1.66	0.84	0.92	0.99
Gal-H3 - Neu5Ac-H3ax	0.43	**0.07**	0.38	0.43	0.59
Gal-H3 - Neu5Ac-H8	0.34	0.45	**0.14**	0.33	0.54
Gal-H1 - GlcNAc-OH6	**-0.11**	-0.38	-0.43	-0.45	-0.52
Gal-OH2 - GlcNAc-H6	-1.20	-0.54	-0.70	-0.59	-0.81[A]
Gal-OH2 - Neu5Ac-H8	-0.23	-0.22	-0.12	-0.19	
Fuc-H1 - GlcNAc-NH2	**-0.81**	-2.61	-2.27	-1.34	-1.75(β)
Gal-OH2 - Fuc-H6	**-0.04**	-0.18	-0.18	-0.11	-0.13
Gal-OH4 - Fuc-H6	-0.29	**-0.64**	**-0.48**	**-0.60**	-0.18
Gal-OH4 - Fuc-H4	**-0.10**	**-0.87**	-0.37	-0.44	-0.33
Gal-OH4 - Neu5Ac-H3eq	**-0.03**	**-0.03**	**-0.02**	**-0.03**	-0.12
Gal-OH2 - Neu5Ac-H3ax	-0.44	**-0.15**	**-0.34**	**-0.35**	-0.87
Gal-H3 - Neu5Ac-HO8	**-0.06**	**-0.08**	-0.25	**-0.05**	-0.47
Gal-OH4 - Fuc-H3	**-0.13**	**-0.46**	**-0.55**	**-0.62**	<-0.04

(a) Cross-peaks overlapping.

Table 6.9 - Experimental trans-glycosidic scalar coupling constants in sialyl Lewis^x vs. theoretical values computed from the 1ns MD simulations using time-averaged restraints.

Trans-glycosidic Coupling	Unrestrained	Restrained $\tau = 0.05$ps	Restrained $\tau = 5$ps	Restrained $\tau = 50$ps	Experimental Values (Hz)[a]
Neu5Ac-C1 - Gal-C3	1.5	1.3	1.7	1.5	n.d.
Neu5Ac-C3 - Gal-C3	2.4	**3.2**	2.4	2.5	2.1
Neu5Ac-C2 - Gal-C2	1.8	1.3	1.8	1.8	1.3
Neu5Ac-C2 - Gal-C4	1.1	1.1	1.2	1.1	n.c.
Gal-C2 - GlcNAc-C4	**1.6**	**3.7**	3.2	3.5	2.9
Gal-C1 - GlcNAc-C3	**0.9**	**1.5**	**1.6**	**1.6**	~2.3
Gal-C1 - GlcNAc-C5	**1.8**	0.8	0.9	0.8	n.c.
Fuc-C2 - GlcNAc-C3	**1.3**	2.9	2.6	2.7	3.3
Fuc-C1 - GlcNAc-C2	**1.7**	0.6	1.0	0.8	n.c.
Fuc-C1 - GlcNAc-C4	**1.1**	2.1	2.2	2.2	2.2
Neu5Ac-C2 - Gal-H3	**4.5**	5.0	**4.4**	**4.6**	5.4
Gal-H1 - GlcNAc-C4	**3.5**	2.4	2.6	2.5	2.8
Gal-C1 - GlcNAc-H4	4.7	5.2	4.9	5.1	4.8
Fuc-H1 - GlcNAc-C3	**3.8**	3.3	2.9	2.9	2.8
Fuc-C1 - GlcNAc-H3	**4.3**	4.5	**4.1**	**4.2**	5.0 - 5.2

(a) Errors in these measurements estimated as ±0.5 Hz.

6.3.6 Bound Conformation of Sialyl Lewis^x

A preliminary investigation of the bound conformation of sialyl Lewis^x with E-selectin was performed using a 3D TRNOESY-HSQC experiment. The aim of the current study was to investigate the applicability of ^{13}C-enriched oligosaccharides in binding studies, and not a full investigation into the conformation of sialyl Lewis^x when bound to E-selectin.

The optimum conditions for the measurement of TRNOEs have been published (Scheffler *et al.*, 1995, 1997), and only the mixing time of the NOESY experiment was optimised. It was found that the build up of TRNOEs was rapid and that the signals had decayed away with mixing times greater than 100ms, with 50ms being the optimum length. This rapid build up and decay is indicative of a ligand with restricted mobility (Campbell and Sykes, 1993). Interestingly previous studies with unlabelled sialyl Lewis^x with the same E-selectin chimera yielded optimum mixing times of about 150ms. A possible explanation maybe the ligand:protein ratio used in the previous study compared to this one. Although the ligand to protein ratio could not be measured accurately due to the unknown weight of ligand and protein used, a comparison of the 1D spectra to that with a known ligand:protein ratio,15:1, (Weimar, T., 1997, personal communication) suggests that the ratio is substantially less than 15:1 (data not shown). Theoretical analysis of the TRNOE has shown that the build up and decay of the TRNOE is dampened with respect to higher ligand:protein ratios (Campbell and Sykes, 1993).

Selective shifting of resonances is indicative of the ligand stacking against an aromatic residue (ring current shifts), and from mutagenesis studies (Erbe *et al.*, 1992; Kogan *et al.*, 1995), Tyr48 and Tyr94 are found to have an affect on the binding of sialyl Lewis^x. Therefore, possible perturbations of selective resonances might be expected. In the ^{1}H-^{13}C HSQC spectrum of sialyl Lewis^x in the presence of E-selectin (*figure 6.3B*) it can be clearly seen that no resonances experience a shift. Intriguingly, the resonances for the GlcNAc residue appear stronger in this spectrum than in a similar HSQC spectrum of sialyl Lewis^x in free solution (*figure 6.3A*). This suggests that the resonances for the other residues are experiencing line broadening due to chemical exchange or intimate contacts with the protein, whilst the GlcNAc residue is not. This is in agreement with functional group analysis that

has shown that groups on the fucose, galactose, and sialic acid residues are essential for binding, whilst the GlcNAc residue makes no contact with the protein.

From the *F2F3* plane of the 3D TRNOE-HSQC spectrum at the *F1* chemical shift of Gal-H3 (*figure 6.11B*), an inter-glycosidic TRNOE is observed to Neu5Ac-H8, but no TRNOE is observed to the folded-in Neu5Ac-H3ax (^{1}H 1.80ppm, ^{13}C 94.3ppm) which is characteristic of conformer 'B'. This suggests that only a subset of conformational space is accessed on binding to E-selectin. Other inter-glycosidic TRNOEs observed in this 3D spectrum are Gal-H2 - Fuc-H5 and H6, and Fuc-H1 - GlcNAc-H3, Gal-H1 - GlcNAc-H4 and H6's, the latter TRNOE has only been observed recently in a 3D HOHAHA-TRNOESY experiment (Scheffler *et al.*, 1997). The TRNOEs to Gal-H1 are shown in a ^{1}H-^{13}C (*F3F2*) plane from the TRNOE-HSQC spectrum at the *F1* chemical shift of Gal-H1 (*figure 6.11A*). These inter-glycosidic NOEs were used in the restrained simulated annealing.

Using the ten computer models of sialyl Lewis^x generated previously from an unrestrained high-temperature (750K) MD simulation (with all torsion terms scaled by a factor of seven to prevent unrealistic ring distortions). Each pseudo-random structure was input into restrained simulated annealing using the restraints in Table 6.9, and a dielectric constant of 4.0 to mimic the protein environment of the bound ligand.. Eight of the ten structures annealed to a single conformation about the Neu5Ac-Gal linkage, conformer 'A' (*figure 6.12*, Table 6.10). The other two structures violated the distance restraints. All of the structures annealed to a single conformation about the Gal-GlcNAc linkage, but one structure annealed to an anomalous conformation about the Fuc-GlcNAc linkage.

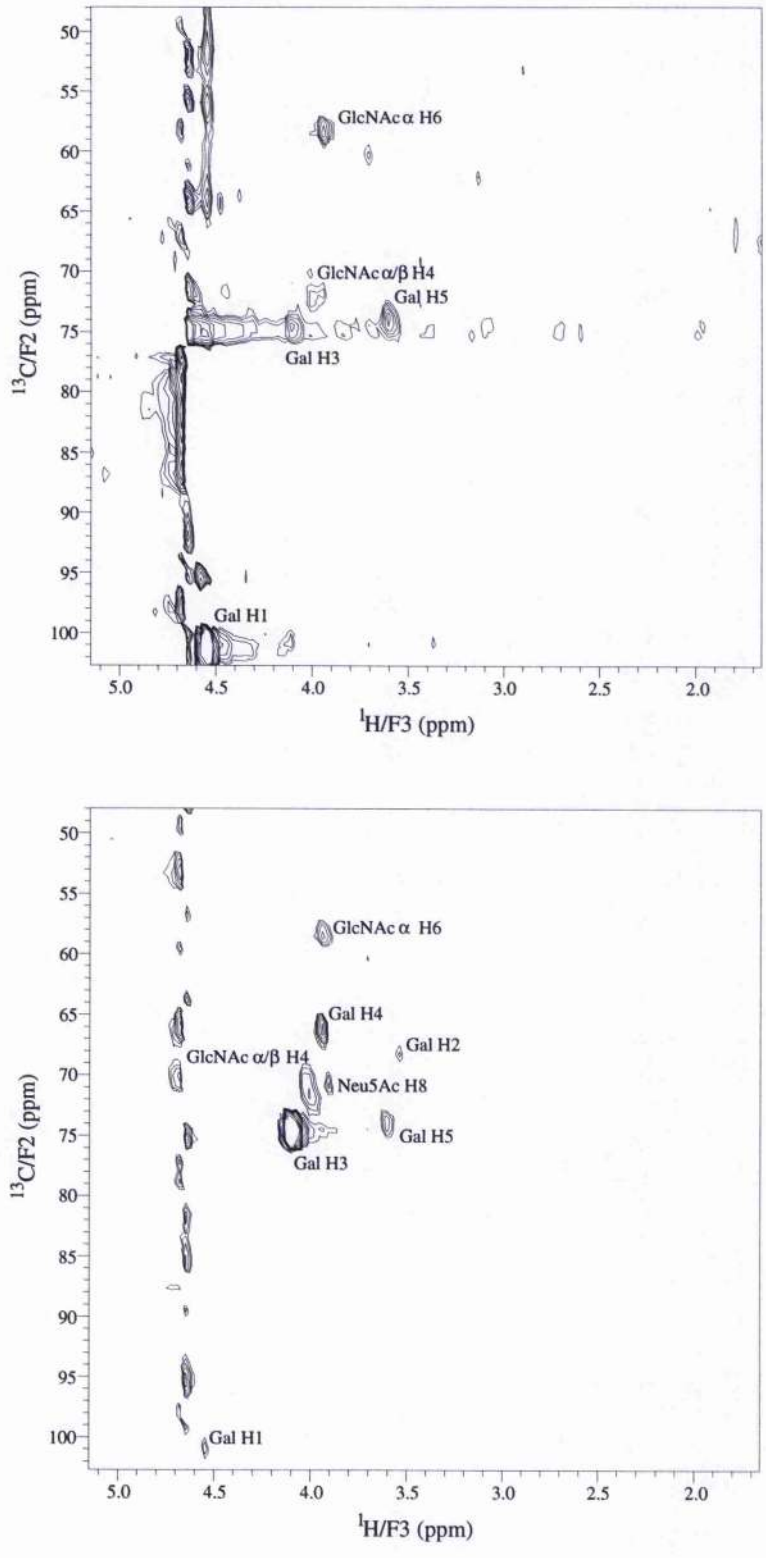

Figure 6.11 - Regions of the *F2F3* planes from the three dimensional TRNOESY spectrum of sialyl Lewis^x in complex with E-selectin at the proton chemical frequencies of (A) Gal-H1, and (B) Gal-H3.

Table 6.10 - Energies and torsion angles of structures from the simulated annealing process which satisfied the distance restraints obtained from TRNOESY data at 310K.

Structure	Conformer	Neu5Ac-Gal		Gal-GlcNAc		Fuc-GlcNAc		Energy
		ϕ	ψ	ϕ	ψ	ϕ	ψ	(kcal)
1	A	-80.21	15.15	46.10	10.12	42.90	20.89	40.99
2	A	-79.20	15.28	48.40	9.83	54.08	24.93	40.05
3	A	-74.73	12.23	40.23	12.73	57.72	23.89	42.53
4	A	-71.14	12.00	48.71	15.47	18.26	17.88	41.13
5	A	-77.84	11.59	43.24	11.61	51.44	23.89	43.14
6	A	-71.39	10.31	39.11	12.78	54.81	24.92	42.83
7	A	-70.91	6.94	46.79	7.04	44.14	21.14	42.09
8	A	-72.61	12.52	50.20	9.51	44.14	21.22	38.88

Although in this case no extra TRNOEs were observed, the case for using ^{13}C labelled ligands is powerful. Lower ligand concentrations can be used and still allow the TRNOEs to be observed distinct from the protein resonances. The use of heteronuclear editing of TRNOE experiments allows for unambiguous assignment of TRNOEs and quantitative data, which is complicated in homonuclear experiments using HOHAHA editing of spectra.

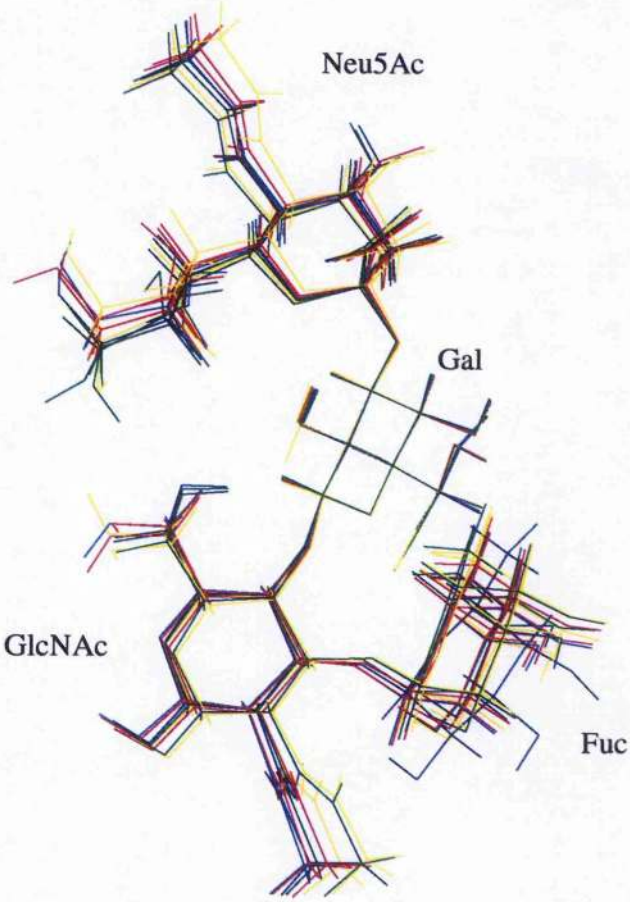

Figure 6.12 - Representation of the structures obtained from simulated annealing corresponding to the conformation of sialyl Lewis^x in the bound state. Eight of the ten structures are shown. The following average values for the glycosidic linkages were obtained: Neu5Ac-Gal, ϕ =-75.7° ± 4.5°, ψ = 11.1° ± 4.2°; Gal-GlcNAc, ϕ = 44.7° ± 5.5°, ψ = 11.3° ± 4.2°; Fuc-GlcNAc, ϕ =50.3° ± 7.4° , ψ = 31.4° ± 3.5°.

6.4 Conclusions

Heteronuclear NMR investigations of the solution behaviour of the tetrasaccharide sialyl Lewis^x antigen has distinct advantages over purely homonuclear methods. In particular complete unambiguous assignment of ROE cross-peaks were possible using a three-dimensional ROESY-HSQC experiment. Additional information on the relative orientation about the glycosidic linkages were made from long range carbon-carbon coupling constants. Further distance restraints were obtained from NOE spectra at low temperatures in a mixture of H_2O and acetone which allows the observation of the exchangeable proton resonances within the oligosaccharide. With these restraints modelling has shown that the NOEs to Gal-OH4 and Neu5Ac-OH8 can only be predicted accurately if within the simulation they are hydrogen bonded to the appropriate oxygen. In contrast, the prediction of NOEs to Gal-OH2, which has also been proposed to be involved in a hydrogen bond, is best suited if in the simulation it is allowed to act as a free rotor. The addition of these extra restraints has also allowed time-averaged restrained molecular dynamics simulations to be used, which are more appropriate than conventional modelling strategies presently used for simulating oligosaccharides which are known to undergo significant conformational fluctuations between two or more low energy structures.

6.4.1 Conformation of the Galβ1-4GlcNAc linkage

The conformation of the Galβ1-4GlcNAc through the series of *N*-acetyllactosamine, sialylα2,3-*N*-acetyllactosamine, and sialyl Lewis^x shows different dynamical properties for each compound. By the use of NOEs to exchangeable protons in the disaccharide it is apparent that the solution conformation cannot adopt a single structure to accommodate all of the distance restraints. In sialylα2,3-*N*-acetyllactosamine the observation of homonuclear ROEs between Gal-H1 - GlcNAc-H3 & H5, which has not been previously unambiguously identified and quantified, suggests that the Galβ1-4GlcNAc adopts the 'anti' conformation and therefore exhibits a high degree of flexibility about this linkage. In contrast, in sialyl Lewis^x this linkage is conformationally restrained with only one of the two conformations observed in the disaccharide populated in solution. This restriction of conformational flexibility occurs because of the stacking of the fucose residue under the galactose.

References

Abbassi, O., Lane, C. L., Krater, S., Kishimoto, T. K., Anderson, D. C., McIntire, L. V. and Smith, C. W. (1991). "Canine neutrophil margination mediated by lectin adhesion molecule-1 *in vivo*." *Journal of Immunology* **147**: 2107 - 2115.

Abbassi, O., Kishimoto, D. C., McIntire, L. V., Anderson T. K. and Smith, C. W. (1993). "E-selectin supports neutrophil rolling *in vitro* under conditions of flow." *Journal of Clinical Investigation* **92**: 2719 - 2730.

Acquotti, D., Poppe, L., Dabroswki, J., von der Lieth, C-W., Sonnino, S. and Tettamanti, G. (1990). "Three-dimensional structure of the oligosaccharide chain of G_{M1} ganglioside revealed by a distance mapping procedure: A rotating and laboratory frame nuclear Overhauser enhancement investigation of native glycolipid in dimethylsulfoxide and in water-dodecylphosphocholine solutions." *Journal of the American Chemical Society* **112**: 7772 - 7778.

Adams, B. and Lerner, L. (1992). "Observation of hydroxyl protons of sucrose in aqueous solution: no evidence for persistent intramolecular hydrogen bonds." *Journal of the American Chemical Society* **114**: 4827 - 4829.

Adams, B. and Lerner, A. (1992). "A simple one-dimensional method for measuring proton exchange rates in water." *Journal of Magnetic Resonance* **96**: 604 - 607.

Adams, B. and Lerner, L. (1993). "Measurement of long-range ^{1}H-^{13}C coupling constants using selective excitation of carbon-13." *Journal of Magnetic Resonance Series A* **103**: 97 - 102.

Alon, R., Rossiter, H., Wang, X., Springer, T. A. and Kupper, T. S. (1994). "Distinct cell surface ligands mediate T lymphocyte attachment and rolling on P and E-selectin under physiological flow." *Journal of Cell Biology* **127**: 1485 - 1495.

Alon, R., Hammer, D. A. and Springer, T. A. (1995). "Lifetime of the P-selectin - carbohydrate bond and its response to tensile force in hydrodynamic flow." *Nature* **374**: 539 - 542.

Amin, S. R., and Chatterjee, B. P. (1995). "Binding mechanism of methyl-α-*N*-acetyl D-galactopyranosamine to *Artocarpus lakoocha* lectin, *artocarpin*: A proton nuclear magnetic resonance study." *Draft Document.*

Andrews, J. S., Weimar, T., Frandsen, T. B., Svensson, B. and Pinto, B. M. (1995). "Novel disaccharides containing sulfur in the ring and nitrogen in the inter-glycosidic linkage - conformation of methyl 5'-thio-4-*N*-α-maltoside bound to glucoamylase and its activity as a competitive inhibitor." *Journal of the American Chemical Society* **117**: 10799 - 10804.

Arbones, M. L., Ord, D. C., Ley, K., Radich, H., Maynard-Curry, C., Otten, G., Capon, D. J. and Tedder, T. F. (1994). "Lymphocyte homing and leukocyte rolling are impaired in L-selectin (CD62L) deficient mice." *Immunity* **1**: 247 - 260.

Arepalli, S. R., Glaudemans, C. P. J., Daves, G. D., Kover, P. and Bax, A. (1995). "Identification of protein-mediated indirect NOE effects in a disaccharide-Fab complex by transferred ROESY." *Journal of Magnetic Resonance Series B* **106**: 195 - 198.

Asensio, J. L., Canada, F. J. and Jimenez-Barbero, J. (1995). "Studies on the bound conformation of methyl-α-lactoside and methyl-β-allolactoside to ricin B-chain using transferred NOE experiments in the laboratory frame and rotating frames, assisted by molecular mechanics and dynamics simulations." *European Journal of Biochemistry* **233**: 618 - 630.

Atherton, A. and Born, G. V. R. (1972). "Quantitative investigation of the adhesiveness of circulating polymorphonuclear leukocytes to blood vessel walls." *Journal of Physiology* **222**: 447.

Aubin, Y. and Prestegard, J. H. (1993). "Structure and dynamics of sialic acid at the surface of a magnetically orientated membrane system." *Biochemistry* **32**: 3422 - 3428.

Ball, G. E., O'Neill, R. A., Schultz, J. E., Lowe, J. B., Weston, B.W., Nagy, J. O., Brown, E. G., Hobbs, C. J and Bednarski, M. D. (1992). "Synthesis and structural analysis using 2D NMR of sialyl Lewis^x and Lewis^x oligosaccharides: Ligands related to E-selectin binding." *Journal of the American Chemical Society* **114**: 5449 - 5451.

Bargatze, R. F., Kurk, S., Butcher, E. S. and Jutila, M. A. (1994). "Neutrophils roll on adherent neutrophils bound to cytokine-induced endothelial cells via L-selectin on the rolling cells." *Journal of Experimental Medicine* **180**: 1785 - 1792.

Barker, R., Nunez, H. A., Rosevear, P. and Serianni, A. S. (1982). "^{13}C NMR analysis of complex carbohydrates." *Methods in Enzymology* **83**: 58 - 69.

Batta, G. and Kover, K. E. (1987). "Theoretical aspects of one dimensional and two dimensional heteronuclear Overhauser experiments and selective ^{13}C T_1 determinations of heteronuclear distances." *Progress in Nuclear Magnetic Resonance Spectroscopy* **19**: 223 - 266

Batta, G., Kover, K. E., Gervay, J., Hornyak, M. and Roberts, G. M. (1997). "Temperature dependence of molecular conformation, dynamics, and chemical shift anisotropy of α, α-trehalose in D_2O by NMR relaxation." *Journal of the American Chemical Society* **119**: 1336 - 1345.

Bauer, C., Freeman, R. and Wimperis, S. (1984). "Long-range carbon-proton coupling constants." *Journal of Magnetic Resonance* **58**: 526 - 532.

Bax, A., Freeman, R. and Frenkiel, T. A. (1981). "An NMR technique for tracing out the carbon skeleton of an organic molecule." *Journal of the American Chemical Society* **103**: 2102 - 2104.

Bax, A. and Freeman, R. (1982). "Long-range proton-carbon NMR spin coupling constants." *Journal of the American Chemical Society* **104**: 1099 - 1100.

Bax, A. and Davis, D. G. (1985). "Practical aspects of two-dimensional transverse NOE spectroscopy." *Journal of Magnetic Resonance* **63**: 207 - 213.

Bax, A., Clore, G. M., Driscoll, P. C., Gronenborn, A. M., Ikura, M. and Kay, L. E. (1990). "Practical aspects of proton-carbon three-dimensional correlation spectroscopy of ^{13}C labelled proteins." *Journal of Magnetic Resonance* **87**: 620 - 627.

Bax, A., Max, D. and Zax, D. (1992). "Measurement of long-range ^{13}C-^{13}C J couplings in a 20kDa protein-peptide complex." *Journal of the American Chemical Society* **114**: 6923 - 6925.

Bax, A., Vuister, G. W., Grzesiek, S., Delaglio, F., Wang, A. C. and Tschudin, R. (1994a). "Measurement of homonuclear and heteronuclear J-couplings from quantitative J-correlation." *Methods in Enzymology* **239**: 79 - 105.

Bax, A., Delaglio, F., Grzesiek, S. and Vuister, W. (1994b). "Resonance assignment of methionine methyl groups and $\chi 3$ angular information from long range proton-carbon and carbon-carbon J correlation in a calmodulin-peptide complex." *Journal of Biomolecular NMR* **4**: 787 - 797.

Bergwerff, A. A., van Kuik, J. A., Schiphorst, W. E. C. M., Koeleman, C. A. M., van den Eijnden, D. H., Kammerling, J. P. and Vliegenthart, J. P. G. (1993). "Conversion of GalNAcβ1-4GlcNAcβ-OMe into GalNAcβ1-4[Fucα1-3]GlcNAcβ-OMe using human milk α-(3/4)-fucosyltransferase - synthesis of a novel terminal element glycoprotein glycans." *FEBS Letters* **334**: 133 - 138.

Bevilacqua, M. P., Prober, J. S., Mendrick, D. L., Cotran, R. S. and Gimbrone Jnr, M. A. (1987). "Identification of an inducible endothelial-leukocyte adhesion molecule." *Proceedings of the National Academy of Science of the United States of America* **84**: 9238 - 9243.

Bevilacqua, M. P., Stengelin, S., Gimbrone Jnr, M. A. and Seed, B. (1989). "Endothelial leukocyte adhesion molecule-1: An induclible receptor for neutrophils related to complement regulatory proteins and lectins." *Science* **243**: 1160 - 1165.

Bevilacqua, V. L., Thomson, D. S. and Prestegard, J. H. (1990). "Conformation of methyl-β-lactoside bound to ricin B-chain: Interpretation of transferred NOE facilitated by spin simulation and selective deuteration." *Biochemistry* **29**: 5529 - 5537.

Bevilacqua, V. L., Kim, Y. and Prestegard, J. H. (1992). "Conformation of β-methylmelibiose bound to ricin B-chain as determined by transferred NOEs." *Biochemistry* **31**: 9339 - 9349.

Bock, K. and Lemieux, R. U. (1982). "The conformational properties of sucrose in aqueous solution - intramolecular hydrogen bonding." *Carbohydrate Research* **100**: 63 - 74.

Bock, K., Arnap, J. and Lonngren, J. (1982). "The preferred conformation of oligosaccharides derived from complex-type carbohydrate portions of glycoproteins." *European Journal of Biochemistry* **129**: 171 - 178.

Bock, K., Brignole, A. and Sigurskjold, B. W. (1986). "Conformational dependence of ^{13}C NMR chemical shifts in oligosaccharides." *Journal of the Chemical Society, Perkin Transactions II*: 1711 - 1713.

Bock, K., Duus, J. O. and Refn, S. (1994). "Conformational equilibria of 4-thiomaltose and nitrogen analogs of maltose in aqueous solutions." *Carbohydrate Research* **253**: 51 - 67.

Bothner-by, A. A., Stephens, R. L., Lee, J. M., Warren, C. D. and Jeanloz, R. W. (1984). "Structure determination of a tetrasaccharide - transient nuclear Overhauser effects in the rotating frame." *Journal of the American Chemical Society* **106**: 811 - 813.

Bourne, Y., van Tilbeurgh, H. and Cambillau, C. (1993). "Protein-carbohydrate interactions." *Current Opinion in Structural Biology* **3**: 681 - 686.

Brady, J. W. (1986). "Molecular dynamics simulations of α-D-glucose." *Journal of the American Chemical Society* **108**: 8153 - 8160.

Brady, J. W. (1987). "Molecular dynamics simulations of β-D-glucose." *Carbohydrate Research* **165**: 306 - 312.

Breg, J., Kroon-Batenburg, L. M. J., Strecker, G., Montreuil, J. and Vliegenthart, J. F. G. (1989). "Conformational analysis of the sialylα(2-3/6)*N*-acetyllactosamine structural element occurring in glycoproteins, by two dimensional NOE ^{1}H-NMR spectroscopy in combination with energy calculations by hard-sphere with hydrogen-bonding potential." *European Journal of Biochemistry* **178**: 727 - 739.

Breimer, M. E., Karlsson, H., Karlsson, K. A., Nislon, K., Samuelsson, B. E. and Stromberg, N. (1988). "Structures of the 8-sugar to 9-sugar glycolipids of human blood group A erythrocytes." *Carbohydrate Research* **178**: 111 - 120.

Brunger, A. T. (1987). *X-PLOR - A system for X-ray crystallography and NMR (Manual)*, Yale University Press.

Bullard, D. C., Kunkel, E. J., Kubo, H., Hicks, M. J., Lorenzo, I., Doyle, C. A., Doerschuk, C. M., Ley, K. and Beaudet, A. L. (1996). "Infectious susceptibility and severe deficiency of leukocyte rolling and recruitment in E-selectin and P-selectin double mutant mice." *Journal of Experimental Medicine* **183**: 2329 - 2336.

Bundle, D. R., Jennings, H. J. and Smith, I. C. P. (1973). "The carbon-13 Nuclear Magnetic Resonance spectra of 2-acetamido 2-deoxy-D-hexoses and some specifically deuterated, *O*-acetylated, and phosporylated derivatives." *Canadian Journal of Chemistry* **51**: 3812.

Bundle, D. R. and Young, N. M. (1992). "Carbohydrate-protein interactions in antibodies and lectins." *Current Opinion in Structural Biology* **2**: 666 - 673.

Bundle, D. R., Baumann, H., Brisson, J-R., Gagne, S. M., Zdanov, A. and Cygler, M. (1994). "Solution structure of a trisaccharide-antibody complex: Comparison of NMR measurements with a crystal structure." *Biochemistry* **33**: 5183 - 5192.

Campbell, A. P. and Skyes, B. D. (1993). "The 2D transferred nOe effect: Theory and Practice." *Annual Review of Biophysics and Biomolecular Structure* **22**: 99-122.

Casset, F., Imberty, A., Perez, S., Etzler, M. E., Paulsen, H. and Peters, T. (1997). "Transferred nuclear Overhauser enhancement (nOe) and rotating frame NOE experiments reflect the size of the bound segment of the Forssman pentasaccharide in the binding site of *Dolichos biflorus* lectin." *European Journal of Biochemistry* **244**: 242 - 250.

Celi, A., Pellegrini, G., Lorenset, R., de Blasi, A., Ready, N., Furie, B. C. and Furie, B. (1994). "P-selectin induces the expression of tissue factor on monocytes." *Proceedings of the National Academy of Sciences of the United States of America* **91**: 8767 - 8771.

Chen, A., Engel, P. and Tedder, T. F. (1995). "Structural requirements regulate endoprotelytic release of the L-selectin (CD62L) adhesion receptor from the cell surface of leukocytes." *Journal of Experimental Medicine* **182**: 519 - 530.

Church, T., Carmichael, I. and Serianni, A. S. (1996). "Two bond ^{13}C-^{13}C spin-coupling constants in carbohydrates: Effect of structure on coupling magnitude and sign." *Carbohydrate Research* **280**: 177 - 186.

Church, T. J., Carmichael, I. and Serianni, A. S. (1997). "^{13}C-^{1}H and ^{13}C-^{13}C spin-coupling constants in methyl β-D-ribofuranoside and methyl 2-deoxy-β-D-erythro-pentofuranoside: Correlations with molecular structure and conformation." *Journal of the American Chemical Society* **119**: 8946 - 8964.

Clausen, H., Levery, S. B., Nudelman, E., Tsuchiya, S. and Hakomori, S-I. (1985). "Repetitive A-epitope (type 3 chain-A) defined by blood group A1 specific monoclonal antibody TH-1 - chemical basis of quantitative A1 and A2 distinction." *Proceedings of the National Academy of Science of the United States of America* **82**: 1199 - 1203.

Clausen, H. and Hakomori, S-I. (1989). "ABH and related histo-blood group antigens - Immunochemical differences in carrier iostype and their distribution." *Vox Sanguinis* **56**: 1 - 20.

Clore, G. M. and Gronenborn, G. M. (1982). "Theory and applications of the transferred nuclear Overhauser effect to the study of the conformations of small ligands bound to proteins." *Journal of Magnetic Resonance* **48**: 402 - 417.

Clore, G. M. and Gronenborn, A. M. (1983). "Theory of the time-dependant TRNOE: Application to analysis of ligand-protein complexes." *Journal of Magnetic Resonance* **53**: 423 - 442.

Clore, G. M., Nilges, M., Sukumaran, D. K., Brunger, A. T., Karplus, M. and Gronenborn, A. M. (1986). "The 3-dimensional structure of alpha-1-purothionin in solution - combined use of nuclear magnetic resonance, distance geometry and restrained molecular dynamics." *EMBO Journal* **5**: 2729 - 2735.

Clore, G. M. and Gronenborn, A. M. (1991). "Applications of 3-dimensional and 4-dimensional heteronuclear NMR spectroscopy to protein structure determination." *Progress in Nuclear Magnetic Resonance Spectroscopy* **23**: 43 - 92.

Cooke, R. M., Hale, R. S., Lister, S.G., Shah, G. and Weir, M. P. (1994). "The conformation of the sialyl Lewis^x ligand changes upon binding to E-selectin." *Biochemistry* **33**: 10591 - 10596.

Crouch, R. C. and Martin, G. E. (1991). "Selective inverse multiple bond analysis - a simple 1D experiment for the measurement of long-range heteronuclear coupling-constants." *Journal of Magnetic Resonance* **28**: 189 - 194.

Dabrowski, J. and Poppe, L. (1989). "Hydroxyl and amido groups as long-range sensors in conformational analysis by nuclear Overhauser enhancement: A source of experimental

evidence for conformational flexibility of oligosaccharides." *Journal of the American Chemical Society* **111**: 1510 - 1511.

Dabrowski, U., Dabrowski, J., Grosskurth, H., von der Lieth, C. W. and Ogawa, T. (1993). "Solution conformation of the tetrasaccharide glycoside Xylβ1-2(Manα1-3)Manβ1-4Glcβ1-R from the mollu-series glycosphingolipids." *Biochemical and Biophysical Research Communications* **192**: 1057 - 1065.

Dabrowski, J., Kozar, T., Grosskurth, H. and Nifant'ev, N. E. (1995). "Conformational mobility of oligosaccharides: Experimental evidence for the existence of an "anti" conformer of the Galβ1-3Glcβ1-OMe disaccharide." *Journal of the American Chemical Society* **117**: 5534 - 5539.

Daniels, G. L., Moulds, J. J., Anstee, D. J., Bird, G. W. G., Brodheim, E., Cartron, J. P., Dahr, W., Engelfriet, C. P., Issitt, P. D., Jorgensen, J., Kornstad, R., Lewis, M., Levene, C., Lubenko, A., Mallory, D., Morel, P., Nordhagen, R., Okubo, Y., Reid, M. and Rouger, P (1993). "ISBT working party on terminology for red cell surface antigens - Sao Paulo report." *Vox Sanguinis* **65**: 77 - 80.

Derome, A. E., (1987). "*Modern NMR techniques for Chemistry Research.*" Pergamon, Oxford.

de Vlieg, J., Boelens, R., Scheek, R. M., Kaptein, R. and van Gunsteren, W. F. (1986). "Restrained molecular dynamics procedure for protein tertiary structure determination from NMR data - A Lac repressor headpiece structure based on information on J-coupling and from the presence and absence of NOE." *Israel Journal of Chemistry* **27**: 181 - 188.

de Waard, P., Boelens, R., Vuister, G. W. and Vliegenthart, J. F. G. (1990). "Structural studies by ^{1}H,^{13}C 2-dimensional and 3-dimensional HMQC-NOE at natural abundance on complex carbohydrates." *Journal of the American Chemical Society* **112**: 3232 - 3234.

de Waard, P., Leeflang, B. R., Vliegenthart, J. F. G., Boelens, R., Vuister, G. W. and Kaptein, R. (1992). "Application of 2D and 3D NMR experiments to the conformational study of a diantennary oligosaccharide." *Journal of Biomolecular NMR* **2**: 211 - 226.

Dieckmann, T. and Feignon, J. (1994). "Heteronuclear techniques in NMR studies of RNA and DNA." *Current Opinion in Structural Biology* **4**: 745 - 749.

Disdier, M., Morrissey, J. H., Fugate, R. D., Bainton, D. F. and McEver, R. P. (1992). "Cytoplasmic domain of P-selectin (CD62) contains the signal for sorting into the regulated secretory pathway." *Molecular Biology of the Cell* **3**: 309.

Dore, M., Korthuis, R. J., Granger, D. N., Entman, M. L. and Smith, C. W. (1992). "P-selectin mediates spontaneous leukocyte rolling *in vivo*." *Blood* **82**: 1308 - 1316.

Duker, J. M. and Serianni, A. S. (1993). "(^{13}C)-substituted sucrose: ^{13}C-^{1}H and ^{13}C-^{13}C spin coupling constants to assess furanose ring and glycosidic bond conformations in aqueous solution." *Carbohydrate Research* **249**: 281 - 303.

Edge, C. (1994) "The role of glycosylation in disease.". Oxford Glycosystems catalogue**:** 30 - 31.

Edison, A. S., Abildgaard, F., Westler, W. M., Mooberry, E. S. and Markley, J. L. (1994). "Practical introduction to the theory and implementation of multinuclear, multidimensional nuclear magnetic resonance experiments." *Methods in Enzymology* **239**: 3 - 79.

Ejchart. A., D., J. and von der Lieth, C. W. (1992). "Solution conformation of monosyllactoses and difucosyllactoses as revealed by rotating-frame NOE-based distance mapping and molecular dynamics calculations." *Magnetic Resonance in Chemistry* **30**: S105 - S114.

Erbe, D. V., Wolitzky, B. A., Presta, L. G., Norton, C. R., Ramos, R. J., Burns, D. K., Rumberger, J. M., Rao, N., Foxall, C., Brandley, B. K. and Lasky, L. A. (1992).

"Identification of an E-selectin region critical for carbohydrate recognition and cell adhesion." *Journal of Cell Biology* **119**: 215 - 227.

Espinosa, J.-F., Asensio, J. L., Bruix, M. and Jimenez-Barbero, J. (1996). "Solution conformation of chitobiose. Evidences for the existence of conformational averaging around the glycosidic linkages form NMR spectroscopy experiments and molecular dynamics calculations." *Anales de Quimica International Edition* **92**: 320 - 324.

Farmer II, B. T., Macura, S. and Brown, L. R. (1987). "Relay artifacts in ROESY spectra." *Journal of Magnetic Resonance* **72**: 347 - 352.

French, A. D. (1988). "Rigid and relaxed-residue conformational analysis of cellobiose using the computer program MM2." *Biopolymers* **27**: 1519 - 1525.

French, A. D. (1989). "Comparisons of rigid and relaxed-residue conformational maps for cellobiose and maltose." *Carbohydrate Research* **188**: 206 - 211.

French, A. D. and Brady, J. W. (1989). *Computer modelling of carbohydrate molecules.* Washington, American Chemical Society.

Fujimoto, T. and McEver, R. P. (1993). "The cytoplasmic domain of P-selectin is phosphorylated on serine and threonine residues." *Blood* **82**: 1758 - 1766.

Gallatin, W. M., Weissman, I. L. and Butcher, E. C. (1993). "A cell surface molecule involved in organ-specific homing of lymphocytes." *Nature* **304**: 30 - 34.

Gearing, A. J. and Newman, W. (1994). "Circulating adhesion molecules in disease." *Immunology Today* **14**: 506 - 512.

Genest, D. (1989). "A Monte-Carlo simulation study of the influence of internal motions on the molecular conformation deduced from two-dimensional NMR experiments." *Biopolymers* **28**: 1903 - 1911.

Gilhespy-Muskett, A. M., Partridge, J., Jefferis, R. and Homans, S. W. (1994). "A novel ^{13}C isotopic labelling strategy for probing the structure and dynamics of glycan chains *in situ* on glycoproteins." *Glycobiology* **4**: 485 - 489.

Glaudemans, C. P. J., Lerner, L., Davies, G. D., Kovac, P., Venable, R. and Bax, A. (1990). "Significant conformational changes in an antigenic carbohydrate epitope upon binding to a monoclonal antibody." *Biochemistry* **29**: 10906 - 10911.

Goebel, C. V., Dimpfl, W. L. and Brant, D. A. (1970). "The conformational energy of maltose and amylose." *Macromolecules* **3**: 644 - 654.

Goetz, D. J., Grief, D. M., Ding, H., Camphausen, R. T., Howes, S., Comess, K. M., Snapp, K. R., Kansas, G. S. and Luscinskas, F. W. (1997). "Isolated P-selectin glycoprotein ligand-1 dynamic adhesion to P- and E-selectin." *The Journal of Cell Biology* **137**: 509 - 519.

Gorin, P. A. J. (1973). "The position of phosphate groups in the phosphonomannan of *Hansenla capsulata*, as determined by carbon-13 Magnetic Resonance Spectroscopy." *Canadian Journal of Chemistry* **51**: 2105.

Gorin, P. A. J. (1974). "Deuterium iostope effect on shifts of ^{13}C Magnetic Resonance signals of sugars: Signal assignment studies." *Canadian Journal of Chemistry* **52**: 548.

Gorin, P. A. J. and Mazurek, M. (1975). "Further studies on the assignment of signals in ^{13}C Magnetic Resonance spectra of aldoses and derived methyl glycosides." *Canadian Journal of Chemistry* **53**: 1212.

Graves, B. J., Crowther, R.L., Chandran, C., Rumberger, J. M., Li, S., Huang, K-S., Presky, D. H., Familletti, P. C., Wolitzk, B. A. and Burns, D. K. (1994). "Insight into E-selectin/ligand interaction from the crystal structure and mutagenesis of the lec/EGF domains." *Nature* **367**: 532 - 538.

Green, S. A., Setiadi, H., McEver, R. P. and Kelly, R. B. (1994). "The cytoplasmic domain of P-selectin contains a sorting determinant that mediates rapid degradation in lysosomes." *Journal of Cell Biology* **124**: 435 - 448.

Greenwell, P. (1997). "Blood group antigens: molecules seeking a function?" *Glycoconjugate Journal* **14**: 159 - 173.

Griesinger, C., Sorensen, O. W. and Ernst, R. R. (1986). "Correlation of connected transitions by two dimensional NMR spectroscopy." *Journal of Chemical Physics* **85**: 6837 - 6851.

Griesinger, C. and Ernst, R. R. (1987). "Frequency offset effects and their elimination in NMR rotating-frame cross-relaxation spectroscopy." *Journal of Magnetic Resonance* **75**: 261 - 271.

Grzesiek, S. and Bax, A. (1993). "The importance of not saturating H_2O in protein NMR. Application to sensitivity enhancement and NOE measurements." *Journal of the American Chemical Society* **115**: 12593 - 12594.

Ha, S. N., Giammona, A. and Field, M. (1988a). "A revised potential energy surface for molecular mechanics studies of carbohydrates." *Carbohydrate Research* **180**: 207 - 221.

Ha, S. N., Madsen, L. J. and Brady, J. W. (1988b). "Conformational analysis and molecular dynamics simulations of maltose." *Biopolymers* **27**: 1927 - 1952.

Haasnoot, C. A., de Leeuw, F. A. A. M. and Altona, C. (1980). "The relationship between proton-proton coupling constants and substituent electronegativities -1." *Tetrahedron* **36**: 2783 - 2792.

Hakomori, S-I. (1982). "Blood group ABH and Ii antigens of human erythrocytes - chemistry, polymorphism, and their developmental change." *Seminars in Hematology* **18**: 39 - 62.

Hakomori, S-I. (1985). "Aberrant glycosylation in cancer sell membranes as focused on glycolipids: overview and perspectives." *Cancer Research* **45**: 2405 - 2414.

Harlan, J. M. (1993). "Leukocyte adhesion deficiency syndrome: insights into the molecular basis of leukocyte emigration." *Clinical Immunology and Immunopathology* **67**: S16 - 24.

Harris, R., Rutherford, T. J., Milton, M. J. and Homans, S. W. (1997). "Three-dimensional heteronuclear NMR techniques for assignment and conformational analysis using exchangeable protons in uniformly ^{13}C-enriched oligosaccharides." *Journal of Biomolecular NMR* **9**: 47 - 54.

Harrison, J. A., Kartha, K. P. R., Field, R. A., Naismith, J. H. and Schenkman, S. (1997). "Development of a high through-put spectrophotometric assay to monitor *Trypanosoma cruzi trans*-sialidase." *Biochemical Society Transactions* **25**: 424S.

Hartmann, G. (1941). *Blood Group Antigens in Human Organs.* Copenhagen, Munksgaard.

Heidlas, J. E., Watson, W. J., Pale, P. and Whitesides, G. M. (1992). "Gram-scale synthesis of uridine 5'-diphosphoglucosamine: Comparison of enzymatic and chemical routes." *Journal of Organic Chemistry* **57**: 146 - 151.

Hemmerich, S., Leffler, H. and Rosen, S. D (1995). "Structure of the *O*-glycans in GLYCAM-1, an endothelial-derived ligand for L-selectin." *Journal of Biological Chemistry* **270**: 12035 - 12047.

Hensley, P., McDevitt, P. J., Brooks, I., Trill, J. T., Field, J. A., McNulty, D. E., Connor, J. R., Griswold, D. E., Kumar, N. V., Kopple, K. D., Carr, S. A., Dalton, B. J. and Johanson, K. (1994). "The soluble form of E-selectin is an asymmetric monomer." *Journal of Biological Chemistry* **269**: 23949 - 23958.

Holak, T. A., Prestegard, J. H. and Forman, J. D. (1987). "NMR - pseudo-energy approach to the solution structure of acyl carrier protein." *Biochemistry* **26**: 4652 - 4660.

Homans, S. W., Pastore, A., Dwek, R. A. and Rademacher, T. W. (1987). "Structure and dynamics in oligo-mannose type oligosaccharides." *Biochemistry* **26**: 6649 - 6655.

Homans, S. W. (1990a). "A molecular mechanical force-field for the conformational analysis of oligosaccharides - comparison of theoretical and crystal structures of Manα1-3Manβ1-4GlcNAc." *Biochemistry* **29**: 9110 - 9118.

Homans, S. W. (1990b). "Oligosaccharide conformations: Application of NMR and energy calculations." *Progress in NMR Spectroscopy* **22**: 55 - 81.

Homans, S. W. and Forster, M. (1992). "Application of restrained minimisation, simulated annealing and molecular dynamics simulations for the conformational analysis of oligosaccharides." *Glycobiology* **2**: 143 - 151.

Homans, S. W. (1992). "Homonuclear three-dimensional NMR methods for the complete assignment of proton NMR spectra of oligosaccharides - application to Galβ1-4(Fucα1-3)GlcNAcβ1-3Galβ1-4Glc." *Glycobiology* **2**: 153 - 159.

Hricovini, M. and Liptaj, T. (1989). "Measurement of long-range proton-carbon coupling constants in medium sized molecules." *Magnetic Resonance in Chemistry* **27**: 1052 - 1056.

Hsu-Lin, S-C., Berman, C. L., Furie, B. C., August, D. and Furie, B. (1984). "A platelet membrane protein expressed during platelet activation and secretion. Studies using a monoclonal antibody specific for thrombine-activated platelets." *Journal of Biological Chemistry* **259**: 9121 - 9126.

Hwang, T-L. and Shaka, A. J. (1995). "Water suppression that works. Excitation sculpting using arbitrary waveforms and pulse field gradients." *Journal of Magnetic Resonance Series A* **112**: 275 - 279.

Ichikawa, Y., Lin, Y-C., Dumas, D. P., Shen, G-J., Garcia-Junceda, E., Williams, M. A., Bayer, R., Ketcham, C., Walker, LE., Paulson, J. C., Wong, C-H. (1992). "Chemical-

enzymatic synthesis and conformational analysis of sialyl Lewis^x and derivatives." *Journal of the American Chemical Society* **114**: 9283 - 9298.

Ichikawa, Y. (1997). Enzymatic synthesis of oligosaccharides and glycopeptides. *Glycopeptides and related compounds: Synthesis, analysis, and applications*. Editors - Large, D. G., Warren, C. D.: 79 - 205.

Imberty, A., Tran, V. and Perez, S. (1990). "Relaxed potential energy surfaces of *N*-linked oligosaccharides - The mannoseα1-3mannose case." *Journal of Computational Chemistry* **11**: 205 - 216.

Imberty, A. (1997). "Oligosaccharide structures: theory versus experiment." *Current Opinion in Structural Biology* 7: 617 - 623.

Ionides, J. M. C., Keeler, J. and Neuhaus, D. (1995). *Poster presentation at 12th International Meeting on NMR Spectroscopy, Manchester UK.*

Johnson, P. J., Donald, A. S., Feeney, J. and Watkins, W. M. (1992). "Reassessment of the acceptor specificity and general properties of the Lewis blood-group gene associated α-3/4-fucosyltransferase purified from human milk." *Glyconjugate Journal* **9**: 251 - 264.

Johnstone, E. R. and Little Jr, A. B. (1995). "Measurement of proton exchange rates in aqueous solution by selective spin locking of the water resonance." *Journal of Magnetic Resonance Series A* **114**: 113 - 115.

Jones, D. A., McIntire, L. V., Smith, C. W. and Picker, L. J. (1994). "A two step adhesion. cascade for T cell/endothelial cell interactions under flow conditions." *Journal of Clinical Investigation* **94**: 2443 - 2450.

Jung, U., Bullard, D. C., Tedder, T. F. and Ley, K. (1996). "Velocity differences between L- and P-selectin dependent neutrophil rolling in venules of mouse cremaster muscle *in vivo*." *American Journal of Physiology* **40**: H2740 - H2747.

Kansas, G. S. (1996). "Selectins and their ligands: Current concepts and controversies." *Blood* **88**: 3259 - 3287.

Karplus, M. (1959). "Contact electron-spin coupling of nuclear magnetic moments." *Journal of Chemical Physics* **30**: 11 - 18.

Karplus, M. (1963). "Vicinal proton coupling in nuclear magnetic resonance." *Journal of the American Chemical Society* **85**: 2870 - 2871.

Kawabata, J. and Fukushi, E. (1994). "Application of DEPT C-C Relay in spectrum editing by multiplicities of neighbouring protonated carbons and accurate determination of ^{13}C-^{13}C coupling constants." *Journal of Magnetic Resonance Series A* **107**: 173 - 177.

Kay, L. E., Xu, G-Y., Singer, A. U., Muhandiram, D. R. and Forman-Kay, J. D. (1993). "A gradient enhanced HCCH-TOCSY experiment for recording side-chain ^{1}H and ^{13}C correlation in H_2O samples of proteins." *Journal of Magnetic Resonance Series B* **101**: 333 - 337.

Keller, P. J. and Vogele, K. E. (1986). "Sensitivity enhancement of INADEQUATE by proton monitoring." *Journal of Magnetic Resonance* **68**: 389 - 392.

Kessler, H., Bermel, W. and Griesinger, C. (1985). "Determination of carbon-carbon connectivities, assignment of quaternary carbons, and extraction of carbon-carbon coupling constants by carbon-relayed hydrogen-carbon spectroscopy." *Journal of Magnetic Resonance* **62**: 573 - 579.

Kiddle, G. R., Harris, R. and Homans, S. W. (1998). "Heteronuclear Overhauser effects in carbohydrates." *Journal of Biomolecular NMR (accepted).*

Kim, Y. C. and Prestegard, J. H. (1990). "Refinement of the NMR structures for acyl carrier protein with scalar coupling data." *Proteins - Structure, Function, and Genetics* **8**: 377 - 385.

Kim, Y. J. and Varki, A. (1997). "Perspectives on the significance of altered glycosylation of glycoproteins in cancer." *Glycoconjugate Journal* **14**: 569 - 576.

King, M.-J. (1994). "Blood group antigens on human erythrocytes - distribution, structure, and possible functions." *Biochimica et Biophysica Acta* **1197**: 15 - 44.

Kittelmann, M., Klein, T., Kragl, U., Wandrey, C. and Ghisalba, O. (1992). "Preparative enzymatic synthesis of activated neuraminic acid by using a microbial enzyme." *Annals of the New York Academy of Sciences* **672**: 444 - 450.

Koch, H. J. and Perlin, A. S. (1970). *Carbohydrate Research* **15**: 403.

Kogan, T. P., Revelle, B. M., Tapp, S., Scott, D. and Beck, P. J. (1995). "A single amino acid residue can determine the ligand specificity of E-selectin." *The Journal of Biological Chemistry* **270**: 14047 - 14055.

Kouwijzer, M. L. C. E. and Grootenhuis, P. D. J. (1995). "Parametrisation and application of CHEAT95, an extended atom force field for hydrated (oligo)saccharides." *Journal of Physical Chemistry* **99**: 13426 - 13436.

Kover, K. E., Batta, G. and Madi, Z. (1980). *Journal of Magnetic Resonance* **69**: 538 - 541.

Kover, K. E. and Batta, G. (1988). "Sensitivity enhanced 2D heteronuclear NOE spectroscopy - 2-fold to 3-fold improved S/N ratio at quaternary carbons in the MIEMI experiment." *Journal of Magnetic Resonance* **79**: 206 - 210.

Kragl, U. (1990). "Enzymatic synthesis of sialic acid." *European Patent* **EP 0 428 947 A1**.

Krivdin, L. B. and Della, E. W. (1991). "Spin-spin coupling constants between carbons." *Progress in NMR Spectroscopy* **23**: 579 - 594.

Kubes, P. and Kanwar, S. (1994). "Histamine induces leukocyte rolling in post-capillary venules. A P-selectin mediated event." *Journal of Immunology* **152**: 3570 - 3577.

Kunkel, E. J., Jung, U., Bullard, D. C., Norman, K. E., Wolitzky, B. A., Vestweber, D., Beaudet, A. L. and Ley, K. (1996). "Absence of trauma-induced leukocyte rolling in mice deficient in both P-selectin and intercellular adhesion molecule-1 (ICAM-1)." *Journal of Experimental Medicine* **183**: 57 - 65.

Kunkel, E. J., Jung, U and Ley, K. (1996). "Slow leukocyte rolling in TNF-α-treated mouse cremaster muscle venules is mediated by E-selectin." *FASEB Journal* **10**: A1280.

Labow, M. A., Norton, C. R., Rumberger, J. M., Lombard-Gillooly, K. M., Shuster, D. J., Hubbard, J., Bertko, R., Knaack, P. A., Terry, R. W., Harbison, M. L., Kontgen, F., Stewart, C. L., McIntyre, K. W., Will, P. C., Burns, D. K. and Wolitzky, B. A. (1994). "Characterisation of E-selectin deficient mice: Demonstration of overlapping function of the endothelial selectins." *Immunity* **1**: 709 - 720.

Larsen, E., Celi, A., Gilbert, G. E., Furie, B. C., Erban, J. K., Bonfanti, R., Wagner, D. D. and Furie, B. (1989). "PADGEM protein: A receptor that mediates the interaction of activated platelets with neutrophils and monocytes." *Cell* **59**: 305 - 312.

Lawrence, M. B. and Springer, T. A. (1991). "Leukocytes roll on a selectin at physiologic flow rates: Distinction from and prerequisite for adhesion through integrins." *Cell* **65**: 859 - 873.

Lawrence, M. B. and Springer, T. A. (1993). "Neutrophils roll on E-selectin." *Journal of Immunology* **151**: 6338 - 6346.

Lee, K. S. and Morris, G. A. (1986). "Hydrogen-carbon-carbon relay as an alternative to the INEPT-INADEQUATE experiment for unprotonated carbons." *Journal of Magnetic Resonance* **70**: 332 -335.

Lee, Y. C. (1972). "Analysis of sugars by automated liquid chromatography." *Methods in Enzymology* **28**: 63 - 73.

Lemieux, R. U., Bock, K., Delbaere, L. T. J., Koto, S. and Rao, V. S. (1980). "The conformations of oligosaccharides related to the ABH human blood group determinants." *Canadian Journal of Chemistry* **58**: 631 - 653.

Ley, K., Gaehtgens, P., Fennie, C., Singer, M. S., Lasky, L. and Rosen, S. D. (1991). "Lectin-like cell adhesion molecule 1 mediates leukocyte rolling in mesenteric venules *in vivo*." *Blood* **77**: 2553 - .

Ley, K., Tedder, T. F. and Kansas, G. S. (1993). "L-selectin can mediate rolling independent of E- and P-selectin in mesenteric venules *in vivo*." *Blood* **82**: 1632 - 1638.

Ley, K. and Tedder, T. F. (1995). "Leukocyte interactions with vascular endothelium. New insights into selectin-mediated attachment and rolling." *Journal of Immunology* **155**: 525 - 528.

Ley, K., Bullard, D., Arbones, M. L., Bosse, R., Vestweber, D., Tedder, T. F. and Beaudet, A. L. (1995). "Sequential contribution of L- and P-selectin to leukocyte rolling *in vivo*." *Journal of Experimental Medicine* **181**: 669 - 675.

Ley, K., Zakrzewicz, A., Hanski, C., Stoolman, L. M. and Kansas, G. S. (1995). "Sialylated *O*-glycans and L-selectin on myeloid cells subsequently mediate rolling *in vivo*." *Blood* **85**: 3727 - 3735.

Li, Y. C. and Montelione, G. T. (1993). "Solvent saturation-transfer effects in pulse field gradient heteronuclear single quantum coherence (PFG-HSQC) spectra of polypeptides and proteins." *Journal of Magnetic Resonance Series B* **101**: 315 - 319.

Liepinsh, E., Otting, G. and Wuthrich, K. (1992). "NMR spectroscopy of hydroxyl protons in aqueous solutions of peptides and proteins." *Journal of Biomolecular NMR* **2**: 447 - 465.

Lin, Y.-C., Hummel, C. W., Huang, D-H., Ichikawa, Y., Nicolaou, K. C., Wong, C-H. (1992). "Conformational studies of sialyl Lewis^x in aqueous solution." *Journal of the American Chemical Society* **114**: 5452 - 5454.

Lin-Chun Liu, J., Shen, G-J., Ichikawa, Y., Rutan, J. F., Zapata, G., Vann, W. F. and Wong, C-H. (1992). "Overproduction of CMP-sialic acid synthase for organic synthesis." *Journal of the American Chemical Society* **114**: 3902 - 3910.

Lipkind, G. M., Shashkov, A. S. and Kochetkov, N. K. (1985). "Nuclear Overhauser effect and conformational states of cellobiose in aqueous solution." *Carbohydrate Research* **141**: 191 - 197.

Lipkind, G. M., Shashkov, A. S., Kikolaev, A. V., Mamyan, S. S. and Kochetkov, N. K. (1987). "Nuclear Overhauser effect and conformational states of (1-4)-linked glucosylrhamnosides in aqueous solutions." *Bioorganic Khimica* **13**: 1081 - 1092.

Liu, H., Kumar, A., Weisz, K., Schmitz, U., Bishop, K. D. and James, T. L. (1993). "Extracting accurate distance and bounds form 2D NOE exchangeable proton peaks." *Journal of the American Chemical Society* **115**: 1590 - 1591.

Livingston, P. O., Natoli, E. J., Jones-Calves, M., Stockbert, E., Oettgen, H. F. and Old, L. J. (1987). "Vaccines containing purified G_{M2} ganglioside elicit G_{M2} antibodies in melanoma patients." *Proceedings of the National Academy Of Sciences of the United States of America* **84**: 2911 - 2915.

Lloyd, K. O. (1987). "Blood group antigens as markers for normal differentiation and malignant change in human tissues." *American Journal of Clinical Pathology* **87**: 129 - 139.

Lommerse, J. P. M., Kroon-Batenburg, L. M. J., Kroon, J., Kammerling, J. P. and Vliegenthart, J. F. G. (1995). "Conformations and internal mobility of a glycopeptide derived from bromelain using molecular dynamics simulation and NOESY analysis." *Journal of Biomolecular NMR* **5**: 79 - 94.

London, R. E., Kollman, V. H. and Matwiyoff, N. A. (1975). "The quantitative analysis of carbon-carbon couplings in the ^{13}C Nuclear Magnetic Resonance spectra of molecules synthesised from ^{13}C enriched precursors." *Journal of the American Chemical Society* **97**: 3565 - 3573.

Longchambon, F., Ohanessian, J., Gillier-Pandraud, H., Duchet, D., Jacquinet, J. C. and Sinay, P. (1981). "Structure de la *N*-acetyl-lactosamine (acetamido-2-desoxy-2-O-β-D-galactopyrannosyl-4-α-D-glucopyranose)." *Acta Crystallography B* **37**: 601 - 607.

Low, D. G. (1996) "NMR Investigation of molecular contacts in a hapten antibody complex.". *Ph.D. Thesis*, Chemistry, St. Andrews University: 210.

Luscinskas, F. W., Ding, H. and Lichtman, A. H. (1995). "P-selectin and vascular cell adhesion molecule-1 mediate rolling an arrest, respectively, of $CD4^+$ T lymphocytes on tumour necrosis factor-α activated vascular endothelium under flow conditions." *Journal of Experimental Medicine* **181**: 1179 - 1186.

Lynch, S. R., Pelton, J. G. and Tinoco Jr, I. (1996). "NMR assignment of a 2'-hydroxyl proton from UUCG tetraloop through long-range correlations with ^{13}C." *Magnetic Resonance in Chemistry* **34**: S11 - S17.

Marion, D., Driscoll, P. C., Kay, L. E., Wingfield, P. T., Bax, A., Gronenborn, A. and Clore, G. M. (1989). "Overcoming the overlap problem in the assignment of ^1H NMR spectra of larger proteins by use of three-dimensional heteronuclear ^1H-^{15}N Hartmann-Hahn multiple quantum coherence and nuclear Overhauser multiple quantum coherence spectroscopy - application to interleukin-1β." *Biochemistry* **28**: 6150 - 6156.

Marshall, J. L. and Miller, D. E. (1973). "The angular dependence of three-bonded carbon-carbon coupling constants." *Journal of the American Chemical Society* **95**: 8305 - 8308.

Mayadas, T. N., Johnson, R. C., Rayburn, H., Hynes, R. O. and Wagner, D. D. (1993). "Leukocyte rolling and extravasation are severely compromised in P-selectin deficient mice." *Cell* **74**: 541 - 554.

McAuliffe, J. and Hindsgaul, O. (1997). "Carbohydrate drugs - an ongoing challenge." *Chemistry and Industry* **March** (5): 170 - 174

McEver, R. P., Beckstead, J. H., Moore, K. L., Marshal-Carlson, L. and Bainton, D. F. (1989). "GMP-140, a platelet alpha granule membrane protein, is also synthesised by vascular endothelial cells and is localised in Weibel-Palade bodies." *Journal of Clinical Investigation* **84**: 92 -99.

McEver, R. P. (1997). "Selectin-carbohydrate interactions during inflammation and metastasis." *Glycoconjugate Journal* **14**: 585 - 591.

McGarvey, G. J. and Wong, C-H. (1997). "Chemical, enzymatic and structural studies in molecular glycobiology." *Liebigs Annalen/Recueil*: 1059 - 1074.

Milton, M. J. (1997). "Multidimensional and heteronuclear NMR investigations of oligosaccharides in the free and protein bound states." *Ph.D. Thesis,* Chemistry, University of St. Andrews: 247.

Milton, M. J., Harris, R., Probert, M. A., Field, R. A. and Homans, S. W. (1998). "New conformational constraints in isotopically ^{13}C enriched oligosaccharides." *Glycobiology (accepted).*

Montelione, G. T. and Wagner, G. (1989). "Accurate measurements of long-range heteronuclear coupling-constants from homonuclear 2D NMR spectra of isotope enriched proteins." *Journal of Magnetic Resonance* **82**: 198 - 204.

Moore, K. L., Stults, N. L., Diaz, S., Smith, D. F., Cummings, R. D., Varki, A. and McEver, R. P. (1992). "Identification of a specific glycoprotein ligand for P-selectin (CD62) on myeloid cells." *Journal of Cell Biology* **118**: 445 - 456.

Moore, K. L., Eaton, S. F., Lyons, D. E., Lichenstein, H. S., Cummings, R. D. and McEver, R. P. (1994). "The P-selectin glycoprotein ligand from human neutrophils displays sialylated, fucosylated, *O*-linked poly-*N*-acetyllactosamine." *Journal of Biological Chemistry* **269**: 23318 - 23327.

Moore, K. L., Patel, K. D., Breuhl, R. E., Fugang, L., Johnson, D. A., Lichenstein, H. S., Cummings, R. D., Bainton, D. F. and McEver, R. P. (1995). "P-selectin glycoprotein ligand-1 mediates rolling on human neutrophils on P-selectin." *Journal of Cell Biology* **128**: 661 - 671.

Mourant, A. E. (1946). "A "new" human blood antigen of frequent occurrence." *Nature* **158**: 237 - 238.

Neuhaus, D. and Keeler, J. (1986). "False transverse NOE enhancements in camelspin spectra." *Journal of Magnetic Resonance* **68**: 568 - 574.

Neuhaus, D. and Williamson, M. P. (1989). *The Nuclear Overhauser Effect - in structural and conformational analysis.*, VCH.

Neuhaus, D. and van Mierlo, C. P. M. (1992). "Measurement of heteronuclear NOE enhancements in biological macromolecules - a convenient pulse sequence for use with aqueous solutions." *Journal of Magnetic Resonance* **100**: 221 - 228.

Ni, F. (1994). "Recent developments in transferred NOE methods." *Progress in Nuclear Magnetic Resonance Spectroscopy* **26**: 517 - 606.

Ni, F. and Scheraga, H. A. (1994). "Use of transferred nOe to determine the conformations of ligands bound to proteins." *Accounts of Chemical Research* **27**: 257 - 264.

Nicolaou, K. C., Hummel, C. W., Bockovich, N. J. and Wong, C-H. (1991). "Stereo-controlled synthesis of sialyl Lewis^x, the oligosaccharide binding ligand to ELAM-1." *Journal of the Chemical Society, Chemical Communications*: 870 - 872.

Nilges, M., Clore, G. M. and Gronenborn, A. M. (1988). "Determination of 3-dimensional structures of proteins from inter-proton distance data by hybrid distance geometry-dynamical simulated annealing calculations." *FEBS Letters* **229**: 317 - 324.

Noggle, J. H. and Schrimer, R. E. (1971). *The nuclear Overhauser effect, chemical applications.* New York, Academic Press.

Nolte, D., Schmid, P., Jager, U., Boltzlar, A., Roesken, F., Hecht, R., Uhl, E., Messmer, K. and Vestweber, D. (1994). "Leukocyte rolling in venules of striated muscle and skin is mediated by P-selectin, not by L-selectin." *American Journal of Physiology* **267**: H1637 - H1642.

Nunez, H. and Barker, R. (1980). "Enzymatic synthesis and carbon-13 NMR conformational studies of disaccharides containing β-D-galactopyranosyl and β-D-[1-^{13}C] galactopyranosyl residues." *Biochemistry* **19**: 489 - 495.

Oettgen, H. F. (1989). *Gangliosides and Cancer.* New York, VCH.

Ohrui, H., Nishida, Y., Watanabe, M., Hori, H. and Meguro, H. (1985). "Studies on (6R)-deuterated and (6S)-deuterated (1-6) linked disaccharides - Assignment of the preferred rotamers about the C5-C6 bound of (1-6) disaccharides in solution." *Tetrahedron Letters* **26**: 3251 - 3254.

Oriol, R., le Pendu, J. and Mollicone, R. (1986). "Genetics of ABO, H, Lewis, X and related antigens." *Vox Sanuguis* **51**: 161 - 171.

Palcic, M. M. and Hindsgaul, O. (1996). "Glycosyltransferases in the synthesis of oligosaccharide analogs." *Trends in Glycoscience and Glycotechnology* **8**: 37 - 49.

Pardi, A. (1992). "Isotope labelling for NMR studies of biomolecules." *Current Opinion in Structural Biology* **2**: 832 - 835.

Pearlman, D. A. and Kollman, P. A. (1991). "Are time-averaged restraints necessary for nuclear magnetic resonance refinement?" *Journal of Molecular Biology* **220**: 457 - 479.

Perlin, A. S. and Casu, B. (1969). "Carbon-13 and proton magnetic resonance spectra of D-glucose-^{13}C." *Tetrahedron Letters* **34**: 2921.

Peters, T. and Pinto, B. M. (1996). "Structure and dynamics of oligosaccharides: NMR and modelling studies." *Current Opinion in Structural Biology* **6**: 710 - 720.

Picker, L. J., Kishimoto, T. K., Smith, C. W., Warnock, R. A. and Butcher, E. C. (1991). "ELAM-1 is an adhesion molecule for skin-homing T cells." *Nature* **349**: 796 - 799.

Picker, L. J. and Butcher, E. C. (1992). "Physiological and molecular mechanisms of lymphocyte homing." *Annual Reviews in Immunology* **10**: 561 - 591.

Plateau, P. and Gueron, M. (1982). "Exchangeable proton NMR without base-line distortion, using new strong-pulse sequences." *Journal of the American Chemical Society* **104**: 7310 - 7311.

Podkorytov, I. S. (1990). "Seven-pulse sequence DEPT-INADEQUATE." *Journal of Magnetic Resonance* **89**: 129 - 132.

Poppe, L., Dabrowski, J., von der Lieth, C. W., Koike, K. and Ogawa, T. (1990a). "Three dimensional structure of the oligosaccharide terminus of globotriaosylceramide and isoglobotriaosylceramide in solution - A rotating frame NOE study using hydroxyl groups as long range sensors in conformational analysis by ^{1}H NMR spectroscopy." *European Journal of Biochemistry* **189**: 313 - 325.

Poppe, L., von der Lieth, C. W., and Dabrowski, J. (1990b). "Three dimensional structure of the oligosaccharide chain of G_{M1} ganglioside revealed by a distance mapping approach - A rotating frame nuclear Overhauser enhancement investigation of native glycolipid in

dimethyl-sulfoxide and in water dodecylphosphocholine solutions." *Journal of the American Chemical Society* **112**: 7762 - 7771.

Poppe, L. and van Halbeek, H. (1991a). "^{1}H-detected measurements of long-range heteronuclear coupling constants. Application to a trisaccharide." *Journal of Magnetic Resonance* **92**: 636 - 641.

Poppe, L. and van Halbeek, H. (1991b). "Nuclear Magnetic Resonance of hydroxyl and amido protons of oligosaccharides in aqueous solution: Evidence for a strong intermoleclar hydrogen bond in sialic acid residues." *Journal of the American Chemical Society* **113**: 363 - 365.

Poppe, L., Stuike-Prill, R., Meyer, B. and van Halbeek, H. (1992). "The solution conformation of sialyl(2-6)lactose studied by modern NMR techniques and Monte Carlo simulations." *Journal of Biomolecular NMR* **2**: 109 - 136.

Poppe, L., van Halbeek, H., Acquotti, D. and Sonnino, S. (1994). "Carbohydrate Dynamics at a micellar surface: GD1a headgroup transformations revealed by NMR spectroscopy." *Biophysical Journal* **66**: 1642 - 1652.

Poppe, L. and van Halbeek, H. (1994). "NMR spectroscopy of hydroxyl protons in supercooled carbohydrates." *Nature Structural Biology* **1**: 215 - 316.

Poppe, L., Brown, G. S., Philo, J. S., Nikrad, P. V. and Shah, B. H. (1997). "Conformation of sLe^{x} tetrasaccharide, free in solution and bound to E-, P-, and L-selectin." *Journal of the American Chemical Society* **119**: 1727 - 1736.

Poveda, A., Asensio, J. L., Martin-Pastor, M. and Jimenez-Barbero, J. (1996). "Exploration of the conformational flexibility of the Le^{x} related oligosaccharide GalNAcα(1-3)Galβ(1-4)[Fucα1-3]Glc by ^{1}H NMR relaxation measurements and molecular dynamics simulations." *Journal of the Chemical Society, Chemical Communications*: 421 - 422.

Poveda, A., Asensio, J. L., Martin-Pastor, M. and Jimenez-Barbero, J. (1997). "Solution conformation and dynamics of a tetrasaccharide related to the Lewis^x antigen deduced by NMR and relaxation measurements." *Journal of Biomolecular NMR* **10**: 29 - 43.

Probert, M. A., Milton, M. J., Harris, R., Schenkman, S., Brown, J. M., Homans, S. W. and Field, R. A. (1997). "Chemoenzymatic synthesis of G_{M3}, Lewis^x and sialyl Lewis^x oligosaccharides in ^{13}C-enriched form." *Tetrahedron Letters* **38**: 5861 - 5864.

Rice, K. G., Wu, P., Brand, L. and Lee, Y. C. (1993). "Experimental determination of oligosaccharide three-dimensional structure." *Current Opinion in Structural Biology* **3**: 669 - 674.

Rinaldi, R. L. (1983). "Heteronuclear 2D NOE spectroscopy." *Journal of American Chemical Society* **105**: 5167 - 5168.

Rosen, S. D. and Bertozzi, C. R. (1994). "The selectins and their ligands." *Current Opinion in Cell Biology* **6**: 663 - 673.

Rosevear, P. R., Nunez, H. A. and Barker, R. (1982). "Synthesis and solution conformation of the type 2 blood group oligosaccharide Fucα(1-2)Galβ(1-4)GlcNAc." *Biochemistry* **21**: 1421 - 1431.

Rossi, G. L. (1992). "Biological activity in the crystalline state." *Current Opinion in Structural Biology* **2**: 816 - 820.

Rutherford, T. J., Partridge, J., Weller, C. W. and Homans, S. W. (1993). "Characterisation of the extent of internal motions in oligosaccharides." *Biochemistry* **32**: 12175 - 12724.

Rutherford, T. J., Spackman, D. G., Simpson, P. J. and Homans, S. W. (1994). "5 nanosecond molecular dynamics and NMR study of conformational transitions in the sialyl Lewis^x antigen." *Glycobiology* **4**: 59 - 68.

Sanders, J. K. M. and Hunter, B. K. (1987). "*Modern NMR Spectroscopy: A guide for chemists.*" Oxford, Oxford University Press.

Scarsdale, J. N., Ram. P., Prestegard, J. H. and Yu, R. K. (1988). "A molecular mechanics-NMR pseudo-energy approach to the solution conformation of glycolipids." *Journal of Computational Chemistry* **9**: 133 - 147.

Schauer, R. (1982). *Sialic acids - chemistry, metabolism and function*, Springer-Verlag.

Scheffler, K., Ernst, B., Katopodis, A., Magnani, J. L., Wang, W. T., Weisemann, R. and Peters, T. (1995). "Determination of the bio-active conformation of the carbohydrate ligand in the E-selectin/sialyl Lewis^x complex." *Angewandte Chem. Int. Ed. Engl.* **34**(17): 1841 - 1844.

Scheffler, K., Brisson, J. R., Weisemann, R., Magnani, J. L., Wong, W. T., Ernst, B. and Peters, T. (1997). "Application of homonuclear 3D NMR experiments and 1D analogs to study the conformation of sialyl Lewis^x bound to E-selectin." *Journal of Biomolecular NMR* **9**: 423 - 436.

Schwalbe, H., Rexroth, A., Eggenberger, U., Geppert, T. and Griesinger, C. (1993). "Measurement of C,C coupling constants in ^{13}C-labelled proteins: A new method for the stereospecific assignment of γ-methyl groups in valine residues." *Journal of the American Chemical Society* **115**: 7878 - 7879.

Scudder, P., Doom, J. P., Chuenkova, M., Manger, I. D. and Pereira, M. E. A. (1993). "Enzymatic characterisation of β-D-galactoside α2,3-trans-sialidase from *Trypanosoma cruzi*." *Journal of Biological Chemistry* **13**: 9886 - 9891.

Sears, P. and Wong, C-H. (1996). "Intervention of carbohydrate recognition by proteins and nucleic acids." *Proceedings of the National Academy of Science in the United States of America* **93**: 12086 - 12093.

Serianni, A. S., Bondo, P. B. and Zajicek, J. (1996). "Verification of the projection resultant method for two-bond ^{13}C-^{13}C coupling sign determinations in carbohydrates." *Journal of Magnetic Resonance Series B* **112**: 69 - 74.

Sharon, N. and Lis, H. (1972). "Lectins: cell agglutinating and sugar specific proteins." *Science* **177**: 949 - 959.

Sicinska, W., Adams, B. and Lerner, L. (1993). "A detailed ^{1}H and ^{13}C NMR study of a repeating disaccharide of hyaluronan: the effects of temperature and counter-ion type." *Carbohydrate Research* **242**: 29 - 51.

Siebert, H.-C., Reuter, G., Schauer, R., von der Lieth, C-W. and Dabrowski, J. (1992). "Solution conformations of G_{M3} gangliosides containing different sialic acid residues as revealed by NOE-based distance mapping molecular mechanics, and molecular dynamics calculations." *Biochemistry* **31**: 6962-6971.

Simon, E. S., Bednarski, M. D. and Whitesides, G. (1988). "Synthesis of CMP-NeuAc from *N*-acetylglucosamine: Generation of CTP from CMP using adenylate kinase." *Journal of the American Chemical Society* **110**: 7159 - 7163.

Sklenar, V. and Bax, A. (1987a). "Measurement of ^{1}H, ^{31}P NMR coupling-constants in double stranded DNA fragments." *Journal of the American Chemical Society* **109**: 7525 - 7526.

Sklenar, V. and Bax, A. (1987b). "Spin-echo water suppression for the generation of pure-phase two-dimensional NMR spectra." *Journal of Magnetic Resonance* **74**: 469 - 479.

Sklenar, V., Piotto, M., Leppik, R. and Saudek, V. (1993). "Gradient tailored water suppression for ^{1}H-^{15}N HSQC experiments optimised to retain full sensitivity." *Journal of Magnetic Resonance Series A* **102**: 241 - 245.

Smeets, E. F., de Vries, T., Leeuwenberg, J. F. M., van den Eijnden, D. H., Buurman, W. A. and Neefjes, J. J. (1993). "Phosphorylation of surface E-selectin and the effect of soluble

ligand (sialyl Lewis^x) on the half life of E-selectin." *European Journal of Immunology* **23**: 147 - 151.

Sorensen, O. W., Freeman, R., Frenkiel, T., Mareci, T. H. and Schuck, R. (1982). "Observation of ^{13}C-^{13}C couplings with enhanced sensitivity." *Journal of Magnetic Resonance* **46**: 180 - 184.

Sorensen, O. W. (1990). "3-dimensional and 4-dimensional NMR experiments for measurement of spin-spin coupling constants." *Journal of Magnetic Resonance* **90**: 433 - 438.

Spivak, C. T. and Roseman, S. (1959). "Preparation of *N*-acetyl-D-mannosamine and D-mannosamine hydrochloride." *Journal of the American Chemical Society* **81**: 2403 - 2404

States, D. J., Haberkorn, R. A. and Ruben, D. J. (1982). "A 2-dimensional nuclear Overhauser experiment with pure absorption phase in 4 quadrants." *Journal of Magnetic Resonance* **48**: 286 - 292.

Stein, P. E., Boodhoo, A., Tyrrell, J. G., Brunton, J. L. and Read, R. J. (1992). "Crystal structure of the cell binding B oligomer verotoxin-1 from *E. coli*." *Nature* **355**: 748 - 749.

Stoddart, J. F. (1971). "*Stereochemistry of Carbohydrates*." New York, Wiley.

Stonehouse, J. (1994). *Ph.D. Thesis*, University of Cambridge.

Stonehouse, J., Shaw, G. L., Keeler, J. and Laue, E. D. (1994a). "Minimizing sensitivity losses in gradient-selected ^{15}N-^{1}H HSQC spectra of proteins." *Journal of Magnetic Resonance Series A* **107**: 178 - 184.

Stonehouse, J., Adell, P., Keeler, J. and Shaka, A. J. (1994b). "Ultrahigh-quality NOE spectra." *Journal of the American Chemical Society* **116**: 6037 - 6038.

Stott, K. and Keeler, J. (1996). "Gradient-enhanced one-dimensional heteronuclear NOE experiment with ^{1}H detection." *Magnetic Resonance in Chemistry* **34**: 554 - 558.

Stott, K., Keeler, J., Van, Q. N. and Shaka, A. J. (1997). "One-dimensional NOE experiment using pulse field gradients." *Journal of Magnetic Resonance* **125**: 302 - 324.

Subramanian, M., Koedoum, J. A. and Wagner, D. D. (1993). "Divergent fates of P- and E-selectins after their expression on the plasma membrane." *Molecular Biology of the Cell* **4**: 791 - 801.

Swift, T. J. and Connick, R. E. (1962). "NMR relaxation mechanisms of ^{17}O in aqueous solutions of paramagnetic cations and lifetime of water molecules in the first co-ordination sphere." *Journal of Chemical Physics* **37**: 307 - 320.

Tedder, T. F., Penta, A. C., Levine, H. B. and Freedman, A. S. (1990). "Expression of the human leukocyte adhesion molecule, LAM1. Identity with the TQ1 and Leu-8 differentiation antigens." *Journal of Immunology* **144**: 532 - 540.

Tedder, T. F., Steeber, D. A. and Pizcueta, P. (1995a). "L-selectin deficient mice have impaired leukocyte recruitment into inflammatory sites." *Journal of Experimental Medicine* **181**: 2259 - 2264.

Tedder, T. F., Steeber, D. A., Chen. A. and Engel, P. (1995b). "The selectins: vascular adhesion molecules." *FASEB Journal* **9**: 866 - 873.

Thogerson, H., Lemieux, R. U., Bock, K. and Meyer, B. (1982). "Further justification for the exo-anomeric effect. Conformational analysis based on nuclear magnetic resonance spectroscopy of oligosaccharides." *Canadian Journal of Chemistry* **60**: 44 - 57.

Titman, J. J., Neuhaus, D. and Keeler, J. (1989). "Measurement of long-range heteronuclear coupling constants." *Journal of Magnetic Resonance* **85**: 111 - 131.

Titman, J. J. and Keeler, J. (1990). "Measurement of homonuclear coupling constants from NMR correlation spectra." *Journal of Magnetic Resonance* **89**: 640 -646.

Torda, A. E., Scheek, R. M. and van Gunsteren, W. F. (1989). "Time-dependent distance restraints in molecular dynamics simulations." *Chemical Physical Letters* **157**(4): 289 - 294.

Torda, A. E., Scheek, R. M. and van Gunsteren, W. F. (1990). "Time-averaged nuclear Overhauser effect distance restraints applied to tendamist." *Journal of Molecular Biology* **214**: 223 - 235.

Torda, A. E., Brunne, R. M., Huber, T., Kessler, H. and van Gunsteren, W. F. (1993). "Structure refinement using time-averaged J-coupling constant restraints." *Journal of Biomolecular NMR* **3**: 55 - 66.

Tropp, J. (1980). "Dipolar relaxation and nuclear Overhauser effects in non-rigid molecules: The effect of fluctuating internuclear distances." *Journal Chemical Physics* **72**: 6035 - 6044.

Tvaroska, I. and Bleha T. (1989). "Anomeric and Exo-anomeric effects in carbohydrate chemistry." *Advances in Carbohydrate Chemistry and Biochemistry* **47**: 45-123.

Tvaroska, I., Hricovini, M. and Petrakova, E. (1989). "An attempt to derive a new Karplus-type equation of vicinal proton-carbon coupling-constants for C-O-C-H segments of bonded atoms." *Carbohydrate Research* **189**: 359 - 362.

Tvaroska, I. (1991). "Theoretical aspects of structure and conformation of oligosaccharides." *Current Opinion in Structural Biology* **2**: 661 - 665.

Tvaroska, I. and Taravel, F. R. (1995). "Carbon-proton coupling constants in the conformational analysis of sugar molecules." *Advances in Carbohydrate Chemistry and Biochemistry* **51**: 15 - 61.

Uhrin, D. and Liptaj, T. (1989). "Determination and assignment of heteronuclear long-range coupling-constants - methods based on semi-selective INEPT." *Journal of Magnetic Resonance* **81**: 82 - 91.

Uhrin, D., Liptaj, T., Hricovini, M. and Capek, P. (1989). "Determination of long-range proton carbon coupling-constants using modified 2D J-resolved experiments." *Journal of Magnetic Resonance* **85**: 137 - 140.

Uhrin, D., Mele, A., Kover, K. E., Boyd, J. and Dwek, R. A. (1994). "One-dimensional inverse-detected methods for measurement of long-range proton-carbon coupling constants. Application to saccharides." *Journal of Magnetic Resonance Series A* **108**: 160 - 170.

van Halbeek, H. (1994). "NMR developments in structural studies of carbohydrates and their complexes." *Current Opinion in Structural Biology* **4**: 697 - 709.

Varki, A. (1993). "Biological roles of oligosaccharides: all of the theories are correct." *Glycobiology* **3**: 98 - 130.

Vliegenthart, J. F. G., Dorland, L. and van Halbeek, H. (1983). "High resolution, ^{1}H-nuclear magnetic resonance spectroscopy as a tool in the structural analysis of carbohydrates related to glycoproteins." *Advances in Carbohydrate Chemistry and Biochemistry* **41**: 209 - 374.

von Asmuth, E. J. U., Smeets, E. F., Ginsel, L. A., Onderwater, J. J. M., Leeuwenberg, J. F. M. and Buurman, W. A. (1992). "Evidence for endocytosis of E-selectin in human endothelial cells." *European Journal of Immunology* **22**: 2519 - 2526.

von Itzstein, M., Wu, W-Y. and Kok, G. B. (1993). "Rational drug design of potent sialidase-based inhibitors of influenza virus repetition." *Nature* **363**: 418 - 423.

Vuister, G. W., de Waard, P., Boelens, R., Vligenthart, J. F. G. and Kaptein, R. (1989). "The use of 3D NMR in structural studies of oligosaccharides." *Journal of the American Chemical Society* **111**: 772 - 774.

Vuister, G. W., Wan, A. C. and Bax, A. (1993). "Measurement of 3-bond nitrogen carbon J-couplings in proteins uniformly enriched in ^{15}N and ^{13}C." *Journal of the American Chemical Society* **115**: 5334 - 5335.

Vuister, G. W. and Bax, A. (1993). "Quantitative J-correlation - A new approach for measuring homonuclear 3-bond $J_{H(N)H(alpha)}$ coupling constants in N-15 enriched proteins." *Journal of the American Chemical Society* **115**: 7772 - 7777.

Vyas, N. K. (1991). "Atomic features of protein-carbohydrate interactions." *Current Opinion in Structural Biology* **1**: 732 - 740.

Wagner, G. and Wuthrich, K. (1979). *Journal of Magnetic Resonance* **33**: 675.

Walker, T. E., London, R. E., Whaley, T. W., Barker, R. and Matwiyoff, N. A. (1976). "Carbon-13 NMR Spectroscopy of [1-^{13}C] enriched monosaccharides. Signal assignments and orientational dependence of geminal and vicinal carbon-carbon and carbon-proton spin-spin coupling constants." *Journal of the American Chemical Society* **98**(19): 5807 - 5813.

Watkins, W. M. and Morgan, W. J. T. (1959). *Vox Sanguinis* **4**: 97 - 119.

Weimar, T., Harris, S. L., Pitner, J. B., Bock, K. and Pinto, B. M. (1995). "Transferred NOE experiments show that the monoclonal antibody strep 9 selects a local minimum conformation of Streptococcus group A trisaccharide-hapten." *Biochemistry* **34**: 13672 - 13681.

Weiner, S. J., Kollman, P. A., Case, D. A., Chandra Singh, U., Ghio, C., Alagona, G., Profeta, S. P. and Weiner, P. (1984). "A new force-field for molecular mechanical simulations of nucleic acids and proteins." *Journal of the American Chemical Society* **106**: 765 - 784.

Weiner, S. J., Kollman, P. A., Nguyen, D. T. and Case, D. A. (1986). "An all atom force-field for simulations of protein and nucleic acids." *Journal of Computational Chemistry* **7**: 230 - 252.

Weis, W. I. (1997). "Cell-surface recognition by animal and viral lectins." *Current Opinion in Structural Biology* **7**: 624 - 630.

Weller, C. T., Lustbader, J., Seshadri, K., Brown, J. M., Chadwick, C. A., Kolthoff, C. E., Ramnarain, S., Pollak, S., Canfield, R. and Homans, S. W. (1996). "Structural and conformational analysis of glycan moieties *in situ* on isotopically ^{13}C, ^{15}N-enriched recombinant human chorionic gonadotropin." *Biochemistry* **35**(27): 8815 - 8823.

Wilkins, P. P., McEver, R. P. and Cummings, R. D. (1996). "Structures of the *O*-glycans on P-selectin glycoprotein lignad-1 from HL-60 cells." *Journal of Biological Chemistry* **271**: 18732 - 18742.

Woods, R. J. (1995). "Three-dimensional structures of oligosaccharides." *Current Opinion in Structural Biology* **5**: 591 - 598.

Wright, C. S. (1992). "Crystal structure of a wheat germ agglutinin/glycophorin-sialoglycopeptide receptor complex. Structural basis for co-operative lectin-cell binding." *Journal of Molecular Biology* **267**: 14345 - 14352.

Wright, C. S. and Kellog, G. E. (1996). "Differences in the hydropathic properties of ligand binding at four independent sites in wheat germ agglutinin-oligosaccharide crystal complexes." *Protein Science* **5**: 1466 - 1476.

Wu, G. D., Serianni, A. S. and Barker, R. (1983). "Stereo-selective deuterium-exchange of methylene protons in methyl tetrafuranosides - hydroxymethyl group conformations in methyl pentafuranosides." *Journal of Organic Chemistry* **48**: 1750 - 1757.

Wu, J., Bondo, P. B., Vuorinen, T. and Serrianni, A. S. (1992). "^{13}C-^{13}C spin coupling constants in aldoses enriched with ^{13}C at the terminal hydroxymethyl carbon - effect of

coupling pathway on J_{CC} in carbohydrates." *Journal of the American Chemical Society* **114**: 3499 - 3505.

Wuthrich, K. (1986). *NMR of proteins and Nucleic Acids.* New York, Wiley.

Yan, Z-Y. and Bush, C. A. (1990). "Molecular dynamics simulations and conformational mobility of blood group oligosaccharides." *Biopolymers* **29**: 799 - 811.

Yu, C. and Levy, G. C. (1984). "2-dimensional heteronuclear NOE (HOESY) experiments - investigation of dipolar interactions between heteronuclei and nearby protons." *Journal of the American Chemical Society* **106**: 6533 - 6537.

Yu, L., Goldman, R., Sullivan, P., Walker, G. F. and Fesik, S. W. (1993). "Heteronuclear NMR studies of ^{13}C-labelled yeast cell wall β-glucan oligosaccharides." *Journal of Biomolecular NMR* **3**: 429 - 441.

Yvelin, F., Zhang, Y-M., Mallet, J-M., Robert, F., Jeannin, Y. and Sinay, P. (1996). "Crystal structure of the Lewis^x trisaccharide." *Carbohydrate Letters* **1**: 475 - 482.

Zhu, G., Renwick, A. and Bax, A. (1994). "Measurement of two- and three-bond ^{1}H-^{13}C J couplings from quantitative heteronuclear J correlation for molecules with overlapping ^{1}H resonances, using t_1 noise reduction." *Journal of Magnetic Resonance Series A* **110**: 257 - 261.